Calmodulin as a universal regulator of voltage gated calcium channels.

by

Valentina Taiakina

A thesis

presented to the University of Waterloo

in fulfillment of the

thesis requirement for the degree of

Doctor of Philosophy

in

Chemistry

Waterloo, Ontario, Canada, 2014

AUTHOR'S DECLARATION

I hereby declare that I am the sole author of this thesis. This is a true copy of the thesis, including any required final revisions, as accepted by my examiners.

I understand that my thesis may be made electronically available to the public.

Valentina Taiakina

Abstract

Calmodulin (CaM) is a ubiquitous calcium-binding protein responsible for the binding and activation of a vast number of enzymes and signaling pathways. It contains two lobes that bind two calcium ions each, separated by a flexible central linker. This structural flexibility allows CaM to bind and regulate a large number of diverse protein targets within the cell in response to Ca^{2+} gradients.

Voltage gated calcium channels (Ca_Vs), as main sources of extracellular Ca^{2+}, are crucial for a number of physiological processes, from muscle contraction to neurotransmission and endocrine function. These large transmembrane proteins open in response to membrane depolarization and allow gated entry of Ca^{2+} ions into the cytoplasm. Their regulation is currently the subject of intense investigation due to its pharmacological and scientific importance.

CaM has been previously shown to pre-associate and act as a potent inhibitor of one class of high-voltage activated (HVA) channels called L-type channels via its interaction with their C-terminal cytoplasmic region. This interaction is primarily mediated by a conserved CaM-binding motif called the 'IQ' motif (for conserved isoleucine and glutamine residues), although the exact molecular details of its involvement in inactivation are currently unclear. Elucidation of these details was the primary objective of this dissertation.

Recently, a novel sequence motif within this channel called 'NSCaTE' (N-terminal spatial calcium transforming element) has been described as an important contributor to calcium-dependent inactivation (CDI) of L-type channels. It was presumed to be unique to vertebrates, but we also show its conservation in a distantly related L-type channel homolog of *Lymnaea*

stagnalis (pond snail). The interaction of CaM with a number of peptides representing the different regulatory motifs (IQ and NSCaTE) for both mammalian and snail isoforms was characterized in an attempt to better understand their role in CDI. Biophysical work with peptides as well as electrophysiology recordings with an N-terminal truncation mutant of *Lymnaea* Ca_V1 homolog were performed to expand our understanding of how the interplay between these channel elements might occur. In brief, the most striking feature of the interaction concerns the strong evidence for a CaM-mediated bridge between the N- and C-terminal elements of L-type channels.

Further investigation of the CaM interaction with both IQ and NSCaTE peptides using Ca^{2+}-deficient CaM mutants reveals a preference of both peptides for the Ca^{2+}-C-lobe of CaM, and a much higher affinity of CaM for the IQ peptide, suggesting that the N-lobe of CaM is the main interaction responsible for the physiological effects of NSCaTE. These results are consistent with our electrophysiology findings that reveal a distinct buffer-sensitive CDI in wild type LCa_V1 that can be abolished by the N-terminal truncation spanning the NSCaTE region.

In addition to L-type channels, CaM has also been shown to have an indirect role in the regulation of low-voltage activated (LVA) or T-type channels ($Ca_V3.x$), via their phosphorylation by CaM-dependent protein kinase II (CaMKII). Using a primary sequence scanning algorithm, a CaM-binding site was predicted in a cytoplasmic region of these channels that was also previously shown to be important in channel gating. Biophysical experiments with synthetic peptides spanning this gating brake region from the three human and the single *Lymnaea* isoform strongly suggest that there is a novel, *bona fide* CaM interaction in this channel region, and also hint that this interaction may be a Ca^{2+}-dependent switch of some sort. The

results confirm a possible new role for CaM in the direct regulation of these channels, although

the exact mechanism remains to be elucidated.

Acknowledgements

I would like to thank my supervisors, Dr. JG Guillemette and Dr. JD Spafford, for their helpful discussions, guidance and support during my graduate (and undergraduate, in Dr. Guillemette's case) years at the University of Waterloo. Your knowledge and wisdom has kept me on track more than once in these last five years.

I would also like to thank my committee members: Dr. Palmer, Dr. Duncker, Dr. Joseph, Dr. Tupling, and my external examiner, Dr. van Petegem, for their time and consideration of this dissertation. I am grateful to NSERC for providing scholarship funding for the majority of my stay here.

I am also grateful to other graduate students of my chemistry lab, including Erica Lee and Mike Piazza, and my biology lab, including Julia Fux, Wendy Guan, Dr. Adriano Senatore, and of course Dr. Adrienne Boone whose work was instrumental to this thesis. I have enjoyed the friendship and camaraderie of several other graduate students in the department, and will definitely miss our chats and coffee breaks and running practices. An honorable mention goes to Harmen Vander Heide, whose help in rescuing our microcalorimeter allowed me to complete my experiments and finally get to writing of this thesis.

A special mention goes to Cathy van Esch, who is a miracle worker and life saver of many students, myself included, for her seemingly limitless knowledge about the arcane world of administrative procedures, deadlines, persons, and anything else that can't be found on the UW home page.

Several undergraduate students have spent many hours working on this project with me directly or through Dr. Spafford, and I would like to thank them all, including Edmund Luk,

Dedication

To my parents, Irina and Fedor,

whose hard work and commitment to their children are unmatched,

thank you for making this possible.

Table of Contents

List of Figures

List of Tables

List of Abbreviations:

AID	α interaction domain (a β subunit binding site)
ALS	amyotropic lateral sclerosis
AMFE	anomalous mole fraction effect
AMPA	α-amino-3-hydroxy-5-methyl-4-isoxazolepropionic acid (Glu analog)
ASD	autism spectrum disorder
BAPTA	1,2-bis(o-aminophenoxy)ethane-N,N,N',N'-tetraacetic acid
CaM	Calmodulin (apo = Ca^{2+} free, holo = Ca^{2+} replete)
CaMKII	CaM-dependent protein kinase II
Ca_V	see VGCC
CD	circular dichroism
CDF	calcium dependent facilitation
CDI	calcium dependent inactivation
CNG	cyclic nucleotide gated (channel)
COSY	Correlation spectroscopy
Cp	heat capacity
DSC	differential scanning calorimetry
DMSO	dimethyl sulfoxide
DTT	dithiothreitol
EDTA	ethylenediaminetetraacetic acid
EGTA	ethylene glycol tetraacetic acid
ESI MS	electrospray ionization mass spectrometry
FCS	fluorescence correlation spectroscopy
FID	free induction decay
FPLC	fast protein liquid chromatography
FRET	Förster resonance energy transfer
GABA	γ-amino-butyric acid
HCN	hyperpolarization cyclic nucleotide-gated (channel)
HEK	human embryonic kidney
HEPES	4-(2-hydroxyethyl)-1-piperazineethanesulfonic acid
HSQC	heteronuclear single quantum coherence
HVA	high voltage activated
IMAC	immobilized metal affinity chromatography
IPTG	Isopropyl β-D-1-thiogalactopyranoside, a lactose analog
ITC	isothermal calorimetry
IUB	International Union of Biochemistry
IUPAC	International Union of Pure and Applied Chemistry
LB	Luria Bertani (broth culture)
LVA	low voltage activated
MRE	mean residue ellipticity
Na_V	voltage gated sodium channels
NMDA	N-methyl-D-aspartate

NMR	nuclear magnetic resonance
NOESY	Nuclear Overhauser Effect Spectroscopy
NSCaTE	N terminal spatial calcium transforming element
PAGE	poly acrylamide gel electrophoresis
PDB	Protein Data Bank
PKC	protein kinase C
qRT-PCR	quantitative reverse transcription polymerase chain reaction
Q-TOF	quadrupole time-of-flight (in reference to ESI MS)
RyR	ryanodine receptor
SASA	solvent-accessible surface area
SB	superbroth (when in context of protein expression)
SDS	sodium dodecyl sulfate
smMLCK	small myosin light chain kinase
TFE	2,2,2-trifluoroethanol
TM	transmembrane
TRP	transient receptor potential
UTR	untranslated region
VDI	voltage dependent inactivation
VGCC	voltage gated calcium channel (also see Ca_V)
VSD	voltage sensing domain

Primarily the three letter amino acid code is used in this thesis, as outlined in the IUPAC-IUB

Joint Commission on Biochemical Nomenclature (Dixon, 1984). DNA sequences use single

letter abbreviations.

Chapter 1: Background

1.1 Introduction

All living organisms are composed of cells – tiny droplets of biomolecules enclosed in vanishingly thin envelopes of lipid membrane. Since the concentrations of these biomolecules are crucial to sustaining cellular metabolism, the entry and exit of water, gases and solutes across the membrane must be tightly regulated. Ion channels are perfectly suited to fill the latter of these roles; these uniquely shaped, large protein structures span the thickness of the membrane (and often extend quite far into the cytoplasm), and precisely control the entry (or export) of only one or very few different ion species. Not every periodic element has a channel associated with it, but there is at least one channel associated with each of the more common ions (e.g. potassium, sodium, chloride and calcium). Some channels are highly selective, being virtually impermeable to all but their 'chosen' element. Yet others are not truly ion channels but more like aqueous pores that allow many ions and even small molecules through in response to specific stimuli. The opening behavior of different channel species is also quite diverse; some are open for prolonged durations, like the potassium leak channels; some are open for fleeting, several millisecond durations and closed the majority of the time (like many neurotransmitter receptors) (Rosenmund et al., 1995; Perez-Reyes, 1999, 2003). There are as many reasons to study ion channels as there are types of ion channels, for each one of them is uniquely suited to fill the role for which it evolved, and even slight changes in amino acid sequence or expression levels can result in anything from strange behaviors to severe and even lethal conditions (**Figure 1.1**)

Electricity, that is, the movement of charged particles, has been observed by humans for a long time. Speculation aside, the first real experiments with 'electrophysiology' can be credited

to Jan Swammerdam in the 1600s, although he did not claim an electrical nature for the cause of muscle contraction; this idea was proposed (but not experimentally confirmed) by Sir Isaac Newton. It was not until the following century, and the more commonly recognized experiments of Luigi Galvani and his colleague-antagonist, Alessandro Volta, that a concrete idea for the electrical nature of neuronal impulses conducting muscle contraction emerged. Their work with frog muscle and electricity paved the way for modern day understanding of neurotransmission. As scholars refined their techniques and equipment, more elaborate experiments were conducted, and a more complex picture of the nervous system emerged.

We are now able to measure single channel currents, whole cell currents, currents from a single channel type, their amplitude, frequency, open probability, current-voltage dependence and so on and so forth. We can dissect a channel's biochemical profile and binding partners, measure their expression patterns, determine their primary sequence and genetic location, and observe crude (low-resolution) structures with electron microscopy. What we cannot yet do, in many cases, is obtain a high-resolution picture of the three-dimensional structure of these channels and point out how it correlates with their spatial and temporal regulatory mechanisms. Ion channels are simply too large, in most cases, and quite hydrophobic: two main qualities that make a protein difficult to purify and prepare for structural analysis by either X-ray crystallography or NMR spectroscopy. Since modern electrophysiology equipment is not quite automated and most labs do not have access to high-throughput recording equipment, detailed kinetic analyses of channel effectors are rather painstaking. The closest we can get to a 'big picture' is an integration of the current piecemeal approach of mutagenesis, biophysical characterization of channel fragments, molecular modeling and electrophysiology with various surrogate systems (e.g. liposomes or *Xenopus* eggs). Therefore it is important to take all work in

this field with a proverbial grain of salt: one can only infer so much about a room-sized puzzle based on a window-sized arrangement of pieces that seemingly fit together. So far, no single complete molecular model for channel regulation has been accepted, but several working models for various channel groups are being refined.

Below is a brief introduction to the field of voltage gated calcium channels and may be helpful in putting the subsequent chapters into context.

Channel Family	Function	Associated Pathologies	Domain architecture (single subunit)	Holo Channel Architecture
Na$_V$	Na+ currents (rising phase of the AP)	Paramyotonia, hyperkalemic periodic paralysis; Long QT syndrome and ventricular fibrillation; generalized epilepsy with febrile seizures plus[3]		
NALCN	Na$^+$ leak channels	Myotonia and cognitive /developmental problems[1]		
Ca$_V$3	LVA Ca^{2+} channels, 'pacemakers'	Absence epilepsy, chronic pain; possible autism-spectrum disorders (ASD)[2]		
Ca$_V$2	HVA non-L-type Ca^{2+} channels (neuronal)	Episodic ataxia; familial hemiplegic migraine; spinocerebellar ataxia[3]; pain disorders[4]		
Ca$_V$1	L-type Ca^{2+} channels (muscle, neuronal, retinal, auditory)	X-linked congenital night blindness; hypokalemic periodic paralysis; malignant hyperthermia; sinoatrial node dysfunction and deafness; Timothy syndrome[5]		
TRP*	Diverse; sensory; 'transient receptor potential' – many gating variables	Many[6] (examples: pulmonary disease, coronary heart disease, diabetes mellitus, cold/heat/etc. sensitivities, taste and hearing dysfunction, bladder and renal diseases, bowel disease)		
Kv10-12 (KCNH)	'ether-a-go-go' potassium channels, regulate excitability	Long QT syndrome, epilepsy, schizophrenia, cancer[7].		
HCN	Hyperpolarization-cyclic nucleotide-gated current (Na$^+$/K$^+$)	Learning abnormalities, epilepsy, altered vision, ataxia, reduced pain; cardiac abnormalities (sinus arrhythmia, QT prolongation, bradycardia)[8]		
CNG	Cyclic-nucleotide (cGMP/cAMP) gated cation channel; vision/olfactory	Retinitis pigmentosa; axon guidance defects in *C.elegans*; inflammatory pain[9]		
KCa1	'big conductance' (BK) voltage+Ca^{2+}-gated K$^+$ channels	Rheumatoid arthritis[10]; ethanol response in *C.elegans*[11]; hypertension[12]		
KCa2	'small conductance' (SK) Ca^{2+} gated K$^+$ channels	Hypertension[13]		
KCa3	'intermediate conductance' " "			
Kv7 (KCNQ)	Neuronal 'M-current' Voltage gated K$^+$	Benign familial neonatal convulsions (BFNC); various long-QT syndromes: deafness[14]		
Kv1-4 (KCNA)	AP repolarization	Episodic ataxia/myokymia[15]; possible autoimmune disorders (Kv1.3)[16]		
K2P	K$^+$ leak channels	Mental retardation (KCNK9)[17]		
Kir	Inward rectifier K$^+$ channels	Bartter syndrome and renal/electrolyte imbalances; vision loss; neonatal diabetes mellitus; developmental delay/ retardation; seizures; Andersen-Tawil syndrome[18]		
GRIK (KAR)	Ionotropic Glu receptor binds kainate; mostly in PSEP (nonselective)	Epilepsy; autism; mania and mild mental retardation; schizophrenia; Huntington disease; major depression; bipolar disorder[19]		
AMPA	Fast excitatory ionotropic Glu receptor, Na$^+$/K$^+$ only	Alzheimer disease[20]; amyotropic lateral sclerosis[21]		
NMDA	Excitatory ionotropic GluR (Na$^+$/K$^+$/Ca^{2+})	Stroke-related neuronal damage; Alzheimer's; Huntington[22]		
P2X	Purinergic (ATP/ ADP/UDP etc.) gated signaling	Stroke and trauma-related neuronal death; Alzheimer's, Parkinson's, Huntington's, ALS, MS; mood disorders (depression, bipolar); schizophrenia and drug dependence[23]		
'cys-loop' receptors	Neurotransmitter-gated ion channels (both cation and anion)	Various. Ex.: epilepsy (GABA$_A$R and neuronal nAChR); congenital myasthenic syndrome or CMS (muscle nAChR); hyperekplexia (GlyR)[24]		
CLC	Voltage-gated chloride channels	Myotonia; epilepsy; osteoporosis and lysosomal storage disease; Bartter's syndrome; glioma; Dent's disease[25]		

Figure 1.1: Summary of phylogeny, function, architecture and common associated disorders of main types of ion channels.
Left side: color coding indicates the approximate evolutionary timing of the divergence between the channel families (blue = basal metazoans, red = single-celled eukaryotes, green = prokaryotes, black = various/emergent/unknown). **Right side**: domain architecture, subunit organization. Color coding indicates the individual distinct subunits. Separate polypeptide chains are different colors; pore-forming domains are denoted by cartoons with central 'holes'. Family-unique features, such as CaM and nucleotide binding domains, are indicated. Cartoon design and phylogeny information adapted from (Jegla et al., 2009); neither are to scale. References for the channel functions and channelopathies are cited below, along with abbreviations and other relevant numbered notes.

(1)(Al-Sayed et al., 2013) (2) (Perez-Reyes, 2003; Splawski et al., 2006) (3) (Cooper and Jan, 1999; Kullmann and Hanna, 2002) (4) (Wilson et al., 2011) (5) (Striessnig et al., 2010; Bidaud and Lory, 2011; Napolitano and Antzelevitch, 2011) Timothy syndrome is a multi-organ disorder characterized by cardiac abnormalities, webbed digits (syndactyly), facial dismorphy, ASD and developmental delay. It is typically lethal by early childhood. (6) TRP family of channels is very diverse (28 genes in humans), gated by any number of stimuli, from temperature to pH to cell volume to sometimes voltage. Not surprisingly, a large number (upwards of a 100) of human diseases is associated with one or more members of this family; the subject has received an excellent review (Nilius, 2007) (7) These channels bear some similarity to the CNG/HCN channels in having a cyclic nucleotide binding homology domain or CNBHD, but are not actually regulated by cAMP (Haitin et al., 2013) (8) (Postea and Biel, 2011) (9) (Ashcroft, 2000; Heine et al., 2011) (10) (Hu et al., 2012) (11) (Davies et al., 2003) (12) (Sobey, 2001) (13) (Dalsgaard et al., 2010) (14) (Jentsch, 2000) (15) Ataxia (loss of muscle control) and myokymia (muscle rippling) of this disorder are also linked to the P/Q ($Ca_V2.1$) type Ca^{2+} channel (Shieh et al., 2000); KCNA1 is homologous to the well characterized Shaker channel from *Drosophila* (16) (Beeton et al., 2006) (17) (Barel et al., 2008) (18) Bartter syndrome is a cluster of symptoms resulting from renal malfunction (hypokalemic alkalosis, hyperprostaglandinuria, hypercalciuria). Andersen–Tawil syndrome is a rare autosomal dominant disorder that manifests in a number of physical and neurological defects (periodic paralysis, arrhythmia, facial and limb abnormalities and developmental problems) (Pattnaik et al., 2012) (19) (Lerma and Marques, 2013) PSEP = post-synaptic excitatory potential (20) AMPA = α-amino-3-hydroxy-5-methyl-4-isoxazolepropionic acid (Glu analog) (Henley and Wilkinson, 2013) (21) (Corona et al., 2007) sALS (sporadic ALS) is associated with a mutation in one of the AMPAR subunits that renders the channel Ca^{2+}-permeable when it normally isn't (22) NMDA = N-methyl-D-aspartate (Rothman and Olney, 1995) (23) MS = multiple sclerosis (Burnstock et al., 2011) (24) GABA (γ-amino-butyric acid) and glycine receptors are anion-selective (thus inhibitory). nAChR (nicotinic acetylcholine receptors) are cationic (excitatory). Hyperekplexia is 'excess surprise' or startle disease, characterized by an exaggerated startle response and subsequent hypertonia (Sine and Engel, 2006; Pless and Lynch, 2008) (25) Bartter's syndrome can also be caused by K_{ir} mutations (different clinical form). Dent's disease is a form of X-linked recessive nephrolithiasis (kidney stones) and associated proteinuria, hypercalciuria and hyperphosphaturia (Jentsch et al., 2005; Puljak and Kilic, 2006; Planells-Cases and Jentsch, 2009)

1.2 Structure, Nomenclature, and Evolution of Ion channels

The basic conducting pore subunit of an ion channel has existed in one form or another for hundreds of millions of years; there are prokaryotic ancestor forms for nearly every major channel family found in mammals (Anderson and Greenberg, 2001; Jegla et al., 2009). There is no one 'template' for an ion channel sequence, as there are at least 5 different basic protein subunit configurations in which the different channel types can meet the ion-conducting requirement. Nature's 'solutions' to this range from a simple 'transmembrane bundle' in the manner of the Shaker potassium channel[1] to the much more complex topology of the chloride channels (CLCs), which contain 2 identical subunits with a pore each. The lack of any similarity between even the most primitive members of each archetype suggests that channels evolved multiple times, independently, pointing to convergent evolution for ion selectivity in some cases (Jegla et al., 2009). The great diversity in ion channel isoforms (over 200 genes for most metazoan species) came about from gene duplication and specialization that accompanied the evolution of a more complex nervous system (Piontkivska and Hughes, 2003). This is especially evident in the case of the voltage-gated potassium and sodium channels; the general topology of these two is quite similar, but the former is a single-homology-domain channel (e.g. forms a tetramer) while the latter is a single polypeptide consisting of 4 highly similar TM domains, each of which bears homology to the voltage-gated potassium channel (Anderson and Greenberg, 2001). It is quite likely that the sodium/calcium four-domain architecture is a result of serial gene duplication of a more potassium-channel-like ancestor. While there is an apparent trend in the accumulation of channel diversity in higher organisms, there is no correlation between the size/complexity of the nervous system and the number of ion channel genes in metazoans (Jegla

---

[1] *Shaker*, a *Drosophila* gene, codes for a homolog of mammalian $K_V1.2$ and is a homotetramer of 6TM helix subunits (see **Figure 1.1**)

et al., 2009); humans have twice those of a barnacle, but about 50% less than a puffer fish. In fact, most of the unique channel classes found in Mammalia are also found in most Cnidarian genomes, and there has been little 'innovation' to the basic subunit archetypes in the time since the divergence of cnidarians from bilateral metazoans. Presumably, this 'core set' represents a functionally non-redundant set of channel types required for basic functioning in modern metazoan life forms, while the gene diversification *within* channel families was a result of tissue-specific requirements arising from higher life form complexity (Piontkivska and Hughes, 2003; Jegla et al., 2009).

The nomenclature of voltage-gated channels has been a subject of much revision since their very discovery. Before the advent of molecular cloning techniques and amino acid sequence analysis, different channel types could only be distinguished by their functional or physiological characteristics, e.g. current properties and sometimes tissue distribution. The broad distinction between the different groups of calcium channels (high-voltage-activated and low-voltage activated) as well as the different current types (L, N, P/Q, R and T type) still gets plenty of use today. However, individual channel genes are typically referred to by one of the more common nomenclature types that aim to distinguish each unique isoform. The International Union of Basic and Clinical Pharmacology (IUPHAR, http://www.iuphar-db.org/index_ic.jsp) uses an intuitive naming convention, using selectivity and gating mechanism as identifiers, e.g. Kv for voltage-gated potassium channel. On the other hand, the Human Genome Organization (HUGO) Gene Nomenclature Committee (www.genenames.org) uses gene names and numbers approximately correlating to the order of discovery or localization (e.g. CACNA1S for the skeletal muscle $Ca_V1.1$). There is yet a third system for voltage gated calcium channels that identifies the pore-forming subunits ($\alpha 1$) approximately identified by their HUGO named

counterparts (e.g. α1s for CACNA1S). To reduce confusion and because most channel

researchers use the IUPHAR system, this method will be predominantly used. A synopsis of

channel and current nomenclature is available in Table 1.1

Table 1.1: Nomenclature, current classification and tissue distribution of voltage-gated calcium channels.
Adapted from (Kang and Campbell, 2003)

Gene	IUPHAR designation	Primary tissues	Current type
CACNA1S	$Ca_V1.1$	Skeletal muscle	L-type
CACNA1C	$Ca_V1.2$	Heart, smooth muscle, brain, adrenal, pituitary	
CACNA1D	$Ca_V1.3$	Brain, pancreas, kidney, ovary, cochlea	
CACNA1F	$Ca_V1.4$	Retina	
CACNA1A	$Ca_V2.1$	Brain, cochlea, pituitary	P/Q type
CACNA1B	$Ca_V2.2$	Brain, nervous system	N-type
CACNA1E	$Ca_V2.3$	Brain, cochlea, retina, heart, pituitary	R-type
CACNA1G	$Ca_V3.1$	Brain, nervous system	T-type
CACNA1H	$Ca_V3.2$	Brain, heart, kidney, liver	
CACNA1I	$Ca_V3.3$	Brain	

1.3 Voltage-gated calcium channels: History and Background

Despite their ubiquity and key roles in many physiological processes, voltage-gated calcium channels (VGCCs) were slow to emerge to the forefront of electrophysiology research, probably due to the much higher abundance and availability of Na^+ and K^+ channels, as well as a much smaller concentrations of calcium in both the cytoplasm and extracellular space (relative to Na^+ and K^+). Their discovery was largely an accident, and came amidst a bustling new field that was still in its infancy. It took nearly two decades from the original paper by Fatt and Katz in 1953 for the scientific world to accept Ca^{2+} channels as a rule rather than exception (Zamponi, 2005). Further studies revealed their pivotal role in neurotransmission, in addition to the previously described cardiac contraction and excitation-contraction coupling – soon after which VGCCs were at the forefront of neuroscience research. The channels were initially considered to be the same across all vertebrate species as well as tissues, but this soon proved to be inaccurate. They were later classified as either high-voltage-activated (HVA) or low-voltage-activated (LVA), first described as "type I and II" respectively by Hagiwara and colleagues while working with starfish eggs (Hagiwara et al., 1975). The evidence was entirely based on electrophysiological recordings; very little biochemistry had been done at the time to give a molecular basis to this distinction. HVA channels were distinguished by the much higher voltage step required for activation, speed of inactivation (faster than LVAs), resistance to 'run-down' or loss of activity following patch excision or dialysis of cytosol (LVAs are more resistant than HVAs) and sensitivity to cadmium (LVAs are more resistant). The L-type channels (HVA) were so named because of their *l*arge and *l*ong-lasting unitary conductance to Ba^{2+} (which was used as a charge carrier to avoid rapid inactivation associated with Ca^{2+} -- a very distinct property of several VGCCs discussed in a later section). The T-type (LVA) channels were named after their *t*iny

conductance to Ba^{2+} and had a *t*ransient average current with a characteristically slow deactivation following sudden repolarization; both T- and L-type were found in heart tissue. The third, new, category was essentially a designation for channels that did not exhibit typical L- or T-type properties and was primarily confined to *n*eurons and had i*n*termediate Ba^{2+} currents but required high voltage for activation and were thus *n*either L- nor T-type. It was thus aptly named N-type. The difficulty with the distinction was palpable due to the coexistence of various channel types in same cell and tissue types and furthermore a lack of any biochemical way of confirming a particular channel type. Nonetheless, research continued, aided by the discovery of compound families capable of modulating channel activity. Nowycky and colleagues showed that L-type channels are selectively affected by Bay K8644[2], which belongs to the dihydropyridine class of drugs; these can act as either agonists or antagonists, depending on the particular activation state of the channel in which they bind most strongly (Sanguinetti et al., 1986). Furthermore, work with various paralytic toxins from cone snails and funnel web spiders led to the discovery of very specific peptide blockers of individual channel types, a pharmacological breakthrough that also greatly simplified the identification and isolation of VGCCs long prior to their eventual cloning and biochemical characterization. As a result of this work, new channel types were identified that had different pharmacological properties from any of the previously described types according to the tripartite model (N, L, T) – these were primarily isolated because of their resistance to drugs known to inhibit the known channels, not for unique electrophysiological characteristics. These were named P-type (found in *P*urkinje cells), Q-type (granular cells) and eventually R-type (for *r*esistant; these currents remained even at saturating concentrations of all known blockers). Subsequent success with molecular cloning of the pore-forming α1 subunits of the channels

---

[2] Bay K8644, a structural analog of nifedipine, is both an agonist as an R-isomer (-), and an antagonist as a S-isomer (+).

revealed that P and Q type were different splice isoforms of the same gene product; additionally the actual subunit composition and interacting proteins (which differ for the P and Q channels) were found to greatly influence the electrophysiology of the complete channel structures (Zamponi, 2005). First to be cloned were the skeletal muscle L-type channels, likely due to their ready availability and abundance, using high-affinity binding antagonists. The SDS PAGE revealed 4 distinct bands that co-migrate when the purified channels were separated; these were identified as the major channel subunits: $\alpha 1$, $\alpha 2\delta$, β, and γ. Similar work was performed with cardiac L-type and brain N-type channels with similar results; however, no γ subunits were found with the latter two. The $\alpha 1$ subunits are highly homologous and have a significant degree of amino acid similarity to the pore-forming subunits in Na_V and K_V channels; it was correctly hypothesized that they constitute the main pore-forming subunit and voltage sensor of the channel (Catterall, 2000, 2011). An $\alpha 1$ subunit consists of four very similar domains (I-IV), each containing 6 transmembrane helices (S1-S6). The S4 segment contains positive residues in every third or fourth position (all facing in the same way) which allows it to respond to voltage changes and act as the gating sensor (described in more detail in a later section). The re-entrant P-loop between the S5 and S6 of each domain is believed to form the actual channel pore through which ions pass. Since the first $\alpha 1$ subunit was identified in skeletal muscle ($\alpha 1_S$), 9 others have been cloned, and eventually each has been assigned to one of the different described current types (e.g. L type, N type etc.) (Zamponi, 2005). The $\alpha 1$ subunit is sufficient to produce functional channels through heterologous expression but such channels exhibit low surface expression and abnormal gating kinetics (Perez-Reyes et al., 1989), which can be alleviated to a high degree by co-expression of the $\alpha 2\delta$ and especially the β subunits (see Section 1.3.1). Through a number of biochemistry techniques, it was shown that the β subunit is intracellular

and has no transmembrane domains, while the γ subunit is a transmembrane glycoprotein. The α2 subunit was thought to be another large anchored glycoprotein but was found to have no transmembrane domains; it is actually held in place by its interaction with the δ subunit through the latter's short C-terminal transmembrane region (Robinson et al., 2011; Dolphin, 2013). The α2 and δ subunits are products of one gene that is post-translationally cleaved and held together by a disulfide bond (Catterall, 2011). However, there are a number of different β and α2δ subunits, and each seem to confer slightly different kinetic properties when co-expressed with a given α1 subunit, with the β subunits causing the greatest variety of effects (Walker et al., 1998). More details regarding subunits and their properties can be found below.

1.3.1 Auxiliary Subunits

T-type channels are monomeric (contain only the α1 subunit), while all other Ca_Vs contain auxiliary subunits that modulate the currents of the pore-forming subunit with which they associate, or its expression. The functional effects of their interactions have been mostly characterized, but the mechanisms by which the regulation occurs are still not fully understood. Below is a brief overview of the three major subunit classes found in association with α1.

1.3.1.1 α2δ

HVA Ca_Vs are typically composed of four subunits, α1 (pore-forming), β, γ and α2δ. The latter was initially believed to be a tight association of two different subunits but was later determined to be a single post-translationally cleaved gene product. The two resulting polypeptide chains remain linked by a disulfide bond. Of these, the C-terminal end of the δ fragment contains a single transmembrane motif which anchors the entire subunit, while the larger N-terminal product (α2) is wholly extracellular. Both δ and α2 are heavily glycosylated. Interestingly, the post-translational cleavage of α2δ is often incomplete in heterologous systems; only about 30% of the gene-product is found in the processed form when expressed alone (Davies et al., 2006). Very little is currently known about the mechanism or the role of this processing on the subunit function, and the cleavage link sequence is not very well conserved among the isoforms. Mutagenesis studies place the location of the cleavage recognition sequence between R941 and V946 and show reduced whole cell currents of the heterologously co-expressed α1 subunits for unprocessed mutants, suggesting reduced surface trafficking (Andrade et al., 2007).

There are currently 4 known vertebrate isoforms of α2δ, and there are also a number of splice variants of each of these. The isoforms are fairly well conserved (≥30% identity) and

structurally similar (Davies et al., 2007). The different isoforms can be reconstituted with a

variety of α1 isoforms *in vitro* (heterologous expression) but are most likely less promiscuous *in

vivo*. All α2δ subunits enhance Ca^{2+} currents through their associated α1 subunits, but the

mechanism is still uncertain (Davies et al., 2007; Dickman et al., 2008). However, it seems that

an associated α2δ is not always required for functional expression of α1 (at least in heterologous

systems) (Davies et al., 2006). There appears also to be a pool of α1's that are not associated

with α2δ and so there could potentially exist an on/off equilibrium between the two states of α1,

which in itself could represent a regulatory mechanism for specific channel kinetics (Obermair et

al., 2008). Furthermore, glycosylation of consensus asparagines (N136 and N184) in α2δ is

required for its current enhancing effects on α1, but has no effect on the channel

gating/activation properties, as shown by mutagenesis studies (Sandoval et al., 2004).

1.3.1.2 γ

Gamma subunits were a late addition to the accepted VGCC archetype because for some time it

was believed that their expression was required for proper channel function only in muscle but

not neuronal tissue, and was thought to be a tissue-specific isoform requirement. However, it was

subsequently shown that a second, neuronal isoform γ2 has a fairly severe "*stargazer*" phenotype

in mice, characterized by uneven gait and random head elevations (Letts et al., 1998; Letts,

2005). Subsequently, γ subunit mutations resulting in ataxia and epilepsy have fuelled scientific

interest and 6 more isoforms have been identified by sequence alignment and cloned (Kang and

Campbell, 2003). In addition, this very finding (the *stargazer* or *stg* mouse) brought the merely

accessory role of the auxiliary VGCC subunits into question, particularly with respect to γ2.

Surprisingly, the *stg* mice did not have any functional AMPA receptors on the post-synaptic

membranes of cerebellar granule cells, a defect that was specifically attributed to the absence of

γ2 (Hashimoto et al., 1999). AMPA, or α-amino-3-hydroxy-5-methyl-4-isoxazolepropionic acid, is an artificial glutamate analog; its ionotropic receptor mediates fast synaptic transmission in the CNS (DiGregorio et al., 2002). Later, co-immunoprecipitation studies confirmed 'stargazin'(γ2) binding to AMPARs, and knock-in experiments showed restoration of full AMPA glutamate signaling with re-introduced γ2 (Chen et al., 2000). If or how these effects pertain to Ca_V regulation is unclear.

The biochemical aspects of γ subunits are not fully elaborated, which is in part due to lack of a crystal structure (typical roadblock for membrane proteins). Tissue expression profiles are known, but the specific combinations of γ and α1 subunits that occur *in vivo* are only known for a few isoforms. Electrophysiology studies have produced contradictory results; however most current research literature indicates that γ subunits in general act to inhibit channel activity by hyperpolarizing the inactivation curve[3] and in some cases lowering the current densities (Kang and Campbell, 2003). More biochemistry studies are required to elucidate the mechanisms by which these effects take place.

---

[3] In this dissertation and most neuroscience literature, 'hyperpolarization of a curve' is set to mean that it is shifted to more negative potentials, e.g. requires a lower membrane potential for a particular effect. Conversely, a depolarized curve is one that is shifted to the right, to more positive membrane potentials.

1.3.1.3 β

Perhaps the second best studied (after the α1 subunit), due to its vast number of regulatory effects, is the β subunit. It is also fairly small (~50kDa, varies with isoform) and completely cytosolic, and thus soluble, which has facilitated its (partial) structural determination– something that has not been achieved for other subunits, as of yet. Nonetheless, even with the amount of biophysical information available, many functional and mechanistic details of how β subunits regulate α1 subunits remain open to debate.

The first β subunit, much like its α1 counterpart, was cloned from human skeletal muscle ($Ca_V1.1$), and subsequently called β1a (Dolphin, 2003b). The β subunit family of VGCCs is highly diverse; while there are only 4 known genes (β1-4), their typical genomic structure is comprised of 13 exons and several of those can be alternatively spliced, giving rise to a large combinatorial potential (Dolphin, 2003a, 2009; Richards et al., 2004). The sequence alignments suggest a shared 5-domain structure (D1-5 or also A-E), with the second and fourth domains being highly conserved among the 4 β genes and the other three quite variable (Hidalgo and Neely, 2007). Homology modeling analysis places the β subunits into the family of membrane-associated guanylate kinase proteins (MAGUKs), which are scaffolding proteins for various signaling complexes and contain multiple protein interaction domains (He et al., 2007). The two conserved domains in β are thought to mediate these interactions; a Src-homology 3 domain (SH3, binds proline-rich sequences) "B", and the putative guanylate kinase domain "D". Despite the name and proposed relationship to *bona fide* GKs, β subunits themselves do not appear to possess kinase activity, presumably because their ATP-binding domain residues are not sufficiently conserved (Dolphin, 2003a, 2003b). The GK domain also contains the consensus "β interaction domain" (BID), which is the region initially believed responsible for the β subunit

16

binding to α1 subunits at their "α1 interaction domain" (AID), located in the linker loop between transmembrane domains I and II of the α1 subunit. A few studies claim absolute requirement of BID for functional regulation of VGCC by the β subunits and that it is often obligatory for proper (heterologous) channel expression (Dolphin, 2009). However, structural studies of three β subunits alone and in complex with an AID point to there being a lack of accessibility of the BID region for binding and suggest that the AID binding occurs through a hydrophobic pocket formed by a distal region of the β subunit nucleotide kinase domain – see Figure 1.2 (Chen et al., 2004; Opatowsky et al., 2004; Van Petegem et al., 2005). The authors suggest that the previously observed BID effects are more likely due to the disruption of proper β-subunit folding and/or function, rather than its interaction with the α1 subunit. One study examined several BID-independent properties of α1-β binding, where two new "short" splice variants of β2 lacking the BID were described. These variants lack the BID and parts of SH3 and GK domains, yet they apparently bind and facilitate functional expression of α1c ($Ca_V1.2$) subunits, and to some extent modulate their biophysical properties (Harry et al., 2004). An interesting observation that raises additional questions from a study by Harry *et al* was that the lack of the 'core' B and D domains in the "ultra-short" β2 manifested as a complete loss of calcium-dependent inactivation (CDI) of $Ca_V1.2$ (Harry et al., 2004).
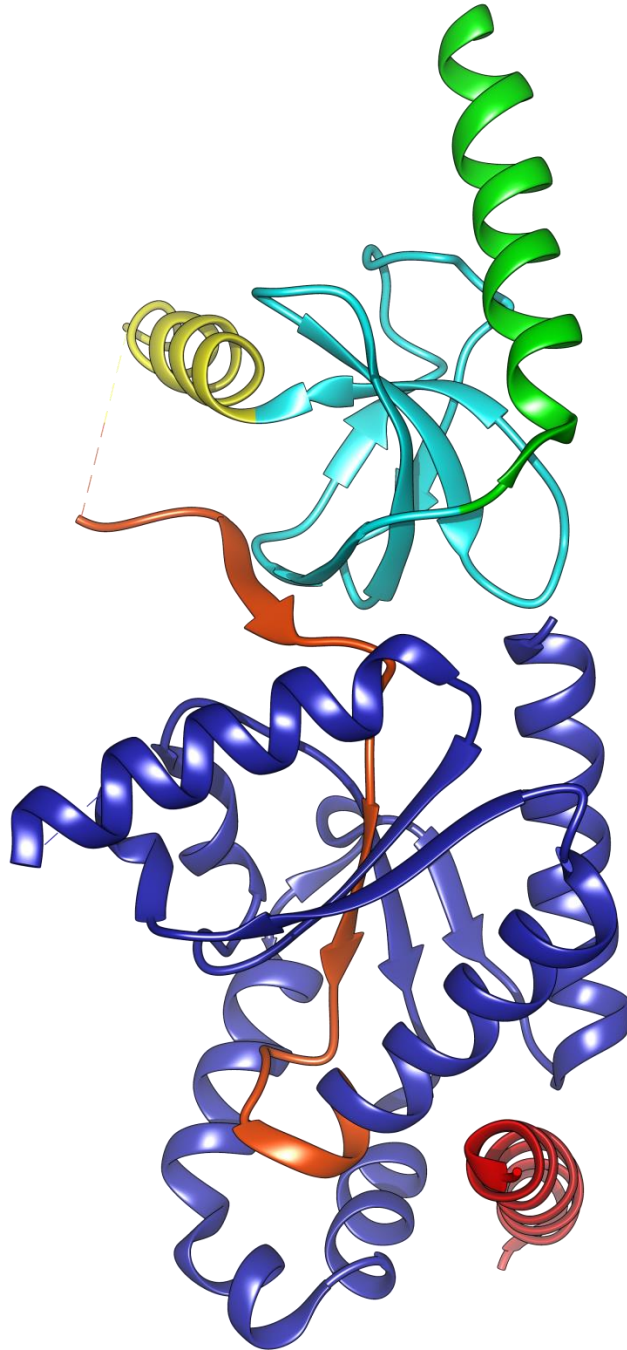
Figure 1.2: Crystal structure of β₃ subunit bound to the AID of Ca_V1.2
 The AID (residues 442-446) peptide is in red, with the view facing its N-terminus. Yellow is the HOOK domain, cyan is the SH3 domain, and blue is the guanylate kinase domain of the β3. The previously implicated "B-interaction domain" or BID is in orange; as can be seen here it is not accessible to the AID region as originally thought. The figure was generated in UCSF Chimera 1.8.1 using the PDB entry 1VYT (Chen et al., 2004)

The mechanism by which β subunits modulate their associated α1 currents remains unclear; however, a number of studies suggest distinct roles for the chaperone effect associated with increased channel trafficking to the plasma membrane (Bichet et al., 2000), and the direct hyperpolarizing effect on channel activation and inactivation (Dolphin, 2003b). This likely pertains directly to the modular nature of the β subunit domains as well as the variety of the different possible isoform combinations of β and α1 subunits. An interesting attempt to answer these questions was made by Arias et al., who created chimeras of T-type channels with regions of the I-II linker of $Ca_V2.2$ (N-type or α1B). They conclude that IS6 (the sixth and last TM repeat in domain I) is important in the interaction with the β subunit, and given its prominent role in channel gating, propose a universal model by which channel regulation is achieved by the β subunits (Arias et al., 2005). Unfortunately, only a handful of different β isoforms were used in the study (and only the IS6 region from N-type channels); so the true universality of this model is uncertain.

1.3.1.4 α1

It is necessary to also describe the molecular and biochemical details of the actual channel pore if one is to talk about its regulation. The pore-forming subunit of VGCCs (α1) is undoubtedly the best studied; however it is also the most difficult to characterize biochemically because of its great size and hydrophobicity. Nonetheless, with the advent of electron microscopy and various labeling techniques it has been possible to determine a number of key features responsible for the function of this subunit and the channel as a whole.

Since a crystal structure of a whole calcium channel is not currently available, all of the existing information here comes from either electron microscopy or, more commonly, homology modeling with other voltage gated channels (usually prokaryotic). Although the sequences

between the different channel groups are quite distinct, similar principles of gating and selectivity appear to govern all members of the 6TM family of channels. There are gross differences in the interdomain cytoplasmic regions, often even among different isoforms of the same channel gene, likely owing to their specific physiological roles and relevant regulatory mechanisms. Yet, the process by which the channels sense voltage changes, open, and pass ions through, despite individual channel adaptations, is similar for all of them. The actual pore of a channel contains three separate regions: the selectivity filter, followed by a water-filled cavity, which extends into a narrow gate region. The selectivity filter and gate are of primary interest, and each has a key role in channel conductance, described below.

1.4 Selectivity

How is it that a Na^+ channel does not allow the passage of identically charged K^+ ions and vice versa? If one uses ionic size as the only criterion, it only explains one and not the other. Furthermore, a hydrated Na^+ is larger than a hydrated K^+ while the reverse is true for the exposed ions. For a long time, this question has remained unanswered. It has recently been solved with the help of the KcsA crystal structure and molecular dynamics software. KcsA is a pH-gated potassium channel ("K^+ crystallographically-sited activation channel") from *Streptomyces lividans* (Doyle, 1998; Li et al., 1998), and has been used extensively as a template for modeling other voltage-gated ion channels (Sansom et al., 2002).

The selectivity filter of KcsA is characterized by 5 ultra-conserved residues[4], TVGYG (Lu et al., 2001). Interestingly, it is their backbone and not the side chains that form hydrogen bonds with the incoming ions (**Figure 1.4**) – a situation which is reversed in the four-homology

---

[4] The selectivity filter residues are usually highly conserved within channel groups. Thus nearly all voltage-gated potassium channels share the 'TVGYG' sequence, Na_Vs have DEKA, Ca_Vs have either EEEE (HVA) or EEDD (LVA).

domain channels like Na_Vs and Ca_Vs. In nearly all cases, however, the actual opening through which an ion must pass is smaller than the hydrated ionic radius of the cognate ion. This means that the ion must lose its hydration shell in order to pass through, which requires energy (but gains in entropy) (Corry et al., 2001). The energy is recovered when the ion makes bonds with the selectivity filter ligands, the residues in which are spaced precisely so as to maximize the favorability of this transfer (Lipkind and Fozzard, 2001, 2008). Hence a Na^+ is too small when dehydrated to fully compensate for the energy it loses when dehydrating, to pass through a K^+ channel. It also explains why Cd^{2+} (cadmium), which is of a very similar ionic size (both hydrated and not) to Ca^{2+}, is highly toxic and will block VGCCs. It also means that small neutral molecules (e.g. urea, glycerol, formamide, etc) can pass through pores larger than their radii (Huang et al., 1978). Interestingly, anion channels typically select for larger ions, but are generally far less selective than cation channels (Kunzelmann et al., 1991; Hille, 2001; Gillespie et al., 2002), likely because there are no other small anions to contend with, other than Cl_- and HCO_3^-.

There is also a question of how the ion actually travels down the channel pore. Various crystallography studies and modeling showed two possible conformations for the pore; one in which there were two ions in the filter and the other in which there were three, in exactly the opposite locations, sandwiched between water molecules (Sansom et al., 2002). This suggested that a 'knock-on' process was responsible, e.g. electrostatic repulsion of newly entering ions propelled the already present ions further into the channel (into the cavity), aided by the concentration gradient inward. This model requires that there be ions of the selected type already present in the channel for it to function; indeed, when a Ca^{2+} channel is reconstituted in a membrane without Ca^{2+} present in the environment, it will allow the passage of Na^+ ions (which

are of a remotely comparable size) as well as small organic molecules but will not pass them if there is any Ca^{2+} present. There are some channels which are less selective than others; likely this has to do with the flexibility as well as the spacing of the ion coordinating residues and their side chains, as well as surrounding residues. Presumably, when a divalent ion is not present to offset the electrostatic repulsion between the coordinating glutamate carboxyl groups, they face away from the pore and the channel becomes more 'open' and thus more permeable (Lipkind and Fozzard, 2001). The model presented by Lipkind and Fozzard has a conical outer vestibule about 18Å tall that tapers from around 20Å at its widest down to sub 6Å within the glutamate 'circle' of the selectivity filter formed by the P-loops (re-entrant helix/loop/helix motif in between S5 and 6 segments of each domain), in which all four glutamates are perfectly positioned to interact with a single Ca^{2+} ion.

The selectivity filter sequence in (most) VGCCs is EEEE, one conserved glutamate from each of the four domains, e.g. E393, 736, 1145 and 1446 in rabbit $Ca_V1.2$. In Na_Vs it is DEKA, and substituting one for the other is usually sufficient to convert one channel selectivity into the other (Lipkind and Fozzard, 2001). Ryanodine receptors, which are specialized Ca^{2+} channels in the sarcoplasmic reticulum, have DDDD (Gillespie et al., 2005). The actual side chains form hydrogen bonds with the cations, in contrast to what is seen with KcsA and K_V channels. Intriguingly, extant bacterial sodium channels (NaChBac) that share ancestral homology with the major voltage-gated ion channel families (K_V, Na_V and Ca_V) have a domain architecture reminiscent of K_Vs (four-homology domain, e.g. homo-tetramers) yet their selectivity filter sequence (EEEE) is closer to Ca_Vs. Molecular dynamics and energy calculations for single residue mutants in this region of NaChBac suggest that the size of the pore and thus, the number of indirect metal ion-water-carboxyl contacts, determines the relative selectivity of a pore

between Na^+ and Ca^{2+} (Dudev and Lim, 2012). Essentially the pore length, charge distribution and volume are all commensurate with the channel's permeability to a monovalent vs. a divalent ion (Malasics et al., 2009). In contrast, the cause of discrimination of a channel among different size monovalent ions is less clear. For instance, KcsA and similar K_V channels require a K^+ ion for structural stabilization of their selectivity filters, and removal of K^+ entirely results in pore collapse, converting the channel into a non-conductive, inactivated state ("C-inactivation" similar to that seen at low pH) (Bhate and McDermott, 2012). NaChBac is permeable to both Na^+ and K^+ and has a selectivity filter containing TVGDG/A instead of the consensus TVGYG of KcsA. It also does not require ionic 'support' to maintain its pore in a conductive state (Shi et al., 2006). Presumably, the difference in Na^+/K^+ selectivity is due to geometric, rather than electrostatic constraints in the amino acid stacking surrounding the ion binding site (Malasics et al., 2009).

This thermodynamic/electrostatic explanation has held true to a large extent: consider that if a channel is bathed in a mixed solution of all possible monovalent ions (Li^+, K^+, Na^+, Rb^+, Cs^+) in equimolar amounts, 120 possible orders of preferential selectivity are possible. Of those, only 11 have been found in nature (the so-called 'Eisenman sequences'), with the most common being the straight forward size prohibition series ($Li^+ > K^+ > Na^+ > Rb^+ > Cs^+$) (Krauss et al., 2011). This model, along with the currently accepted 'textbook' explanation of channels' ion selectivity (Hille, 2001), is based on a barrier model, where individual ions get passed along from site to site within the selectivity filter, similar to the free energy wells of the transition states in a reaction profile. A similar approach is taken by most molecular dynamics simulations where the number of modeled particles is limited and can be predicted with some accuracy. There are issues with this model, however, as it does not take into account the frictional forces

associated with ion-ion and ion-fluid interactions while passing through a narrow pore (Gillespie and Boda, 2008). Additionally, a more recent crystal structure of a bacterial sodium channel Na_VAb (from *Arcobacter butzleri*) in its closed state shows that it passes Na^+ ions in at least a semi-hydrated state. In fact, the entire KcsA selectivity filter could fit inside that of Na_VAb (Payandeh et al., 2011). The selectivity filter of Na_VAb contains a narrow, negatively charged opening at the top of the pore, thus making an inverted funnel shape, with the narrowest point being extracellular – in contrast to the 'right side up' funnel shape seen in KcsA and most other voltage gated channels. The rest of the vestibule is larger and accommodates a Na^+ ion with its primary hydration shell, and presents a hydrophobic surface over which the ions disperse rapidly, thus accounting for the high conductance of these channels. A very recent review suggests there is a high level of correlation between the structural features of Na_VAb and what is known about the gating kinetics of vertebrate Na_Vs (Catterall, 2014). Much of the future advancement in this field rests on the availability of structural data from a vertebrate four-domain channel.

Some channels that can pass more than one ion type display a behavior called the 'anomalous mole fraction effect' or AMFE, which occurs when the conductance of the channel changes non-linearly with the relative concentration of that ion in the bath while the total ionic strength of the bath is kept constant (Friel and Tsien, 1989; Nonner et al., 1998; Gillespie and Boda, 2008). Previously, the consensus explanation for this effect was related to the multi-ion occupancy model of the selectivity filter as in the KcsA channel (Hille, 2001); the AMFE was supposed to reflect the varying relative binding affinity of the several ion binding sites. In this regard, having an AMFE for a channel would be synonymous to having a multi-ion pore. However, several discrepancies have since shown this assumption to be false. Firstly, all mutagenesis studies point to Ca_Vs as having a single high-affinity Ca^{2+} site (the coordinating

24

glutamates) rather than the single-file multi-ion pore seen in potassium channels, or any multi-pore or multi ion combination (Corry et al., 2001; Hille, 2001; Lipkind and Fozzard, 2001; Zamponi, 2005; Gillespie and Boda, 2008; Malasics et al., 2009; Dudev and Lim, 2012; Park et al., 2013). Furthermore, an AMFE can be observed in simple 50Å plastic nanopores in mixed solutions, evidently without the requirement of multiple ion binding sites, ion interaction/hydration or single file permeation (Gillespie et al., 2008). The latter finding essentially invalidates everything previously generalized for all channels about the nature of AMFE and permeation. Mathematical models of bulk ion movement in fluids have been applied to this problem, with a modified Poisson-Nernst-Planck (PNP) equation being successfully used to predict the AMFE in both an artificial oligopeptide channel (Chen et al., 1997) and more complex systems such as the ryanodine receptor RyR (Gillespie et al., 2005; Gillespie and Boda, 2008). Essentially, the model treats the channel as a series of resistors formed by depletion zones resulting from electrostatic effects of localized ion binding at the different affinity sites inside the pore. This model does not call for ion single file passage through the pore (and thus accurately predicts the AMFE in nanopores), but obviously requires some knowledge of the pore interior for accurate predictions – and in many cases extensive mathematical modeling.

Calcium channels vary in their permeability; however, all HVA Ca_Vs are largely impermeable to Na^+ in the presence of at least 1µM Ca^{2+}, but are quite permeable to Na^+ in the absence of Ca^{2+}, and are typically at least twice as permeable to Ba^{2+} as to Ca^{2+} (Hille, 2001; Zamponi, 2005). They are not permeable to any particles larger than tetramethylammonium (TMA), but can pass ions smaller than it, in a selectivity sequence of $Ca^{2+} > Ba^{2+} > Li^+ > Na^+ > K^+ > Cs^+$. LVA or T-type channels (Ca_V3.x) have a different selectivity filter sequence (EEDD),

and have different permeability/selectivity ratios in their various isoforms (Perez-Reyes, 2003; Talavera et al., 2003; Shcheglovitov and Shuba, 2006; Park et al., 2013).

1.5 Voltage Sensing and Gating

Gating is the process of opening (activation) of the channel in response to a specific stimulus, and is tightly linked to inactivation. Thus, gating is an even more complex subject than selectivity due to the great deal of controversy regarding the molecular mechanisms involved.

Most voltage-gated channels have similar topology, in which the first four helices of their basic domain unit constitute a voltage sensing domain, with the fourth helix (S4) of every domain serving as the main voltage sensor. Sequence alignments show that the S4 transmembrane helix in all voltage-gated cation channels is structured so that about every third residue is positively charged, creating a molecular 'strip' of positive charge along one face of the helix. The importance of these positive charges, and surprisingly some of the neutral residues around them, was pointed out in a number of different mutagenesis studies (see Hille 2001, Tombola et al. 2006, Bezanilla 2006, and the references therein). Interestingly, not all mutations had a similar effect: some are hyperpolarizing, while the rest are depolarizing[5]. A change in membrane potential (e.g. depolarization), causes a corkscrew-like movement in S4, resulting in translocation of charged residues across portions of the membrane – a recordable phenomenon known as 'gating current' (Peterson et al., 1999; Hille, 2001; Doyle, 2004; Bezanilla, 2005, 2006; Zamponi, 2005; Chanda et al., 2005; Long et al., 2005; Tombola et al., 2006; Elinder et al., 2007; Catterall, 2011). Initially, gating mechanisms were modeled based on the structures of bacterial and archaeal channels, namely KcsA, MthK and KvAP (from *Streptomyces lividans*,

---

[5] One would expect that removing the positive 'sensor' charges from S4 would reduce the open probability (Po) due to reduced voltage sensing and cooperativity; however it appears that some changes actually *increase* Po by lowering the threshold potential (hyperpolarizing the current-voltage curve).

Methanobacterium thermoautotrophicum, and *Aeropyrum pernix*, respectively) (Tombola et al., 2006), although their structural similarity to eukaryotic channels is modest. There is a dearth of structural data for 4-domain channels (e.g. Na_V and Ca_V), and eukaryotic channels in particular. The most commonly used structure for homology modeling is the $K_V1.2$ channel (Chen et al., 2010), which, like other K_V channels, has a single domain architecture and forms a tetramer.

Whereas mutagenesis and modeling studies involving the known structures of single TM domain channels (e.g. various potassium channels) affect each of the four monomers identically, the same cannot be said of the S4 segments in each domain of the 4-TM domain channels (e.g. Na_V, Ca_V). Several mutagenesis studies in sodium channels point to the S4 of domain IV (DIV-S4) as being the slowest to respond to depolarization, and thus rate-limiting for activation, and suggest a degree of cooperativity between the S4 helices of the four domains. This might explain the fast kinetics of the sodium channel, a necessary feature of action potential propagation (Bezanilla, 2006).

Voltage sensing is fairly well understood: the change in membrane potential results in gating currents caused by rearrangement of the sensor charges in response to the electric field disturbance. The molecular details of how this movement occurs, and more importantly, how it is transduced into the gating region to actually open the channel, are less clear. Numerous kinetic models have been developed that treat the opening process as any biochemical reaction, with a number of energy lows and highs, with discrete equilibrium constants governing the probability of the channel occupying each state versus the membrane potential. These models are usually empirically derived, as very few structural models exist to confirm and correlate a particular kinetic step to a physical state of the channel. The larger the number of these elementary 'steps', the smaller the individual gating current associated with each 'step' should be. In contrast, early

work with sodium (Conti and Stühmer, 1989) and potassium (Mika and Palti, 1994) channels in patch clamp experiments suggests that the actual number of discrete gating states is low.

So how does the S4 helix actually move to open the channel? Several models have been developed, although most of the early ones (full translocation and moving orifice, and later the 'paddle' model) did not bear out with the growing body of evidence, with the notable exception of the helical screw model (Keynes and Elinder, 1999), which is still widely discussed today (Elinder et al., 2007; Broomand and Elinder, 2008; Nishizawa and Nishizawa, 2008; Catterall and Yarov-Yarovoy, 2010). The 'paddle' model was introduced using a crystal structure in which the S4-5 linker 'paddle' was immobilized using monoclonal antibodies in several configurations, which suggested there was a large transverse motion of this linker within the membrane (Jiang et al., 2003b). However, it has since been demonstrated that the antibody-bound conformation changes are distorted and not representative of native channel states. The helical screw model was proposed by studies using cysteine substitutions in S3 and S4 with subsequent monitoring of disulfide bridge formation during S4 motion (reviewed in Catterall and Yarov-Yarovoy, 2010), in which S4 rotates slightly about its axis in response to depolarization. Contrasting these results, various fluorescence studies that have quantitated the motion of the S4 helices report that the depolarization-associated movement (either radial or translational) is remarkably low (2-4Å), a finding that is hard to reconcile with even the most conservative predictions of a helical screw model (Chanda et al., 2005; Posson et al., 2005). In an attempt to reconcile all these findings, a modified model incorporating the 'rotation-in-place', 'moving orifice' and charge translocation has been suggested, called the 'transporter' model (Bezanilla, 2006; Tombola et al., 2006). Here the charges in S4 are in contact with two different aqueous reservoirs, a large interconnected internal crevice (in the closed state) and a shallower externally

connected one (in the open state). Depolarization presumably results in a rearrangement of the hydrogen bond network of S4 and these reservoirs. In a series of elegant studies by Bezanilla and his group, Arg-to-His substitutions in the gating-charge-carrying S4 residues converted the voltage sensing domain (VSD) of the Shaker potassium channel into a proton shuttle (Tombola et al., 2006), strongly supporting their 'transporter' model. This is another instance where a complete solution structure of the channel may go a long way in settling the debate, although it would be difficult to obtain structures of a channel in the resting state since neither NMR nor X-ray crystallography are amenable to maintaining an intact cell membrane at resting potential.

What constitutes the actual 'gate' of the pore and how does S4 cause it to open? Crystal structures of KcsA, MthK and KvaP present us with a general shape reminiscent of an 'inverted teepee' (Doyle, 1998; Jiang et al., 2002, 2003a), with an internal water filled cavity beneath the selectivity filter (**Figure 1.4**), followed by the 'gate' formed by the crossing of the S6 helices at the 'peak' of this teepee bundle (**Figure 1.5**). Experimental evidence shows that quarternary ammonium (QA) compounds used intracellularly block potassium currents, but can be 'trapped' in the aqueous cavity by a strong and rapid hyperpolarization (which closes the channel), locking it 'open' (Swartz, 2004a; Elinder et al., 2007). This led to the idea that a swiveling motion of the S6 helices about the 'tip' of the cone constitutes the opening process of the channel. Mutagenesis studies with various S6 residues changed to cysteines and subsequent probing by thiol-reactive agents (methanethiosulfonates or MTS as well as the silver ion Ag^+), in the open and closed states, largely supported this 'pivot' model. Additional crystal structures from MthK show a much larger opening in the 'gate' region than that of KcsA. KcsA was crystallized 'locked open' by an artificial Cys-Cd^{2+}-His bridge, which is impossible for the distance observed in MthK ($\approx$12Å). This indicates a higher degree of rotational movement at the

'hinge' region of the gate and a more 'bent' S6 in MthK. The 'hinge' region appears to be a conserved glycine residue in the S6 of prokaryotic channels, and either the glycine or a 'PVP' motif further down the S6 helix in Shaker and Kv channels (Swartz, 2004a; Long et al., 2005; Tombola et al., 2006; Elinder et al., 2007). Mutation of the second proline of this motif in *Shaker* (a *Drosophila* $K_V1.2$ homolog) uncouples it from its VSD, resulting in a constitutively active channel (Sukhareva et al., 2003). The distal end of S6 and the residues downstream of PVP appear to serve as a coupling site for the actual mechanical transduction of activation for the S4-5 linker and the VSD (Swartz, 2004a, 2004b; Long et al., 2005; Tombola et al., 2006; Elinder et al., 2007). The linker crosses over the 'bent' S6 from a neighboring subunit, making several contacts in Kv1.2 (Long et al., 2005); chimeric channels with mismatched S4-5 linkers and C-terminal S6 sequences (from different channels) show very little voltage regulation (Lu et al., 2001; Lu, 2002). Whether the mutations render the channel constitutively closed or open appears to depend on the resulting change in the angle at which the S6 helices converge, thus further supporting the idea of the C-terminal ends of S6 as being the functional 'gate'.
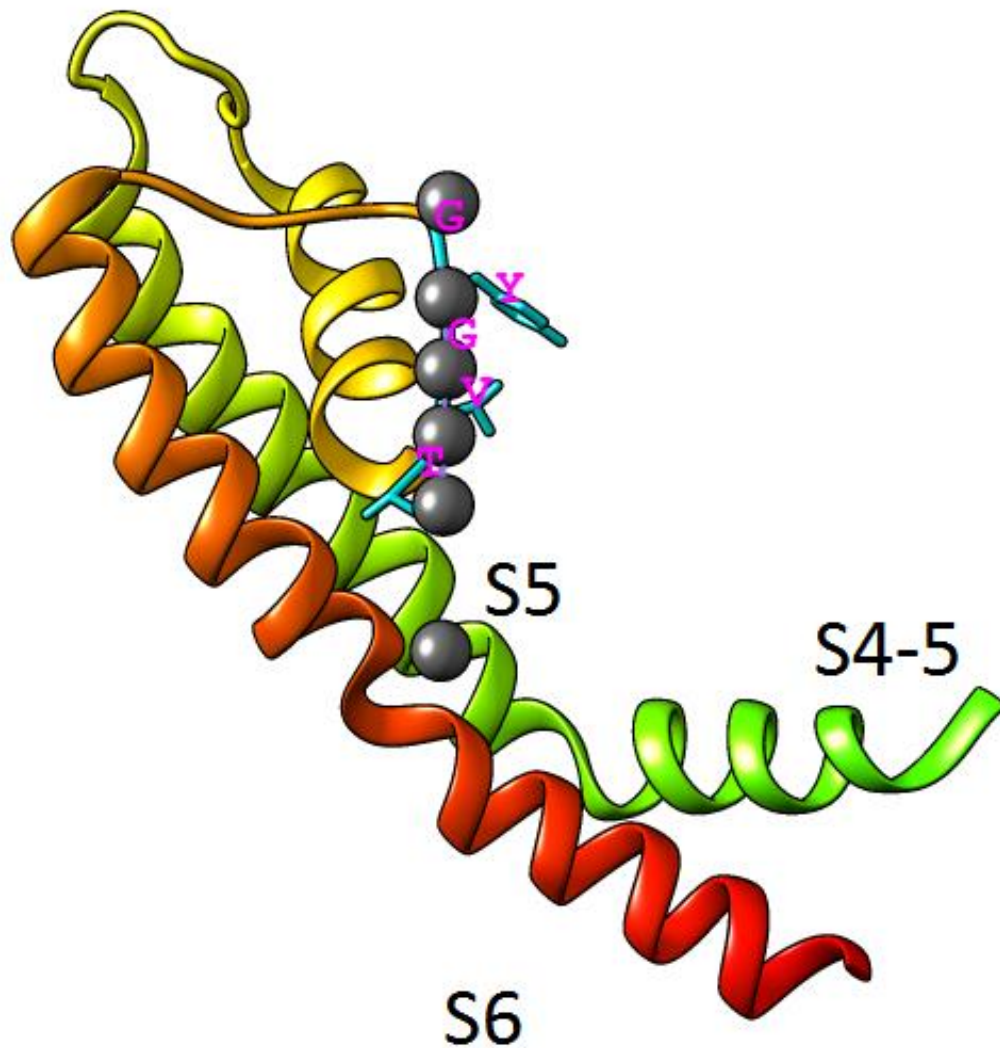
Figure 1.3: Structural depiction of the 'gate' region (one subunit) in K$_V$1.2.
Generated using Chimera (PDB ID#: 2A79) (Long et al., 2005)

The gating transduction pathway is not fully understood, but so far has been shown to involve the S4-5 linker, several contacts between the S4 and S5 helices themselves , as well as an isolated 'gating' motion of S4 that occurs as the final step in the sequence of 'opening steps' involved in gating charge motion (Tombola et al., 2006). This last 'gating' step carries little charge and can be isolated from actual voltage sensing in Shaker through conservative mutagenesis of several hydrophobic S4 residues (the "ILT" mutant V369I, I372L, S376T), and it

is this final motion of S4 that supposedly imparts cooperativity to the opening of the channel (Ledwell and Aldrich, 1999; Pathak et al., 2005). The extent to which we can extrapolate this information onto four homology domain channels like Na_V and Ca_V remains to be seen (Bezanilla, 2006). Lack of structural data for these larger channels has been a major roadblock in obtaining a functional model. Furthermore, there are additional layers of regulation imparted by the presence of auxiliary subunits (see section 1.3.1) and calcium-binding proteins such as calcium binding proteins (CaBP1-4) and calmodulin (CaM). The latter is nearly universal for all HVA channels (Peterson et al., 1999; DeMaria et al., 2001; Erickson et al., 2001), regardless of species, and is the main subject of the research covered by this dissertation. Thus, it follows that a brief introduction to this crucial protein is necessary, and can be found in the next section.
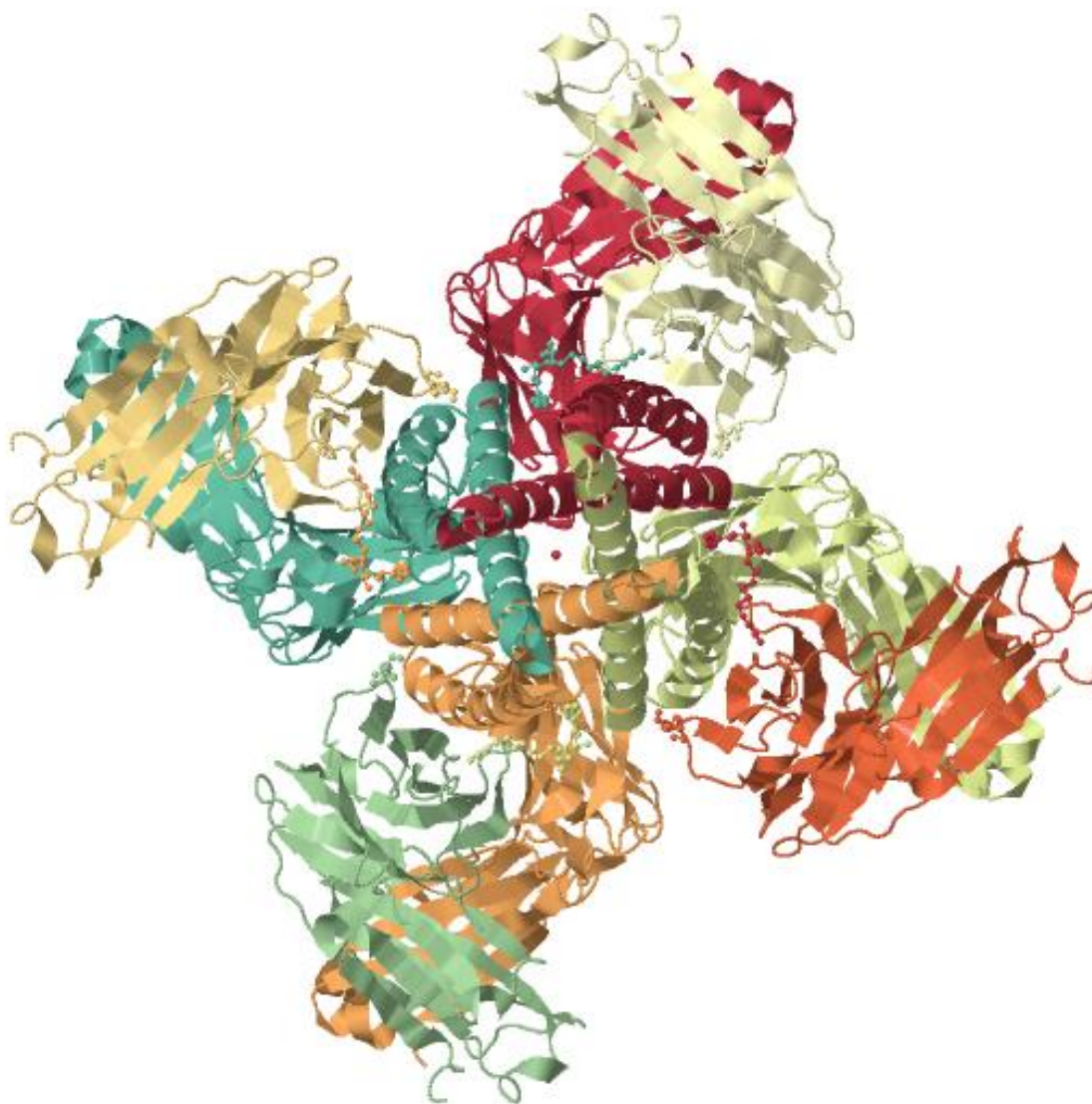
Figure 1.4: Ribbon-format structure of KcsA.
Transverse inverted view (e.g. looking into the bottom of the channel, where the S6 helices converge). Generated using Jmol viewer on the PDB web site (KcsA entry ID: 1K4C). The different chains are color coded. The pore-forming domain at the center is comprised of S5 and 6 helices from each subunit, while the pH-sensing/activation domains roughly corresponding to the VSDs of voltage-gated channels are positioned on the outside in an opposing manner – see also **Figure 1.1** for architectural diagrams.
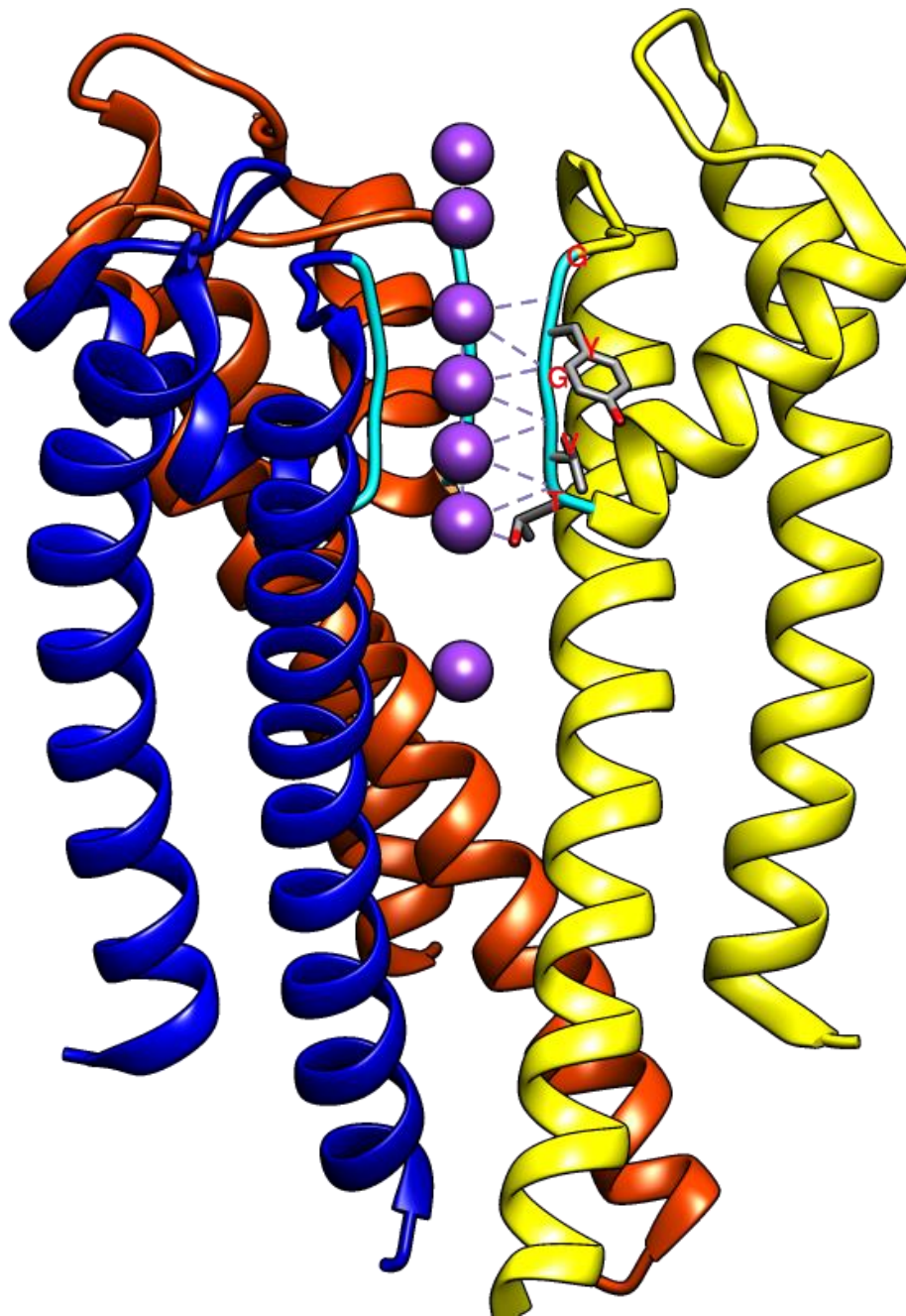
Figure 1.5: A 'dissected' view of KcsA pore-domain (S5-6).
Three of the four subunits shown for clarity (color coded). K$^+$ ions are purple. Selectivity filter (P-loop) sequence TVGYG is in cyan, only one is annotated for clarity. Generated using UCSF Chimera molecule modeling software (http://www.cgl.ucsf.edu/chimera/) and the PDB entry for KcsA (1K4C).

1.6 Calcium and Calmodulin

1.6.1 Calcium

Calcium, while being present at much lower concentrations in biological systems than either

potassium or sodium, has a much greater chemical gradient across the plasma membrane, by at

least three orders of magnitude[6](Simons, 1988; Hille, 2001; Tuckwell, 2012). It is very

ubiquitous in nature, being the fifth most common element in the lithosphere, and many of its

salts have low solubility. Ca^{2+} tends to cross-link macromolecules resulting in aggregation and

precipitation (Zhou et al., 2013), which is likely the reason why evolution has favored its

exclusion from the intracellular space and carefully maintained distribution and storage

(Berridge et al., 2000). Free internal calcium concentrations range anywhere from 20 to 200nM,

comparable to that of protons (Berridge et al., 2000; Hille, 2001). This is achieved by the

existence of several plasma membrane Ca^{2+}-ATPases and Na^+-Ca^{2+} exchangers, as well as Ca^{2+}

pumps in the mitochondria and endoplasmic reticulum (Clapham, 2012). Chemical interaction of

metal ions becomes more covalent across the periodic table, favoring interaction with less

electronegative ligands such as sulphur and nitrogen. Ca^{2+} and the metals in its group, in

contrast, are highly ionic in their character, favoring interaction with oxygen based ligands

(carbonyl, carboxyl, alcohols and ethers), a flexible coordination geometry (4-8) and fast binding

kinetics (Grabarek, 2005; Zamponi, 2005; Gifford et al., 2007; Zhou et al., 2013). This

combination of features makes it excellently suited for its role as a cellular messenger; indeed,

the number of regulatory pathways in which Ca^{2+} is involved is staggering (Berridge et al., 2000;

Clapham, 2012; Zhou et al., 2013). Of course, having a Ca^{2+} binding motif in every potential

---

[6] Exact numbers are cell-specific, but most never exceed 1μM free internal Ca^{2+} (Berridge et al., 2000), whereas plasma concentrations are usually around 1mM free Ca^{2+}, in contrast to the 140/10 and 20/100 mM (out/in) range of concentrations found for Na^+ and K^+

regulatory target protein would be physiologically costly (and redundant). Fortunately, nature's solution to this problem was the evolution of 'translator' proteins that bind Ca^{2+} as well as diverse protein targets; this allows a small number of conserved Ca^{2+} motifs to have a vast number of downstream targets depending on what combination of 'detector' and 'effector' domains are present.

1.6.2 The EF hand motif

There are several common calcium-coordinating motifs in proteins, but the most ubiquitous of those is the EF hand motif, at least among cytoplasmic proteins. There are five other types of Ca^{2+} binding proteins found outside the cell, and a number of different ER/SR-localized proteins, phospholipid-binding 'annexins', C2-domain proteins like PKC and synaptotagmin inside the cell, suggesting that Ca^{2+} binding proteins may have arisen more than once in evolution (Clapham, 2012). The first study to characterize the EF hand motif in carp parvalbumin used alphanumeric indexing of the protein helices, A-F (only the C-terminus of this protein binds Ca^{2+}). The helix-loop-helix structure formed upon Ca^{2+} binding resembles a pair of hands facing each other with thumbs perpendicular to the index fingers, thus giving the motif its characteristic name (Figure 1.6). Each Ca^{2+} binding loop contains 12 residues, 6 of which provide seven coordinating ligands: 3-4 side chain carboxyl groups of acidic residues (positions 1,3,5, typically Asp), a backbone carbonyl of a rather variable residue (pos7), an Asp-polarized water (9) and both side chain oxygens of the final Glu residue (12). Interestingly, two non-coordinating residues also appear to be crucial, or at least, invariable in most EF hands: a Gly in (6), likely to accommodate the bend in the loop necessary for proper geometry, and a hydrophobic residue in (8) (Ile, Leu or Val) (Gifford et al., 2007). The latter is proposed to be needed to make inter-helix van der Waals contacts in the collapsed apo-form, and hydrogen

36

bonds (via backbone) between the 2 loops in the Ca^{2+}-replete holo form of CaM (Grabarek, 2005). The strength of the inter-helix coupling appears to be a factor in the cooperativity of Ca^{2+} binding (Linse et al., 1991; Nelson et al., 2002), thus in nearly all known EF-hand containing proteins these motifs happen to occur in pairs. The actual arrangement of EF-hand *domains*, however, especially their relative orientation and linker flexibility, is quite variable in nature and is the salient feature of all Ca^{2+}-signal transducing proteins, to which they owe their vast regulatory target repertoire – CaM in particular (Chou et al., 2001; Hoeflich and Ikura, 2002; Vetter and Leclerc, 2003; Yamniuk and Vogel, 2004; Gifford et al., 2007). Ca^{2+} binding to EF hands realigns the two helices from nearly anti-parallel to more perpendicular (e.g. opens the 'hand', see **Figure 1.6**), and allows the exposure of hydrophobic side chains which are often involved in subsequent target binding (Zhang et al., 1995; Ikura, 1996; Hoeflich and Ikura, 2002).

1.6.3 Calmodulin: general background

Calmodulin is the prototypical EF hand protein, belonging to a family collectively termed 'CTER' for each of the most abundant four members: **c**almodulin, **t**roponin C and **e**ssential and **r**egulatory myosin light chains. CaM contains two EF hand domains, each containing a pair, for a total capacity of four Ca^{2+} ions. The CaM EF domains share a 46% sequence identity, separated by a 27 residue flexible linker, roughly resembling a 'dumb bell' shape (Chou et al., 2001). Calcium binding to EF hands in CaM is thought to occur in the sequence of III-IV-I-II, in a cooperative manner, although unusual target-bound conformations where only the N-lobe is Ca^{2+}-saturated do exist (Vetter and Leclerc, 2003) (see Table 1.2). The C lobe has a 6-fold higher affinity for Ca^{2+} than the N-lobe (Linse et al., 1991), which gives CaM an additional level of

regulatory complexity by increasing the effective range of cellular Ca^{2+} concentrations to which it can respond (Zhang et al., 2012).

CaM is an essential protein; its knockouts are lethal in *Drosophila* and yeast (Davis et al., 1986; Heiman et al., 2010), although maternal CaM sustains fruit fly larvae for up to 2 days. Intriguingly, gross behavioral abnormalities in CaM knockouts of *Drosophila* (spontaneous backwards movement) parallel some CaM mutation effects in *Paramecium* (aberrant backward motion) (Hinrichsen, 1992). This observation supports the role of CaM in regulation of neuronal activity related to Ca^{2+} current modulation – although this was not directly confirmed until nearly the turn of the century (Peterson et al., 1999). Not surprisingly, given CaM's essential role, its expression in mammals is multi-genetic: there are three non-allelic mammalian *CALM* genes, all sharing a high degree of nucleotide sequence identity ($\approx$80% in humans), which all translate into the same amino acid sequence. At first glance, this arrangement would seem like a good 'backup' strategy for an essential protein, but a closer inspection reveals a high degree of variation in their untranslated regions (UTRs), typically associated with protein transcriptional control (Toutenhoofd and Strehler, 2000). This would suggest that the different *CALM* genes may actually serve as a way of controlling the availability of local CaM pools for different targets. The expression of CaM is highly variable and appears to be finely regulated, with the highest levels of total CaM found in the brain and testis (Kakiuchi et al., 1982) and typically ranging from 1 µM (erythrocytes) to 30 µM (cerebral cortex).

In terms of its biochemistry, CaM is a relatively small (16.7 kDa), ubiquitous, highly soluble, acidic (pI $\approx$ 4) protein of 148 amino acids. It has a high frequency of methionines (9 total, making up $\approx$ 6% of the protein), greater than the average for the animal proteome (2-3%) (DePristo et al., 2006). The methionines are thought to be crucial to CaM's versatility in target

binding (Gellman, 1991; Zhang et al., 1994; Yuan and Vogel, 1999; Yamniuk and Vogel, 2004) and almost half of holo-CaM's hydrophobic solvent accessible surface area (SASA) is contributed by these Met residues (O'Neil and DeGrado, 1990). Not surprisingly, Met oxidation is associated with a loss of target binding by CaM and increased proteasomal degradation (Gao et al., 1998; Snijder et al., 2011), although the effect may be residue- and target-specific (Montgomery et al., 2003).

1.6.4 CaM target binding

Actual CaM binding target sequences range widely but have a few common properties and several conserved motifs, typically differing in the arrangement and spacing of their hydrophobic anchor residues that interact with CaM (hence names like 1-5-8-14, as in smMLCK). Some representative examples and sequences are outlined in Table 1.2

A common feature of these sequences is their propensity to form an amphipathic, basic α-helix, with the bulky anchor residues presumably facing the same way on one side of the helix (Vetter and Leclerc, 2003; Yamniuk and Vogel, 2004), at least for the majority of the 'canonical' type recognition sequences (Rhoads and Friedberg, 1997). Admittedly, an increasing number of new CaM target structures reveal unusual conformations not consistent with the Ca^{2+} binding mechanics of CaM (e.g. the small conductance SK channel, *B.anthracis* edema factor protein, etc.). There are instances of CaM being reciprocally regulated by its actual target. For example, the IQ motif of the voltage gated sodium channel $Na_V1.2$ actually preferentially binds the C-lobe of apo-CaM over holo-CaM (either lobe), and subsequently reduces its affinity for Ca^{2+} by over 2 orders of magnitude (Feldkamp et al., 2011). Interestingly, this channel also binds Ca^{2+}-CaM at an alternate site upstream of the IQ motif, and the two are likely in competition *in vivo*, serving as a molecular Ca^{2+}-dependent switch. Similar Ca^{2+}-affinity tuning effects have been observed

with other targets as well (Putkey et al., 2008; Zhang et al., 2012), as well as targets that increase

CaM's affinity for Ca^{2+} (reviewed in Jurado 1999). Hence the availability of CaM, in any of the

Ca^{2+}-bound forms (0, 2, or 4- Ca^{2+} ions) is subject to its retention by different cell-specific and

common high-affinity targets. Several studies point to CaM-dependent kinase II as being one

such 'CaM-trap' molecule (Kim et al., 2004b; Sanabria et al., 2008). CaMKII is dodecameric,

with at least as many high-affinity Ca^{2+}-CaM binding sites, and is able to increase its own CaM

affinity via auto-phosphorylation upon CaM binding. Not all CaM 'traps' are high-capacity,

however. Strong, nearly irreversible binding of CaM to certain targets can also reduce the pool of

available CaM, especially if the concentration of these targets is high. These 'constitutive' CaM

binding proteins essentially treat CaM as an integral subunit. An example is the inducible nitric

oxide synthase (iNOS), which binds CaM at basal Ca^{2+} levels but requires Ca^{2+} for full

activation, and is highly expressed in macrophages upon immune activation by cytokines (Cho et

al., 1992; Censarek et al., 2004; Spratt et al., 2006). In fact, iNOS cannot even be heterologously

expressed at a practical level without any CaM present, due to severe aggregation, suggesting

CaM might also be acting as a chaperone in this case (Wu et al., 1996). Another low-capacity,

high-affinity CaM sequestering protein is neurogranin (NG), which contains an IQ-motif and,

like $Na_V1.2$, attenuates the Ca^{2+} affinity of CaM (Kubota et al., 2007). NG is responsible for the

fine-tuning of long-term potentiation (LTP) in post-synaptic neurons, although the exact

mechanism is still unclear.

As a result of such regulatory controls, CaM availability appears to be limiting in the cell

(Persechini and Stemmer, 2002), with one study involving cardiomyocytes proposing a $[CaM]_{free}$

range of 50-75nM, which is only 1% of total CaM in those cells, even at resting Ca^{2+} (Wu and

Bers, 2007). Another study in kidney cells using a biosensor that binds both apo- and holo-CaM

estimates the total available CaM for resting cells to be in the micromolar range, with an approximately 50-fold decrease upon cellular $[Ca^{2+}]_{free}$ elevation (Black et al., 2004). This allows for selective activation of specific CaM-mediated signaling networks that is both spatially and temporally controlled in response to Ca^{2+}, as a complex function of the number of targets and Ca^{2+} gradients (Slavov et al., 2013). On the other hand, overexpression of CaM can also lead to pathological effects, although there are comparatively few studies that have been done to characterize them[7].

Considering that perturbations in CaM Ca^{2+} binding can have devastating consequences, such as recurrent cardiac arrest in infants (Crotti et al., 2013), understanding the mechanism by which CaM exerts its effects is paramount. As a first step in this direction, biophysical characterization of the target binding sites in voltage-gated ion channels has been largely successful, with a number of published structural and functional studies revealing several conserved CaM binding sites in a number of channels (reviewed in Kovalevskaya et al., 2013). That number is poised to increase yet further, aided by the findings contained within this dissertation. The three main groups of voltage-gated calcium channels ($Ca_V1,2,3.x$) are all represented here (with more emphasis on L- and T-type channels than others). Established, canonical binding sites (e.g. the IQ motif) are compared, and novel, moderately conserved binding sites are explored and characterized, all with the ultimate goal of understanding how CaM may affect the (in)activation profiles of these large, essential proteins.

---

[7] CaM overexpression in pancreatic β-cells results in Ca^{2+}-induced cell apoptosis and subsequent diabetic symptoms (Yuzawa et al., 2008). CaM overexpression in cardiomyocytes leads to hypertrophy via a calcineurin/CaMKII-dependent pathway (Obata et al., 2005).
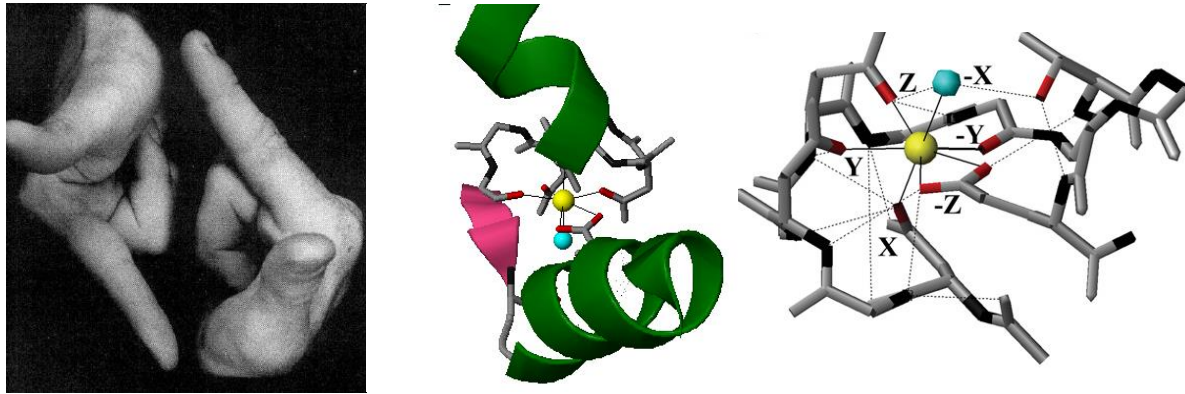
Figure 1.6: Schematic representation and structural view of the EF hands of CaM.
(left) EF 'hand' as represented by a pair of hands; the right index finger is 'E' and thumb is 'F' (middle), corresponding to the PDB structure for the EF hand from CaM of *Paramecium* (PDB code 1EXR) (right), visualized with Jmol. The helices are in green, whereas the short inter-helix anti-parallel β-sheet (only one hand shown for clarity) is in pink. Coordinating oxygens are red; peptide bonds in black, the coordinating water molecule is blue and Ca^{2+} ion is yellow.

Table 1.2: Brief overview of prototypical (and some atypical) CaM binding targets and their defining features.
Content adapted from (Rhoads and Friedberg, 1997; Vetter and Leclerc, 2003; Yamniuk and Vogel, 2004). Sequences for the first 5 peptides are taken from one of those three references. Hydrophobic anchor residues are bolded; consensus 'IQ motif' sequences are underlined. Special notes and source references: (1) The 'CaM binding database' (Yap et al., 2000) as well as (Yamniuk and Vogel, 2004), list CaMKK (both α and β isoforms) as a 1-16 motifs, not as 1-5-16 as in (Vetter and Leclerc, 2003). (2) The initial PMCA-CaM structure study used a shorter PMCA fragment that only bound the C-lobe of CaM (reflected in Vetter and Leclerc, 2003) in a different conformation than seen in the more recent NMR study with a larger peptide (Juranic et al., 2010). (3) (Schumacher et al., 2001). (4) The sequence is actually a prediction from the edema factor of *B. anthracis* adenylyl cyclase gene (GB ID M24074.1) CDS analyzed by the prediction search algorithm of the CaM binding database (Yap et al., 2000) and structure obtained from (Drum et al., 2000). (5) The study actually reveals a reduction of CaM C-lobe affinity for Ca^{2+} when bound to the $Na_V1.2$ IQ peptide (Feldkamp et al., 2011) (6) (Van Petegem et al., 2005) (7) (Kim et al., 2008) (8) based on a crystal structure from (Houdusse et al., 2006); myosin V contains multiple IQ motifs with quite variable sequences; the more variable residues in the second (C-terminal) half of the IQ motifs make contacts with the N-lobe of CaM and alter its relative orientation.

42

CaM Target	Sequence	(Target / CaM) structural conformation	Motif name	CaM lobes bound to #(Ca^{2+}) ions
smMLCK	RRKWQKTGHAVRAIGRLSSS	Helix /collapsed antiparallel	1-8-14	N, C (4)
skMLCK	KRRWKKNFIAVSAANRFKKISS	Helix/ collapsed antiparallel	1-5-8-14	N, C (4)
CaMKII	FNARRKLKGAILTTMLATR	Helix /collapsed antiparallel	1-5-10	N, C (4)
CaMKKβ	IPSLATVILVKTMIRKRSFGNPF	Helix –β hairpin loop /parallel	1-16[1]	N, C (4)
Ca^{2+} pump	LRRGQILWFRGLNRIQTQIKVVKAFHSS	Helix /collapsed antiparallel	1-18[2]	N, C (4)
K^+ channel	TQLTKRVKNAAANVLRETWLIYKNTKLVKKIDHAKVRKHQRKFLQAIHQLRSVKMEQRKLNDQANTLVDLAK[3]	3 helix/ extended 2:2 complex	Non classsical	N (2)
Anthrax edema factor	*HIFSQEKKRKISIFRGIQAYNEIEN* [4]	? /Extended non-classical	Unknown	C (2)
Na$_V$1.2 IQ domain	KRKQEEVSAIV**IQRAY**RR**Y**LLKQKVKK	Helix/ 'open' 'parallel', C-lobe only[5]	Canonical IQ motif	Apo-CaM
Myosin V motor domain	1) ACIRIQKTIRGWLLRKRY 2) AAITVQRYVRGYQARCYA	Helix / antiparallel Semi-open C-lobe, Closed N-lobe	Canonical IQ motif (x2)	Apo-CaM
L-type IQ (Ca$_V$1.2)	VGKFYATFLIQEYFRKFKKRKEQ	Helix/ compact Parallel[6]	IQ-like motif	N, C (4)
P/Q type IQ (Ca$_V$.2.1)	VGKIYAAMMIMEYYRQSKAKKLQ	Helix /compact Anti-parallel[7]	IQ-like motif	N, C (4)

1.7 CaM regulation of other channels

While voltage-gated calcium channels and their modulation by Ca^{2+}/CaM are certainly the best studied, they are not alone in being subject to CaM control. A large number of other channels from rather distant lineages (see **Figure 1.1**) are all subject to direct modulation by CaM. Many more are subject to some indirect control of CaM, such as a phosphorylation pathway, but the latter are beyond the scope of this dissertation and will not be touched upon. Among those directly regulated by CaM are (in order of most related/similar to Ca_Vs, and also the best studied, to least): voltage-gated sodium channels (Na_Vs), ryanodine (RyR) and inositol triphosphate (IP_3R) receptors, voltage-gated potassium channels ($K_V11.1$ and $K_V7.4$), small conductance Ca^{2+}-activated K^+ channels (SK or KCNN), transient receptor potential channels (TRPV1,5,6), cyclic nucleotide-gated channels (CNGs) and certain ligand-gated channels (NMDA and metabotropic Glu receptors) (Kovalevskaya et al., 2013). CaM also regulates the plasma membrane Ca^{2+} ATPase (PMCA), although it is not strictly an ion 'channel' (Boschek et al., 2008; Juranic et al., 2010). The interactions are quite diverse and so is our level of understanding regarding their mechanisms and effects. Below is a brief summary of what is known regarding a select number of representative examples; for a more comprehensive examination the reader is directed to several reviews (Saimi and Kung, 2002; Kovalevskaya et al., 2013) and the references therein.

1.7.1 Voltage gated sodium channels

As mentioned earlier in this chapter, Na_Vs are closely evolutionarily related to Ca_Vs (Anderson and Greenberg, 2001; Goldin, 2002; Piontkivska and Hughes, 2003). It is therefore not surprising that these channels also possess two EF hands and an IQ motif in their C-terminus. At present,

the textbook description of inactivation in Na_Vs is a similar process to that in K_Vs, in that a

cytoplasmic region of the channel (DIII-IV linker, or 'lid') swings over the inner mouth/pore of

the channel rapidly and inactivates it ('hinged lid' mechanism) (Catterall, 2000; Hille, 2001; Yu

and Catterall, 2003; Zamponi, 2005). Interestingly, the III-IV linker also contains a CaM-binding

site (Sarhan et al., 2012), which preferentially binds the Ca^{2+}-C-lobe of CaM and has a

prominent attenuating effect on channel inactivation. This region is also a hotspot for disease-

associated mutations affecting channel gating kinetics (Potet et al., 2009; Sarhan et al., 2012). In

contrast, the IQ motif in these channels preferentially binds apo-CaM (Potet et al., 2009;

Feldkamp et al., 2011) and its effects on inactivation appear to lack Ca^{2+} dependence.
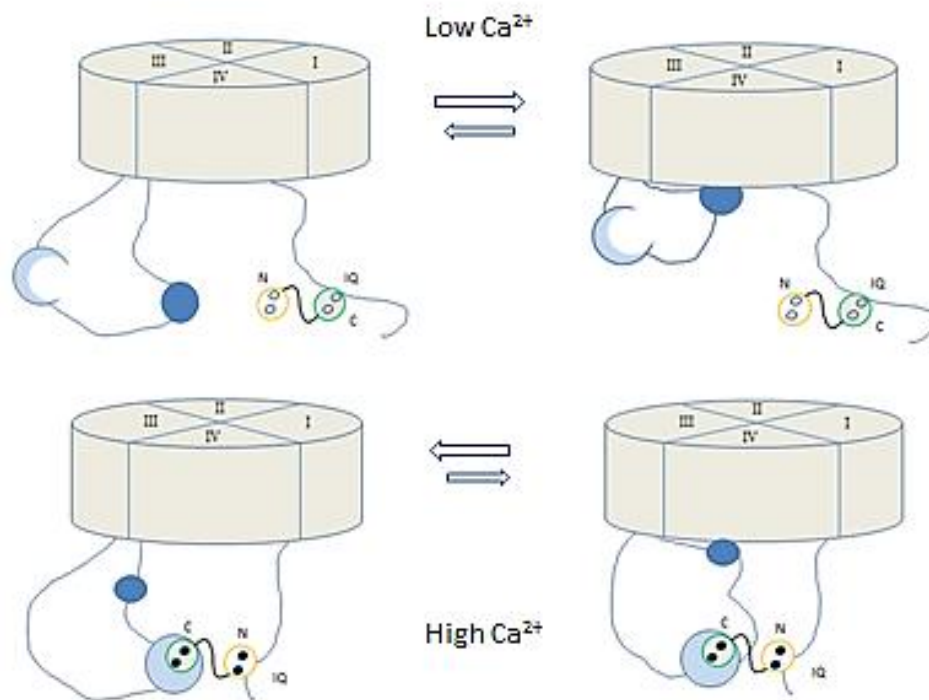
Figure 1.7: Model summarizing the proposed CaM regulation of Na_V1.5
In resting Ca^{2+}, apoCaM remains tethered to the IQ motif via its C-lobe, allowing the 'lid' region (blue circle) to freely interact with the docking site, causing rapid channel inactivation. When cellular Ca^{2+} rises, its binding to the C-lobe of CaM causes it to dissociate from the IQ motif and bind instead to the

CaM binding site in the III-IV linker (crescent moon), which destabilizes the lid-pore complex and results in increased channel opening (higher Po) (Sarhan et al., 2012; Van Petegem et al., 2012).

The effects of the two CaM binding sites (IQ and III-IV linker) on the calcium/CaM dependent modulation of the channel remain controversial, however, as conflicting results have been obtained in different studies, depending on isoform, mutation, and even cell lines used for expression, with the general consensus that the IQ motif is not actually essential for the Ca^{2+}-specific effects on inactivation (Van Petegem et al., 2012). The Na_V IQ motif has also been shown to bind CaM with a few variable, isoform-specific differences in conformation, such as $Na_V1.5$ (Sarhan et al., 2012) vs. $Na_V1.6$ (Reddy Chichili et al., 2013), something that is also true for the CaM-IQ structures of various Ca_Vs (Kim et al., 2008). The most recently proposed model describes the C-terminal $Na_V1.5$ IQ motif as a 'tether' for apo-CaM, whereby the apo-C-lobe interacts with the C-terminus in absence of Ca^{2+}, for which it has a higher affinity than the apo N-lobe (Figure 1.7). But as soon as allosteric Ca^{2+} signals (either from nearby Ca_Vs or RyR-ER activation) allow Ca^{2+} to bind the C-lobe of CaM, which has a higher Ca^{2+} affinity than the N-lobe, there is structural rearrangement leading to the relocation of the Ca^{2+}-C-lobe to the III-IV linker, and an opening for the N-lobe to now bind the C-terminus. This bridging of the two intracellular domains presumably leads to a destabilization of the inactivation gate from its putative docking site in the S4-5 linkers of DIII and IV, leading to a depolarizing shift (e.g. increased channel availability) in the activation curve. In simplified terms, CaM acts as a 'clamp' on the inactivation 'lid', reducing its mobility or occluding the docking site, and allows the channels to remain open longer or at more negative potentials (Van Petegem et al., 2012). This is especially interesting in regard to its potential similarity to the regulation of Ca_Vs, albeit with different molecular elements (the domain I-II linker, NSCaTE, etc. – see Chapters 2 and 3). It

will be interesting to see whether some form of this model holds true for all 'lid' type inactivating channels.

1.7.2 Calcium-gated potassium channels

Despite being loosely grouped within the voltage gated channel family, the small conductance potassium channels (SK, or $K_{Ca}2.1$-3) are solely activated by Ca^{2+} via a constitutively bound CaM. These channels are tetramers of the standard S1-6 TM architecture, with a distinct regulatory Ca^{2+}/CaM binding domain in their cytoplasmic C-terminus, immediately downstream of the pore-forming domain. SK channels are fairly unique in their regulatory mechanism and structural interaction with CaM (as explained below), far different from the more 'canonical' 1:1 complexes seen with CBDs of other channels, showing yet again just how flexible CaM is as an effector molecule.

There are two striking features of CaM regulation of SK channels. First, is that upon Ca^{2+} level increase, only the N-lobe of CaM binds Ca^{2+}, while the C-lobe remains in the apo form, although some of its hydrophobic residues do get repacked differently in the transition (Schumacher et al., 2001, 2004; Lee et al., 2003b). Note that the Ca^{2+} source has to be a nearby Ca^{2+} channel[8] or global cellular Ca^{2+} elevation, since SK channels do not pass Ca^{2+}. Secondly, is that while the apoCaM C-lobe interacts with a relatively small (~10 residue) region of the SK2 CBD, the rest of which remains unbound and flexible, binding of Ca^{2+} induces large scale rearrangement leading to dimerization of the CBDs of adjacent subunits. In the much less flexible dimer form, the Ca^{2+}-N-lobe of one CaM interacts with a C-terminal region of the adjacent CBD, while the C-lobe repacks itself to cross-link two of the helices in its own CBD,

---

[8] There is evidence of T-type channels being physically and/or functionally coupled to certain potassium channels, such as K_V4 and SK (Wolfart and Roeper, 2002; Anderson et al., 2013)

resulting in an unusual two CaM, three helix structure (Schumacher et al., 2004). The proximity of this complex to the S6 (and therefore, the channel 'gate') presumably destabilizes the inactivated state and results in the opening of the channel, although this motion has not yet been verified.

1.7.3 Ryanodine Receptors

RyRs are Ca^{2+} release channels found on the sarcoplasmic or endoplasmic reticulum, and often found coupled to voltage gated calcium channels (e.g. $Ca_V1.1$ in skeletal muscle) that direct their opening. These massive (approximately 10 times larger than Na_V and Ca_Vs) cation-selective channels are homotetramers of ~5000 residue subunits, large N-terminal portions of which are facing into the cytoplasm in a roughly square pattern (Zalk et al., 2007). The majority of the sequence is associated with regulatory functions, whereas only about the last 10% of the protein contains the transmembrane segments; a truncated ~1000 C-terminal residue subunit was sufficient to create a Ca^{2+} sensitive pore in one study (Bhat et al., 1997).

Remarkably, CaM is a multi-tier regulator of the RYR1 isoform found in skeletal muscle, via its C-lobe binding directly to the 3614-43 region of RYR1, as both apo and holo CaM, as well as by competing for binding of the $Ca_V1.1$ C-terminus to this region (Sencer et al., 2001; Maximciuc et al., 2006). The 3614-3643 region of RYR1 binds CaM in an anti-parallel fashion in a novel '1-17' conformation, with the two CaM lobes binding with relative independence of each other (Maximciuc et al., 2006). The N-lobe of CaM is also thought to bind to a more upstream region (1975-1999, 'site 1') of an adjacent RYR1 subunit. Furthermore, CaM competes for binding to 3614-43 ('site 2') with a downstream region of RYR1 (4064-4210, 'site 3'), which is predicted to have a CaM-like fold (Xiong et al., 2006), and may play a role in channel activation by blocking CaM from its interaction with site 2. Even more bewildering is that CaM

48

is also able to bind to this third site itself, in the apo state, with very high affinity (Lau et al., 2014), although the physiological effect of this interaction is unknown. Interestingly, CaM binding site 3 (CBS3) is very weakly conserved and does not appear to affect the Ca^{2+}/CaM regulation of RYR1 gating in deletion studies; thus it may simply be a CaM tethering site, or have another, isoform-specific role. Additionally, all three RYR isoforms contain one or more EF hands in various locations (in RYR1, there are three tandem EF hands just downstream of the third CaM binding site), although their roles are still not fully understood. Ca^{2+} has a bimodal effect on the gating of RYR1; at low concentrations (nanomolar) it is stimulatory and at higher (micromolar) concentrations, it is inhibitory. In contrast, in cardiac RYR2, CaM is inhibitory at all Ca^{2+} concentrations (Zalk et al., 2007). Whether or not this is a consequence of different CaM-RYR interactions, or the differences in the position and properties of the RYR EF hand motifs, or a combination of these and other effects remains to be elucidated.

1.7.4 Transient Receptor Potential Channels

TRP channels are essentially the cell 'sensors' towards various external stimuli, and comprise a large number (over 20 different isoforms in mammals) of different genes, broadly categorized into seven groups. They share a similar topology (6TM, heterotetramer) with other voltage-gated channels but are typically not gated by voltage. Instead, they are often capable of responding to numerous (and often seemingly disparate) physiological stimuli, and display an impressive range of cation selectivities and cytoplasmic domain diversity. They are also often found associated with other channels as effectors, and in many cases this interaction is essential for the TRP function (e.g. the IP3 receptors) (Venkatachalam and Montell, 2007). Many human inherited diseases are associated with mutations in this channel family (see **Figure 1.1**).

At least three isoforms are thought to interact with CaM (Numazaki et al., 2003; Kovalevskaya et al., 2012), TRP1, 5 and 6. TRPV1 is the 'classical' TRP channel and responds to heat, capsaicin, camphor and several other pharmacological agents. It thus acts as a generic polymodal 'pain receptor', and is the primary TRP channel in sensory neurons. Pain desensitization via capsaicin application is thought to be a result of inactivation of TRPV1 currents, and is a Ca^{2+}-dependent process attributed to CaM binding to TRPV1 at a 35 residue site in the C-terminus (E767-T801). Intriguingly, this interaction occurs in both presence and absence of Ca^{2+}, but the desensitization process requires extracellular Ca^{2+} (Numazaki et al., 2003). The process may prove to be qualitatively similar to CDI in L-type channels, or the CaM regulation of Na_Vs; the exact molecular mechanisms of this process remain to be elucidated.

TRPV5 and 6 are the most Ca^{2+}-selective of the group and may have involvement with store-operated Ca^{2+} currents; TRPV5 mutations are associated with high urinary Ca^{2+} excretion and osteoclast Ca^{2+} resorption defects (Nilius, 2007; Venkatachalam and Montell, 2007). Little is known about the effects of Ca^{2+} and CaM on the current/voltage properties of these channels. However, there has been at least one study suggesting that up to five CaM binding sites may be involved (Kovalevskaya et al., 2012), thus the process is likely quite complex if these are all indeed physiologically relevant. So far, only their *in vitro* CaM binding properties have been analyzed.

1.7.5 NMDA receptors

Neurotransmission is a complex process involving several different classes of channels: sodium and potassium channels for action potential propagation, voltage gated calcium channels for neurotransmitter release, and finally, neurotransmitter receptors on the post-synaptic neuron

membrane (Bezanilla, 2006). The latter are highly specialized among neurons and even by location, and, unsurprisingly, have highly complex architectures. Glutamate is a key neurotransmitter in excitatory signaling. NMDA is an analog of glutamate, and its receptors are heterotetramers of two types of subunits: NR1 and NR2(A-D), with additional variation contributed by splice isoforms of NR1[9]. NMDARs are one of the most Ca^{2+}-selective ligand channels, and are subject to regulation by CaM. Binding of CaM to NMDARs reduces their open probability and mean open time (Rosenmund et al., 1995; Zhang et al., 1998)

Interestingly, CDI in NMDARs is also strongly affected by cytoskeleton-disrupting agents, suggesting that physical coupling of the channel domains to the cytoskeleton may be involved in their inactivation. In fact, addition of α-actinin2, an actin associated protein, abolishes CaM-induced CDI (Zhang et al., 1998). There has been controversy regarding the binding between NR1 and α-actinin2, with one study suggesting that a direct interaction is responsible (Merrill et al., 2007), and another showing a lack of any interaction (Wang et al., 2008); thus, a clear model is lacking. Furthermore, the interaction between CaM and CBS1 of NR1 is Ca^{2+}-dependent and does not likely support a pre-association mode for CaM. Additionally, CaM may bind CBS1 with a 1 : 2 (CaM : CBS) stoichiometry, suggesting that functional channel dimerization (in a Ca^{2+}-dependent manner) drives CDI. Only the C-lobe of CaM needs to be Ca^{2+}-replete for the interaction with CBS1, and likely proper folding of the C-terminus, but either lobe is sufficient to displace α-actinin2. Additionally, the regulation by Ca^{2+}-CaM may be at least in some part attributed to the action of CaMKII, which is able to bind to NR1 C0 if α-actinin2 is first displaced (Merrill et al., 2007). Much additional research is still

---

[9] The three mammalian NR1 exons (C0-2) are known; C0 is invariant (and contains the first CaM-binding site CBS1) and C1 and 2 are developmentally regulated (Wang et al., 2008). C1 contains the higher affinity CBS2 that appears to lack any effect on CDI.

needed to decipher the exact role CaM plays in the regulation of NMDARs, and settle the
controversy.

1.7.6 Summary

As evident from this section, the regulation of different channel types by CaM is both intricate
and varied, and may rely on anywhere from just one to many binding sites. The prevailing
molecular mechanism archetypes are either A) several short, contiguous motifs, typically in the
C-terminus, with distinct Ca^{2+} dependences and therefore, functional effects, or B) distinct,
distant binding sites that may be brought close *in vivo* by their interaction with holoCaM, with
direct biophysical effects on channel activity. As only a handful of channel proteins have had
their structural elements and biochemical properties of CaM binding sites elucidated, at this time
it is nearly impossible to derive a 'template' for channel CaM regulation that can accurately
predict a particular model solely from primary sequence. However, if we were to obtain such
information for a much greater repertoire of channels, perhaps a clearer trend could be observed.

1.8 Research Objectives

The main goal of this thesis is to further our understanding of voltage gated calcium channel
regulation by calmodulin. The main hypothesis concerns the role of NSCaTE, which is a novel
N-terminal CaM-binding motif in L-type channels, in global or local CDI, as well as the extent
of its conservation. We propose that this motif is present in *Lymnaea* and performs a conserved
role in all L-type channels. The questions to be answered in this dissertation are:

1. What are the effects of NSCaTE on L-type channel regulation of diverse phyla?

    Hypothesis: NSCaTE is a conserved motif involved in some type of CDI in L-type

    channels of diverse phyla.

2. How do NSCaTE and/or IQ motif interact with CaM to elicit CDI? This is to be answered using biophysical analysis with various CaM mutants and through peptide binding studies. Hypothesis: CaM interacts with NSCaTE, in a way or conformation that is distinct from its interaction with the IQ motif, and consistent with its role outlined in 1)

3. Does CaM regulate other channels through other possible mechanisms? (HVA or LVA). Hypothesis: CaM is a universal regulator of Ca_Vs.

To complete these objectives, a combination of biophysical studies using peptides corresponding to the regulatory motifs (IQ and NSCaTE) of their cognate channels were performed, as well as electrophysiology recordings with an NSCaTE deletion mutant of LCa_V1. These studies include spectropolarimetry (circular dichroism), native PAGE studies, steady-state fluorescence and isothermal calorimetry. The results obtained in this thesis will help further our understanding of the molecular mechanisms governing the Ca^{2+}-CaM regulation of voltage-gated calcium channels.

Chapter 2: Characterization of a Novel Short Linear Motif in the N-terminus of an Invertebrate L-type Channel

2.1 Introduction

L-type calcium channels (Ca$_V$s) have key roles in a number of physiological processes (Catterall, 2011). The molecular endpoints of both voltage-dependent inactivation (VDI) and calcium-dependent inactivation (CDI) of Ca$_V$s have both been extensively studied, and although no universal model exists, many key elements have been determined and characterized (Zühlke et al., 2000; Kim et al., 2004a; Cens et al., 2006; Barrett and Tsien, 2008; Findeisen and Minor, 2009; Cui, 2010; Tadross et al., 2010). Calmodulin (CaM), a small (16.7 kDa) bi-lobed Ca^{2+} signal transducing protein, is an essential factor for CDI (Tang et al., 2003; Tadross et al., 2008; Guo et al., 2010) and is found pre-associated with these channels *in vivo*, regardless of its Ca^{2+}-binding state (Erickson et al., 2003). The difficulty of working with holo-channels has precluded a detailed structural analysis of this interaction, but various mapping studies have pointed to the IQ motif and surrounding sequences in the C-terminus and a small region of the N-terminus of Ca$_V$s as likely targets of CaM binding and regulation (Ivanina et al., 2000; Dick et al., 2008; Benmocha et al., 2009; Asmara et al., 2010; Liu and Vogel, 2012). The N-terminal region of Ca$_V$ 1.2 and 1.3 has been described as an "N-terminal spatial calcium transforming element" or NSCaTE (Dick et al., 2008), because of its dominant-positive 'knock-in' effect when fused to Ca$_V$2.2, resulting in robust, buffer-insensitive CDI that is not normally present in this channel (Peterson et al., 1999). Despite this profound effect, the actual role of NSCaTE *in vivo* is unclear. Several key mutations (W82, I86 and R90) do not greatly affect CDI even if they affect CaM binding (Benmocha et al., 2009), but the deletion of the entire N-terminus has an attenuating effect on CDI (Ivanina et al., 2000). To clarify the role of NSCaTE in CDI, we have

characterized a homologous sequence in the L-type channel of *Lymnaea stagnalis* (pond snail) or LCa$_V$1. This channel has been previously characterized and shown to have a very strong resemblance to mammalian Ca$_V$1.2 (Spafford et al., 2006; Senatore et al., 2011a), including all the hallmarks of CDI *in vivo* as well as when heterologously expressed in HEK cells. It has striking sequence homology to α1c and α1d in the C-terminal region, particularly the IQ motif, and a distinct yet similar 'NSCaTE' motif. Wild type LCa$_V$1 and a deletion mutant (ΔNT LCa$_V$1, without the first 112 residues) were recorded in the whole-cell voltage clamp mode, using both Ca^{2+} and Ba^{2+} as charge carriers to distinguish the effects on CDI and VDI, respectively. In addition, biophysical studies using synthetic peptides corresponding to the IQ and NSCaTE motifs of both LCa$_V$1 and Ca$_V$1.2 with wild type mammalian CaM were performed in an attempt to establish a molecular mechanism for the effects observed with electrophysiology recordings. We confirm the existence of NSCaTE in invertebrates and show its conservation coincides with the evolution of the IQ motif to a much greater extent than previously thought, and show it has a weak binding affinity for CaM as well as a modest and buffer-sensitive attenuating effect on Ca^{2+} currents.

2.1.1 *Lymnaea* as a model organism

Lymnaea stagnalis, or the great pond snail, is an excellent model organism for neuroscience research. Like all invertebrates, it has a relatively simple nervous system. It is inexpensive to maintain, has a low generation time, has had most of its already sequenced and is in the process of having its genome sequenced (Feng et al., 2009; Sadamoto et al., 2012). The genome of the marine gastropod *Aplysia*, its close relative, is already known. In contrast to *Aplysia*, however, *Lymnaea* is significantly easier to keep in a modest laboratory setting. Furthermore, many *Lymnaea* neurons have been identified with specific behaviours, and detailed neural networks

with corresponding behavior maps have been described (Ito et al., 1999; Feng et al., 2009 and the references therein). Just as early electrophysiology studies with squid giant axon have paved the way towards our understanding of the electrochemical gradient and the action potential, subsequent work in *Aplysia* (Eckert and Tillotson, 1981) and then *Lymnaea* (Byerly and Yazejian, 1986) were the first to illustrate the basic mechanisms governing calcium channel currents. There is a high level of conservation, both mechanistic and at the sequence level, among the regulatory elements of L-type channels (Spafford et al., 2006); in fact it is not unusual to co-transfect mammalian accessory subunits with a *Lymnaea* channel for recording to simplify the analysis. Another advantage of using the *Lymnaea* model is that it has only one isoform of each channel type (L-type, non-L-type HVA and T-type, corresponding to LCa_V1, 2 and 3 respectively), in contrast to its numerous vertebrate homologs (there are 10 total human Ca_V isoforms, see Chapter 1,

Table 1.1). This simplifies recordings in neurons where only a single Ca^{2+} current may be present, and fewer splice isoforms complicate the picture. The obvious downside to this is that subtle isoform-specific effects present in mammalian systems cannot be inferred from their counterparts in *Lymnaea*.

2.1.2 Current overview of mechanisms involved in CDI and VDI

Before covering the controversial subject of the molecular relatedness of these two processes, it is first necessary to describe the method by which currents passing through channels are measured, that is, electrophysiological recording. The basic setup of an electrophysiology recording rig is shown in **Figure 2.1**. Different techniques can be used to gather different types

of information regarding the channel in question. Firstly, one can monitor currents while keeping the voltage across the cell membrane constant, - the so-called voltage patch clamp. Alternatively, voltage changes associated with injecting current into the cell via an electrode can be measured, e.g. 'current clamp'. The former is much more commonly used to study the behavior of channels, whereas the latter is more featured in neurotransmission research. The term "patch clamp" refers to the fact that only a small portion of the cell membrane (a 'patch') is targeted for recording; only the channels found in this region of the membrane will be studied. There are also more exotic alternatives of patch clamp that involve disconnecting it from the cell (basically ripping out the patch from the plasma membrane), e.g. inside-out-patch, outside-out-patch. If a patch is small enough, or the level of channel expression is sparse, unitary channel currents can be measured. Single channel recording is perhaps the most sensitive and arguably the most valuable (and also difficult) method in the study of channel behavior. However, since the channel current is usually a fixed value, depending on the number of channel 'open states', the magnitude of whole-cell currents cannot be measured this way unless exact expression levels and open probability and mean open time are known. For this purpose, whole-cell voltage clamp can be used. In this case the glass pipette containing the electrode is introduced into the cell through a disruption of the membrane patch ('breakthrough') and continuity between the electrode solution ('internal') and the cell cytoplasm is achieved. Because of this electrical connection, the currents now measured by the electrode reflect the currents of the whole ensemble of channels found in the cell. There is a caveat to this: unless all other possible currents are blocked or cell expression is limited to only the channel under study, the whole cell current can be a mixture of different ion/current types. This is the main reason HEK293 and other non-electrically active cell lines are most often used as surrogate channel expression systems.

Since unitary channels cannot effectively describe inactivation[10], whole-cell currents are typically used. In this regard, the time-profile of inactivation is seen as a reduction of whole-cell current from its peak. Whether the reduction in current is due to increased channel inactivation (via gating or allosteric mechanisms) or a reduction of *activation* can be further determined by measuring the change (if any) in gating currents (see Chapter 1, section 1.5). Allosteric inactivation mechanisms (e.g. pore occlusion by mobile cytoplasmic domains, as in the 'ball and chain' mechanism of K_V channels) do not typically alter gating currents.

The driving force for a particular ion current is directly proportional to that ion's gradient across the cell membrane, as described by the Nernst equation:

$$E = \frac{RT}{F} \ln \frac{[M^+]_{out}}{[M^+]_{in}}$$

Where R is the universal gas constant, T is temperature and F is the Faraday's constant, and E is the equilibrium potential (also 'reversal' potential) for that ion. As there are several important ions both inside and outside the cell, the resting membrane potential is slightly different from the equilibrium potential for each ion, and can be summarized by the Goldman equation:

$$E_m = \frac{P_{K^+}}{P_{tot}} E_{K^+} + \frac{P_{Na^+}}{P_{tot}} E_{Na^+} + \frac{P_{Cl^-}}{P_{tot}} E_{Cl^-}$$

Where E_m is the membrane potential, P_X is the relative permeability of ion X (typically in Siemens) and P_{tot} is the total ion permeability of the membrane for all three ions, and E_X is the reversal potential of that ion (see previous equation).

As per Ohm's law, current is directly proportional to voltage (e.g. membrane potential), and inversely proportional to resistance. The resistance in the case of ion channels is described

---

[10] "Inactivation" for a single channel means a reduction in the open probability or mean open time, which cannot be seen on a time course due to the stochastic opening behavior of single channels

by the conductance and density of channels, as well as their open probability. As for the ion gradients, *in vivo* concentrations of Ca^{2+} are very low, but the membrane gradient is very high (low milimolar range in extracellular space and nanomolar in resting cytoplasm) (Berridge et al., 2000; Hille, 2001; Clapham, 2012; Zhou et al., 2013). Electrophysiology recording often involves over-activation of ion channels and much larger Ca^{2+} load into the cells than physiological for achieving maximal current amplitude. Thus for maintaining the high Ca^{2+} gradient, as well as staving off the Ca^{2+}-associated cytotoxicity, intracellular recording solutions usually contain Ca^{2+} chelators (EDTA, EGTA, BAPTA). Depending on the rate of Ca^{2+} entry into the cell, this may also prevent the CaM N-lobe from binding Ca^{2+} and initiating processes requiring higher cellular $[Ca^{2+}]_{free}$. The concept of 'local' and 'global' Ca^{2+} sensing via the magnitude and spatial distribution of Ca^{2+} gradients was partially uncovered by reducing the concentration of these internal Ca^{2+} buffers during recording such that 'low buffer' inactivation due to a rise in whole-cell 'global' calcium was permitted (Liang et al., 2003). This 'local/global' idea was extensively modeled by the Yue lab (Peterson et al., 1999; DeMaria et al., 2001; Liang et al., 2003; Dick et al., 2008; Tadross et al., 2008, 2010; Tadross, 2009). It suggests that Ca_Vs are able to differentiate (via CaM) the Ca^{2+} signals occurring through single channel events (local, transient, nanodomain Ca^{2+}) from higher Ca^{2+} accumulations due to multiple depolarizations and/or channel clustering (global, microdomain Ca^{2+}). While there is evidence to support this model in many cases, the scope of its applicability remains to be established.

In the case of HVA channels, which are characterized by a much more depolarized current-voltage relationship (I-V curve) than the LVA (T-type) channels, inactivation can occur by at least two separate mechanisms. When Ca^{2+} is used as the charge carrier, L-type channels inactivate much more rapidly (calcium-dependent inactivation, or CDI), than when Ba^{2+} is used

as a charge carrier (reviewed in Tuckwell, 2012). The latter is thus commonly referred to as 'voltage-dependent' (VDI), since Ba^{2+} does not effectively bind CaM yet passes through the selectivity filter at least as well as Ca^{2+}. Whether or not inactivation can occur in absence of *any* ions has not been determined (unless closed state inactivation is considered), thus Ba^{2+} serves as the approximate surrogate. The term 'VDI' is really a misnomer; it should instead be termed 'generic current dependent inactivation' or at least 'Ca^{2+}-INdependent inactivation', but VDI seems to be the *de facto* term in literature.
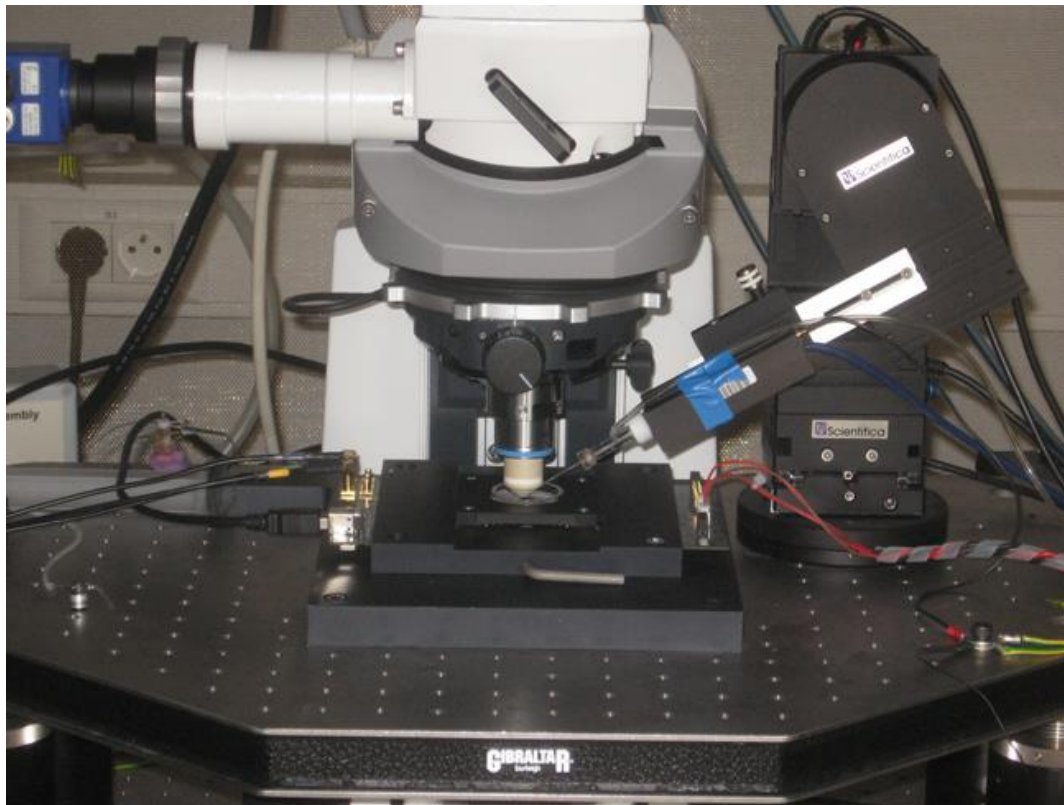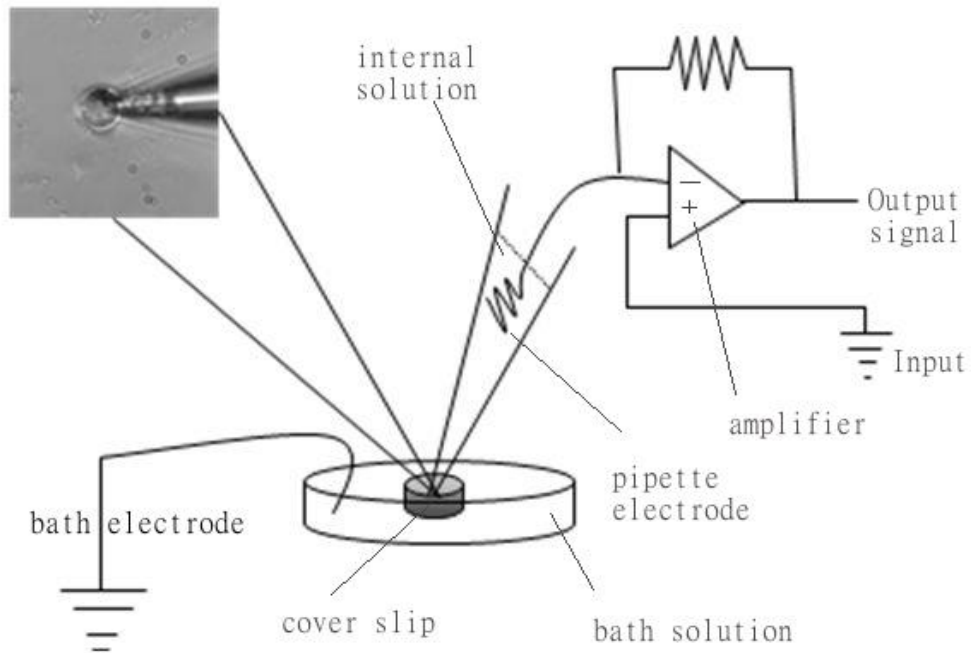
Figure 2.1: Typical electrophysiology rig setup.
The top figure represents the mechanistic basis for patch clamp recording (not to scale), including a stock image of a patched cell. The bottom image is a generic stock picture of an electrophysiology rig, where the culture dish and recording pipette/electrode can be seen along with the microscope; the entire set up is placed on a specialized vibration dampening table, and often within a Faraday cage to minimize interference.

CaM, as well as a functional IQ motif and a 'derelict', e.g. non-Ca^{2+} binding EF hand in the C-terminus of L-type channels are required for CDI (Peterson et al., 1999, 2000; Zühlke et al., 2000; Pitt et al., 2001; Kim et al., 2004a; Van Petegem et al., 2005; Fallon et al., 2009; Halling et al., 2009). While apoCaM pre-association with $Ca_V1.2$ is known to occur in the channel's C-terminus (Erickson et al., 2001), the exact localization of this interaction is unknown. Three putative regions[11] have been implicated, and while some of the constructs partly encompass the IQ motif, the IQ motif itself is not sufficient for the interaction with apoCaM (Tang et al., 2003; Kim et al., 2004a).

VDI is less rapid than CDI and is strongly modulated by the β-subunit of Ca_Vs binding to a region of the I-II linker in the α-subunit called AID (α-interaction domain), with isoform-specific effects (see Chapter 1, section 1.3.1.3) (Dafi et al., 2004; Opatowsky et al., 2004; Zhang et al., 2005; Lao et al., 2008). There is some experimental evidence that hydrophobic residues lining the inner 'mouth' of the channel pore are important in VDI, which may hint that a pore-occlusion type mechanism may be involved, possibly through the docking of the linker to this hydrophobic region, much like the 'hinged lid' mechanism in Na_Vs (Shi and Soldatov, 2002; Stotz et al., 2004; Tadross et al., 2010).

VDI is also dependent on the formation of a rigid α-helix by the region encompassing the sequence between the IS6 (last TM segment of domain I) and the AID, which binds the β subunit (Findeisen and Minor, 2009). Most interesting, however, is that not only do mutations disrupting this linker helix affect VDI; they also reduce the apparent CaM effects (CDI and CDF[12] in P/Q

---

[11] In human $Ca_V1.2$, regions 'A' = residues 1609-1628, 'C' = 1627-1652, and the IQ motif = 1665-1685 (Tang et al., 2003)

[12] CDF (Ca^{2+}-dependent facilitation) is normally only observed in $Ca_V2.1$ (P/Q type), although current enhancement due to β-adrenergic activation of cardiomyocytes (which pass primarily L-type current via $Ca_V1.2$) and phosphorylation of β subunit by CaMKII has been observed.

type channels). Additionally, removing pre-associated CaM ablates CDI and accelerates VDI (Liang et al., 2003). To complicate matters further, one study points at the defunct EF hand of $Ca_V1.2$ as also reducing VDI (Bernatchez et al., 1998), although the mechanism is unclear. This study also used *Xenopus* oocytes for recording, which express other channels that may have complicated the analysis.

Altogether, these studies suggest that VDI shares at least some structural determinants with CDI and cannot be treated independently as once suggested (Cens et al., 2006; Barrett and Tsien, 2008; Minor and Findeisen, 2010; Tadross et al., 2010).

2.1.3 Review of literature and experimental goals

Several key studies provided the context from which the experimental framework of this chapter was built. In 2008, a groundbreaking study by Yue and colleagues revealed an unexpected effect of CaM binding to the N-terminus of L-type channels when the latter was genetically fused to N-type channels ($Ca_V2.2$), which resulted in its name 'N-terminal Spatial Calcium Transforming Element' or NSCaTE (Dick et al., 2008). N-type channels do not normally show CDI in standard recording (with 'high' or 10mM EGTA or BAPTA in the internal solution), but they do when NSCaTE is present, regardless of EGTA or BAPTA. Furthermore, NSCaTE appears to act this way via binding to the N-terminal lobe of CaM, as shown by using CaM mutants deficient in Ca^{2+} binding to either the N or C lobe[13]. Intriguingly, CaM binding to the N-terminus of L-type channels has been shown before (Ivanina et al., 2000), but not in the context of its effects on CDI. Yue attributes the fast CDI component to the N-lobe of CaM acting via NSCaTE, and the slow component, which is spared by high buffering, NSCaTE deletion and CaM_{12} mutations, to the C-lobe of CaM. While the binding of NSCaTE to CaM has been studied further (Benmocha

---

[13] CaM_{12} and CaM_{34}, respectively

et al., 2009; Asmara et al., 2010; Guo et al., 2010; Liu and Vogel, 2012), the effects on CDI and VDI remain controversial. The goal of the experiments covered in this chapter was to demonstrate that NSCaTE is far more conserved that originally suggested, as well as its ability to bind CaM (either apo, holo, or both) alone or concurrently/competitively with the L-type IQ motif. Biophysical characterization of CaM interaction with NSCaTE and IQ motifs from both mammalian and snail L-type channels was completed. Electrophysiological recording of wild type LCa_V1 and a truncated mutant ($\Delta NTLCa_V1$, sans first 112 residues) was performed to lend relevance to the biochemistry results and attempt to reconcile the findings with those previously published.

2.2 Methods

2.2.1 Cloning of the L-type N-termini from LCa_V1 and $Ca_V1.2$

Both $Ca_V1.2$ and LCa_V1 N-termini were PCR-amplified from their respective wild type plasmid constructs (in PMT2 and pIRES2 vectors, respectively – See Appendix Figure A.3) using the following primers:

$Ca_V1.2$ FW   5'-CTT TAA GAA GGA GAT ATA CAT ATG GTC AAT GAA AAC ACG AGG ATG TAC

$Ca_V1.2$ RV   5'- GTG GTG GTG GTG GTG GTG CTC GAG CCA TTC AAC AAT AGA GAT GCA TGC -3'

LCa_V1 FW   5'-CTT TAA GAA GGA GAT ATA CAT ATG GCC AGT TCG CCA ACA GGG GTT CAC

LCa_V1 RV   5'- GTG GTG GTG GTG GTG GTG CTC GAG TAT TCT GCA ACC TGT ATA CAA AAT -3'

These primers contain both the restriction sites (NdeI and XhoI) and part of the sequence for pET22b (C-terminal 6HIS-tag, T7 promoter, Novagen) expression vector for either restriction-free (van den Ent and Löwe, 2006) or standard cloning. Amplification of NSCaTE was done

using AccuTaq polymerase (Sigma Aldrich). Reaction conditions: 0.25μL of each primer (0.1μM stock) 0.4mM dNTPs, 2.5mM $MgCl_2$, ammonium sulfate PCR buffer at 1X and 200-500ng of template, 25μL final volume. Cycle conditions for the first stage amplification: hot start (3min @94ºC) 1 unit of AccuTaq (0.2μL of 5U/μL); touchdown section: 30s @ 94ºC, 30s @ 59→42ºC(Δ-2ºC), 60s @ 72ºC; amplification section: {30s @ 94ºC, 30s @ 54ºC, 60s @ 72ºC}x10, {30s @ 94ºC, 30s @ 50ºC, 60s @ 72ºC}x10; final extension: 5min @ 72ºC. Second stage (restriction-free cloning/amplification) reaction conditions: 1μg template (pET22b), 0.4mM dNTPs, 80ng of gel-extracted 1st stage product as primer, 1X Expand PCR buffer (without $MgCl_2$) (Roche), 1mM $MgSO_4$. Cycle conditions: 3min @94ºC hot start, added 0.3μL of Pwo polymerase (Roche). Touchdown: 30s @ 94ºC, 30s @ 58 → 42(Δ-2ºC), 10min @ 68ºC. Amplification: same as touchdown but instead 10 cycles each where the annealing step was 1min @ 48, 56 and 66ºC (30 total).The product was then DpnI digested and transformed into XL1 blue electro-competent *E.coli* (originally from Invitrogen) for screening. The second stage PCR was only successful for $Ca_V1.2$. LCa_V1 was cloned into pET22b the 'old school way'[14] with NdeI and XhoI. All constructs were sequence verified by The Centre for Applied Genomics (Sick Kids, Toronto).

2.2.2 Protein Expression

Wild type rat calmodulin was purified using Phenyl Sepharose 6 fast flow high sub from GE Healthcare, packed to approximately 10mL volume, by gravity flow at 4ºC. pET9d (a T7 *E.coli* expression vector, with kanamycin resistance marker, from Novagen) containing the codon-optimized CaM ORF was transformed into BL21 DE3 *E.coli* using electroporation and plated on kanamycin media at 37ºC. Overnight cultures of ~50mL LB supplemented with kanamycin were

---

[14] Using standard DNA restriction and ligation techniques

used to inoculate 1L of either LB or superbroth with 30mg/mL kanamycin (10mL of inoculum per1L) and grown at 37ºC and 200rpm to OD of 0.4 – 0.6 (for LB) or 0.5-0.9 (for SB), at which point they were induced by 1mM added IPTG and grown for another 4 (for SB) to 6 (for LB) hours. Robust expression of soluble CaM was confirmed by SDS PAGE. Cells were collected by centrifugation at ~4000g, then lysed in high salt buffer (0.1M Tris-Cl pH 7.5, 0.5M NaCl, 0.5M ammonium sulfate, 1mM DTT) using an Avestin Emulsiflex homogenizer at 15-20 000 psi with jacketed water cooling, through which the cells were passed about three times on average. The cell lysate was clarified by centrifugation at 20000rpm in SS-34 rotor (approx. 50000g) at 4ºC for 30min. To the cleared lysate, $CaCl_2$ was added to a final concentration of 10mM; this lysate was then applied to the gravity phenyl sepharose column equilibrated with the same high salt buffer (and 1mM $CaCl_2$). It was extensively washed with high-salt buffer and CaM was then eluted using 10mM Tris-Cl and EDTA solution (pH 7.5). The highest fractions were pooled, concentrated, and applied to the prep grade Superdex 75 16/60 column (GE Healthcare) on an AKTA FPLC system. Typical injection volume was 1mL, and the gel filtration buffer (50mM Tris-Cl pH 7.5, 150mM NaCl, 1mM $CaCl_2$) was set to flow at 1mL/min. Wild type CaM reproducibly elutes at ~68mL on this column. Elution peak width is dependent on the amount of CaM present; routinely up to ten 1mL fractions were obtained of concentrations 200-400μM; these were pooled and concentrated using the spin-concentrators from Sartorius or Amicon (10,000 MWCO). Extinction coefficient of 3006 $M^{-1}cm^{-1}$ at A_{276} was used (Potet et al., 2009) and the final protein stock was aliquotted to 500μL and stored at -80ºC.

RN (rat NSCaTE) and LN (*Lymnaea* NSCaTE) HIS fusion constructs in pET28a (N-terminal 6xHIS T7 expression vector from Novagen) were expressed in a similar manner to CaM, except that growth was done at 25ºC, in Superbroth. Collected cells were resuspended in

lysis buffer (20mM sodium phosphate 500 mM NaCl, 20 mM imidazole, 1 mM $MgCl_2$, 1 mM

PMSF, and lysed using the Avestin Emulsiflex homogenizer. Inclusion bodies containing the

protein constructs were collected by centrifugation at 20000 rpm in the SS-34 tubes (~50000g),

and resuspended further in 8M urea IMAC buffer (8M urea, 20 mM TrisHCl, 500 mM NaCl, 5

mM imidazole, 1 mM β-mercaptoethanol). This solution was applied to the 1mL His Spin-Trap

(IMAC) columns from GE Healthcare, washed with the same buffer, and eluted with the same

buffer supplemented with 500mM imidazole. Step-wise dialysis was then done to remove urea

from the sample, by solution changes in 2M increments (6, 4, 2, 0) down to 0M Urea, 20mM

Tris pH 7.5, 500mM NaCl and either 20μM $CaCl_2$ or EDTA. When no exogenous CaM was

added, His-RN did not remain in solution throughout the steps, precipitating more and more

along each step. When CaM was added, but the dialysis was done in EDTA, similar results were

seen. However, when $CaCl_2$ and CaM were used, HisRN remained visibly more soluble (see

Figure 2.7). Typically a large molar excess of CaM was added, as judged by the BioRad protein

assay of the His-RN fusion construct. Despite comparable treatment of HisLN, it did not appear

to remain in solution in detectable amounts by SDS PAGE (data not shown).

2.2.3 Bioinformatic analyses of oligonucleotide and peptide sequences

Oligonucleotide design was performed using the wild type sequences for LCa_V1 (Spafford et al.,

2006) and rat $Ca_V1.2$ (GI 158186632), and codon optimization and hairpin/dimer analysis was

done using the tools found on the Integrated DNA Technologies web-site (www.idtdna.com).

Protein parameters (pI and MW) were determined using the prediction tool in ExPaSy

(http://web.expasy.org/protparam/) and the aggregation propensity was determined using the on-

line software at Centre for Genomic Regulation (http://tango.crg.es/). All phylogenetic

alignments were done using variations of the BLAST tool on the GenBank web site. The CaM

binding site prediction database (http://calcium.uhnres.utoronto.ca/ctdb/contacts/index.htm) was used to search for other possible 'hits' in the channel ORFs (Yap et al., 2000) and to design optimal peptide sequences for synthesis.

Table 2.1: List of L-type peptides ordered from CanPeptide

Name	Sequence	Position	MW	pI
rat-long (RN)	SWQAAIDAARQAKLMGS	22-38	1804.07	8.46
snail-long (LN)	GWSTALAAAQGAATVRK	93-109	1658.89	11
Rα1c-long (IQc)	KFYATFLIQEYFRKFKKRKEQ	1466-1486	2799.34	10.12
LC1-long (LIQ1)	KFYATFLIQDYFRRFKKRKEQ	1551-1571	2813.27	10.28

Table 2.2: List of L-type peptides ordered from Genscript

Name	Sequence	Position	MW	pI
$Ca_V1.2$ IQ (IQc)	KFYATFLIQEYFRKFKKRKEQ	1466-1486	2799.34	10.12
LCa_V1IQ (LIQ1)	KFYATFLIQDYFRRFKKRKEQ	1551-1571	2813.27	10.28
LCa_V2IQ (LIQ2)	KIYAGLLISENWKAYKASQNA	1592-1612	2368.7	9.4

2.2.4 Gel Shift Mobility Assay

All gels with L-type channel peptides (Table 2.1 and Table 2.2) were run in native, urea-free buffer. 15% acrylamide separating and 4% stacking gels were used. Running buffer: 192mM glycine, 50mM Tris-Cl pH 8.3. Separating gel buffer (2x): 0.7M Tris-Cl pH 8.8, 1mM $CaCl_2$ (or EDTA); stacking buffer (2x): 0.5M Tris-Cl pH 6.7 (1mM $CaCl_2$ or EDTA). Peptides were incubated with CaM for ≥ 1hour at 4ºC in gel filtration buffer (150mM NaCl, 50mM Tris-Cl pH 7.5, 1mM $CaCl_2$) prior to loading; 50% glycerol in gel filtration buffer and <0.1% bromophenol blue (as tracker dye) was used at 1:2 sample volume just prior to loading for each sample. Gels were run at 100V in 4ºC jacketed /ice bath conditions for 6-8 hours as needed.

2.2.5 Native Trp fluorescence

Steady state measurements were obtained using a Photon Technologies International (PTI) Quantamaster Fluorimeter (London, ON) in a 50μL 1mm fluorescence cuvette from Hellma at

room temperature. The same buffer was used as for gel filtration and ITC experiments (50mM

Tris-Cl pH 7.5, 150mM NaCl) with either 1mM $CaCl_2$ or 10mM EDTA where indicated; buffer

was used as a baseline for subtraction. To the cuvette containing the starting peptide solution

(25µM), increasing amounts of CaM were added (in increments corresponding to ~2.5µM).

Emission scans from 300 to 400nm using a 280nm excitation wavelength and 1nm slit width

(averaging over 1s each) and step size were performed. Traces were exported to .csv format and

analyzed with MS Excel.

2.2.6 Dansyl-CaM fluorescence

Dansyl (5-(dimethylamino)naphthalene-1-sulfonyl chloride) is an amine-reactive fluorescent dye

(see Figure 2.2). Dansyl-CaM was prepared as previously described (Kincaid et al., 1982). CaM

(1 mg/ml) was transferred into 10 mM $NaHCO_3$, 1 mM EDTA, pH 10.0, at 4°C. 30 µl of 6 mM

dansyl-chloride (1.5 mol/mol of CaM) in DMSO was added to 2 ml of CaM, with stirring. After

incubation for 12 hours at 4°C, the mixture was first dialyzed against 500 volumes of 150 mM

NaCl, 1 mM EDTA, 20 mM Tris-HCl, pH 7.5, at 4°C, and then exhaustively dialyzed against

500 volumes of water. Labeling yields were determined from absorbance spectra using the ε_{320} of

$3,400 \ M^{-1}cm^{-1}$ and were compared to actual protein concentrations determined using the

Bradford method with wild-type CaM used as the protein standard (Chen, 1968). ESI-MS was

used to confirm successful dansyl-labeling of CaM protein. The concentration of dansyl-CaM in

all experiments was 2 µM.
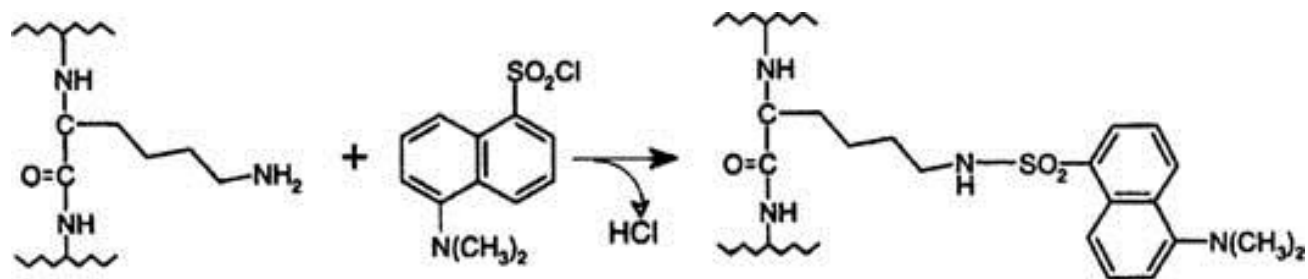
Figure 2.2: the dansylation reaction (for a Lys residue).

Steady state fluorescence was performed in a similar manner as the Trp experiments, except that a newer Florolog3-22 (Horiba Scientific, Ltd.) fluorimeter (kindly offered by Dr. Elizabeth Meiring's lab) was used, and the buffer used was 10mM HEPES (pH 7.0) with supplemented 0.1 mM $CaCl_2$

2.2.7 Circular Dichroism

CD measurements were performed using the Jasco-715 spectropolarimeter (Jasco Instruments, NS), using the following parameters: 250-190nm range, 20nm/min speed, 1s response time, 0.5nm bandwidth and 100mdeg sensitivity at room temperature. Recordings were made in a 1mm cuvette, in 10mM sodium phosphate buffer with 0.1mM added $CaCl_2$, and used as baseline, which was subtracted from each recording. For CaM+peptide spectra, the same solution of 10μM CaM was scanned before stock (1mM) peptide was added in incremental amounts before being scanned again. The resulting spectra were subtracted (e.g. CaM+peptide – CaM alone) to extract the spectrum corresponding to the change associated with adding the peptide. Every recording was an average of at least 16 accumulations and subsequently corrected for protein concentration (converted to units of mean residue ellipticity or MRE). These were smoothed and exported into ASCII format for analysis with Excel and either SOMCD (http://geneura.ugr.es/cgi-bin/somcd/index.cgi) or Dichroweb K2d algorithm (http://dichroweb.cryst.bbk.ac.uk).

70

Trifluoroethanol (TFE) recordings were performed using pure 2,2,2-trifluoroethanol (Sigma Aldrich) at 10%, 25% and 50% after thorough pre-mixing and incubation with peptides in the phosphate buffer, baseline corrected against the same TFE/buffer solution without peptide.

2.2.8 Cloning and Expression of ΔNT-LCa$_V$1

PCR was used to create LCa$_V$1 with an alternative start site 112 amino acids downstream of the long form of the channel, removing a predicted NSCaTE sequence at positions 90 to 101 in the existing full-length LCa$_V$1 (Genbank: AF484079) cloned in mammalian expression vector, pIRES2-EGFP plasmid (Spafford et al., 2006; Senatore et al., 2011a). pIRES2 is a bicistronic vector which generates an EGFP reporter for easy detection of LCa$_V$1 expressing channels using green fluorescence on an epifluorescence microscope. Plasmid sequences were verified by sequencing (TCAG, Sick Kids Hospital, Toronto, ON). LCa$_V$1 channels were transiently transfected along with required α2δ1 and either β1b or β2a subunits in HEK293T cells using calcium phosphate precipitation (Senatore et al., 2011b). Plasmids for rat α2δ1 (NM_012919), rat β2a (NP_446303) and rat β1b (NM_017346) were a generous gift from Terry Snutch (Univ. British Columbia) via Gerald Zamponi (Univ. of Calgary).

2.2.9 Electrophysiology

Electrophysiological recordings were carried out at room temperature with an Axopatch 200B or Multiclamp 700B amplifier (Axon Instruments, Union City, CA) through a PC computer equipped with a Digidata 1440A analog-to-digital converter in conjunction with pClamp10.1 software (Molecular Devices, Sunnyvale, California). Cells were bathed in external solution containing barium (10 mM BaCl$_2$) or calcium (10 mM CaCl$_2$) as the charge carrier and 1 mM MgCl$_2$, 10 mM HEPES, 40 mM tetraethylammonium chloride (TEA-Cl), 80 mM CsCl, 10 mM

glucose, pH adjusted to 7.2 with TEA-OH, filtered through 0.22 μm filter). Patch pipettes (World Precision Instruments, Sarasota, Florida were filled with internal solution (106 mM Cs-methanesulfonate, 4 mM $MgCl_2$, 9 mM EGTA, 9 mM HEPES, 2 mM MgATP adjust pH to 7.2 with CsOH, filtered through a 0.22 μm filter) and had resistances of 2–5 MΩ. For the low EGTA experiments, the internal solution was 114.5 mM Cs-methanesulfonate, 4 mM $MgCl_2$, 0.5 mM EGTA, 9 mM HEPES, 2 mM MgATP pH adjusted to 7.2 with CsOH.

Recorded currents were digitized at a sampling frequency of 2 kHz and filtered at 10 kHz using a low-pass Bessel filter. Only recordings with minimal leak (<10%) were used for analysis, and offline leak subtraction was carried out using the Clampfit 10.1 software (Molecular Devices, Sunnyvale, California). Series resistance was compensated to 70% (prediction and correction; 10 ms lag). All values are expressed as the mean ± SEM, with statistical analyses using a one-way ANOVA. Current-voltage relationships were obtained by holding cells at -60 mV before stepping to test potentials ranging from +25 to +60 mV for 300 ms. Cell culture, transfection and data analysis was performed as described previously (Senatore et al., 2011a, 2011b).

2.2.10 Data-mining and Computational Analyses of L-type Orthologs

N-termini and C-termini sequences were gathered for orthologs of L-type channels by BLAST data-mining of available genomic databases such as NCBI (Bethesda, MD), Joint Genome Institute, Department of Energy and University of California (DOE-JGI), Washington University in St. Louis (Genome Institute at WUSTL), Baylor College (HGSC), Broad Institute of MIT and Harvard. Multiple alignments of amino acid sequences and gene tree making were conducted using Phylogeny.fr (Dereeper et al., 2008). Running window of amino acid similarity of multiple aligned sequences was conducted using Plotcon within EMBOSS (Rice et al., 2000).

2.2.11 qRT-PCR of LCa$_V$1 and ΔNT-LCa$_V$1 N-termini

mRNA was extracted from embryos, identified by morphological features of animals within egg capsules, and by the shell lengths (1–1.5 cm and 2–2.5 cm respectively) of juvenile and adult snails respectively (Marois and Croll, 1992; McComb et al., 2005). LCa$_V$1 transcripts were amplified by quantitative RTPCR (qPCR) with a forward and reverse primer pair designed against LCa$_V$1 to amplify a 138 bp sequence just upstream of the NSCaTE sequence, respectively (LCa$_V$1-Met1f: 5' GAGGTAGAGGAAGGAGGAGGAG 3' and LCa$_V$1-Met1b: 5'-GCCAGAGTCTGTTGTATTCAGAG-3'), and a primer pair designed to amplify a 145 bp sequence just downstream of NSCaTE: (LCa$_V$1-Met$_2$f: 5' TACAGGTTGCAGAATACAAAGCAT 3' and LCa$_V$1-Met$_2$b: 5' AAGACATATTCAAT CCGATCCAGT 3'). Amplification efficiencies (E values) for each primer pair was determined by generating standard curves using 1:5 serial dilutions of pooled cDNA from all RNA extracts as template. By plotting the cycle threshold (C$_T$) values[15] vs. log of template concentration (copy number) and determining the slope, one can determine the efficiency (slope = -1/logE). C$_T$ values for each amplicon were averaged (n = 4) and normalized against averaged C$_T$ data for control gene HPRT1 using the ratio

$$E_{NSCaTE}^{\Delta CT_{NSCaTE}} / E_{HPRT1}^{\Delta CT_{HPRT1}} \text{ (Pfaffl, 2001).}$$

---

[15] C$_T$ is the cycle number at which a particular fluorescence level (e.g. detection) is achieved.

2.3 Results

2.3.1 Conservation of NSCaTE in L-type channels

The alignments in this section were compiled by Dr. JD Spafford, and were published recently (Taiakina et al., 2013). They show a ubiquitous presence of an NSCaTE motif in L-type channels of most bilateral animal phyla (Figure 2.4, top panel). NSCaTE appears to be missing in several arthropod species, notably *Drosophila* and certain vertebrate L-type isoforms. Interestingly, nematodes and mosquitoes may have evolved an NSCaTE region independently, based on the clustering of their sequence variation, divergence of position of NSCaTE within the N-terminus, and presence of an additional intron in nematodes. The actual position of NSCaTE within the N-termini of L-type channels, as well as the degree of sequence conservation (**W**xx**AI/L**xAx) are quite variable, which may explain why previous studies have underestimated its evolutionary age and/or missed it entirely. Indeed, only the tryptophan residue seems invariably conserved, which most likely means it is crucially involved in CaM binding and explains why it strongly affects CDI (Dick et al., 2008; Benmocha et al., 2009; Asmara et al., 2010; Guo et al., 2010). The other likely hydrophobic anchor candidate is the conserved I/L in the middle of NSCaTE; the remainder of the sequence is highly variable among phyla. The key feature of this sequence is the high content of Ala, which is known for its tendency to occur in α-helices, as well as basic Arg/Lys residues – also one of the defining characteristics of CaM targets (O'Neil and DeGrado, 1990; Vetter and Leclerc, 2003). Conserved flanking residues surrounding NSCaTE could provide the fine tuning of affinity and regulatory effects of CaM binding.

2.3.2 NSCaTE as an optional motif

Another interesting outcome of the multiple sequence alignments and conservation plots of IQ and NSCaTE motifs is that for the vast majority of NSCaTE-containing channels, there is a downstream Met with an alternate Kozak sequence which produces an NSCaTE-less channel. Indeed, this shortened isoform was used in the electrophysiology recordings of LCa_V1 (the 'short' isoform was generated using PCR to amplify the rest of the CDS from the second, downstream-of-NSCaTE methionine as the start codon). Upon further inspection, it was observed that a second start site was also present in the rat L-type homolog $Ca_V1.2$, and human $Ca_V1.2$ and $Ca_V1.3$. Translational read-through has recently become more recognized as a source of protein diversity and regulatory network complexity (Bazykin and Kochetov, 2011), and has already been described in TRP channels before (Honoré, 2008). To verify that both 'short' and full-length (e.g. Met_2 and Met_1, respectively) forms are expressed natively, we would need to perform Western blots using NSCaTE-specific and generic, LCa_V1-specific antibodies with L-type channels purified from *Lymnaea* tissues. Considering that purification of ion channels is already fraught with practical limitations of expression and solubility, the generation of such antibodies was a daunting task we were too time-constrained to undertake. Instead, we sought to eliminate the possibility that there was any regulation at the transcriptional level.

Quantitative reverse-transcription PCR (qRT-PCR) of snail tissues and whole animals (embryos, juveniles and adults) has been applied previously to map expression and gain clues to protein function (Senatore and Spafford, 2010, 2012; Senatore et al., 2013). In this case, it was used to find whether both +NSCaTE (Met_1) and −NSCaTE (Met_2) channels were being generated transcriptionally through mRNA editing or alternate splicing (although no intron junctions in this channel exist in the cytoplasmic N-terminus). The results clearly indicate that no such

transcriptional selection exists, and approximately all LCa_V1 transcripts contain the Met_1 sequence (Figure 2.3). These experiments were carried out by Julia Fux (M.Sc candidate) and Adriano Senatore (Ph.D.) under the supervision of Dr. JD Spafford.
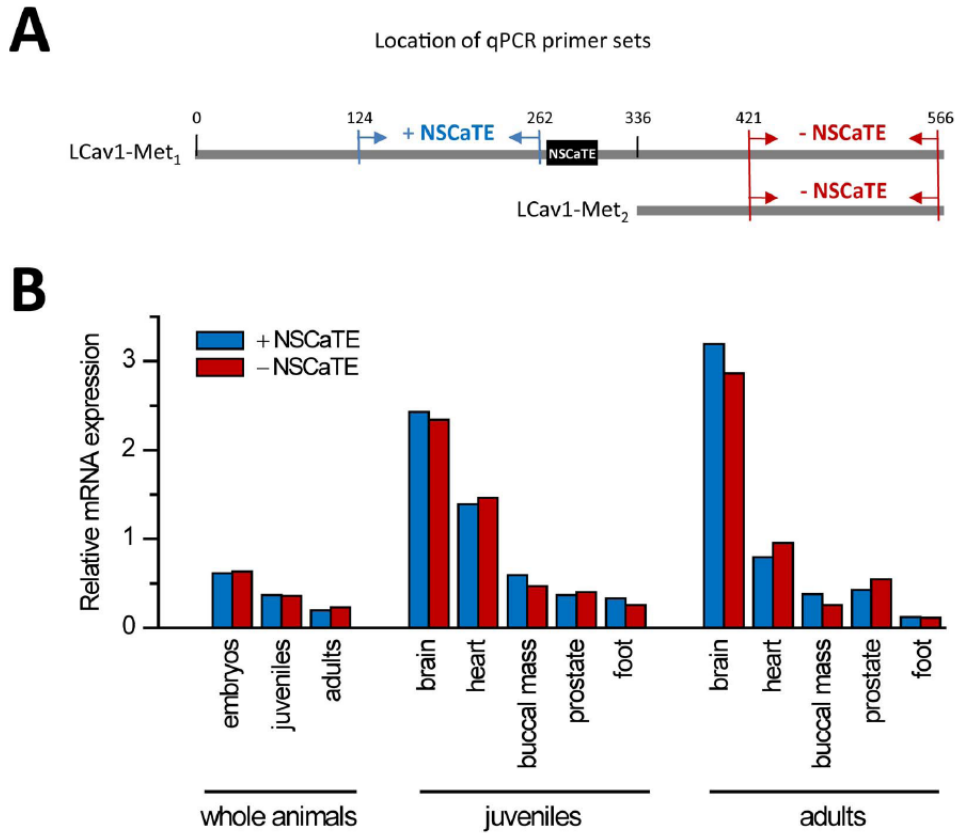
Figure 2.3: qRT-PCR of Met_1 and Met_2 LCa_V1, showing lack of transcriptional differences.
A: location of primer sets. B: fold difference in mRNA levels relative to those of a housekeeping gene, HPRT1.
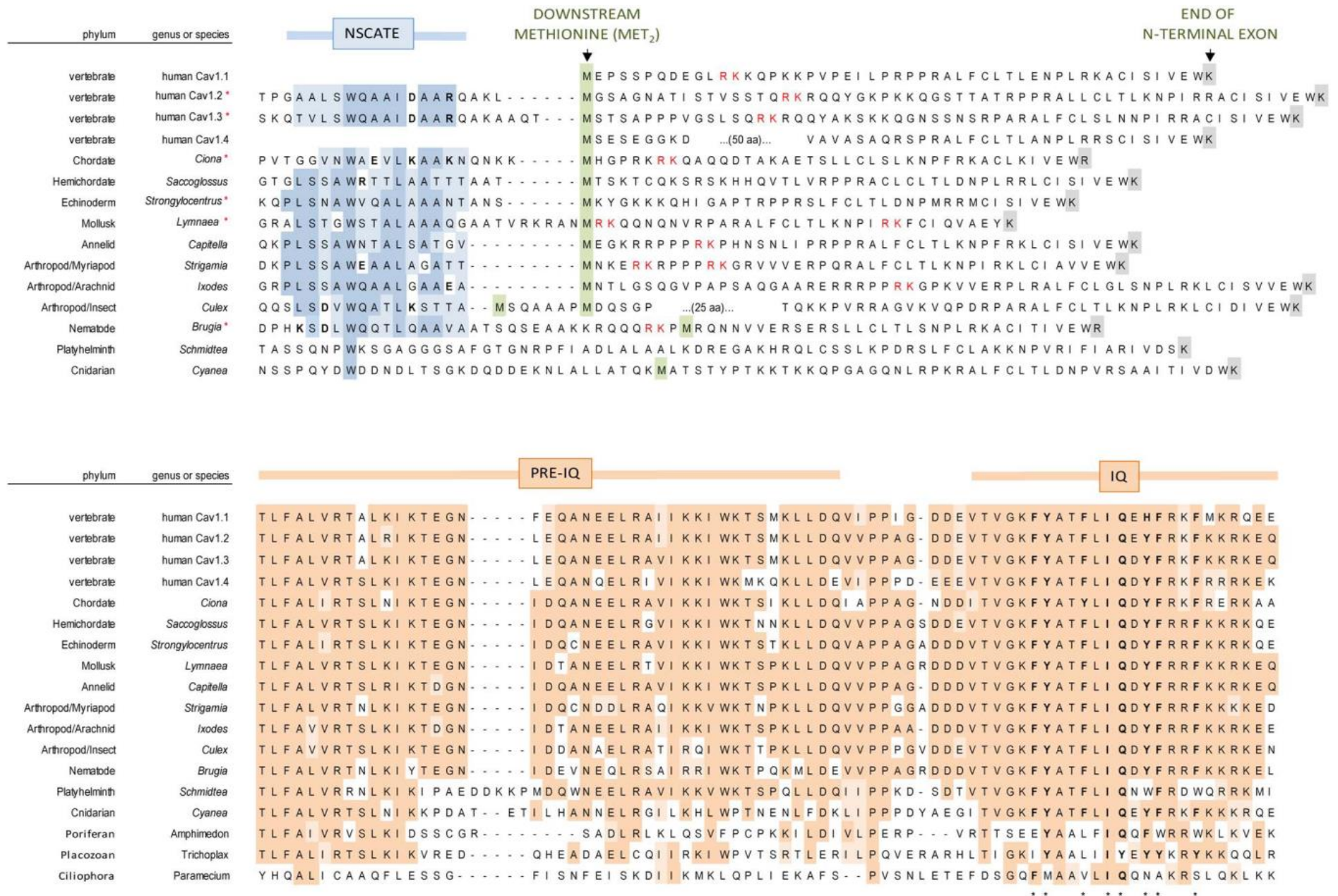
Figure 2.4: Sequence alignment of NSCaTE and Pre-IQ/IQ motifs across animal phyla.

2.3.3 Electrophysiology recordings of LCa$_V$1: Met$_1$ and Met$_2$.

Whole-cell voltage patch clamp recordings of HEK293T cells expressing either full-length, wild

type LCa$_V$1 (Met$_1$) which contains NSCaTE, and a truncated NSCaTE-less LCa$_V$1 (ΔNT-LCa$_V$1,

Met$_2$), were performed by Dr. Adrienne Boone. Their analyses were performed by Dr. Boone

and Dr. Spafford, using ClampFit 10.1 and Origin software, with a one-way ANOVA (analysis

of variance).

The initial recordings of the 'short' LCa$_V$1 (Met$_2$) were discouraging; no significant

difference in CDI, VDI or any other biophysical parameter were found from wild type ('long' or

Met$_2$) LCa$_V$1. The only exception is the recovery of channels from inactivation after a 1s

depolarization in Ca^{2+} (Table 2.3, Figure 2.5), which appears to be slightly higher with NSCaTE

present. NSCaTE deletion corresponds to a lower recovery from inactivation in Ca^{2+}, which

makes it near-identical to that of Ba^{2+}, but the effect is small. However, when standard recording

solution (9mM EGTA) was replaced with a low-EGTA recipe presumably resembling a

'physiological' level of Ca^{2+} buffering (0.5mM EGTA) (DeMaria et al., 2001; Liang et al., 2003;

Dick et al., 2008), a significant effect on CDI was observed in Met$_2$ channels (Figure 2.5, Table

2.3). Ba^{2+} currents and VDI were not affected. R$_{300}$ values, which correspond to the fractional

amount of I_{max} present at 300ms of a test pulse, are typically used to quantitate inactivation,

since absolute currents can vary greatly. Quantitation of CDI is routinely reported as an f-value

(e.g. f$_{300}$), which is the ratio of R values at that time point (e.g. $f_{300} = R_{300}^{Ca^{2+}}/R_{300}^{Ba^{2+}}$). Thus, f$_{300}$

for the wild type (Met$_1$) LCa$_V$1 is 0.21 ± .026 and for the truncated (Met$_2$) LCa$_V$1 is 0.435 ± 0.04,

a twofold reduction of CDI. Perhaps even more importantly, the R$_{300}$ values in Ca^{2+} for Met$_2$ are

comparable in both low and high internal EGTA (0.37 and 0.31, respectively), whereas for Met$_1$

the R_{300} for Ca^{2+} goes down almost two-fold in low EGTA (from 0.32 to 0.18). This strongly suggests that NSCaTE acts to accelerate CDI under high-Ca^{2+} load conditions, potentially through a similar CaM N-lobe-mediated mechanism as that of mammalian $Ca_V1.2$ NSCaTE (Dick et al., 2008).
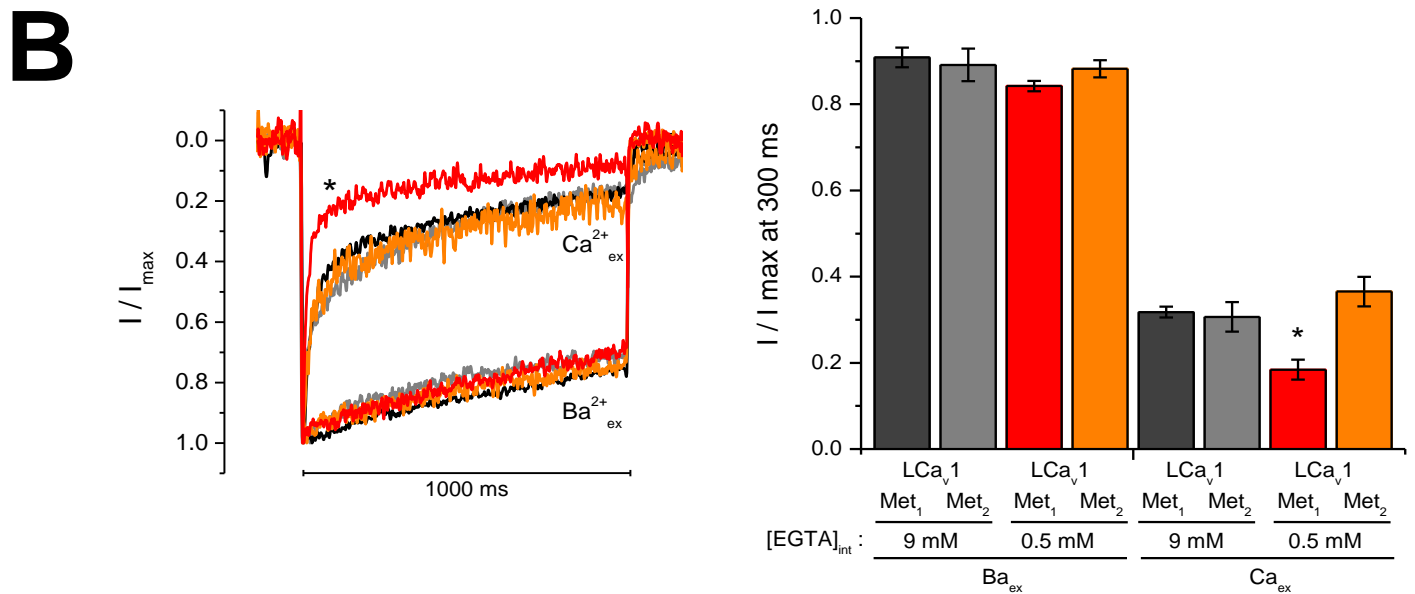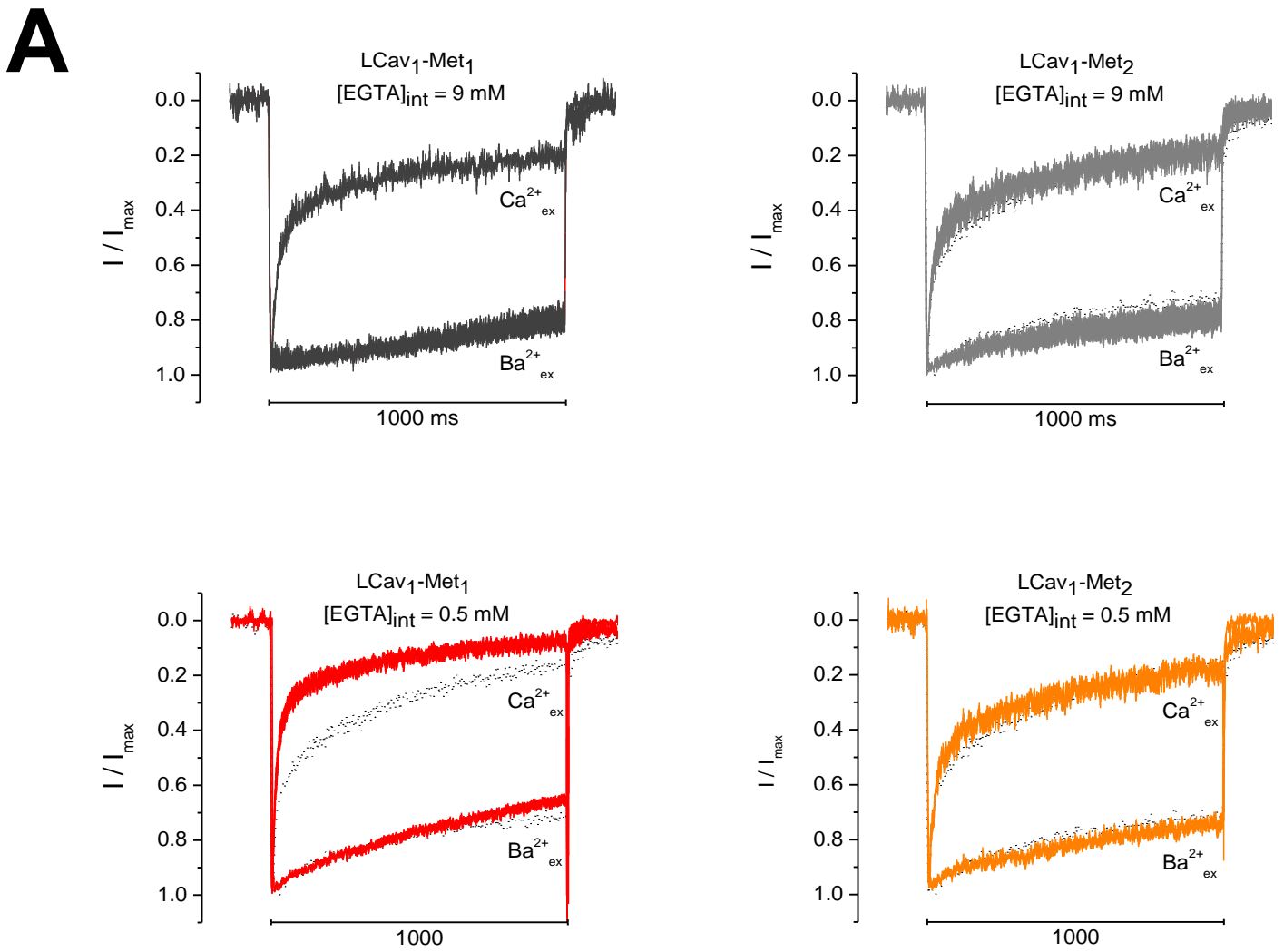
Figure 2.5: Electrophysiology traces and summary of results of wild type and ΔNT LCaV1.
A) Each cell that was recorded (in both Ca^{2+} and Ba^{2+}) had its current normalized to the peak Ba^{2+} current, and for each recording condition (Ca^{2+}, Ba^{2+}, low and high EGTA, Met_1 or Met_2) the corresponding normalized traces from a representative number of cells were averaged. B) Overlaid traces from A (left), summarizing the results in bar graph form (right). See also Table 2.3, including *n* values. Met_1 = wild type LCa_V1. Met_2 = ΔNT LCa_V1.

Table 2.3: Summary of N-terminal deletion effects on LCaV1 currents.
Similar but expanded data from Figure 2.5. LCa_V1Met_1 = wild type *Lymnaea* Ca_V1. LCa_V1Met_2 = ΔNTLCa_V1, lacking the first 112 amino acids including NSCaTE (93-109).

| | [Ba_ex] = 10 mM | | | | | | [Ca_ex] = 10 mM | | | | | | Statistical significance | | | |
| | LCav_1Met_1 | | | LCav_1Met_2 | | | LCav_1Met_1 | | | LCav_1Met_2 | | | [Ba_ex] | [Ca_ex] | [Ba_ex] vs [Ca_ex] | |
	n	mean	SEM	n	mean	SEM	n	mean	SEM	n	mean	SEM	Met_1 vs Met_2		Met_1	Met_2
[EGTA]_in = 9 mM EGTA																
Activation:																
V_1/2 (mV)	10	-3.31	0.28	10	-3.13	0.32	10	5.17	0.26	10	5.12	0.36	n.s.	n.s.	***	***
slope	10	5.90	0.33	10	5.92	0.28	10	6.49	0.20	10	6.83	0.32	n.s.	n.s.	***	***
Inactivation:																
V_1/2 (mV)	10	-19.78	1.12	10	-20.69	1.18	6	-25.69	1.14	6	-25.32	1.10	n.s.	n.s.	***	***
slope	10	8.14	0.99	10	8.67	1.04	6	7.74	1.03	6	6.61	0.96	n.s.	n.s.	***	***
Inactivation recovery:																
% recovery at 1 sec	4	41.88%	2.56%	4	40.87%	3.30%	4	46.87%	3.31%	4	39.82%	2.33%	n.s.	*	*	n.s
I_max amplitude:																
Ba:Ca size ratio	10	2.02	0.19	6	1.91	0.12							n.s.			
Inactivation kinetics:																
R_300	5	0.91	0.023	5	0.89	0.038	5	0.32	0.013	5	0.31	0.034	n.s.	n.s.	***	***
[EGTA]_in = 0.5 mM EGTA																
Inactivation kinetics:																
R_300	5	0.85	0.012	5	0.86	0.020	5	0.18	0.023	5	0.37	0.034	n.s.	***	***	***

n.s. not significant;
*$p<0.05$;
**$p<0.005$;
***$p<0.001$.

2.3.4 Expression of N-terminal HIS-tag fusion construct of Ca$_V$1.2 and LCa$_V$1

Attempts were made to study the interaction of CaM with both mammalian and snail NSCaTE. In theory, having an expression system for the larger NSCaTE-containing N-terminal region would facilitate pull-down assays, mutagenesis studies, and potentially even a solution NMR structure down the road. To this end, cloning attempts were made for the rat NSCaTE (Ca$_V$1.2) and *Lymnaea* Ca$_V$1 using synthetic oligos spanning the entire N-terminal cytoplasmic tail of each channel, codon optimized and flanked by appropriate restriction sites for cloning into a pET expression vector (pET28a). After a series of many expression attempts, it was found that the solubility of the rat NSCaTE protein construct was very poor in native conditions; typical protocols allowed only a small fraction of the expressed protein to be collected, or none at all in the case of snail NSCaTE (**Figure 2.6**). Using 8M urea improved the yield, but the process of removing urea from solution caused aggregation and precipitation of the NSCaTE fusion protein. As a last resort, in an attempt to maintain solubility of the protein, pure wild type recombinant CaM was added in various amounts to the IMAC-purified NSCaTE prior or during the removal of urea. Satisfyingly, the soluble fraction was greatly enriched in the protein expressed by the HIS-NSCaTE construct as a result (**Figure 2.7**). Notably, this enhancement was only observed under Ca^{2+}-replete conditions, suggesting that NSCaTE binding to CaM is Ca^{2+}-dependent, an observation that was subsequently supported by other experiments, and indeed a number of later published studies (Benmocha et al., 2009; Asmara et al., 2010; Guo et al., 2010; Liu and Vogel, 2012).

In the meantime, similar treatment of the *Lymnaea* NSCaTE construct proved unsuccessful. While it was presumably well-expressed, it did not appear to be stable enough in solution under the conditions used to isolate the mammalian NSCaTE construct.

The SDS PAGE and expression experiments and gel images in this section were done by Erica Lee as part of her CHEM 494 project for the Department of Chemistry at University of Waterloo.
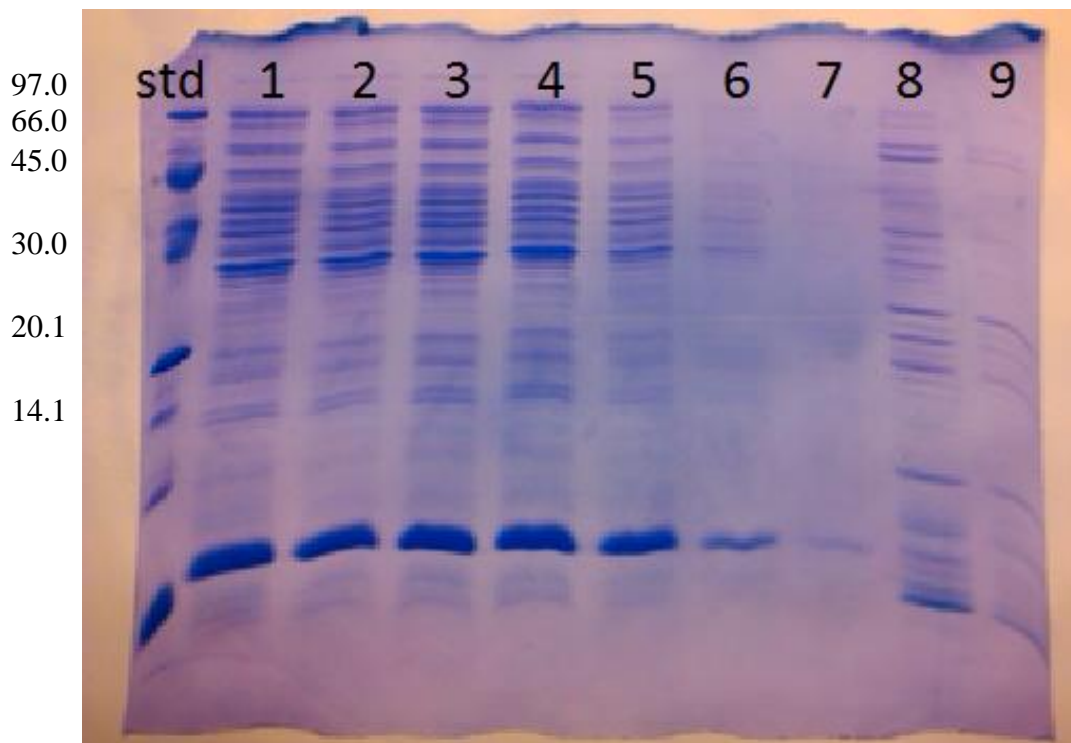
Figure 2.6: **SDS-PAGE results of snail NSCaTE purification using IMAC**.
Legend (from left to right) – unpurified sample (1), 1st flowthrough (2), 2nd flowthrough (3), 3rd flowthrough (4), 1st wash (5), 2nd wash (6), 3rd wash (7), 1st elution (8), and 2nd elution (9). The most pronounced band corresponds well to the NSCaTE construct size (~15kDa); however it appears to be near-absent in the elution fractions (last two lanes), suggesting poor protein stability, column binding, or solubility.
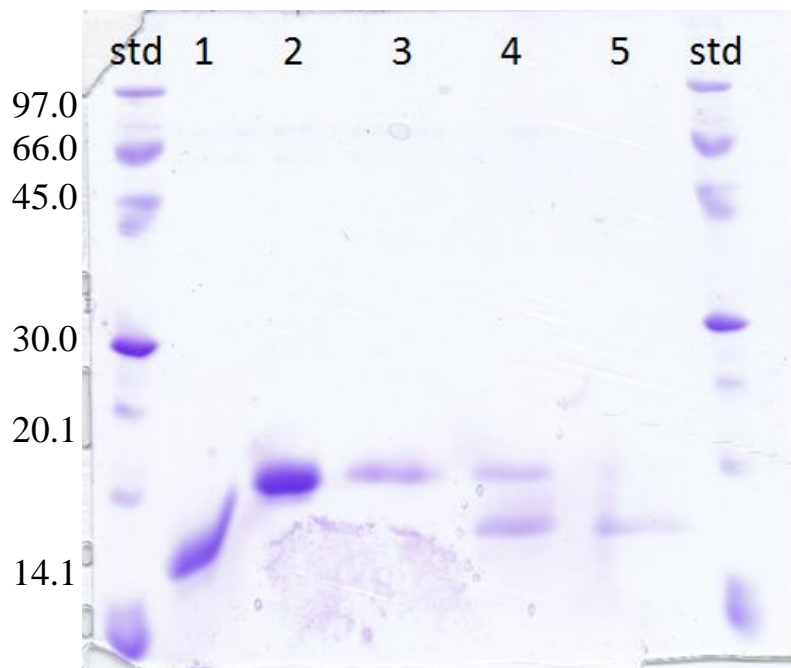
Figure 2.7: Purification of soluble rat NSCaTE is aided by Ca^{2+}-CaM.
Legend: ladder, (1) CaM in CaCl$_2$,
(2) CaM in EDTA,
(3) HisRN, supernatant of HisRN - CaM sample dialyzed in CaCl$_2$,
(4) supernatant of HisRN - CaM sample dialysed in EDTA, and ladder

As a follow up to these experiments, we attempted to generate shorter NSCaTE constructs with

fewer hydrophobic regions. The downside of such truncation was that the new DNA constructs

were at the limit of what can be reasonably purified with a gel-extraction kit (QIAGEN), e.g. sub

200bp. Upon further consideration, the cloning attempts and expression trials were suspended in

favor of more readily amenable biophysical studies using synthetic peptides corresponding to

both IQ and NSCaTE motifs from both Ca$_V$1.2 and LCa$_V$1. They are subsequently denoted

"LIQ1" for LCa$_V$1 IQ, "IQc" for Ca$_V$1.2 IQ (rat α1c), RN for rat NSCaTE and LN for *Lymnaea*

NSCaTE (Table 2.1 and Table 2.2).

2.3.5 Gel Shift Mobility Studies of L-type channel peptides

L-type channel peptides were ordered from CanPeptide, specified to >95% purity. Subsequently it was found that some of these peptides, LN in particular, were not fully soluble in water. As a result, DMSO was added in varying amounts (up to 5% v/v) to aid in solubilization. Unfortunately, this caused a number of artifacts to be observed with fluorescence and circular dichroism. In addition, IQ peptides starting with the conserved Ile were found to be lacking several residues required for CaM binding and did not appear to interact with CaM (as determined by gel shift assays, CD and fluorescence with dansylated CaM). Eventually, new peptides were ordered including a portion of the "pre-IQ" region (5 residues preceding the Ile and +2 C-terminal residues), as well as slightly longer (+4 C-terminal residues) snail and rat NSCaTE peptides, specified to >98% purity. These new peptides (see Table 2.1 and Table 2.2) were ordered from CanPeptide as well, and appeared to be fully water soluble and capable of binding CaM as determined by gel shift and fluorescence results (see sections 2.3.5 and 2.3.6). Peptides corresponding to the IQ motifs of LCa_V1 and rat $Ca_V1.2$ (IQc) were ordered from Genscript, specified to >98% purity, and were found to be soluble in water.

2.3.5.1 Conformation

It has been observed that CaM has different mobility in PAGE depending on its conformation (e.g. apo vs. holo forms, or peptide-bound vs. free). To make use of this property, wild type CaM was incubated with increasing amounts of each peptide and each combination was run on a native PAGE (no urea) and semi-native PAGE (4M urea). In the presence of EDTA, no shift was observed with any of the peptides (data not shown). In the presence of $CaCl_2$ (1mM), both IQ motif peptides (IQc and LIQ1) were seen to have a distinct reduction of CaM mobility (Figure 2.9). In contrast, no shift was seen with either LN or RN peptides, regardless of $CaCl_2$, EDTA,

urea or native conditions. To determine whether this was due to a lack of binding or a lack of conformational change in CaM, subsequent biophysical studies (such as fluorescence, CD and ITC) were performed. These confirmed that CaM is indeed binding to both rat and snail NSCaTE, albeit with a low affinity. The gel pictures in this section do not utilize urea, as there appears to be no urea effect on the peptide interaction with CaM. It was also noted that none of the previous studies including gel-shift experiments and NSCaTE or IQ/CaM used urea in their methods (Peterson et al., 1999; DeMaria et al., 2001; Erickson et al., 2001; Liang et al., 2003; Dick et al., 2008).

The gel shift and spectropolarimetry data together suggest that the binding of CaM to IQ and NSCaTE peptide is fundamentally different: in the case of the latter, there is little change in CaM itself and significant change in the conformation of the peptide. This is indicated by a lack of a gel mobility shift in CaM upon binding NSCaTE, yet significant change in α-helical content upon peptide addition to CaM. In contrast, the conformation of CaM when binding to IQ is altered enough to cause a gel mobility shift, and modest changes in peptide conformation. This is consistent with the previously published structure of CaM and $Ca_V1.2$ IQ peptide (Figure 2.8) (Van Petegem et al., 2005)
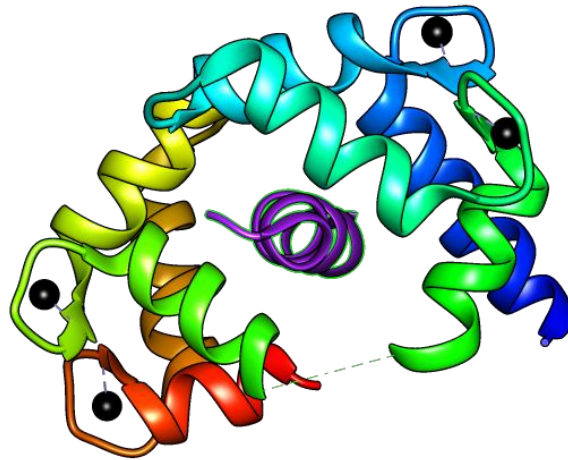
Figure 2.8: Crystal structure of Ca$_V$1.2 IQ bound to Ca^{2+}-CaM
(Top-down view facing the N-terminus of IQ). Ca^{2+} ions are in black. Generated with UCSF Chimera using the 2BE6 PDB entry (Van Petegem et al., 2005) .
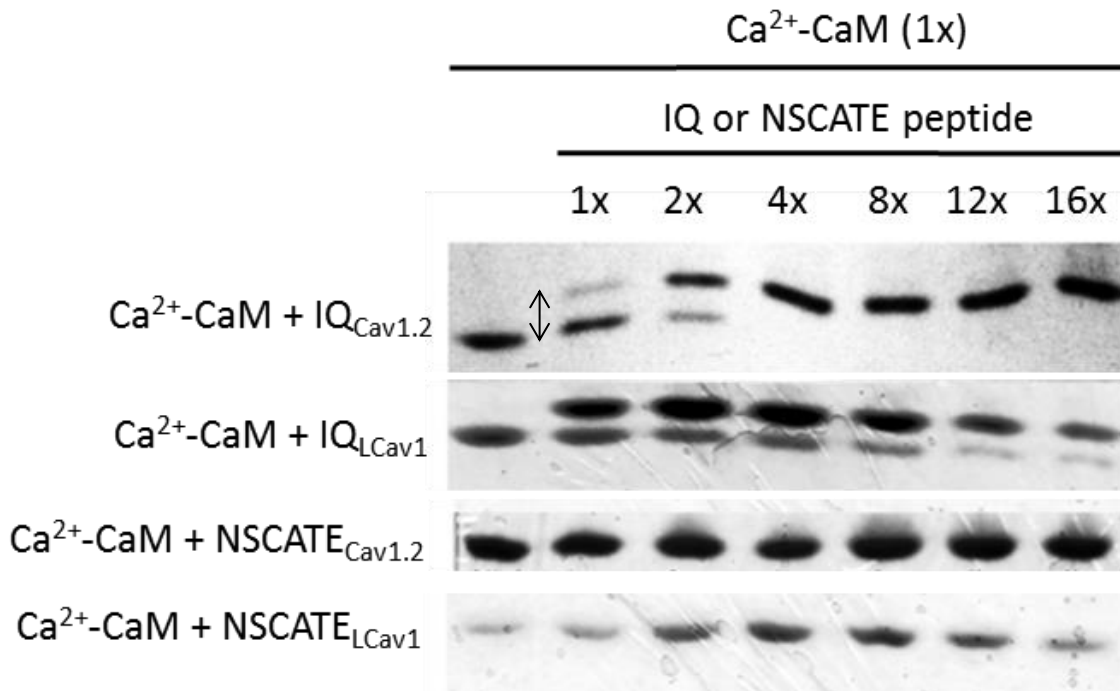
Figure 2.9: Effects of peptide binding on CaM conformation in PAGE mobility.
First lane in each gel is CaM alone control; subsequent lanes have an increasing amount (indicated by the relative ratio number at the top) of each peptide. IQ peptides cause a shift in CaM's mobility (arrow), while NSCaTE peptides do not.

2.3.5.2 Competition Experiments

To further demonstrate an effect of LN and RN peptides on CaM mobility in PAGE, displacement experiments using combinations of IQ and NSCaTE peptides were performed. In each set, an IQ peptide from the respective mammalian or snail channel was pre-bound to holo-CaM at an empirically determined ratio that facilitated a complete shift to the slower CaM mobility (approximately 1.5 peptide to 1 CaM for both IQc and LIQ1). To this mixture, increasing amounts of corresponding channel's NSCaTE were added, incubated further, and then run on the gel. As expected, high excess of NSCaTE peptides resulted in a reversal of CaM mobility to the faster-migrating non-IQ-bound state. This further supported the idea that NSCaTE is capable of binding CaM, albeit at a lower affinity and in a different conformation than the IQ motif.
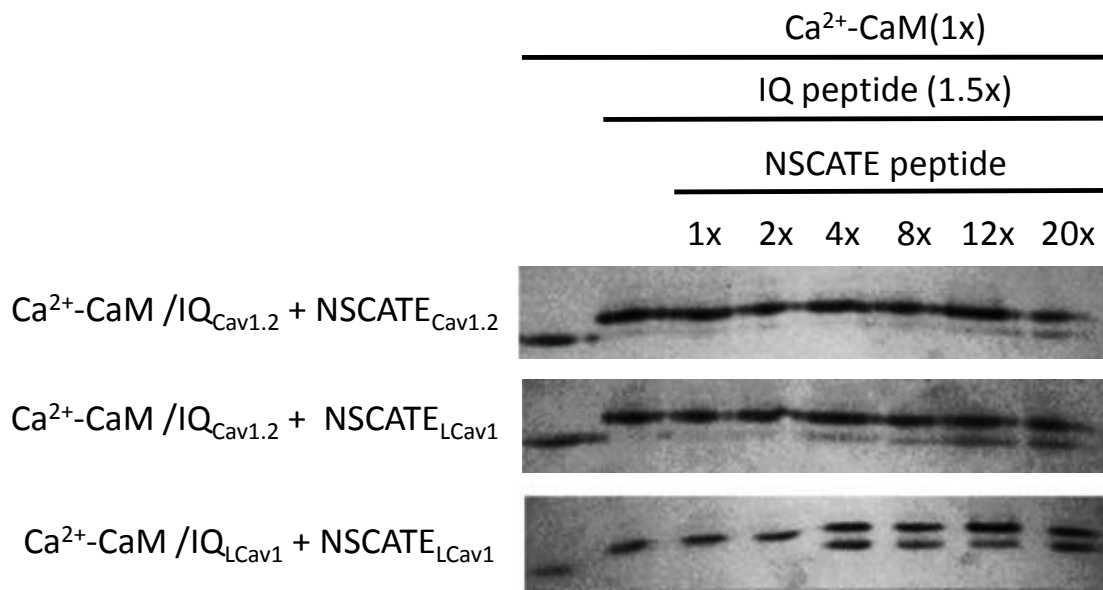
Figure 2.10: Competition gel shifts of NSCaTE vs. IQ bound to CaM.
First lane in each gel is CaM alone; second lane is CaM + IQ peptide (at 1.5x) with no NSCaTE. Subsequent lanes each contain an increasing amount of competing NSCaTE peptide (ratio relative to CaM indicated at the top). Both NSCaTE peptides partially return CaM to the native (faster) mobility when present in excess. In all cases native 15% gels and Coomassie staining was used (see section 2.2.4).

2.3.6 Fluorescence studies of L-type peptides

Fluorescence measurements can offer a substantial amount of insight into protein-protein or protein-peptide interactions in terms of the types of interactions involved, orientation, and even kinetics and binding affinities (Brown and Royer, 1997; Park and Raines, 2004; Roder et al., 2004; Sharma and Deo, 2005; Ciruela, 2008). Typically synthetic fluorophores are covalently linked to the protein under investigation, and its excitation-emission spectra monitored using a spectrofluorimeter. Steady-state fluorescence is most often used to determine simple binding parameters such as stoichiometry and changes in the fluorophore's local environment. Stopped-flow fluorescence, fluorescence correlation spectroscopy (FCS), fluorescence polarization and other variations of combined kinetic and spectroscopic techniques allow for a more detailed quantitative assessment of the interaction, such as binding kinetics (on/off rates) and affinities; however they are more difficult to set up and analyze correctly. The following section details the spectroscopic studies performed with the peptides corresponding to the L-type channel fragments from rat and *Lymnaea* to study their interaction with CaM, both via native Trp fluorescence of the NSCaTE peptides, and using dansyl-labeled CaM.

2.3.6.1 Tryptophan fluorescence

Steady-state fluorescence experiments were performed with wild type unlabeled CaM and NSCaTE peptides at varying ratios with both Ca^{2+} and EDTA. Both rat and snail NSCaTE have an invariable Trp in their N-termini. Native tryptophan fluorescence has been used to monitor protein interactions previously (Kilhoffer et al., 1992; Vivian and Callis, 2001; Li et al., 2003; Ciruela, 2008). This method relies on the sensitivity of the indole ring moiety of the residue's side chain to its environment; significant changes in emission maxima can be observed upon

altering the solvent accessibility of the Trp due to protein-protein interaction (Vivian and Callis, 2001). Thus, it was no surprise that the emission peaks of both rat and snail NSCaTE were considerably blue-shifted from about 355nm to 320nm for LN and 325nm for RN, and enhanced, from ~40% increase for RN to over 100% increase for LN (Figure 2.11 and Figure 2.12). Base fluorescence was higher for RN than LN, but the increase observed was much more significant for LN (Figure 2.13). As expected, no increase or shift was observed with EDTA, confirming the interaction with CaM as Ca^{2+}-dependent. To control for the possible background fluorescence from CaM (which has no Trp, but several Tyr residues), emission scans of holo-CaM alone were done (data not shown). As expected, the peaks were near 310nm as expected for tyrosine, and substantially lower in intensity than tryptophan (around 45000 RFUs at the highest concentration of CaM used in any titration, e.g. ~25µM) and thus did not contribute significantly to the NSCaTE peptide spectra.
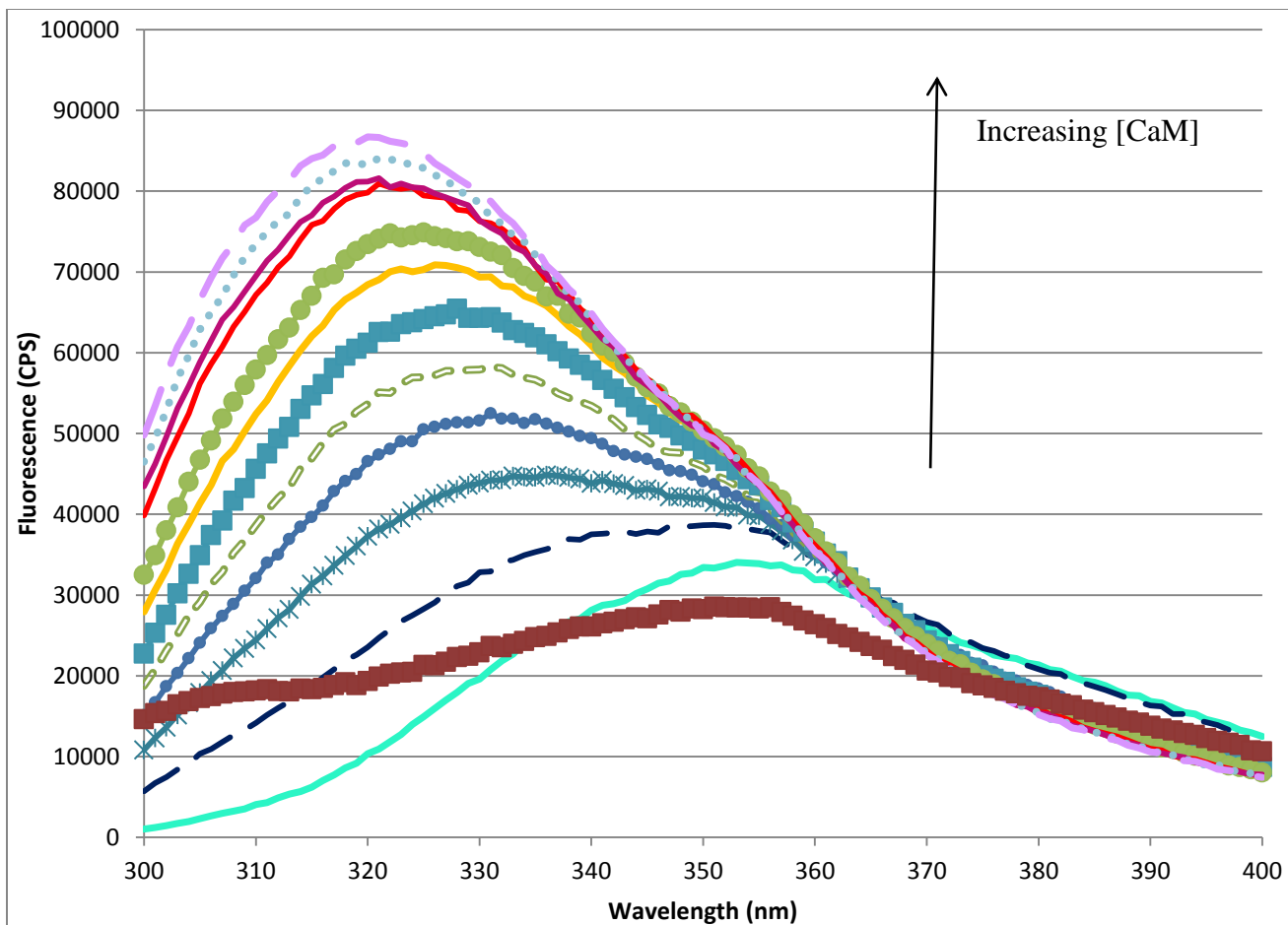
Figure 2.11: Native Trp fluorescence of LN with addition of CaM.
To the cuvette containing 25μM LN, incremental amounts of Ca^{2+}-CaM were added (2.5μM steps; each step produced an increase in signal, thus a legend was omitted for clarity). Highest fluorescence (light purple dashed) value obtained was with 30 μM CaM, corresponding approximately to a 1:1 CaM : peptide ratio. No CaM added trace (LN peptide only) is in cyan. +CaM and +EDTA (30μM and 20mM, respectively) trace is in maroon. This confirms the binding of CaM to NSCaTE and that it is a Ca^{2+}-dependent process.
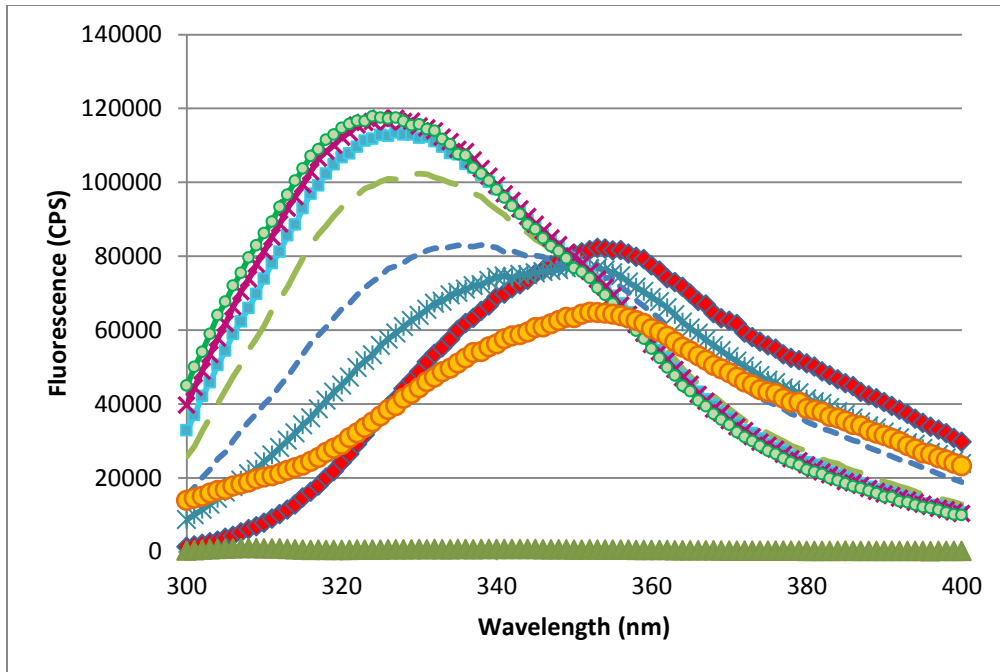
Figure 2.12: Native Trp fluorescence of rat NSCaTE with CaM.
Rat NSCaTE (RN) was scanned at 25µM just as with *Lymnaea* NSCaTE (LN) in the previous figure, then wild type Ca^{2+}-CaM incrementally added to a maximum of 25µM (dappled green, top trace). RN alone (no CaM) is in red, CaM+RN+EDTA (25µM-25µM-20mM, respectively) is in yellow.
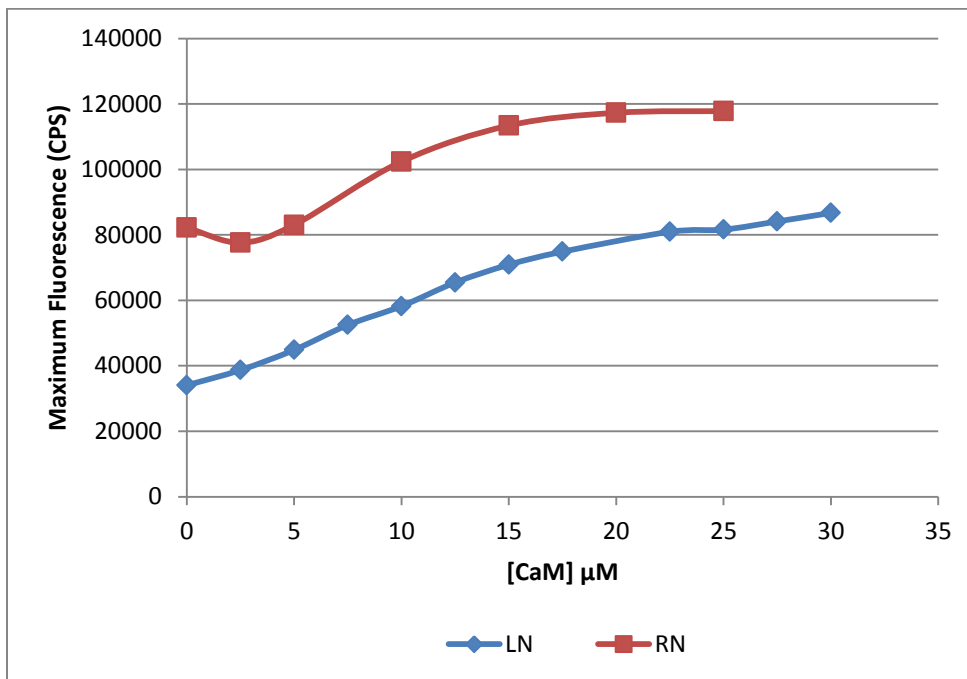
Figure 2.13: Summary plot of fluorescence vs. the amount of CaM added to the NSCaTE peptides.
NSCaTE peptides were scanned first at 25µM, and increasing amounts of stock CaM (0.3mM) were added. All conditions were the same for each peptide. The resulting maximum fluorescence (at 320nm) value for each trace was plotted vs. the concentration of CaM.

2.3.6.2 Dansyl-CaM fluorescence

The IQ peptides do not contain a tryptophan, thus a similar native fluorescence experiment (as NSCaTE) could not be performed. Instead, we dansyl-labeled wild type CaM, and performed steady-state fluorescence experiments with both IQ peptides. Dansyl is an amine-reactive label that is also sensitive to its environment; it absorbs maximally (when covalently bound) at around 340nm and emits anywhere from 450 to 550nm. In contrast to the much greater blue-shifts observed with the Trp of NSCaTEs, the fluorescence change we observe in dans-CaM upon IQ peptide addition is much smaller (10% increase or less), even at four-fold molar excess of peptide (Figure 2.14). The small effect is likely due to the low labeling yield of CaM (about 1/10) and possibly heterogeneous labeling (it is not really possible to control which amines dansyl reacts with).
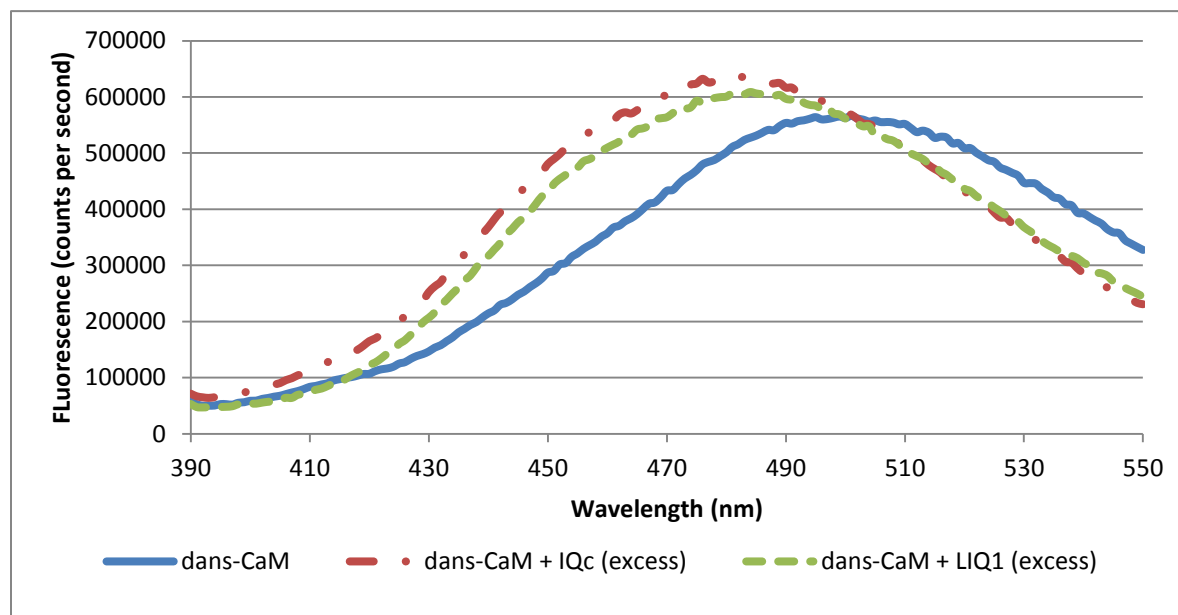
Figure 2.14: Dansyl-CaM fluorescence with IQ peptides.
The same 2µM dans-CaM was used in each trace, and stock (1mM) peptide was added to a final 4 fold molar excess, up to 8µM final (intermediate titrations not shown for clarity).

2.3.7 Circular Dichroism of L-type peptides

The principle of spectropolarimetry is fairly simple: chiral molecules, such as the amino acids making up a polypeptide chain, absorb circular left (counter-clockwise) and right (clockwise) plane-polarized light differently. The effect is quantitated on a spectropolarimeter in machine units or millidegrees, but typically converted to "mean residue ellipticity" (to normalize for protein content) in published work and calculation algorithms.

The application of spectropolarimetry for rough estimate of secondary structure content of proteins and peptides has been extensively examined (Kelly et al., 2005). It is fast and relatively straightforward, except sometimes where the analysis of complex spectra is involved. Different algorithms employed by software can give widely ranging outputs for actual fractional content of each secondary structure type for the same data set. Most of these algorithms rely on an existing reference set of proteins for which crystal structures and CD data are precisely known. There is less consistency between the different algorithms for proteins whose α-helical content is low and/or combined with significant β-sheet content or random coil. Often complications arise from high background absorbance of buffer components, especially in far-UV ($\leq$ 200nm).

α helices have characteristic CD spectra with a maximum of ~190 nm, and minima at 208 and 222 nm, which are due to the electronic transition of $\pi_0 \rightarrow \pi^*$ and $n \rightarrow \pi^*$, respectively, in the amide bond. Most proteins contain a mixture of different secondary structures, and rather than quantitating each, the studies that are performed are of a more qualitative nature (e.g. observing changes due to ligand binding or mutations). In the case of CaM, however, the secondary structure is largely composed of α helies (Chou et al., 2001; Zhang et al., 2012), and thus CaM has a very distinctive CD spectrum characteristic of an α helix. In contrast, most of its

94

target peptides are unstructured in solution, although this may not necessarily be the case where they are part of a larger protein (O'Neil and DeGrado, 1990; Vetter and Leclerc, 2003; Yamniuk and Vogel, 2004; O'Donnell et al., 2009). Irregular structures appear as a weak and broad negative peak around 200nm (cf. Figure 2.21, blue trace). Often, however, CaM induces a conformational change in its target peptide, resulting in the peptide adopting a more helical conformation (Brokx et al., 2001; Hoeflich and Ikura, 2002; Vetter and Leclerc, 2003; Lang et al., 2005; Radivojac et al., 2006; Spratt et al., 2007). This effect can be quantitated by subtracting the spectrum for the same solution of CaM from one with the peptide in question added; the resulting difference is then indicative of the changes occurring as a result of CaM-peptide binding[16]. The values also need to be corrected for total protein content and reported in units of 'mean residue ellipticity' (MRE) $deg \cdot cm^2 \cdot dmol^{-1}$.

Unfortunately, since the ellipticity change is typically subtle, even modest noise results in fairly large errors in all the structure calculation algorithms. There are also problems with calculation of CaM-induced changes in peptides that are already α-helical. Nonetheless, even by visual inspection it is possible to observe a change in ellipticity at 222 nm, and to a lesser extent at 208 and <200 nm.

Addition of trifluoroethanol (TFE) aids in helix formation, presumably by accelerating the dehydration of key residues involved (Kelly et al., 2005). If a peptide is capable of forming an α-helix, TFE at concentrations of up to 50% (v/v) will promote its transition, but only up to what is physiochemically possible at the backbone level. In other words, if the peptide does not have a sequence conducive to helix formation (α-helical propensity), the observed structural change will be relatively small. However, if the peptide regularly undergoes random coil – helix

---

[16] It is not easily possible to distinguish the secondary structure changes in CaM from those in its target peptide using the subtraction method; it is therefore advisable to look at both the CaM and TFE data together.

transitions, such as many CaM binding targets *in vivo*, it will show a profound change in the ellipticity signal at 208 and 222 nm (Moorthy et al., 1999; Vetter and Leclerc, 2003; Whitmore and Wallace, 2008). Indeed, this is what was generally observed with all L-type channel peptides, albeit to a varying extent for each (see section 2.3.5).

For helical content calculation, two different online analysis programs were used, SOMCD (self-organizing method CD) (Unneberg et al., 2001) and the K2D algorithm on the Dichroweb server developed by Drs. Whitmore and Wallace from the University of London (Whitmore and Wallace, 2004, 2008). Additionally, relative increase in signal at 208 and 222 nm (vs. peptide only signal) was used for comparison, although these metrics were somewhat difficult to correlate with the two software-based methods above due to the differences in the Y-axis scale. For the SOMCD and K2D algorithms, the Y-values represent fractional structure content (e.g. a total sum of 1 for all possible states). For the 222 nm data, a logarithm of the fold increase in ellipticity had to be used to maintain a reasonable scale for comparison. The 208 nm values are fold differences of the machine unit ellipticities at that wavelength. Overall, we see similar trends between all three methods, but since the use of a buffer caused significant background absorbance at < 200nm, accurate quantitation of secondary structure content in our case was not truly possible. Instead, we use the fold increase at 208 nm and log fold of 222 nm versus the molar ratio of peptide to CaM for the comparison of all of the peptides.

The IQ peptides show a maximum in α helical content at a 1:1 ratio with CaM (Figure 2.15 and Figure 2.16). This makes sense, since the greatest amount of α helix should be present when all of the peptide is in its CaM-bound conformation; any more peptide that can bind to CaM is then simply diluting the signal. However, the situation for NSCaTE peptides is more complicated since the *Lymnaea* peptide (LN) is unstructured and has a slight negative slope in

the % α-helix/[peptide] plot (Figure 2.17) which was not consistent with the increase seen in the IQ peptides. There was no clear 'maximum' unless the 5μM point is considered (lower ratios were not assayed), but visual inspection of the scan suggests there may be an issue with the signal/noise ratio that affected that particular trace (5μM – purple trace in Figure 2.17). The fold difference in MRE signals (both at 208 and 222 nm) for LN with CaM is much greater than for RN, likely because the actual intrinsic α-helical content of RN peptide is much greater (Figure 2.18 and Figure 2.22). LN is also much less affected by TFE, see Figure 2.21. In general terms, this suggests that the structural changes induced by CaM in NSCaTE or vice versa are minor. Moreover, there does not appear to be a consensus in the TFE-induced alpha helical change between the two NSCaTE peptides. While LN continues to gradually increase its α-helical character with addition of more TFE (Figure 2.21), the same is not strictly true for RN, which maintains a consistent level of secondary structure starting with 10% TFE (Figure 2.22). LN has a lower alpha-helical propensity, as it does not approach a detectable level of α helix until 25% TFE is added. The IQ peptides and RN, in contrast, readily respond to TFE and achieve an early maximum at low (10-25%) concentrations of TFE.

Comparing the relative α-helicity of the peptides using both varying concentrations of TFE and their maximal α-helical content with CaM presents a somewhat contrasting picture (see Table 2.4 for a summary). Both NSCaTEs appear to reach a higher maximal % α-helix with CaM (on the order of 60% - Figure 2.17 and Figure 2.18), whereas the IQ peptides are not as strongly affected by CaM (~30%) (Figure 2.15 and Figure 2.16). In contrast, the IQ peptides and mammalian NSCaTE respond more easily to the addition of TFE (Figure 2.22, Figure 2.19 and Figure 2.20), and reach higher α-helical content at lower TFE concentrations. One explanation might be that the subtracted CaM spectra do not take into account the actual α-helical changes

that could be occurring within CaM itself, e.g. the flexible linker region. It is also possible that greater noise at the lower peptide concentrations used with CaM (and the lack of reliable < 200nm data) affect the K2D calculations.

Together these data suggest a significant difference in the modes of binding of IQ and NSCaTE peptides by CaM, as well as a modest difference between the *Lymnaea* and mammalian NSCaTEs. A more in-depth biophysical dissection of the interaction with CaM was performed and analyzed in the following chapter.
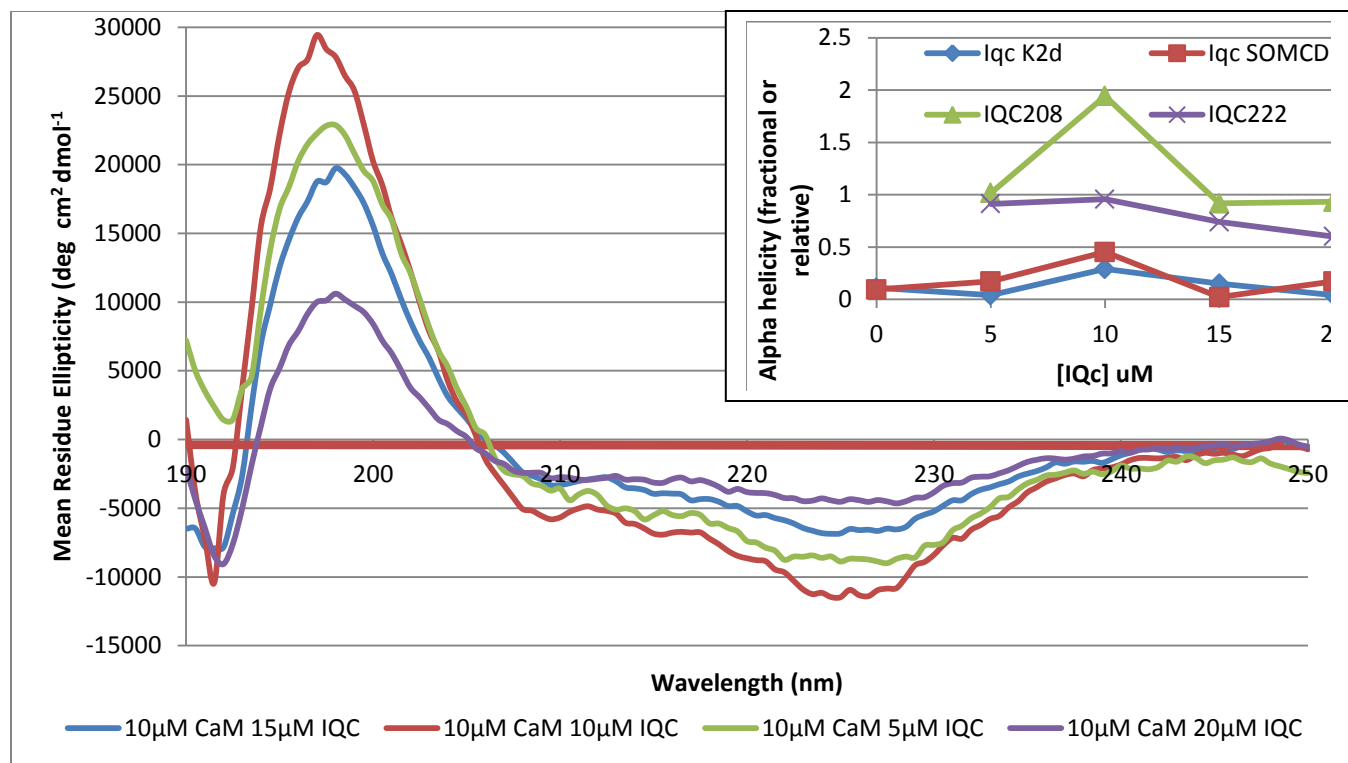
Figure 2.15: CD spectra of IQc with CaM.
Subtracted spectra of (peptide+CaM) – CaM alone, corrected/smoothed. Inset: helical content according to various algorithm calculations vs. peptide concentration. All recordings were done with the same 10 µM CaM in the cuvette. Algorithms are described in Methods. Inset: alpha-helical content vs. the concentration of added peptide, calculated using the 4 different algorithms described in Methods. Here, '0' is actually CaM-free peptide at 50µM (see TFE plots below), not peptide-free CaM, calculated with the K2D and SOMCD algorithms. The 208 and 222 nm data are fold and log fold increases (respectively) over the CaM-free peptide values, which is why they do not contain a data point at 0.
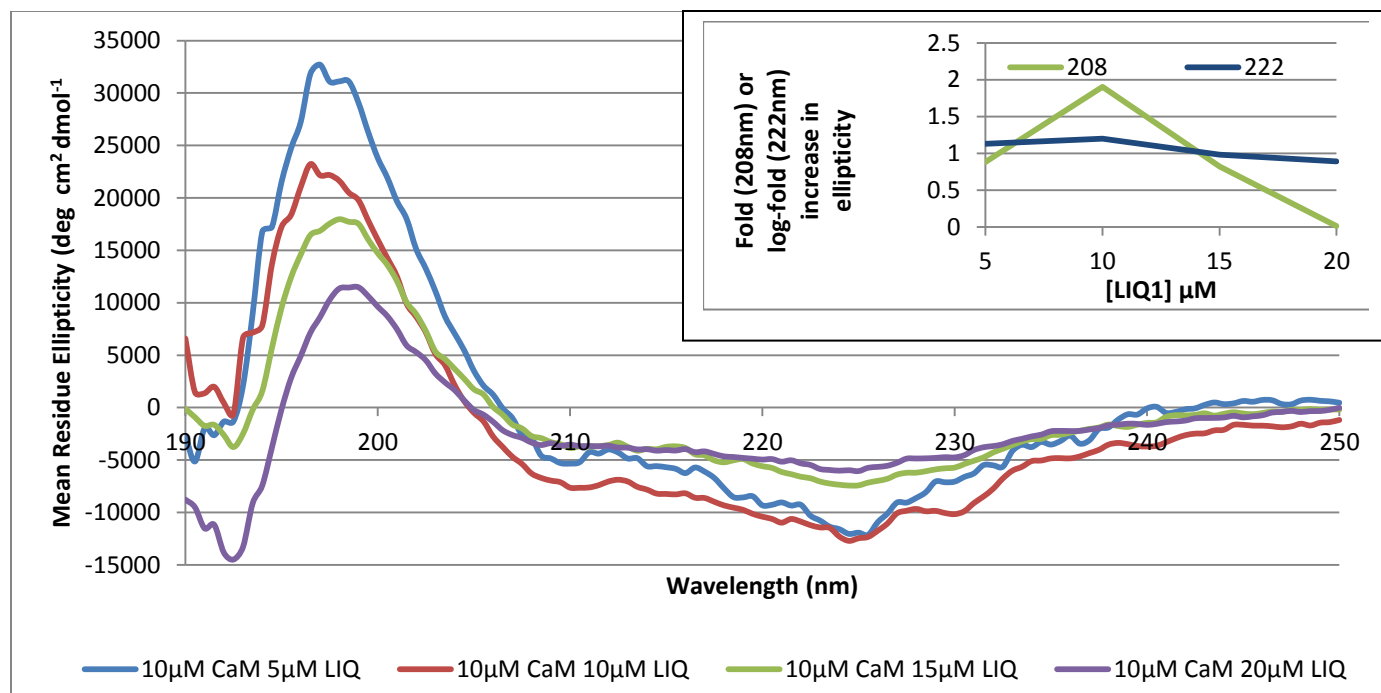
Figure 2.16: LIQ1 with CaM.
Same methodology as Figure 2.15
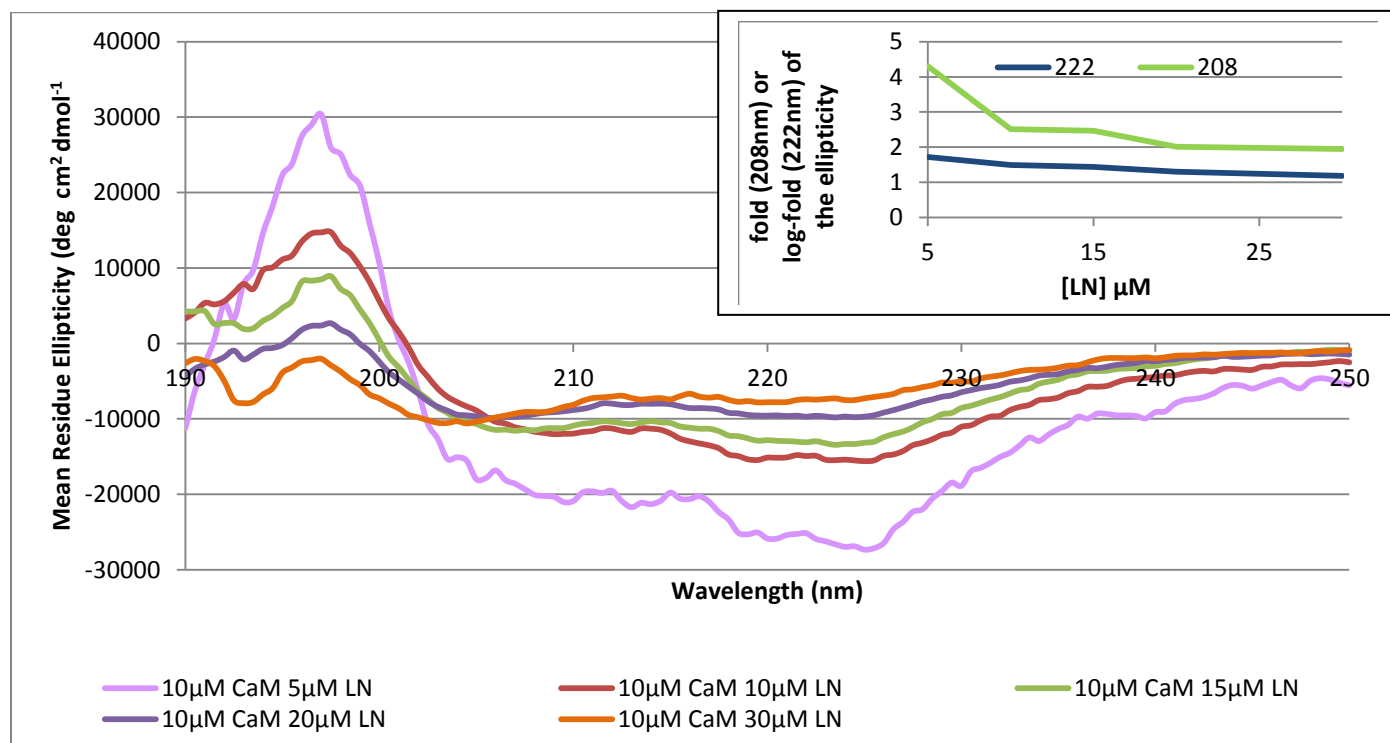
Figure 2.17: LN with CaM. Same methodology as Figure 2.15
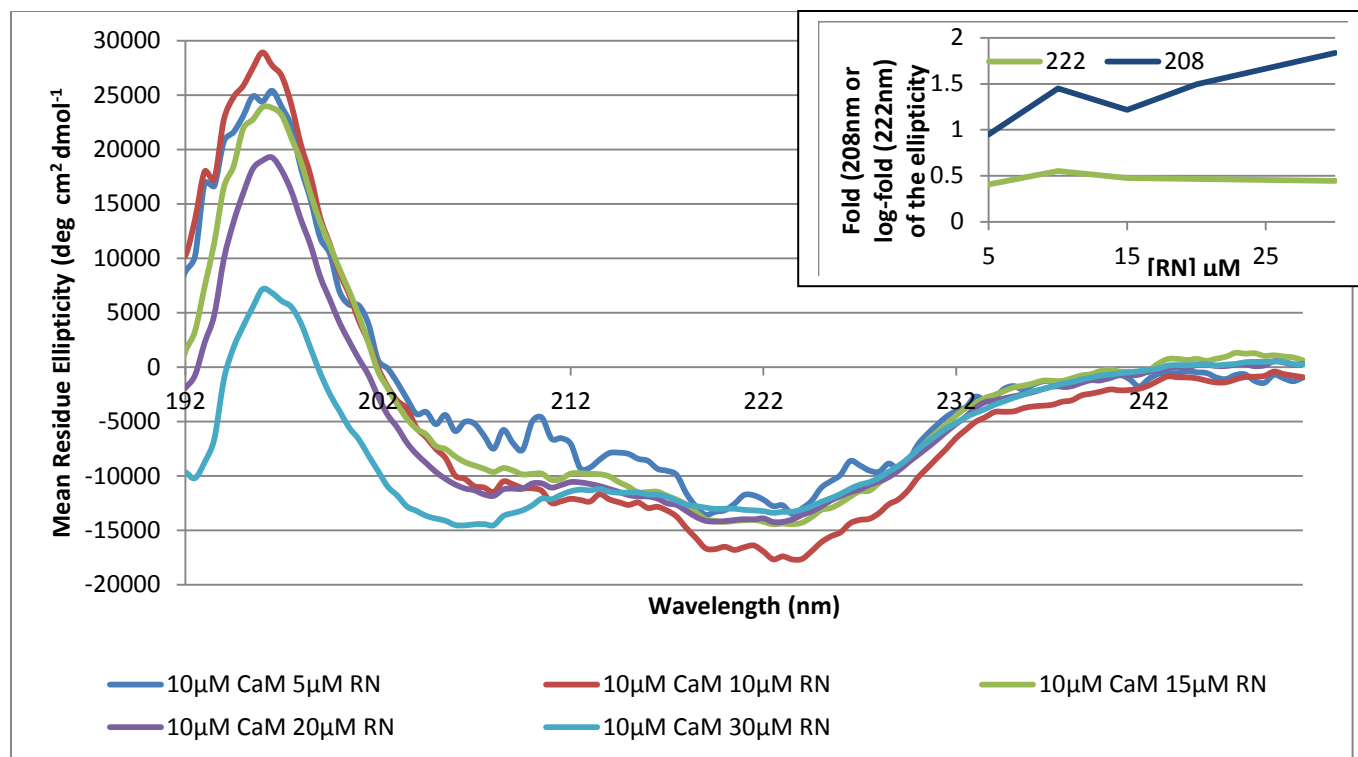
Figure 2.18: RN with CaM.
Same methodology as Figure 2.15
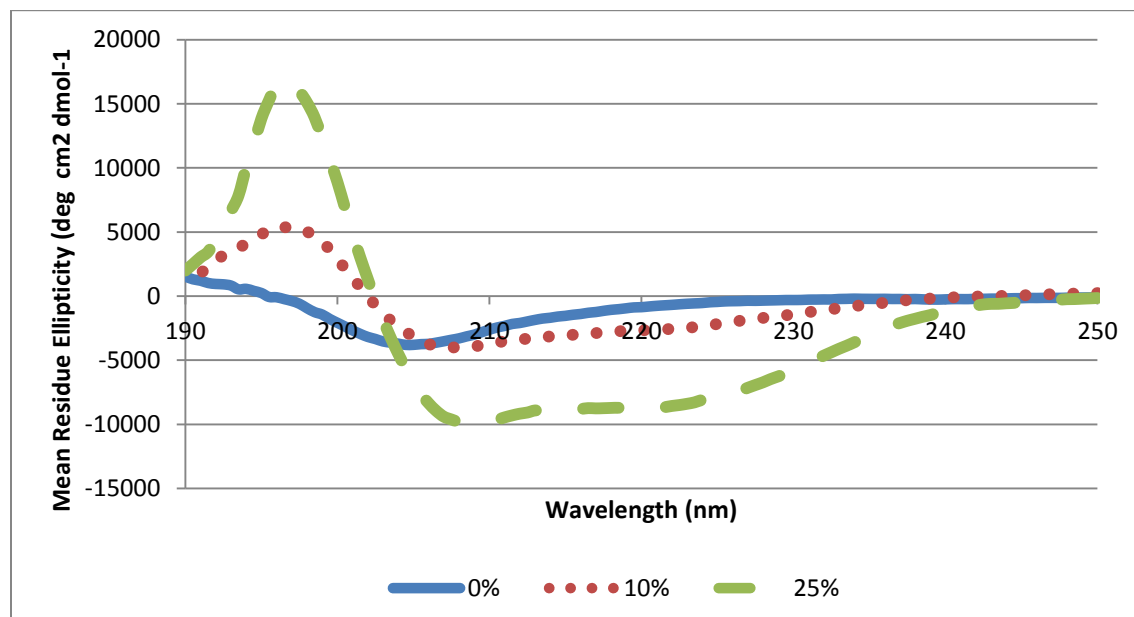
Figure 2.19: LIQ1 with TFE.
Trifluoroethanol (TFE) is an organic solvent used to induce alpha-helical transition in peptides (concentrations used in each trace are indicated). The 50% trace could not be obtained due to peptide aggregation. In all cases 50µM peptide was used.
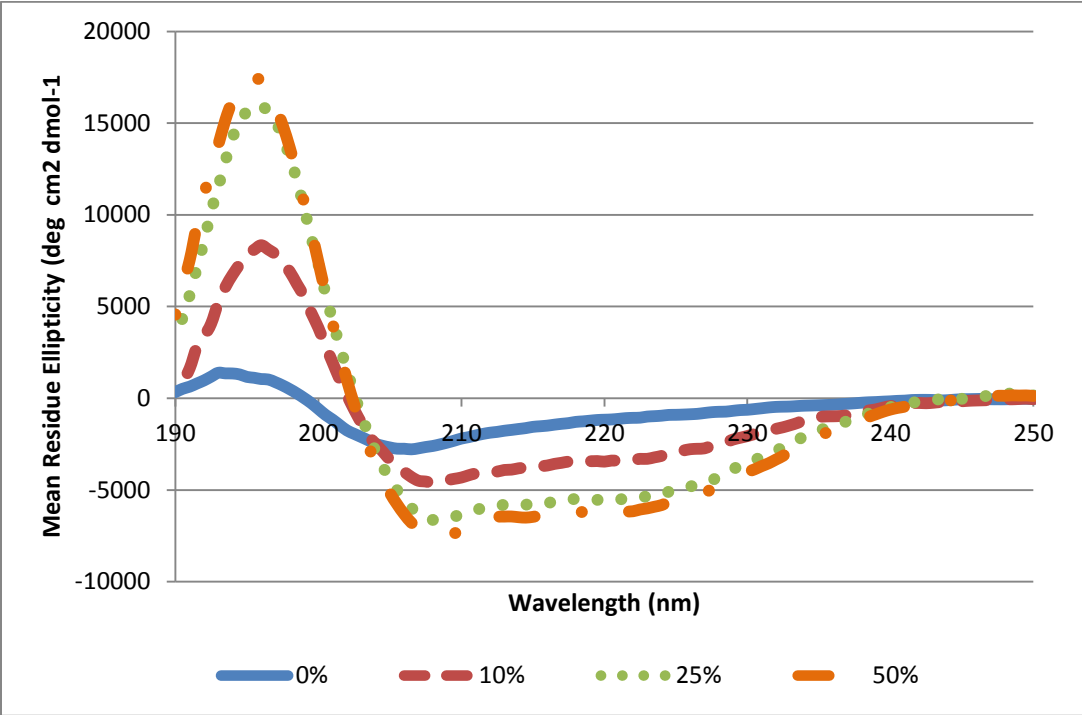
Figure 2.20: IQc with TFE.
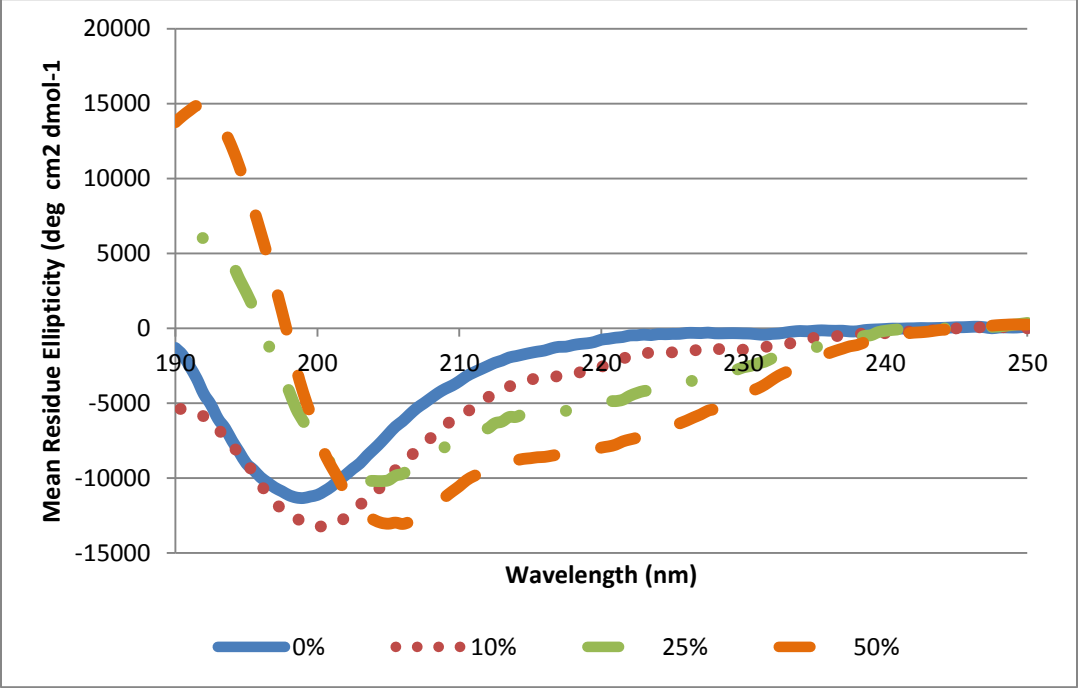
Figure 2.21: LN with TFE.
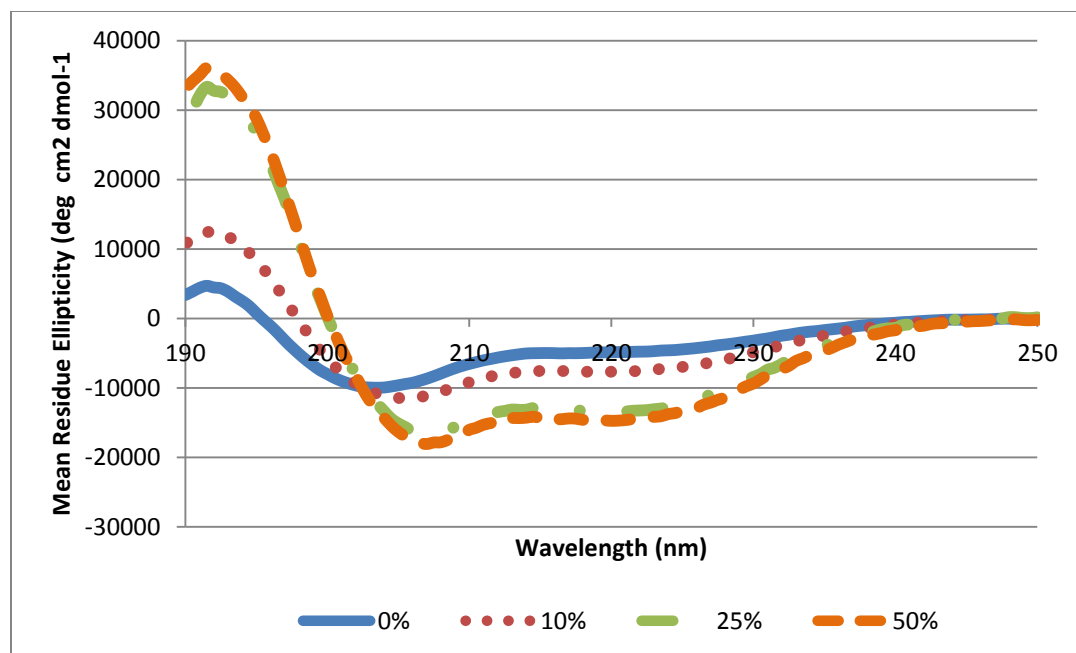
Figure 2.22: RN with TFE.

Table 2.4: Summary of CD results.
The K2D method was used for the fractional helical content calculation. Since the 50% TFE trace was not obtained with LIQ1, some of the calculations were not applicable.

Peptide	% α helix when free in solution (no TFE or CaM)	Maximum % α-helical content (50% TFE)	% of maximum at 10% TFE	% of naximum at 25% TFE	Maximum α-helical content (as%) with CaM
RN	9	41	49	93	58
LN	7	23	30	39	57
IQc	11	31	55	90	29
LIQ1	8	N/A	N/A	N/A	37

2.4 Discussion

The goal of the experiments in this chapter was to establish the existence of, and characterize, an invertebrate NSCaTE homolog from Ca_V1 of *Lymnaea stagnalis*. The effort was largely successful, and interesting new insights into the complex interaction scheme of CaM and L-type channels have been gained, although some findings raise new questions. The latter, and the attempts to answer them, are covered further in the next Chapter.

The conservation of the NSCaTE motif is far more extensive than previously thought; all but the most primitive (basal) metazoans possess an NSCaTE motif in one or more of their channels. Importantly, NSCaTE appears only to occur in L-type channels (but not all isoforms), all of which also contain a highly conserved IQ motif. This IQ motif only binds Ca^{2+}-CaM, unlike the canonical IQ motifs of myosins and Na_Vs, which bind apoCaM (Houdusse et al., 2006; Feldkamp et al., 2011). It is absent in *Drosophila*, but present in *Culicidae* (mosquitoes). NSCaTE is conspicuously absent in $Ca_V1.1$ and 1.4, all the more intriguing because those are 'unusual' L-type channels that do not exhibit the same kind of regulatory feedback (via CDI and VDI) as the 'canonical' L-type channels $Ca_V1.2$ and 1.3 (Peterson et al., 1999; Catterall, 2000; Zamponi, 2005; Striessnig, 2007; Griessmeier et al., 2009). They still possess an IQ motif, which is essential for the excitation contraction coupling role of $Ca_V1.1$ (Stroffekova, 2011), presumably also through an interaction with CaM. In contrast, no channel containing an NSCaTE but lacking an IQ motif is known to exist.

NSCaTE is somewhat atypical for a CaM binding target: it has a relatively low alpha-helical propensity on its own (or with TFE), yet a strong alpha-helical change with CaM (Brokx et al., 2001). The lack of a gel shift effect on CaM by NSCaTE binding can thus be explained by two possibilities. One, there is no conformational change in CaM upon NSCaTE binding

(consistent with the spectropolarimetry results). The other is that the affinity of NSCaTE for CaM is quite low and the fraction of CaM-bound NSCaTE (and the lifetime of the interaction) is too low to be detectable with a gel-shift method. While the results presented in this chapter lack a quantitative description for the affinities of NSCaTE and IQ motifs for CaM (to be addressed in the following chapter), there is clear evidence that both interactions do, in fact, occur. Gel shift data indicates that there is at least some level of competition occurring between the two peptides (or co-interaction, a question we sought to address further), with a clear interaction observed with the IQ motif and either a blocking effect or a weaker interaction occurring with the NSCaTE motif. Secondary structure changes in NSCaTE upon addition to CaM were consistent with a CaM interaction. Most indicative, however, was the strong blue-shift observed with tryptophan fluorescence in NSCaTE upon CaM addition, in a Ca^{2+}-dependent manner. The solubility enhancement of a mammalian NSCaTE fusion construct upon Ca^{2+}-CaM co-incubation is also solid evidence of a persistent CaM binding. Exposed hydrophobic residues in the construct likely contribute to its aggregation; masking of these hydrophobic regions by CaM is the most likely explanation for this effect.

It is possible that NSCaTE fine-tunes CDI, principally acting in response to large Ca^{2+} influxes from prolonged opening or high local density of L-type channels (such as in synapses). This is strongly supported by our results; removal of NSCaTE from LCa_V1 renders it insensitive to internal buffer conditions, and modestly reduces the recovery from inactivation in Ca^{2+} after a prolonged depolarization. This is consistent with previously published NSCaTE deletion and CaM mutant experiments in mammalian channels (Ivanina et al., 2000; Dick et al., 2008; Benmocha et al., 2009; Asmara et al., 2010; Guo et al., 2010). Thus, NSCaTE fulfills the presumed role of a 'global' Ca^{2+} sensor, likely via the less-Ca^{2+} sensitive N-lobe of CaM.

Meanwhile the IQ motif is arraigned as the 'first responder' to transient Ca^{2+} pulses in the immediate channel vicinity, due to its relatively slower off-rate for Ca^{2+} (Tadross et al., 2008). The crystal structure of $Ca_V1.2$ IQ motif bound to CaM shows a parallel (unusual for IQ) orientation with both lobes bound, and half CaM/IQ calorimetric titrations suggest a preference for the C-lobe (Van Petegem et al., 2005). Whether a N(0)-C(2) Ca^{2+} CaM[17] conformation is actually found bound to the IQ motif *in vivo* remains questionable; live-cell FRET studies with large fluorophores (GFP variants, all much larger than CaM) are unlikely to be true representations of a native conformation. Furthermore, it is unclear what constitutes a 'physiological' level of buffering: 0.5mM EGTA is an arbitrary number (the relative amounts of free and bound cellular Ca^{2+} at any given time are controlled by a myriad of factors, from high capacity 'buffer' proteins to Ca^{2+} pumps in both plasma and organellar membranes), and is compounded by the artificial recording conditions. While the relative effects of 'high' and 'low' internal EGTA appear to play a significant role on L-type CDI, the extent of the buffer effect and its relationship with NSCaTE and CaM lobes may be much greater *in vivo*, under native conditions – but quite challenging to actually determine. It is plausible to consider NSCaTE as a secondary switch or 'safeguard' for neurons and cells that are highly electrochemically active, where it can prevent excess Ca^{2+} influx when intracellular levels reach a certain threshold. In this regard, it would be interesting to determine if there is indeed a tissue-biased distribution of L-type channel variants of the same isoform with and without NSCaTE, if the translational regulation (alternate start sites) we observe is indeed physiologically significant. Of course, this would require extensive immunohistochemistry profiling with very specific sets of antibodies: a minimum of a Master's level project all in its own.

---

[17] Here the notation represents the number of Ca^{2+} ions in the indicated lobe, e.g. 0 in the N-lobe and two in the C-lobe

2.5 Conclusions

The primary objective of this chapter was to investigate the *Lymnaea* NSCaTE homolog as a functional regulatory motif of LCa$_V$1, and verify its role in CDI to be similar to that of mammalian NSCaTE. This was indeed accomplished, as we have shown a strong buffer-sensitive component of CDI imparted to LCa$_V$1 by its own NSCaTE, which is qualitatively different from what is seen in the mammalian isoforms (Ca$_V$1.2 and 1.3) by (Dick et al., 2008). Nonetheless, there is a clear interaction between CaM and *Lymnaea* NSCaTE, and even a possibility for co-interaction between NSCaTE, IQ and CaM although we lack concrete evidence for such a complex. We see a possibility of a chaperone effect of CaM due to the improved solubility profile of an NSCaTE-HIS fusion construct when exogenous CaM is applied during refolding. Further experiments with full channel expression as a function of NSCaTE truncation will be necessary to confirm this.

There appears to be a fundamental difference in how NSCaTE and IQ motifs bind CaM; this can be seen with both the native PAGE gel shift and spectropolarimetry results. While CaM exhibits a strong shift in native PAGE with IQ peptides, it does not alter its mobility with NSCaTE to an observable extent. This might suggest that while CaM essentially 'wraps around' the IQ motif, it binds NSCaTE with a much subtler conformational change – perhaps even with a single lobe. A detailed solution structure of CaM-NSCaTE has not yet been published, but solving one may be a possibility in the future.

Additionally, we show that nearly every NSCaTE-containing L-type isoform has a downstream Met that could potentially serve as an alternative start site, resulting in an optional NSCaTE motif that is translationally regulated (we see no difference at the transcript level). In

essence, NSCaTE may serve as a fine-tuning element in CDI that is both tissue and isoform-specific, possibly as a failsafe against excessive Ca^{2+} entry into the cell.

Chapter 3: Thermodynamic analysis of CaM binding to IQ and NSCaTE peptides

3.1 Introduction and Summary

Based on the results of experiments presented in Chapter 2, where we show NSCaTE binding to CaM using gel-shift and fluorescence, the next step was to quantitate this interaction and its thermodynamic parameters using isothermal calorimetry and Ca^{2+}-deficient CaM mutants (CaM_{12}, CaM_{34}). These mutants have critical D$\rightarrow$A substitution in the indicated EF hands (e.g. hands 1 and 2 for CaM_{12}, etc.), thus impairing Ca^{2+} binding in one or both lobes. Experiments with these mutants allowed us to dissect the interaction with L-type channel peptides in detail and to test the relevance of the local-global model[18] to the relative contributions of IQ vs. NSCaTE, based on their CaM lobe preference and relative affinity. We also attempted to determine whether the two peptides could bind CaM simultaneously, although due to a very weak and transient interaction between CaM and NSCaTE, only indirect supporting evidence could be obtained (with ITC).

3.1.1 Isothermal Calorimetry of L-type peptides

Isothermal calorimetry is a biophysical technique used for characterizing the association or disassociation of macromolecules, typically proteins and their ligands, or protein-protein complexes. It relies on the summative changes in the enthalpy of reactants and products, and the total change in system heat; entropy can be inferred from knowing the enthalpy and binding constant. The instrument is described in Figure 1.1. The heat in this case is measured indirectly; the ITC_{200} system uses a specific reference power, which is set by the user (range from 0-

---

[18] Proposed originally by Yue and Tadross (DeMaria et al., 2001; Dick et al., 2008; Tadross et al., 2008)

12μcal/s) that is supplied to both the sample and the reference cell. Deviations from the reference power due to the sample cell either requiring less (for exothermic binding) or more (for endothermic binding) heat to maintain at the set temperature is reflected in the direction of the injection peaks. The peaks are integrated and with the information regarding the concentration of the ligand in the cell, and the protein in the syringe, the experiment is plotted as μcal vs μmol injectant, typically forming a sigmoidal plot. OriginLab, SigmaPlot or similar fitting software with functions pertaining to relevant kinetic models[19] can then be used to fit the resulting data through iterative least-squares type regression. From one experiment, all the relevant interaction data can be obtained: stoichiometry (N), affinity (K_d or K_a), and the enthalpy (ΔH) and entropy (TΔS) associated with the binding. The equation for the corrected heat observed during an injection is:

$$Q_{corr} = Q_{meas} - Q_{dil,ligand} - Q_{dil,macromolecule} - Q_{blank}$$

Where Q_{corr} is the actual heat associated with the binding from one injection, Q_{meas} is the measured heat on the instrument, $Q_{dil,ligand}$ is the heat associated with the dilution of ligand upon being titrated into the cell, $Q_{dil,macromolecule}$ is the small heat associated with the dilution of the macromolecule in the cell, and Q_{blank} is the heat associated with the friction from buffer molecules mixing (buffer into buffer injections), which should be negligible in most cases. Often the correction can be done by subtracting the baseline heats which occur after saturation of the macromolecule with ligand. Errors in software fitting can be mostly avoided by constructing a proper baseline.

The heat per injection (Q_{inj}) can be used to determine the enthalpy ΔH:

---

[19] Standard models are 'one set of sites', 'two sets of sites', 'dissociation' or 'competitive binding'; more complex kinetic models have to be written by the user

$$\Delta H = \frac{Q_{inj}}{V_{inj} \times [ligand]}$$

The stoichiometry is roughly the x-coordinate where the slope of the titration curve is maximal. The relationship describing the shape of a simple single binding event isotherm ('one-set-of-sites' model) can be expressed as:

$$\Theta_j = \frac{[L]K_j}{1 + [L]K_j}$$

$$L_t = [L] + P_t \sum_{j=1}^{k} (n_j \, \Theta_j)$$

where Θ_j is the fraction of site j occupied by ligand, L_t is the total ligand concentration, [L] is the free ligand concentration, P_t is the total macromolecule concentration, K_j is the binding constant of process j, and n_j is the total stoichiometric ratio for process j, each of the equations is defined for all potential binding sites, and solutions for any number of sites can be defined. Substitution of Θ_j from the top equation into the bottom one yields a (k + 1) degree polynomial. Thus, to solve for a one-set-of-sites process, roots of a second degree polynomial must be found (Freyer and Lewis, 2008). Origin is capable of solving up to third degree polynomials, more complex models likely have to be fitted with at least some of the parameters known (or at least empirically estimated). Solving for [L] allows one to find Θ_j:

$$Q = P_t V_0 \left(\sum_{j=1}^{k} n_j \, \Theta_j \Delta H_j \right)$$

Where Q is the total heat evolved in the process j, V_0 is the initial volume of the sample cell and ΔH_j is the molar enthalpy for process j. Using a non-linear least squares regression on the differential heats for each injection one can fit the parameters K, N and ΔH, to which the universal gas law can be applied to obtain TΔS.

Weakly binding ligands require a much higher experimental concentration to get a good fit than high affinity ligands; however the downside of the latter is that depending on the heats of injection, it is often difficult to have a dilute enough sample to get a good signal-to-noise ratio, especially if the enthalpy of reaction is low. The 'c-value' or $N \cdot K_d \cdot M_t$ (where M_t is the total macromolecule concentration, N is the stoichiometry and K_d is the affinity of binding) defines how 'good' the curve is (how amenable to being fitted) and should fall in the range of 1 to 1000 for reliable K_d calculation (Turnbull and Daranas, 2003; Broecker et al., 2011), which puts a practical limit on direct K_d determination for very high-affinity and/or low enthalpy binding. In contrast, very weak binding requires ligand/ macromolecule concentrations that are not achievable or practical in the typical micro-calorimeter, such as the ITC_{200}. Fortunately, such weak interactions (>50µM) between proteins are not usually biologically relevant, at least in the context of CaM interactions. For very high-affinity interactions, it is sometimes possible to determine the K_d indirectly, by having a known concentration of a competing ligand with a precisely known K_d in both cell and syringe, thus reducing the apparent K_d for the experiment and enabling the back-calculation of the actual K_d.
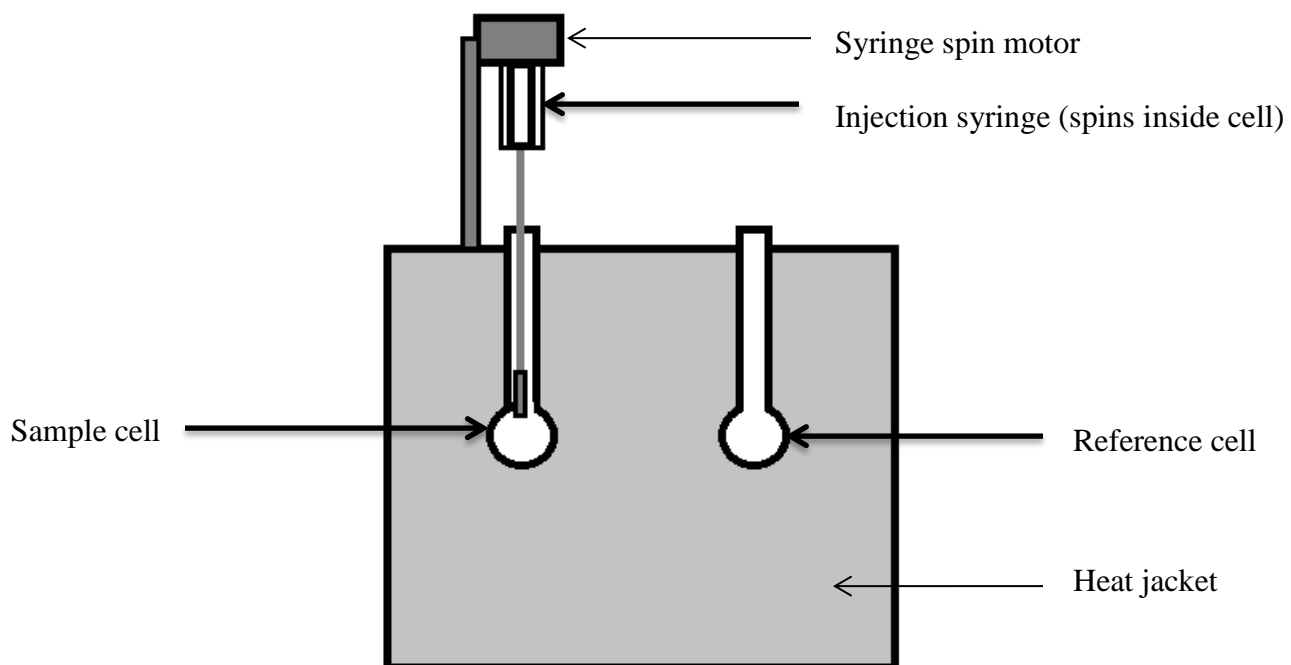
Figure 3.1: The typical components of a calorimeter; not to scale.

3.1.2 Nuclear Magnetic Resonance Spectroscopy (NMR)

One of the two most common techniques in macromolecular structure determination is solution

NMR, in which the macromolecule under study is analyzed in native or near-native conditions

(contrary to X-ray crystallography). While high degree of conformational flexibility and

movement impedes accurate structural assignment by NMR, it can yield information on which

areas of the protein are constrained as a result of binding to a target during titration. Furthermore,

the degree of solvent exposure under different conditions can yield information regarding the

solvent-accessible surface area (SASA), which can be used as an indirect measure of target

binding. Finally, full residue assignment of a multi-dimensional NMR spectrum or of a

combination of several spectra can lead to a high-resolution atomic structure of the

molecule/complex.

The theoretical basis of the methodology in NMR is quite complex and will not be fully

explained here; however, a basic introduction to the concepts will be attempted.

The basis of an NMR signal is the free-induction decay (FID) that occurs when a

transverse magnetization applied via a radio frequency or RF pulse to nuclei that aligned within a

strong external magnetic field. The resulting change in the spin precession of magnetically active

(spin $I > 0$) nuclei is temporary, but since the oscillation ('transverse relaxation') is very well-

defined by a specific frequency, it can be amplified and detected, and then Fourier transformed

to give a single Lorenzian peak. This peak is the basis of the 'chemical shift' often discussed in

NMR literature, which is standardized for every nucleus type and can be looked up from a table

to assist in residue assignment. Shielding from magnetic fields by aromatic electrons, as well as

spin-spin coupling of neighboring nuclei, all have an effect on chemical shifts which can be used

to correlate them and also disperse the spectra of larger proteins with many instances of the same

amino acid. Using several different pulse sequences such as heteronuclear single quantum correlation (HSQC), total correlation spectroscopy (TOCSY) and Nuclear Overhauser Effect Spectroscopy (NOESY), multi-dimensional spectra can be generated with several connections for the same nucleus (typically at least 2 different experiments are needed). The coupling can then be traced in a 'connect-the-dots' manner to assign the backbone nuclei, which can then be used to determine basic secondary structure using dipole couplings and knowledge of torsion angle constraints. Subsequently, through-space interactions (via NOESY) can be used to find non-bonded neighboring nuclei and a more detailed higher-order structure can be solved. The larger the number of NOEs and angle/distance constraints, the higher the quality of the structure that can be obtained. More generally, changes in chemical shifts of specific amino acids in a sequence can be indicative of a structural shift, possibly due to an interaction with a target peptide or protein. This can be observed with a simple HSQC with ^{15}N and/or ^{13}C labeled proteins/peptides, which correlates the amide protons and nitrogen nuclei. Here, we use such information to discern the structural changes for each L-type channel peptide interaction with CaM.

The HSQC spectra used in this and next chapter were acquired by Michael Piazza (Ph.D. candidate).

3.2 Methods

3.2.1 Isothermal Titration Calorimetry

All titrations were performed at 25ºC using 0.5x gel filtration buffer (25mM Tris-Cl pH 7.5, 75mM NaCl) with added 1mM $CaCl_2$ to avoid buffer artifacts and because peptide stocks were made up in MQ water, while CaM stocks were stored in gel filtration buffer after purification.

Mutant CaM concentrations were determined using a Bio-Rad Bradford assay with wild type

CaM used as a standard, using a modified Bradford method (Ernst and Zor, 2010). Depending on

the expected K_d and stoichiometry, the starting concentrations for cell and syringe varied from

10 to 50 µM and 100 to 500 µM, respectively. Most experiments involved between 20 and 30

injections of 1.2 to 1.8 µL at 2-3min intervals. L-type channel peptides with wild type CaM were

titrated at a reference power of 11µcal/s; mutant CaMs were done at 5µcal/s. In all cases, high

feedback gain and 1000rpm stir speed were selected. Mutant CaM experiments were performed

in a 5mM HEPES (pH 7.0) with 1mM $CaCl_2$ buffer, while for wild type CaM experiments the

gel-filtration buffer at half strength (25mM Tris-Cl pH 7.5, 75 mM NaCl) with 0.5 mM $CaCl_2$

was used. HEPES appears to have a lower background heat, which was beneficial for titration of

weakly interacting peptides.

Table 3.1: L-type peptides and their properties.
All peptides were synthesized by Genscript except RN, which is from CanPeptide, and specified to >98% purity and mass spectrometry verified.

Name	Origin	Sequence	MW	pI
RN	rat NSCaTE (Ca_V1.2 or α1c)	SWQAAIDAARQAKLMGS	1804.07	8.46
LN	snail NSCaTE (LCa_V1)	GWSTALAAAQGAATVRK	1658.89	11
IQc	rat α1c IQ (Ca_V1.2), L-type 'cardiac'	KFYATFLIQEYFRKFKKRKEQ	2799.34	10.12
LIQ1	snail L-type IQ (LCa_V1)	KFYATFLIQDYFRRFKKRKEQ	2813.27	10.28
IQa	rat α1a IQ (Ca_V2.1) or P/Q type	KIYAAMMIMEYYRQSKAKKLQ	2799.34	9.87

3.2.2 Purification of Ca^{2+}-deficient CaM proteins.

Since the interaction of CaM with hydrophobic interaction chromatography (HIC) media

depends on its exposure of the hydrophobic residues upon Ca^{2+} binding, the phenyl-sepharose

method is not nearly as efficient for the purification of $CaM_{12/34/1234}$. Instead, we used a

combination of ion-exchange chromatography and subsequent gel-filtration. The latter method is identical to the one described in Chapter 2. For ion exchange, a Q-sepharose (quarternary ammonium) 6mL column from Pharmacia (now GE Healthcare) was used. Lysis and low salt buffer were 5 mM bis-tris pH 6.0 with no Ca^{2+} or EDTA. Lysis buffer also had DTT added to 1 mM final concentration to maintain CaM's methionines in the reduced state. $CaM_{12, 34}$ and $_{1234}$ (in pET28a) were expressed and harvested the same way as wild type CaM (see section 2.2.2). Cells were lysed using the Avestin Emulsiflex homogenizer (>15000 psi), clarified by centrifugation at ~ 50000 g and applied to the column (ion exchange was done using the AKTA FPLC system, same as for gel filtration chromatography). The column was then briefly washed with low salt buffer (5-10 column volumes), and a shallow salt gradient was applied (100mM NaCl over 10 column volumes). Subsequently the column proteins were eluted with a steep gradient (1.6M NaCl over 2 CVs, held for 2 more CVs), after which the column was re-equilibrated or cleaned. The resulting fractions were analyzed by SDS PAGE and absorbance at 278nm, best candidates pooled and concentrated using YM-10 spin columns (Millipore) and further purified by gel filtration chromatography (section 2.2.2). Purity of the CaM proteins was confirmed by SDS PAGE and ESI MS and their concentrations were determined using the modified Bradford assay (Ernst and Zor, 2010) (with wild type CaM as the standard), aliquotted and stored in gel filtration buffer at -80℃.

3.2.3 NMR spectroscopy

CaM for NMR experiments were expressed in M9 minimal media (11.03 g/L $Na_2HPO_4 \cdot 7H_2O$, 3.0 g/L KH_2PO_4, 0.5 g/L NaCl, 2 mM $MgSO_4$, 0.1 mM $CaCl_2$, 5 mg/mL thiamine, 100 μg/mL kanamycin) containing 2 g/L ^{13}C-glucose and 1 g/L $^{15}NH_4Cl$. ^{13}C-^{15}N CaM was purified as

described above. The samples were prepared for NMR experiments via a buffer exchange into

NMR solution (100 mM KCl, 10 mM $CaCl_2$, 0.2 mM NaN_3, 90% H_2O/10% ^2H_2O) at pH 6.0

using a YM10 centrifugal filter device (Millipore Corp., Billerica, USA). All NMR samples

contained 300μM CaM in a total volume of 500 μL. The samples were transferred into 5 mm

NMR sample tubes and stored at 4^oC until required for NMR experiments. NMR experiments on

the complexes were conducted on CaM samples titrated with each peptide to saturation in a 1:1

CaM:peptide ratio. Complex formation was monitored after each addition by acquisition of a ^1H-

^{15}N heteronuclear single-quantum coherence (HSQC) pulse sequence. NMR spectra were

recorded at 25^oC on Bruker 600 and 700 MHz DRX spectrometers equipped with XYZ-gradients

triple-resonance probes (Bruker, Billerica, MA, USA). Spectra were analyzed using the program

CARA (Computer Aided Resonance Assignment) (Keller, 2004).

3.3 Results

Within the first few experiments involving wild type CaM and NSCaTE (both rat and snail) it

was noted that an unusual 2 : 1 (peptide : CaM) stoichiometry was present in every titration.

Upon further analysis and using competition titrations with IQ peptides, it was determined to be

an authentic interaction stoichiometry, and not an experimental or concentration error-related

artifact. Furthermore, subsequent nuclear magnetic resonance (NMR) experiments with NSCaTE

and CaM revealed a similar result, that is, complete signal shift saturation occurring only after

approximately 2 equivalents of peptide were added. Shortly before writing the manuscript

explaining these unusual results (Taiakina et al., 2013), a paper was published by Liu and Vogel

(2012) that provided a structure of each CaM-lobe individually bound to an NSCaTE peptide,

thus supporting our results. In fact, they were unable to actually determine a structure of intact

holo-CaM with 2 peptides, due to 'severe peak broadening', which we suspect is the result of a

rapid on-off equilibrium between free and CaM-bound peptide, as well as the distinct structural changes associated with binding of NSCaTE to the two sites.

In an attempt to determine unambiguously the effects of individual CaM lobes on L-type peptide binding, titrations with Ca^{2+}-deficient CaM mutants were performed. Additionally, competition experiments where either NSCaTE or IQ peptide was first pre-bound to CaM at 1 : 1 (or 2 : 1 in the case of NSCaTE : CaM) stoichiometry and the competing peptide titrated in (Figure 3.4). We also used the Ca^{2+}-deficient CaM mutants CaM_{12} and CaM_{34} to perform the same pre-bound peptide competition titrations to determine the relative lobe/Ca^{2+} preference of the two peptides (Table 3.2).

For the apo-CaM experiments, to ensure that no Ca^{2+} was bound to even just the C-lobe of CaM, a low background concentration of EDTA was used (up to 1mM) and CaM stock was buffer exchanged into water. While these experiments were successful for NSCaTE peptides, the IQ peptides apparently interact with EDTA and precipitate out of solution, likely owing to their extremely high isoelectric point (>10). Anecdotally, the same kind of aggregation was also seen when an inorganic acid buffer was used (sodium phosphate, as low as 10mM). This seems to support the idea that the IQ peptides are essentially forming insoluble salt complexes via their Arg and/or Lys residues. Such an interaction has also been shown between calcitonin (a small peptide hormone) and EDTA; interestingly, calcitonin is also known to bind CaM (Seyferth and Lee, 2003). Aggregation was not diminished in either EGTA or BAPTA. Reducing peptide concentrations and EDTA concentration alleviated the issue to an extent, but due to the sensitivity of ITC and the fitting algorithm, the EDTA-CaM titrations with IQ peptides were questionable. Instead, we opted to use the CaM_{1234} mutant as a proxy for apoCaM.

3.3.1 Isothermal Calorimetry

3.3.1.1 Wild type CaM

There was no interaction between NSCaTE and CaM in the presence of 1mM EDTA. In the presence of Ca^{2+}, both rat and snail NSCaTE (RN and LN, respectively) bound CaM with a 2 : 1 (NSCaTE : CaM) stoichiometry and weak affinity (~1.2 μM for rat and ~13 μM for snail NSCaTE). Both NSCaTE peptides had a much lower (over an order of magnitude higher K_d) affinity for CaM than their respective IQ peptides (Table 3.2, also Figure 3.2). As expected, both rat and snail IQ peptides had very similar affinity for CaM (sub-micromolar) and 1 : 1 stoichiometry. All L-type peptides were found to be exothermic (negative ΔH) and had very weakly negative (mammalian) or positive (snail) entropy (ΔS), indicating that the interaction is primarily enthalpy-driven (Table 3.2). Enthalpy changes are often associated with electrostatic interactions and hydrogen bonding; this suggests a hydrophilic character of NSCaTE/CaM/IQ interactions. EDTA appears to form insoluble complexes with IQ peptides, thus we were unable to determine if wild type apo-CaM binds IQ peptides by ITC. Instead, we used CaM_{1234} (with all four EF hands containing a critical D➔A mutation) which is unable to bind Ca^{2+}. It was found to be incapable of binding either IQc or LIQ1 at a detectable level.
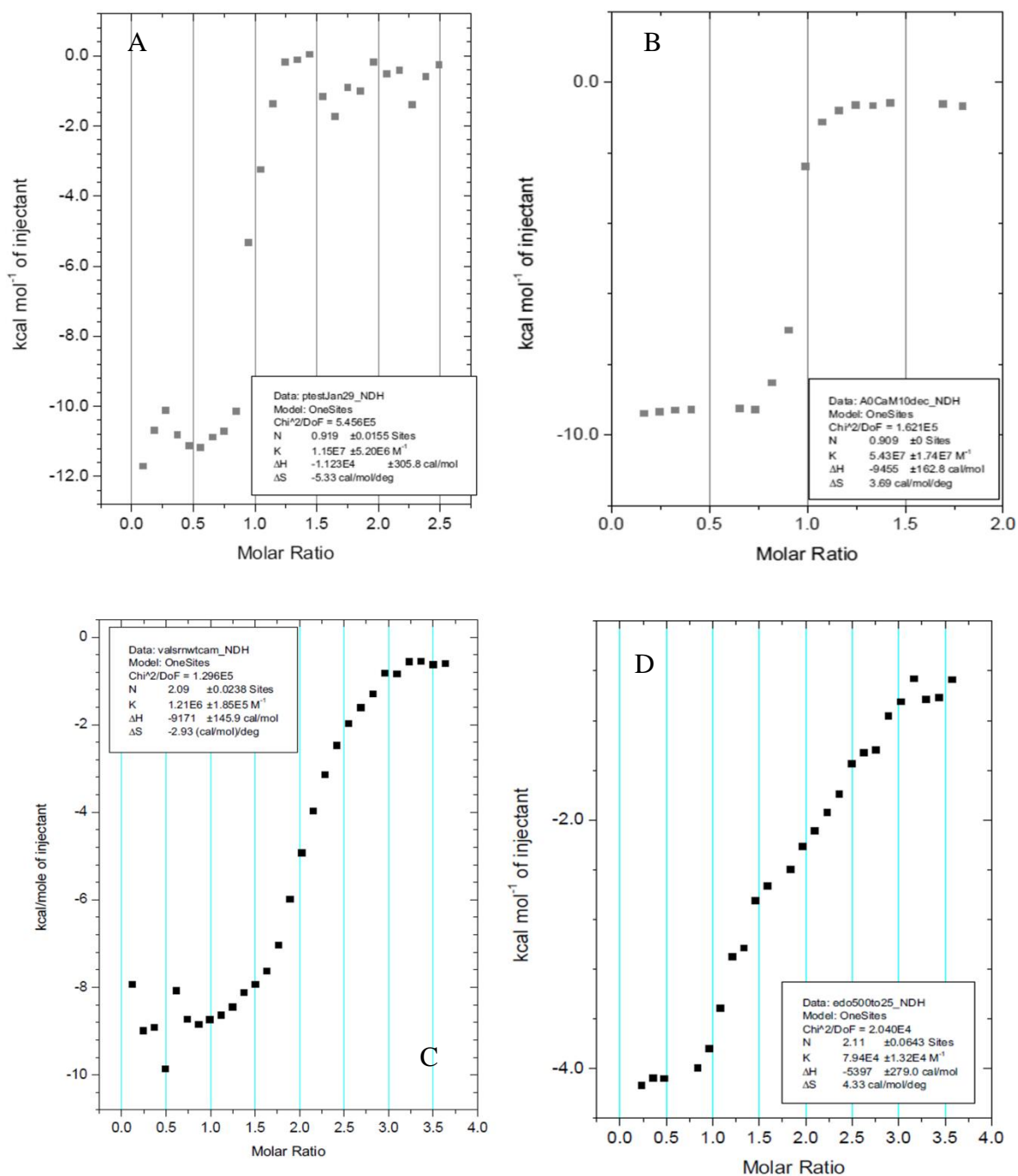
Figure 3.2: Representative ITC results from wild type CaM and L-type peptides.
Each panel contains the integrated peak heats as a function of added titrant (peptide): **A**): IQc (500 μM) into WT CaM (50 μM). **B**): LIQ1 (100 μM into 10 μM). **C**): RN (500 μM into 25 μM). **D**): LN (500 μM into 50 μM). All experiments fit the one-set-of-sites model in OriginLab. Each experiment was repeated at least twice.

3.3.1.2 Competition experiments with wild type CaM

To elucidate the relevance of CaM binding to NSCaTE (and the 2 NSCaTE : 1 CaM stoichiometry) as well as test the possibility that both peptides might be binding CaM simultaneously, competition experiments were performed. The ITC sample cell was filled with an equimolar solution of CaM and peptide (either IQ or NSCaTE), and the opposing peptide titrated in to saturation. The results indicate that the stoichiometry for both peptides when titrated in this way (regardless of order) is 1 : 1, and the binding constants are relatively unaffected, strongly supporting a case for co-interaction (see Figure 3.4). These results indicate that CaM can bind the NSCaTE peptide at two different sites, but not if one of these sites is already occupied by an L-type IQ peptide.

In addition, the NSCaTE 'knock-in' effect (see section 2.1.3), for which the motif was named (Dick et al., 2008), was tested by a competition analysis with the IQ peptide from a rat P/Q-type channel ($Ca_V2.1$), which bears little resemblance to L-type IQ peptides (Table 3.1). There is strong evidence that the previously described transforming effect of NSCaTE (on $Ca_V2.2$ channels) is due to its ability to out-compete the weaker binding IQ motif of this channel. We tested the IQa peptide ($Ca_V2.1$) for its interaction with CaM, by ITC and by gel shift experiments, and found that despite a strong gel-shift, its affinity for CaM is low (~1µM) and it is readily displaced by NSCaTE. Additionally, we see a 2 : 1 stoichiometry for IQa : CaM, and a persisting 2 : 1 stoichiometry for NSCaTE when titrated into CaM pre-bound to IQa, suggesting that NSCaTE fully displaces it from CaM (see Table 3.2 and Figure 3.3). No interaction was observed when IQa was titrated into CaM pre-bound to NSCaTE (data not shown). Effectively, this proves that the 'transforming' effect of NSCaTE is due to its ability to displace the native IQ peptide of non-L-type channels from CaM. Additional implications are discussed below.
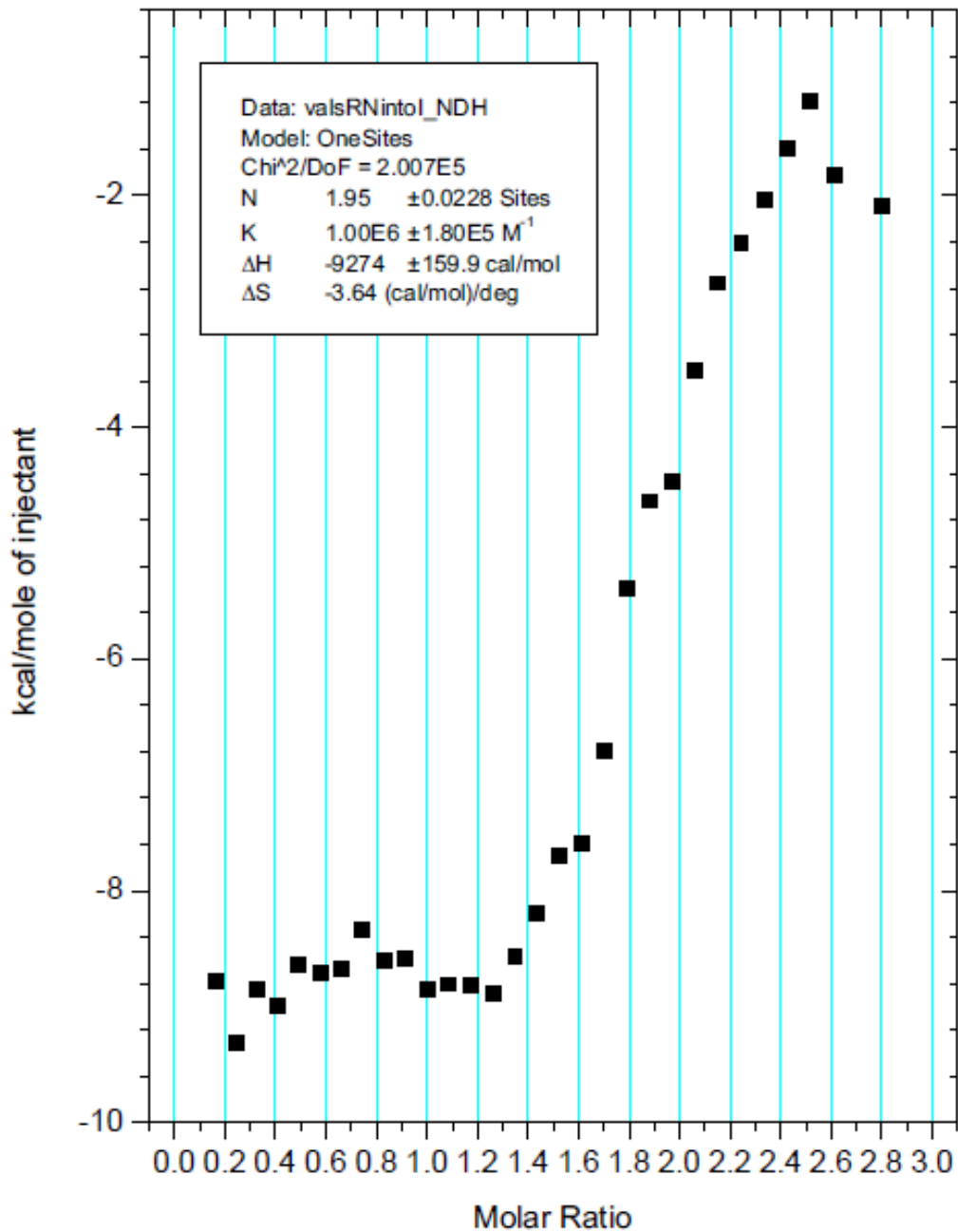
Figure 3.3: NSCaTE (RN) fully displaces the P/Q IQ (IQa) peptide from CaM.
500 μM RN was titrated into 30 μM CaM pre-bound with 30 μM IQa. The resulting isotherm fits the one-sites model in Origin, with an N of approximately 2, and a Kd of $\approx 1.0 \pm 0.18$ μM.

A

kcal mol⁻¹ of injectant → $kcal\ mol^{-1}$ of injectant

Data: IQIQ1x30uM_NDH
Model: OneSites
Chi^2/DoF = 9.184E4
N   0.977   ±0.0169 Sites
K   5.52E5 ±7.69E4 M⁻¹
ΔH   -9366   ±215.0 cal/mol
ΔS   -5.14 cal/mol/deg

Molar Ratio

B

kcal mol⁻¹ of injectant

Data: A1xRN1x30u_NDH
Model: OneSites
Chi^2/DoF = 3.179E5
N   1.06   ±0.0163 Sites
K   7.56E6 ±2.81E6 M⁻¹
ΔH   -1.081E4   ±285.9 cal/mol
ΔS   -4.76 cal/mol/deg

Molar Ratio

C

kcal mol⁻¹ of injectant

Data: A0CtrlJan1_NDH
Model: OneSites
Chi^2/DoF = 1.356E4
N   1.00   ±0.234 Sites
K   2.92E4 ±7.35E3 M⁻¹
ΔH   -7989   ±2352 cal/mol
ΔS   -6.37 cal/mol/deg

Molar Ratio

D

kcal mol⁻¹ of injectant

Data: A0CaM10dec_NDH
Model: OneSites
Chi^2/DoF = 2.752E5
N   0.910   ±0.0102 Sites
K   5.26E7 ±2.31E7 M⁻¹
ΔH   -9398   ±214.0 cal/mol
ΔS   3.82 cal/mol/deg

Molar Ratio

Figure 3.4: Competition experiments with L-type peptides and wtCaM.
A): RN (500μM) into CaM prebound to IQc (both at 30μM). B): IQc (100 μM) into CaM prebound to RN (both 10μM). C): LN (500μM) into CaM prebound to IQc (30μM both). D): LIQ1 (100μM) into CaM prebound to LN (10μM both). We were unable to get a curve that could be fitted with LN into LIQ1+CaM, likely due to its low affinity for CaM; however the LIQ1 and IQc sequences and their properties are very similar.

124

3.3.1.3 EF hand CaM mutants

To elucidate the contribution of each CaM lobe and dissect the putative NSCaTE-IQ-CaM complex, we used CaM mutants incapable of binding Ca^{2+} in either the N- or C- terminal EF hands (CaM_{12} and $_{34}$, respectively). These mutants have critical aspartate to alanine substitutions in their Ca^{2+}-coordinating residues (D21A and D56A for the N-lobe, and D93A + D131A for the C-lobe), and approximate the Ca^{2+}-deficient states of CaM. In addition, CaM_{1234}, in which all four mutations are present, is often used as an apo-CaM proxy, although its *in vivo* relevance and conformational fidelity have become controversial (Jurado, 1999; Xiong et al., 2010). We find that both CaM_{12} and CaM_{34} are capable of binding to both IQ and NSCaTE peptides, albeit with varying effects on K_d and N; most notably, the stoichiometry of NSCaTE with either lobe mutant is altered to 1 : 1, meaning that each lobe is capable of binding an NSCaTE peptide independently, and only when bound to Ca^{2+} (see Table 3.2). This was concurrently confirmed by a structural study (Liu and Vogel, 2012), which also found a preference of NSCaTE for the N-lobe of CaM (with ITC).

Both L-type channel peptides have similar or even slightly higher affinity for CaM_{12} compared to wild type CaM (Table 3.2 and Figure 3.6). The titrations were done in HEPES to reduce the background associated with (de)protonation heat effects. The entropy term (ΔS) for IQc with CaM_{12} is actually slightly larger and positive (as opposed to wild type CaM), which might suggest that the N(0)-C(2) Ca^{2+} CaM conformation is the preferred mode of binding to the IQ motif. In contrast, CaM_{12} and NSCaTE interaction loses entropy (ΔS becomes modestly negative) while gaining slightly in enthalpy (ΔH becomes more negative). Entropy is usually associated with van der Waals effects or solvation changes, often related to conformational rearrangements, or changes in the degrees of freedom of the macromolecular components.

In contrast to CaM$_{12}$ and wild type CaM, both IQ and NSCaTE peptides bind CaM$_{34}$ with a greatly reduced affinity (almost 100-fold higher K$_d$ in the case of IQc), and very large negative entropy, offest by substantial increases in enthalpy (Table 3.2 and Figure 3.6). Whether the result is indicative of the peptides binding to the lower affinity site in the N-lobe or a transitional, conformationally unfavorable state of CaM is uncertain. It may be that the conformational state of CaM is subject to disruption by the EF hand mutations and thus does not represent an authentic N(2)-C(0) Ca^{2+} status of CaM (if such a conformation is even capable of existing outside of some very specific circumstances, such as when interacting with the CaM-binding domain of SK channels). The thermodynamic parameters (great loss in entropy in exchange for high heat of binding) hint at the greatly reduced conformational flexibility associated with CaM N-lobe binding the IQ motif alone. It is possible that the interaction is a non-specific electrostatic effect. Further competition experiments with the EF hand CaM mutants reveal an even more puzzling picture (next section).

126

3.3.1.4 Competition experiments with EF hand mutants

To determine the relative Ca^{2+} and CaM lobe preference of the two peptides, similar competition experiments were performed with the Ca^{2+}-deficient CaM mutants (see section 3.3.1.2 for rationale and methodology and Figure 3.5, Table 3.2 for results). Strangely, both peptides show a discernible isotherm with CaM_{34}, albeit with a greatly reduced ($\geq 10\mu M$) affinity (see Table 3.2). In fact, the K_d for IQc with CaM_{34} pre-bound to RN is nearly at the detection limit of the calorimeter. Regardless of which one is pre-bound first, both IQ and NSCaTE show a 1 : 1 stoichiometry and extremely negative entropy (far more than either peptide with CaM_{34} alone), offset by very large gains in enthalpy (over threefold, in the case of IQc$\rightarrow$RN+CaM_{34}).
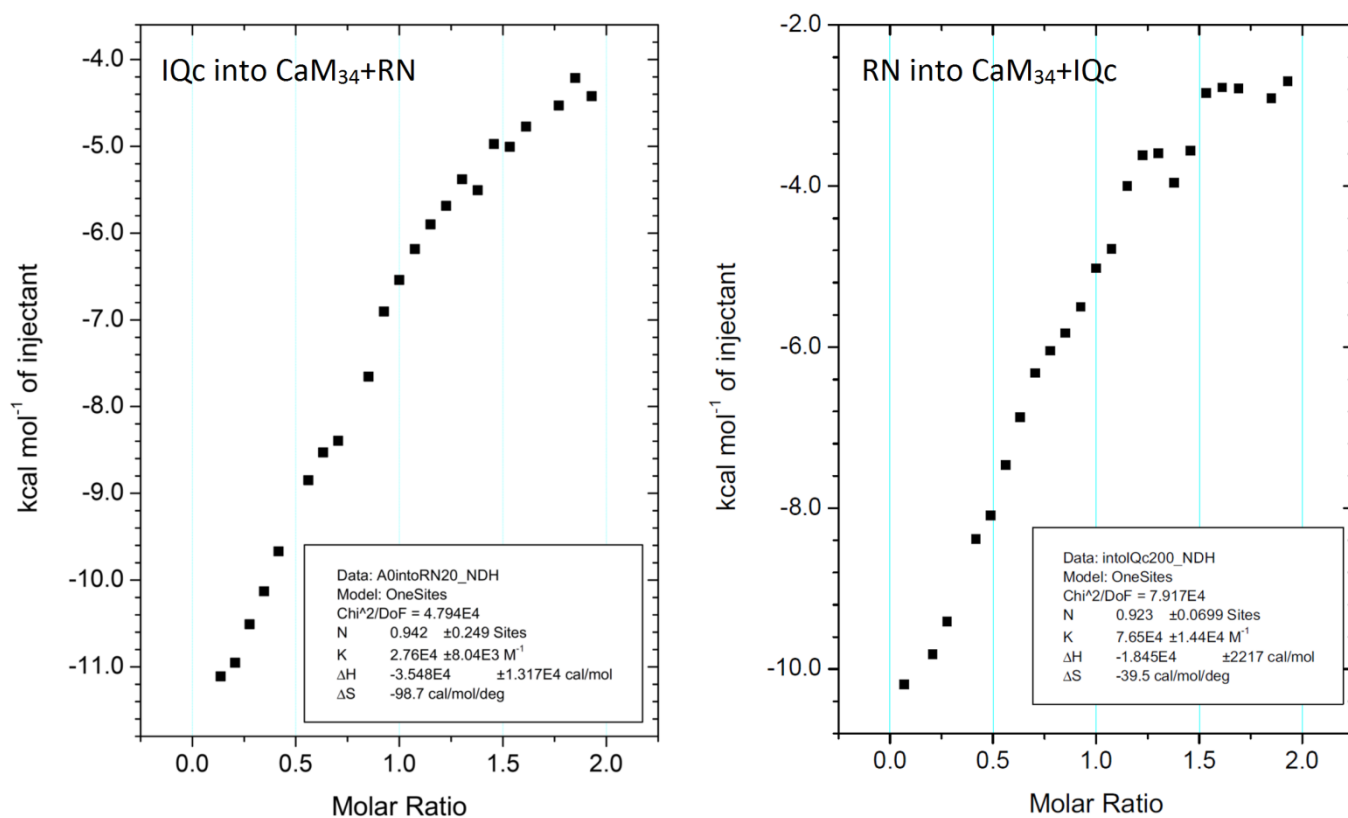
Figure 3.5: ITC competition experiments with CaM_{34} and L-type peptides.
Left: IQc ($200\mu M$) into CaM_{34}+RN ($20\mu M$ each). Right: RN ($200\mu M$) into CaM_{34}+IQc ($20\mu M$ each).

As for CaM_{12}, it appears that competition experiments do not follow the same straight-forward logic as with wild type CaM. We expected that due to the higher affinity of the IQc peptide for CaM_{12}, it would outcompete RN, especially given their 1 : 1 stoichiometry; however, no such trend was observed (Table 3.2). There is no apparent interaction when RN is titrated into CaM_{12}+IQc, suggesting it is unable to displace IQ if it is bound to CaM_{12} first (data not shown). We were also unable to obtain an interpretable isotherm with IQc titrated into CaM_{12} pre-bound to RN. This is difficult to reconcile with the previous result (CaM_{12} with either peptide alone), and suggests that the interaction isn't strictly mutually exclusive, nor is it mutually independent. On the other hand, it further casts doubt on whether the EF hand mutants are viable representations of an authentic CaM conformation for biophysical studies.
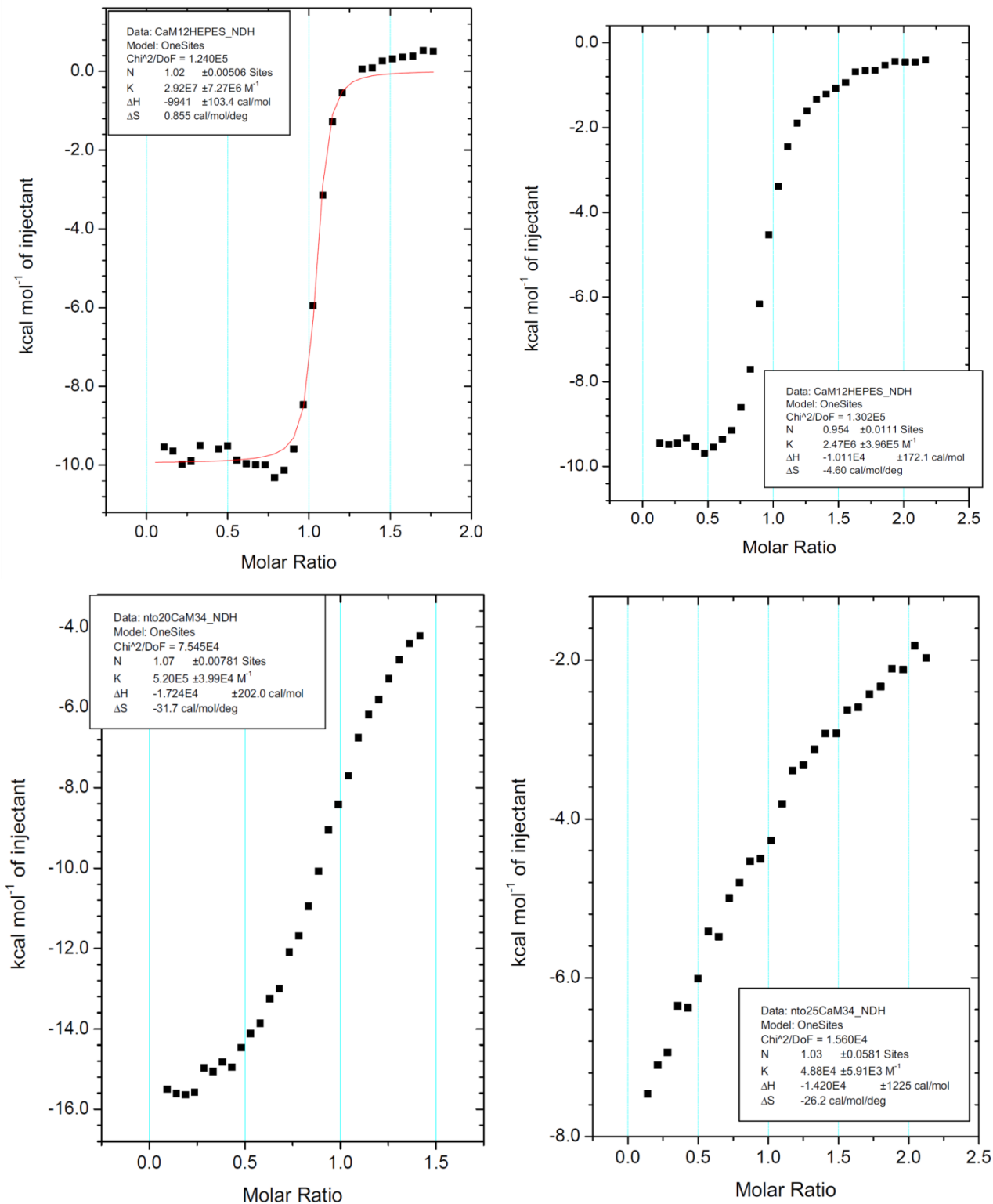
Figure 3.6: Representative ITC results of EF hand CaM mutants with L-type peptides.
Top left: IQc (200μM) into CaM$_{12}$ (20μM). Top right: RN (300μM) into CaM$_{12}$ (25μM). Bottom left: IQc (200μM) into CaM$_{34}$ (20μM). Bottom right: RN (300μM) into CaM$_{34}$ (25μM).

Table 3.2: Summary of ITC results with the L-type calcium channel peptides and CaM (mutant and wild type).

Titration conditions are described in methods. In all case CaM was in the cell and peptide was in the syringe; in competition experiments CaM was pre-bound to the indicated peptide at stoichiometric ratios (1 : 1). Each experiment was performed at least twice to ensure consistent results.

Experiment	N (sites)	±	Kd (µM)	±	ΔH (cal/mol)	±	ΔS (cal/mol/deg)
Single peptides with wild type CaM							
RN	2.09	0.030	1.16	0.290	-8340	163	-0.784
LN	2.05	0.081	13.51	2.831	-5694	387	3.2
IQc	0.92	0.016	0.09	0.039	-11230	305	-5.33
LIQ1	0.91	0.000	0.02	0.005	-9455	163	3.69
IQa	1.90	0.022	0.95	0.162	-9246	155	-3.43
Competition with wild type CaM:							
IQc into RN	1.06	0.016	0.13	0.049	-10810	286	-4.76
RN into IQc	0.99	0.018	1.78	0.253	-9700	233	-6.23
RN into IQa	1.95	0.023	1.00	0.180	-9274	160	-3.64
LN into IQc	1.10	0.075	13.79	2.321	-7476	717	-2.84
LIQ1 into LN	0.91	0.010	0.02	0.008	-9398	214	3.82
+CaM$_{12}$							
RN	0.95	0.011	0.40	0.065	-10110	172	-4.6
IQc	1.02	0.005	0.03	0.009	-9941	103	0.855
+CaM$_{34}$							
RN	1.03	0.058	20.49	2.482	-14200	1225	-26.2
IQc	1.07	0.008	1.92	0.148	-17240	202	-31.7
RN into Iqc	0.92	0.070	13.07	2.461	-18450	2217	-39.5
IQc into RN	0.94	0.249	36.23	10.555	-35480	13170	-98.7

3.3.2 Qualitative NMR analysis

HSQC spectra of wild type ^{15}N CaM with various peptide combinations were obtained. While no structure determination has been achieved yet, several interesting observations can be made. The overlaid spectra for CaM and each peptide alone, or sequential titrations of one then the other as indicated reveal distinct binding conformations for a number of combinations. Future work and additional spectra will allow full assignment and possibly a solution structure for one or more of these complexes.

Predictably, CaM's amide peaks shift when bound to either IQ or NSCaTE (only mammalian peptides were analyzed), with a greater number of distinct shifts seen with the IQ peptide, suggesting a greater degree of conformational change, consistent with our gel-shift results (Chapter 2). There is little obvious structural change in CaM upon binding NSCaTE, and a few small but significant changes upon binding the IQ peptide (Figure 3.7). What is far more interesting, the structural changes observed with binding either IQ or NSCaTE alone are only partly represented when IQ is first pre-bound to CaM and then titrated with NSCaTE (one equivalent of each). There are distinct peaks in this spectrum (Figure 3.8, purple) not seen with either peptide + CaM or CaM alone, and some peaks that are missing (Figure 3.7). With a few additional experiments (likely a NOESY at the very least), enough data can be gathered to solve a structure and determine with certainty whether or not a simultaneous co-interaction between CaM and both peptides is actually occurring.
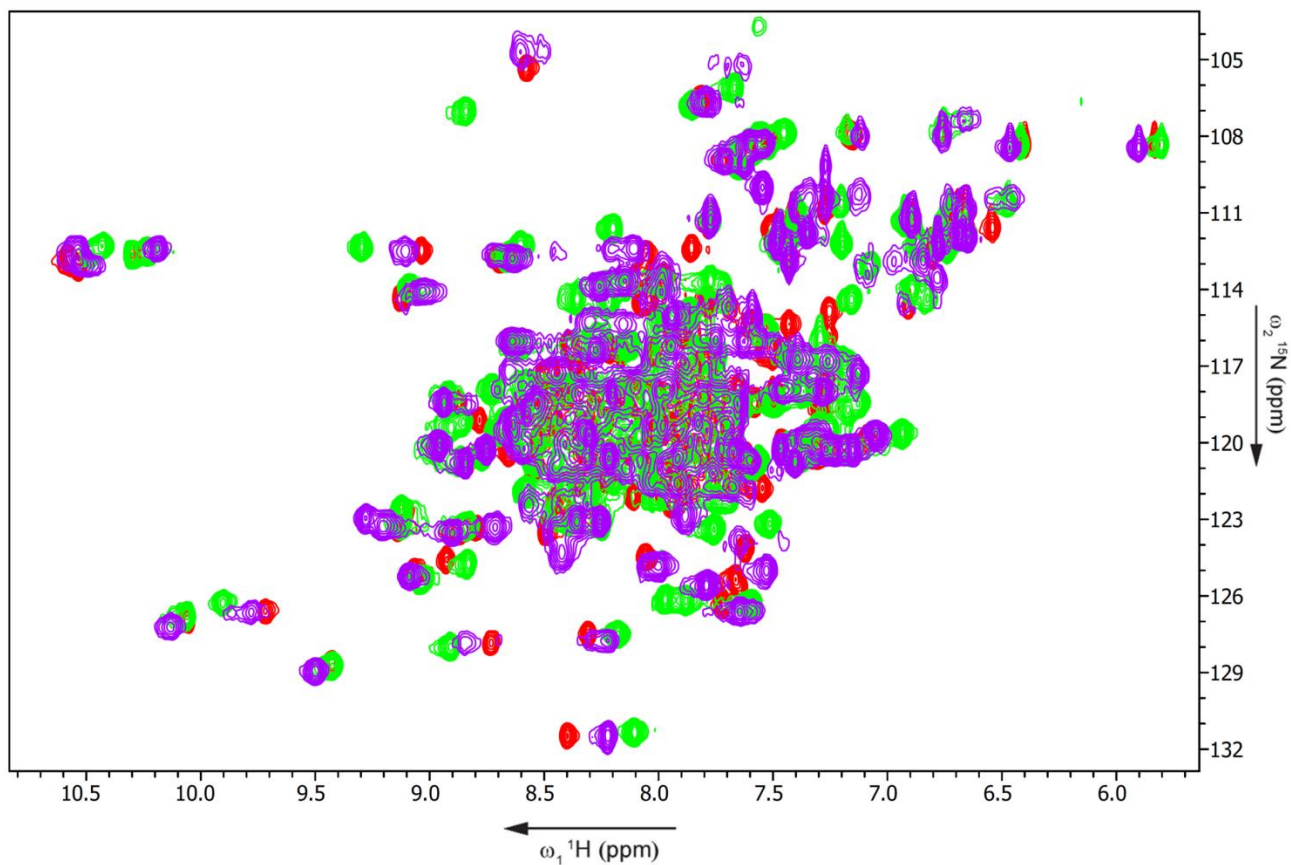
Figure 3.7: ^{15}N HSQC of holo-CaM alone (red), CaM + IQc (green) and CaM + RN (purple).
X axis is proton chemical shift, Y axis is nitrogen chemical shift (in ppm). One equivalent of IQc and two equivalents of RN were used in their respective spectra**.**
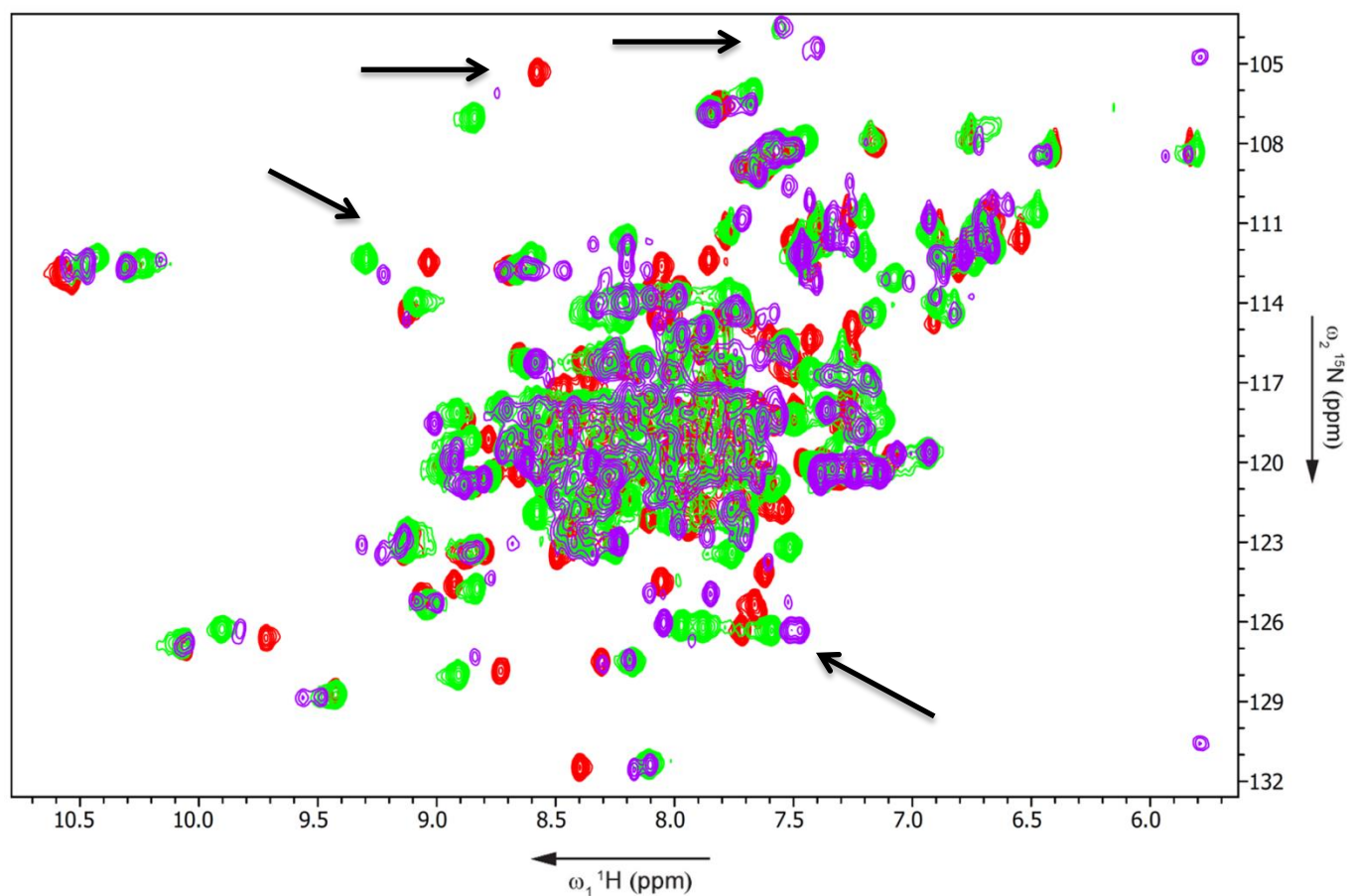
Figure 3.8: ^{15}N HSQC of holo-CaM alone (red), CaM titrated with IQc (green), and CaM pre-bound to IQc and titrated with RN (purple).
Same axes as Figure 3.7. One equivalent of IQc was used and two equivalents of RN; however there was no change after the 1 : 1 (RN : CaM-IQc) ratio was achieved. Arrows indicate peaks that may be of interest (not yet assigned).

3.4 Discussion

In this chapter, we sought to obtain a biophysical perspective and a possible mechanistic insight into the regulatory effect of CaM on L-type channels via its interaction with the IQ and NSCaTE motifs. Using isothermal calorimetry, we find major differences between the CaM-binding affinities of IQ and NSCaTE, as well as between the mammalian vs. snail NSCaTE. What is more, both NSCaTEs bind CaM with a 2 : 1 stoichiometry, which was confirmed by a concurrently published study (Liu and Vogel, 2012), and consistent with our NMR results. The L-type IQ peptide binds CaM with a more typical 1 : 1 stoichiometry and sub-micromolar affinity.

This stoichiometry persists when NSCaTE is titrated into CaM pre-bound to an IQ motif from a P/Q channel (α1A or Ca_V2.1), which suggests that its dominant positive effect on CDI seen in (Dick et al., 2008) is due to the much weaker affinity of the Ca_V2.1 IQ motif for CaM (the IQ_A peptide cannot displace NSCaTE from CaM based on our ITC data). Interestingly, IQ_A also possesses a 2 : 1 stoichiometry with CaM. Obviously, there is little physiological relevance to such ratios because it is highly unlikely that two large, membrane-associated proteins (> 250kDa) can be cross-linked by a single CaM molecule. Instead, this suggests conformational diversity and a presence of more than one binding mode as well as competing interactions from multiple CaM-binding sites. In other words, the same peptide may bind CaM differently depending on its local conformational terrain, CaM's Ca^{2+} occupancy and any competing interactions. In a fascinating twist, CaM's stoichiometry with NSCaTE is altered to 1 : 1 when an L-type IQ peptide is first pre-bound to CaM (or vice versa), suggesting that CaM is capable of co-interaction with both regions of the channel. Results with Ca^{2+}-deficient CaM mutants also lend support to this theory. CaM_{12} and CaM_{34} both have a 1:1 stoichiometry with NSCaTE.

CaM$_{34}$ appears to have poor binding to either IQ or NSCaTE, and may not be a true representation of the N(2)-C(0)Ca^{2+}-CaM conformation. CaM$_{12}$ is even more perplexing, because, while it binds with high affinity to either IQ or NSCaTE peptide alone (with an altered 1 : 1 stoichiometry for the latter), there is no discernible interaction when either peptide is pre-bound to CaM$_{12}$ first. This somewhat confounds the notion that NSCaTE's role is as a 'global' CDI regulator via the N-lobe of CaM, since its affinity for CaM$_{12}$ is at least 50-fold higher than CaM$_{34}$.

Unfortunately, CaM$_{12}$ and CaM$_{34}$ likely do not truly represent the Ca^{2+}/apo-lobe conformational states they are intended to, even if they are close approximations for the non-mutated lobes. To really dissect the lobe contributions, half-CaMs[20] and Ca^{2+} concentrations reminiscent of those found *in vivo* need to be tested. Controlling Ca^{2+} concentrations *in vitro* typically involves the addition of a set concentration of CaCl$_2$ and a chelator (EDTA/EGTA/BAPTA etc). Much to our chagrin, the IQ peptides form insoluble complexes with chelating agents, making the latter strategy inapplicable. Competition ITC experiments with half-CaMs will be a valid alternative strategy in future experiments, and several such experimental designs are proposed in Chapter 5.

Other than the ITC experiments, we have no other direct evidence to support a co-interaction between IQ/CaM/NSCaTE; several experiments were attempted, but not successful, including formaldehyde cross-linking and native gel filtration; see Appendix (Figure A.4-Figure A.7). Fluorescence labeling of IQ peptides to attempt FRET experiments using tryptophan and dansyl as FRET pairs was problematic (or FITC and dansyl, which was worse); fluorescent labels appear to interfere with the peptides' ability to bind CaM. The interaction between NSCaTE and CaM may be too weak and/or transient to allow for capture of a stable complex

---

[20] Constructs containing only one lobe of CaM and optionally, the central linker.

using standard separation techniques, which has led one previous study to conclude the absence of such a co-interaction (Benmocha et al., 2009). Taking our ITC data into account, we disagree. Indeed, a very recent study by the same group which initially characterized NSCaTE predicts the same model we describe here (N-lobe + NSCaTE/ C-lobe + IQ), albeit with a different mechanistic explanation and no direct biophysical evidence (Johny et al., 2013).

NMR spectra of both peptides bound to CaM may not represent a single population of CaM conformations; e.g. a spectrum may represent a combination of CaM bound to one or the other peptide, with peaks from either conformation. However, the presence of unique peaks in the HSQC spectrum containing both IQ and NSCaTE bound to CaM is promising. Solving a structure of CaM with both peptides bound may be necessary to unequivocally prove that the IQ-NSCaTE bridging by CaM does indeed occur, and should be the focus of future experiments.

If such a co-interaction were indeed real, and in fact occured *in vivo* (which would be substantially more difficult to show explicitly), the implications on our understanding of L-type channel regulation by CaM would be far-reaching. On the one hand it is difficult envision a physical process that would bring the two termini of the channel molecule into close proximity – that is, within a distance spanned by one CaM molecule, or about 40Å. But on the other hand it is even less plausible that CaM binds to NSCaTE independently from the IQ motif, for which it has a much higher affinity, when CaM is presumably limiting in the cell and is found pre-associated with Ca_V C-termini (Persechini and Stemmer, 2002; Erickson et al., 2003; Liang et al., 2003; Sanabria et al., 2008; Evans et al., 2011). A more likely scenario is that CaM first binds to the IQ motif, and a structural change in the holo-channel then allows the N-terminus to come in close enough proximity to the IQ-CaM complex for NSCaTE to bind to CaM, most likely at the N-lobe. Exactly what this process entails and how it affects the open probability or inactivation

gating is far from clear, but considering the major effects of NSCaTE on 'global' Ca^{2+} feedback (see section 2.3.3), it likely involves a rapid closing mechanism that has yet to be described. The 2 : 1 stoichiometry is probably due to a reduced selectivity of NSCaTE for CaM lobes; e.g. the secondary site is more or less an artifact due to its similarity to the *bona fide* interaction site. It may also explain the positive transforming effect of NSCaTE on $Ca_V2.2$ ($\alpha1B$) (Dick et al., 2008), which normally does not have buffer-resistant (e.g. 'local') CDI, a seemingly contradictory result due to NSCaTE's presumed interaction with the N-lobe of CaM, which is presumably involved in 'global' or buffer-sensitive CDI. The most plausible explanation is that in this case, NSCaTE is not just binding the N-lobe of CaM, but *also* the C-lobe of CaM, because it can outcompete the indigenous IQ motif of $Ca_V2.2$, and subsequently act as a 'surrogate' L-type IQ motif and produce a similar effect on CDI. In this sense, it would be interesting to see if there is a docking site somewhere on the channel (either $Ca_V1.2$ or 2.2) for CaM lobes bound to either IQ or NSCaTE.

Based on previous studies and our own cursory bioinformatics scan using the CaM binding site prediction database (Ivanina et al., 2000; Yap et al., 2000; Pitt et al., 2001; Stotz et al., 2004; Findeisen and Minor, 2009), the most likely candidate is the distal I-II linker in the L-type channels (downstream of the AID). Indeed, a few basic ITC experiments[21] we performed (Appendix, Figure A.8) reveal that these are capable of binding CaM with low micromolar affinity. The fact that other studies show an effect of I-II linker mutations on CDI (Findeisen and Minor, 2009), as well as a confirmed biophysical interaction between the I-II linker and CaM (Ivanina et al., 2000; Pitt et al., 2001; Zhou et al., 2005; Christel and Lee, 2012), points to a 'hinged-lid' type mechanism by which CaM may be exerting its effects, similar to the process in

---

[21] We did not attempt to do any competition or co-interaction experiments, but that data could become valuable in the future

Na$_V$s that involves the III-IV linker of this channel (see section 1.7.1). Therefore, a possible mechanistic model (see Figure 3.9) is that 1) apoCaM is tethered at a C-terminal site upstream of the IQ motif, but then 2) progressively recruits various other channel regions upon Ca^{2+}-binding first to the C-lobe ('local' CDI, via the IQ motif), and then 3) the N-lobe binds to either IQ and/or 4) NSCaTE), cross-links these different domains and 5) docks them near the I-II linker in a configuration that restricts channel opening (or physically blocks it). Whether the 'lid' process is shared for the 'local' and 'global' versions of CDI, whether the β-subunit may be involved, or how it proceeds at all, is unclear. A number of experiments can be used to test this hypothesis (see last chapter).
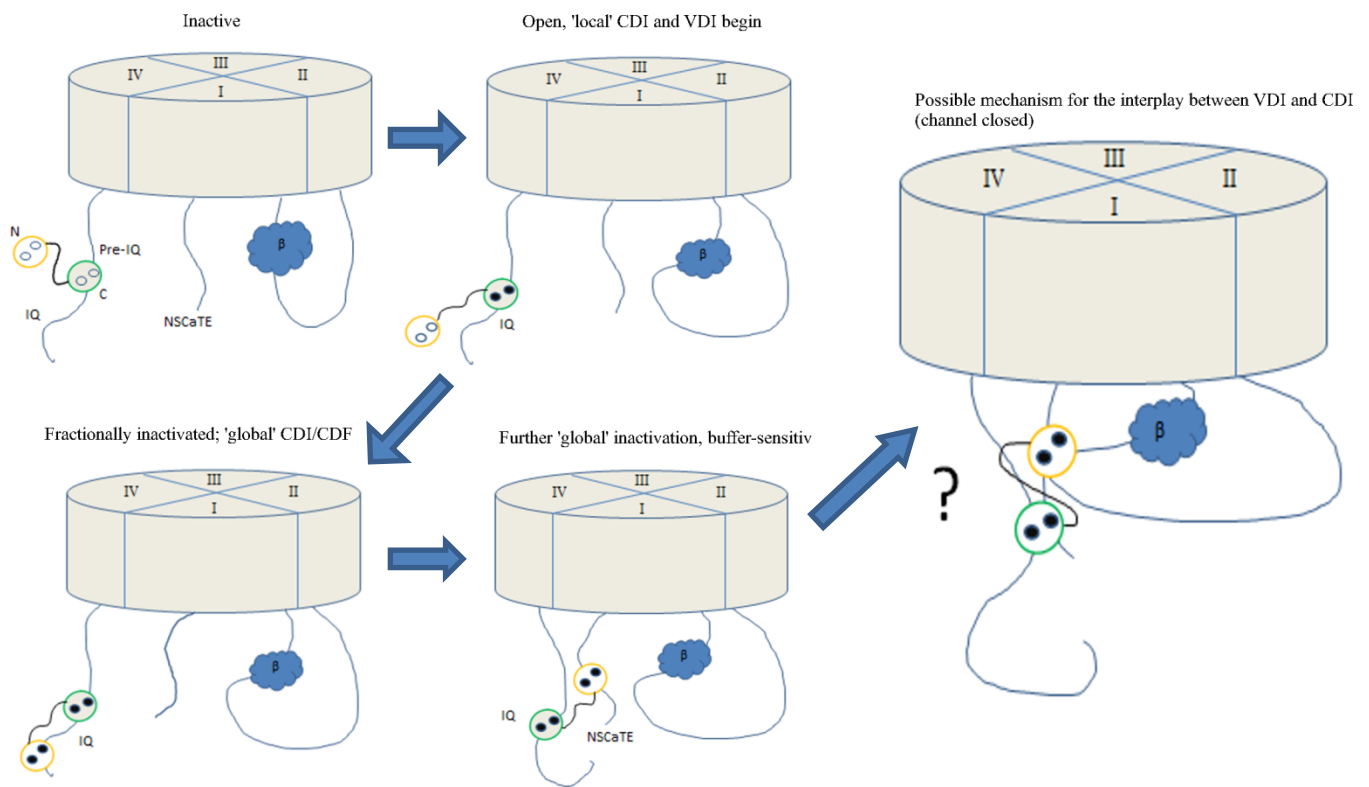
Figure 3.9: Proposed mechanistic model of L-type calcium channel modulation by calmodulin.
Open circles indicate absent Ca^{2+} ions, filled indicate bound Ca^{2+}. Not to scale.

3.5 Conclusions

The main objective of this chapter was to characterize the details of the molecular interaction of CaM and NSCaTE, as well as any possible co-interaction with the IQ motif. Although no direct biophysical evidence[22] was obtained to confirm such a co-interaction, we present convincing calorimetric evidence that this is indeed a possibility. Unusual NSCaTE: CaM stoichiometry (2 :1) that was also confirmed by (Liu and Vogel, 2012) is replaced by a more physiological 1 : 1 stoichiometry when CaM is first pre-bound to the IQ motif peptide (or vice versa). The relative affinities of snail and mammalian NSCaTE, and IQ and NSCaTE peptides differ by about an order of magnitude each. The IQ motifs of mammalian and snail L-type channels are actually remarkably conserved and bind CaM with a very similar affinity and thermodynamic parameters (enthalpy and entropy). The dominant effects on CDI seen by NSCaTE fusion to a non L-type channel (α1B or N-type) reported in the formative NSCaTE study (Dick et al., 2008) can most likely be explained by the relatively higher affinity of NSCaTE for CaM, which we observe with another non L-type peptide (α1A or P/Q type). The latter can be fully displaced from CaM when NSCaTE is titrated into the complex.

Additionally, we see a strong preference of both IQ and NSCaTE peptides for the Ca^{2+}-C-lobe of CaM, as evidenced by their much higher affinity for the CaM_{12} mutant over CaM_{34}. None of the peptides were capable of binding apo-CaM, suggesting their effects are tied solely to active channel regulation (e.g. post-Ca^{2+}-entry).

---

[22] Such as an actual molecular complex captured, or structure solved

Chapter 4: Characterization of a novel CaM-binding site in the I-II linker of low-voltage activated channels

4.1 Introduction

T-type ('transient' and 'tiny' currents, also low-voltage activated "LVA") channels are distinct from the high voltage activated ($Ca_V1.x$ and $Ca_V2.x$) channel group in many ways. They are evolutionarily distant from other Ca_Vs (see Chapter 1), less conserved among themselves (there are 3 splice isoforms in mammals), and have distinct and sometimes cryptic physiological roles (Perez-Reyes, 1999, 2003; Senatore and Spafford, 2010). Generally speaking, there is far less known about them than the HVA channels, which have been studied for much longer. While the LVAs are categorized as 'calcium' channels, their actual selectivity for Ca^{2+} (over Na^+) is often much lower than HVA channels, in most cases by over an order of magnitude ($P_{Ca}/P_{Na} < 100$, while for HVAs it is typically ≈ 1000) (Shcheglovitov and Shuba, 2006). Their Ca^{2+}/Ba^{2+} selectivity varies by isoform. Interestingly, the selectivity filter that in HVA channels contains an invariable E-E-E-E, is altered in T-type channels to E-E-D-D, while in Na_Vs, it is D-E-K-A in the equivalent positions (Talavera et al., 2003; Yu and Catterall, 2003; Talavera and Nilius, 2006; Park et al., 2013). More interestingly, substitution of the T-type selectivity filter residues to the 'consensus' E-E-E-E does not strictly convert the T-type channels into a more Ca^{2+}-selective channel, in fact, for $Ca_V3.2$ it greatly increases the Ca^{2+}/Ba^{2+} selectivity, the opposite of what is expected. In contrast, replacing only the first aspartate actually reduces the Ca^{2+} selectivity; in all cases, D$\rightarrow$E (of E-E-D-D) mutations reduced macroscopic currents from wild type $Ca_V3.2$ (Park et al., 2013). There is also some evidence that these residues not only control selectivity, but also the gating properties (depolarization of the I-V curve and slope

increase of activation) as well as sensitivity to protonation (Talavera et al., 2003; Talavera and Nilius, 2006).

In most cells that express them, T-type channels act as 'first responders', opening at sub threshold voltages (-65 to -30mV, as opposed to the L-type -20 to +20 mV), and inactivating rapidly before the HVA channels activate. The overlap of voltage-dependence for activation and inactivation in T-type channels causes a 'window' current of Ca^{2+}, thus allowing Ca^{2+} entry at basal levels (Cain and Snutch, 2010). In some neurons, the window current is sufficient to generate action potentials ('burst firing'), such that the T-type channels in these cells contribute to their pacemaker activity (Perez-Reyes, 2003). Furthermore, inactivation rate and recovery are often dictated by preceding membrane potential changes, which suggests that these channels have a role in short-term synaptic plasticity (Cain and Snutch, 2010). Mutations in T-type channels are often associated with certain epilepsy disorders (Singh et al., 2007). Due to their ubiquity and importance, these channels present a new promising field for pharmacological development (Kochegarov, 2003), as well as basic biophysical and biochemical research.

There is not much known about the regulatory mechanisms controlling the gating of T-type channels; few unique conserved motifs have been described. Like other Ca_Vs, there is a great deal of splice variation even within a single T-type isoform (some genes contain over 30 exons) and several of these have highly variable biophysical effects (Perez-Reyes, 1999; Senatore and Spafford, 2012). Electrophysiological recording of T-type channels presents a challenge as well, since they are rather quick to inactivate, share a common activation voltage range with TRPs, HCNs and other channels, and lack the many pharmacological tools (specific channel blockers) that have been developed for HVAs.

A common approach for investigating the role of specific channel domains in their regulation involves the use of chimeric channels in which a signature region (e.g. the IQ motif, AID, I-II or II-III domain linkers, etc.) from the more commonly studied $Ca_V1.x$ or $Ca_V2.x$ channels is used to replace the native corresponding domains in a T-type channel. Such an approach has revealed some interesting results, for example the distinct role of the domain II S4 segment in activation (Talavera and Nilius, 2006). However it is best to interpret such results with caution. NSCaTE is an excellent case in point: its effects on $Ca_V2.2$ (N-type, or α1B) channels, when fused as a chimera, are very striking, yet bear no physiological relevance or say much about the native regulation of the channel other than that its own IQ motif is dissimilar in its regulatory mechanisms from the L-type IQ motif. Thus, to really tease apart the contribution of the different domains, site-directed mutagenesis and isolated biophysical studies have to be undertaken with the channel's own domains.

One of the more interesting findings of the chimeric studies was that transferring the I-II linker of a $Ca_V2.2$ into $Ca_V3.1$ (α1G) channel, instead of conferring β-subunit regulation on the latter, presumably via AID, actually generated an ultra-low voltage gated channel (Perez-Reyes, 2003, 2010; Arias et al., 2005). More generally, it has been observed that several mutations in the I-II linker of $Ca_V3.2$ (α1H) are often associated with childhood absence epilepsy (Khosravani et al., 2004), and those of $Ca_V3.1$ have been implicated in idiopathic generalized epilepsy (Singh et al., 2007). The proximal I-II linker is a putative helix-loop-helix motif, with the second helix being crucial to the gating/activation properties of the channel (Perez-Reyes, 2010); without it, the channel is able to open at more negative voltages. This gating brake is highly conserved across all three channel isoforms, and, more interestingly, even shows a high degree of similarity in its single *Lymnaea* homolog (LCa_V3) (see Figure 4.1). Previous work in Dr. Spafford's lab has

included a detailed characterization of the *Lymnaea* T-type homologue, which shows some

distinct (and some similar) characteristics to its mammalian counterparts (Senatore and Spafford,

2010, 2012).

```
CaV3.1     --SCYEELLKYLVYILRKAARRLAQV--------SRAAGVRVGLLSSPAP
CaV3.2     ---CYEELLKYVGHIFRKVKRRSLRL--------YARWQSRWRKKV----
CaV3.3     PGDCYEEIFQYVCHILRKAKRRALGL--------YQALQSR-RQALGPE-
LCaV3      PGGYYSELLKLVAQVYRRVKRKVIKTRGLQKINPEKSLSLR-RKKSKKKG
               *.*::: :   : *:. *: *                 *
```

Figure 4.1: Alignment of the gating brake in human and *Lymnaea* T-type I-II linker.
(Only the second helix is shown). Predicted CaM-binding region is in yellow.

So far, no direct Ca^{2+}-specific regulation such as CDI or CDF has been shown for T-type

channels. Whether this is due to a genuine lack of such effects, or simply a limitation associated

with recording of these channels, which (in)activate very rapidly, is uncertain. Several studies

point to G-protein and tyrosine kinase (CaMKII in particular) regulation of $Ca_V3.2$, the latter

being localized to the II-III linker (Welsby et al., 2003; Talavera and Nilius, 2006). T-type

channels are thought to be monomeric; that is, they require no accessory subunits for efficient

expression and activity (Walsh et al., 2009). They also lack a cognate IQ motif and EF hand in

their C-termini, in contrast to HVAs. Since HVAs are also regulated by CaMKII[23], we sought to

determine whether a previously uncharacterized CaM-binding site may be involved in the

interaction of CaM/CaMKII and Ca_V3 channels, or otherwise linked to their regulation.

We expected to find a cryptic CaM-binding site, possibly in the C-terminus or the II-III

linker of $Ca_V3.2$, with which CaMKII is thought to associate, so we submitted the entire protein

sequence to the CaM binding site prediction tool (see section 2.2.3) (Yap et al., 2000). To our

---

[23] Directly in the case of $Ca_V2.1$ and indirectly via the phosphorylation of the β2a subunit of associated $Ca_V1.2$ or 1.3 (Grueter et al., 2006; Jiang et al., 2008)

greatest surprise, we found that the putative gating brake region of all T-type channels is a strongly predicted CaM binding site. This site directly spans the second helix of the helix-loop-helix motif of the proximal I-II linker in all 3 mammalian as well as the *Lymnaea* Ca$_V$3 channels (Figure 4.1). Skeptical, we first obtained the LCa$_V$3 I-II linker peptide (from Genscript: YSELLKLVAQVYRRVKRKVIKTYYKT) and tested it for binding to CaM. To our even greater surprise, we found it to bind CaM with nanomolar affinity and with a strongly positive enthalpy. Subsequently, we obtained linker peptides corresponding to the gating brake of the three mammalian isoforms, as well as a α1H (Ca$_V$3.2) linker mutant in which the helical structure is disrupted by several Pro-Gly residues in place of the native sequence. We characterized all these peptides using similar methods as in Chapter 2 & 3. There are interesting isoform specific differences but also similarities across all isoforms, which are relevant to the physiological characteristics of the channels and may have important biophysical and pharmacological implications. These findings will fundamentally alter the knowledge base of T-type channel regulation.

4.2 Methods

Table 4.1: T-type gating brake peptides and their parameters.
All peptides were synthesized by Genscript (specified to >98% purity, MS and HPLC verified), made up to 1mM stocks in MQ water shortly before use.

Name	Source	Sequence	MW	pI
LCa$_V$3	*Lymnaea* T-type I-II linker gating brake	YSELLKLVAQVYRRVKRKVIKTYYKT	3246.9	10.29
Ca$_V$3.1(G)	human α1G I-II linker GB	YEELLKYLVYILRKAARRLAQVSRAA	3094.7	10.16
Ca$_V$3.2(H)	human α1H GB	YEELLKYVGHIFRKVKRRSLRLYARW	3381.03	10.61
Ca$_V$3.3(I)	human α1I GB	YEEIFQYVCHILRKAKRRALGLYQAL	3182.76	9.52
Ca$_V$3.2mut	mutant human α1G GB	YEELLK**PGPGPG**RKVKRRSLRLYARW	3126.71	11.0

4.2.1 Gel shift mobility assays

The assays were performed in both native conditions and with 4M urea (see Chapter 2 Methods section). Other than urea, the buffer and gel composition for the experiments were identical. For Ca^{2+}-CaM experiments, 1mM $CaCl_2$ was used in the gel and 0.1mM $CaCl_2$ in the running buffer. For EDTA experiments, 0.1 mM EDTA was used in all solutions. As before, all experiments were run with ice bath and cooler jacketing set to 4°C, at 120-200V. Pre-incubation buffer for all experiments was 10mM Tris-Cl (pH 7.5) with 0.1 mM $CaCl_2$ or EDTA (no urea).

4.2.2 NMR Spectroscopy

Identical protocol and CaM/peptide concentrations were used as in Chapter 3 (Section 3.2.3).

4.2.3 Spectropolarimetry

The same JASCO-715 spectropolarimeter was used as in Chapter 2. Scans were done at 50nm/min, over 250-190nm range with 1s response time, 1nm bandwidth and 16-25 accumulations depending on signal quality. Buffer composition for LCa_V3 and α1H mutant linkers was PBS (10mM sodium phosphate pH 7.3, 137mM NaCl, 2mM KH_2PO_4, and 2.7 mM KCl). The other linker peptides were characterized in low ionic strength buffers due to severe aggregation issues in PBS; for these 3 peptides ($Ca_V3.1-3$), 10mM HEPES (pH 7) was used. In all cases a 0.1cm quartz cuvette (Hellma) was used. CaM binding experiments were performed by adding increments of stock (1mM) peptide to the same cuvette containing 10 μM CaM (300 μL). Subsequent scans would then have the CaM-only trace subtracted and be corrected for total peptide concentration, smoothed, converted to MRE units and exported to .csv format.

4.2.4 Isothermal Calorimetry

Due to severe aggregation issues with some of the mammalian linker peptides in any amount of salt, we had to use a low ionic strength (10mM HEPES, pH 7.0, 0.1mM $CaCl_2$) buffer in all cases. All the experiments were performed at 25ºC, with 1000rpm stirring, 5µcal/s reference power and high feedback gain. Injection conditions were typically 1.2-1.8µL each (22-28 injections) and cell/syringe concentrations optimized for individual experiments (c value between 10 and 1000) (Turnbull and Daranas, 2003; Freiburger et al., 2009; Broecker et al., 2011), but typically between 10 and 50 µM for cell and 100 to 500 µM for the syringe. Periodically, water-water and buffer-buffer controls were conducted to ensure the syringe and cell were clean and in good working order. Most of the endothermic titrations had to be baseline subtracted against the final injection heats (end-weighted auto-baseline or manual baseline for $Ca_V3.3$ to correct for the heat of dilution) due to fitting artifacts from the isotherm passing through the x-axis. Baseline-corrected curves were all fitted to a one-set-of-sites model in Originlab with satisfactory results.

4.3 Results

4.3.1 Gel shift mobility assays

We found urea to have an attenuating effect on the mobility shifts with all peptides (c.f. left and right panels of **Figure 4.2**), although LCa$_V$3 peptide was least affected. Omitting urea in the experiment allowed a very weak (unobservable in the presence of urea) gel shift with α1I (Ca$_V$3.3) to be observed (bottom right panel). It also allowed for a more complete shift with α1H (Ca$_V$3.2) and α1G (Ca$_V$3.1). No shift was observed under any conditions with the mutant α1H peptide. No shift was observed with any of the peptides in the presence of EDTA.
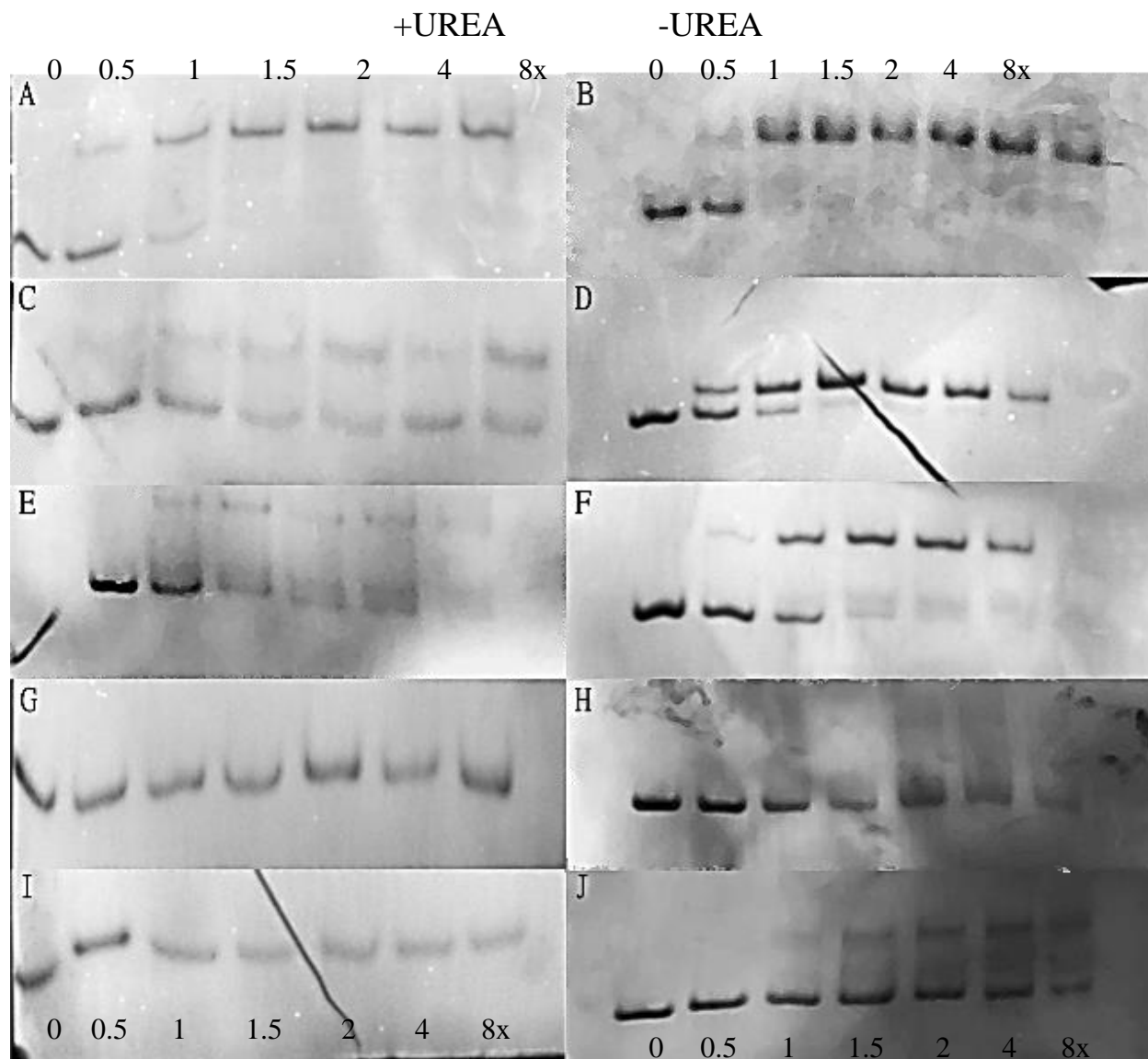
Figure 4.2: T-type gating brake peptide gel shift results with Ca²⁺-CaM.
Left side has urea present, right side is urea-free gels (Coomassie stained). A,B – LCa$_V$3. C,D – α1G. E,F – α1H. G,H – α1H mutant. I,J – α1I. See methods for peptide sequences and properties. EDTA gels are not shown (none of the EDTA gels exhibited any shift; for example, see panel G and H and I). First lane in each gel is CaM alone; subsequent lanes have increasing amounts of indicated peptide (ratios: 0.5, 1, 1.5, 2, 4, 8 molar excess of peptide).

4.3.2 NMR:

Only the *Lymnaea* gating brake peptide was analyzed by NMR due to scheduling and time

constraints. The results are consistent with the gel shift and ITC results in that a 1 : 1

stoichiometry was observed. There are several noticeable peak shifts in the ^{15}N HSQC spectrum

of Ca^{2+}-CaM bound to LCa$_V$3 gating brake peptide, but the majority of the structure is unchanged (Figure 4.3). A complete structure solution will require additional types of experiments. Peptide structure solution will require a labeled peptide and several more NMR spectra.
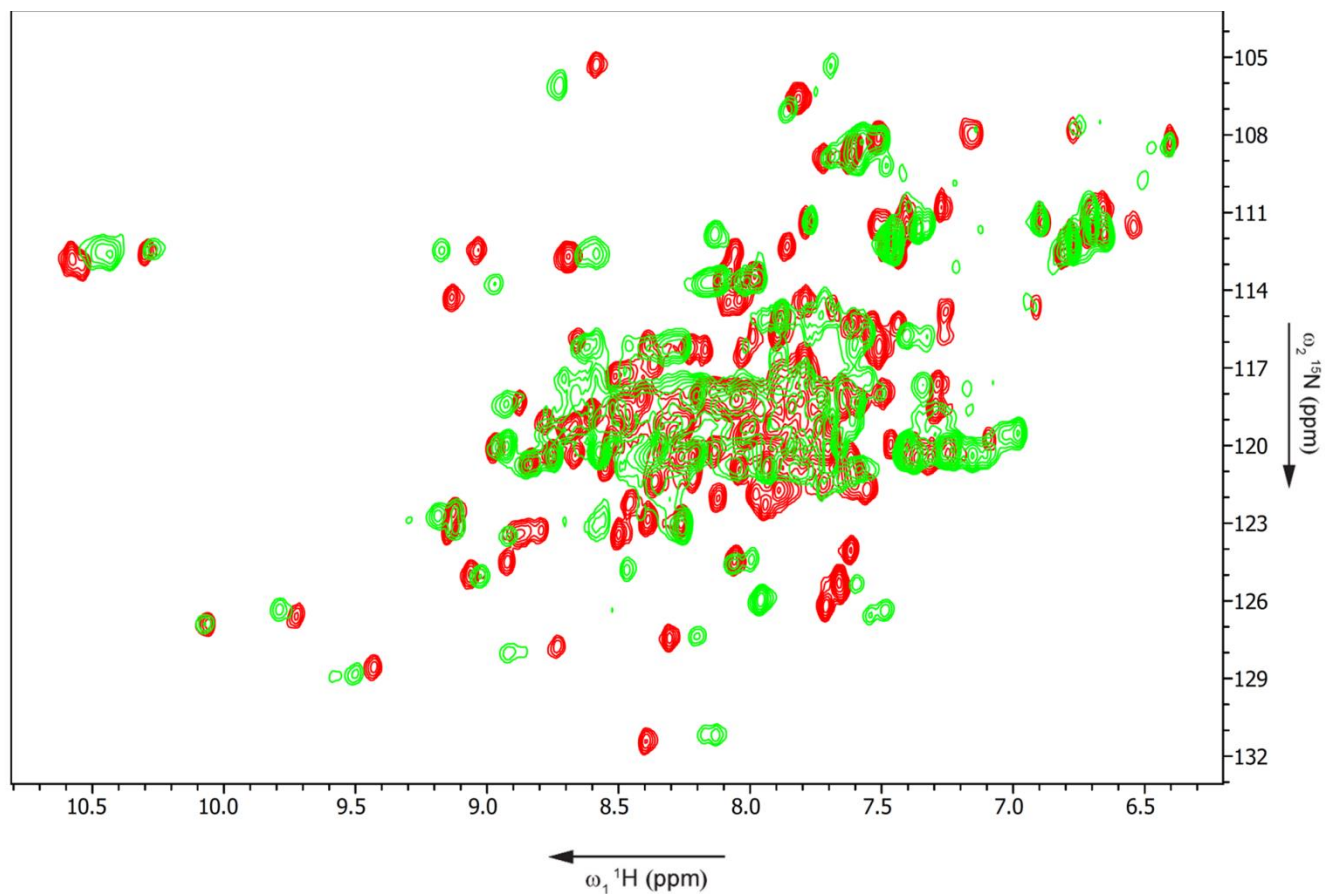
Figure 4.3: NMR results with LCa$_V$3 gating brake peptide and Ca^{2+}-CaM.
X axis is proton chemical shift, Y axis is nitrogen chemical shift (in ppm). CaM alone is red; peptide+CaM is green. Backbone assignments are in progress.

4.3.3 Circular Dichroism:

Secondary structure calculation (with the software algorithms from Chapter 2, e.g. K2D and SOMCD) was not feasible with many of the peptides with largely unstructured or partially structured spectra. The two algorithms also gave widely divergent results, with high levels of error for several spectra. We therefore forgo a detailed quantitative analysis of the secondary structure in this chapter.

Qualitatively speaking, $Ca_V3.1$ had the most α-helical secondary structure of all the linker peptides (Figure 4.5), while the mutant $Ca_V3.2$ had virtually none (Figure 4.7). All other peptides were able to adopt at least some degree of α-helix upon TFE addition and CaM binding (Figure 4.4-Figure 4.8). In most cases, the binding of each peptide to CaM is comparable to adding a low concentration of TFE.
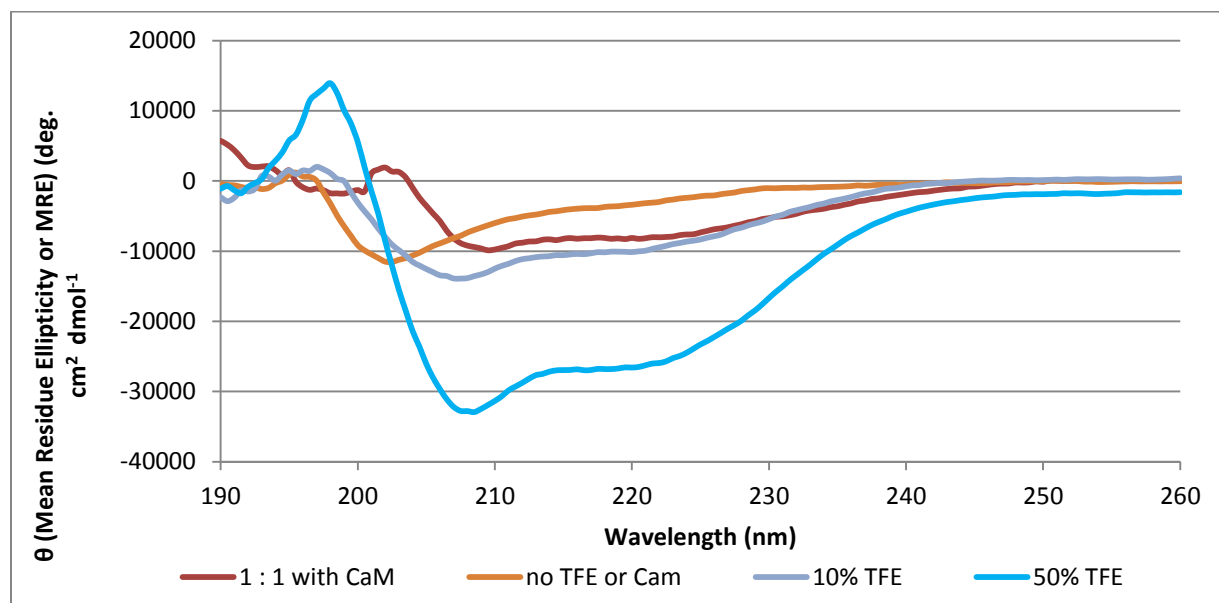
Figure 4.4: LCa$_V$3 gating brake peptide CD spectra.
20μM of wild type CaM in the cuvette was used; to this, increasing amounts of stock (1mM) peptide were added (1.5μL increments into a 300μL total volume, corresponding to 5μM concentration steps). From each peptide+CaM spectrum, the CaM-alone spectrum was subtracted, result converted to MRE and smoothed. For TFE experiments, 50μM peptide in PBS buffer was used (baseline corrected against PBS as background). *Lymnaea* gating brake peptide has little to no intrinsic secondary structure, but becomes progressively more α-helical with increasing amounts of added TFE. Adding a stoichiometric amount of CaM elicits modest structural change, in comparison.
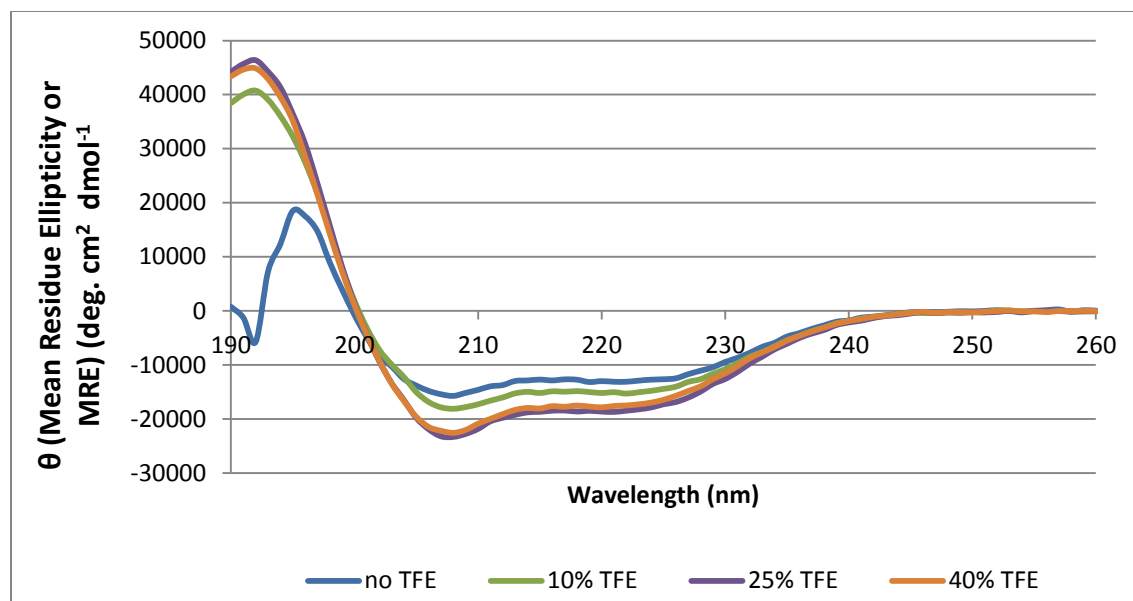
Figure 4.5: Ca$_V$3.1 (α1G) secondary structure is primarily α-helical in solution.
No CaM titrations were performed because the peptide is already α-helical (with little effect even at high %TFE), and would not provide meaningful analysis. Methods are the same as in **Figure 4.4**.
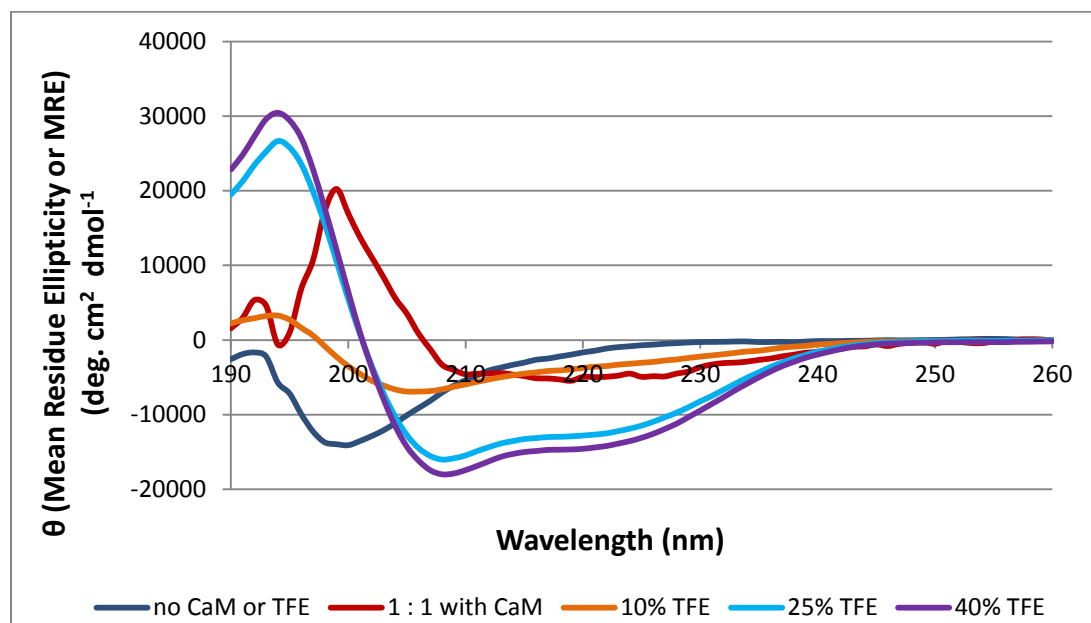
Figure 4.6: Ca$_V$3.2 (α1H) gating brake peptide secondary structure is strongly affected by TFE and somewhat less by CaM.
10μM CaM was used in the cuvette; 10mM HEPES as buffer. Methods are the same as in Figure 4.4. Similar to *Lymnaea* gating brake, human α1H has little to no intrinsic secondary structure, but is strongly affected by the addition of TFE, and substantially less by the addition of CaM.

151
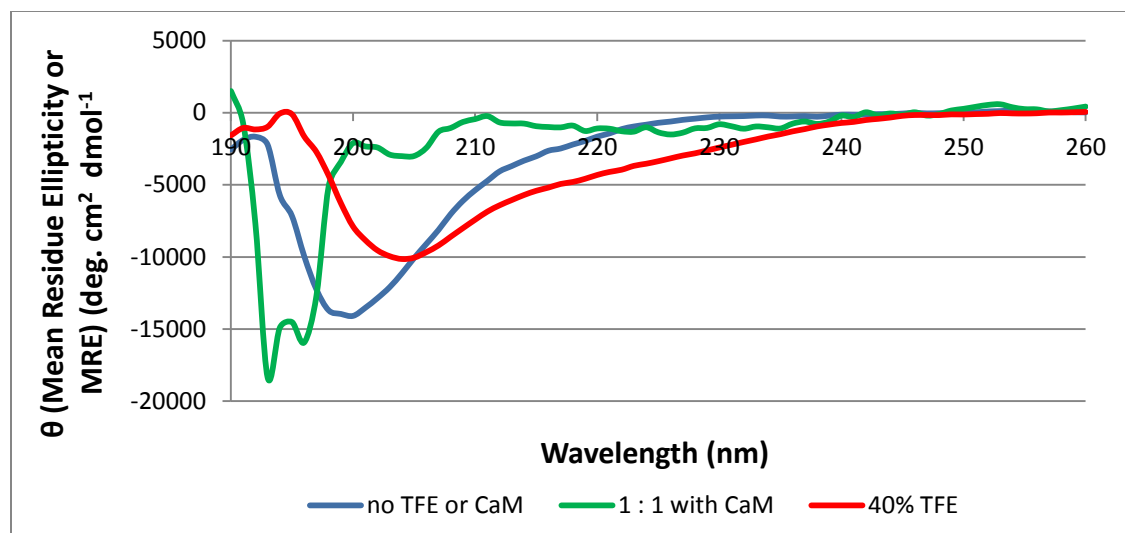
Figure 4.7: Mutant Ca$_V$3.2 gating brake peptide has very little secondary structure.
Same methods as Figure 4.6. The large 'peaks' below 200nm are likely subtraction/noise artifacts. This peptide has little to no α-helical propensity, owing to its Pro substitutions.
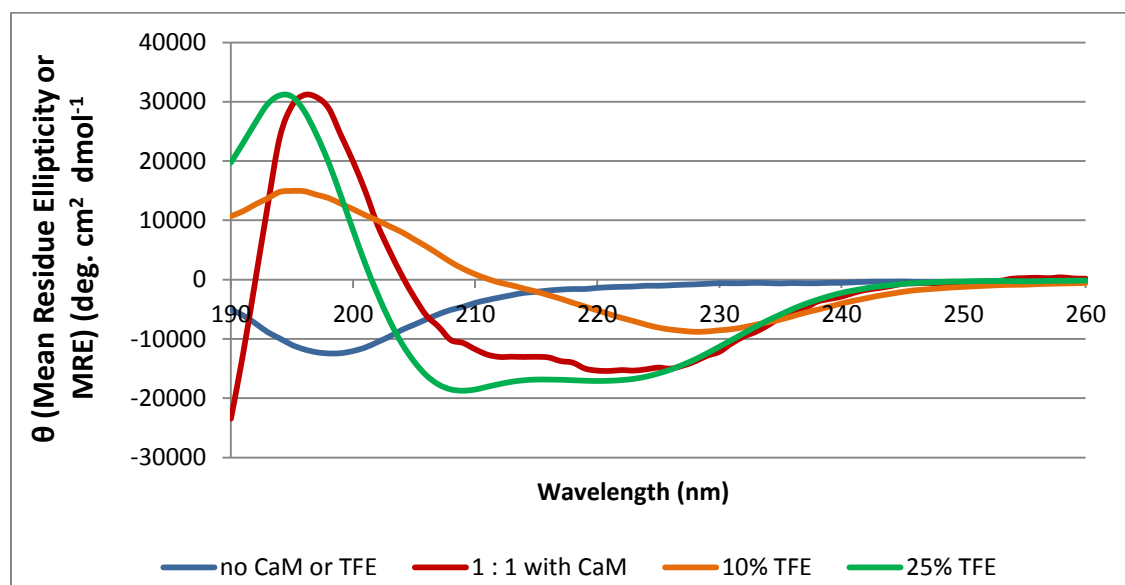
Figure 4.8: Ca$_V$3.3 gating brake peptide secondary structure is strongly affected by both CaM and TFE.
Human α1I is similar to α1H and *Lymnaea* gating brake peptides in that there is almost no intrinsic structure present, but it exhibits profound increase in α-helical content upon CaM and TFE addition. Same methods as in Figure 4.6. 40% TFE trace was not obtained due to peptide aggregation.

4.3.4 ITC

The relative affinities of each gating brake peptide are summarized in Table 4.2
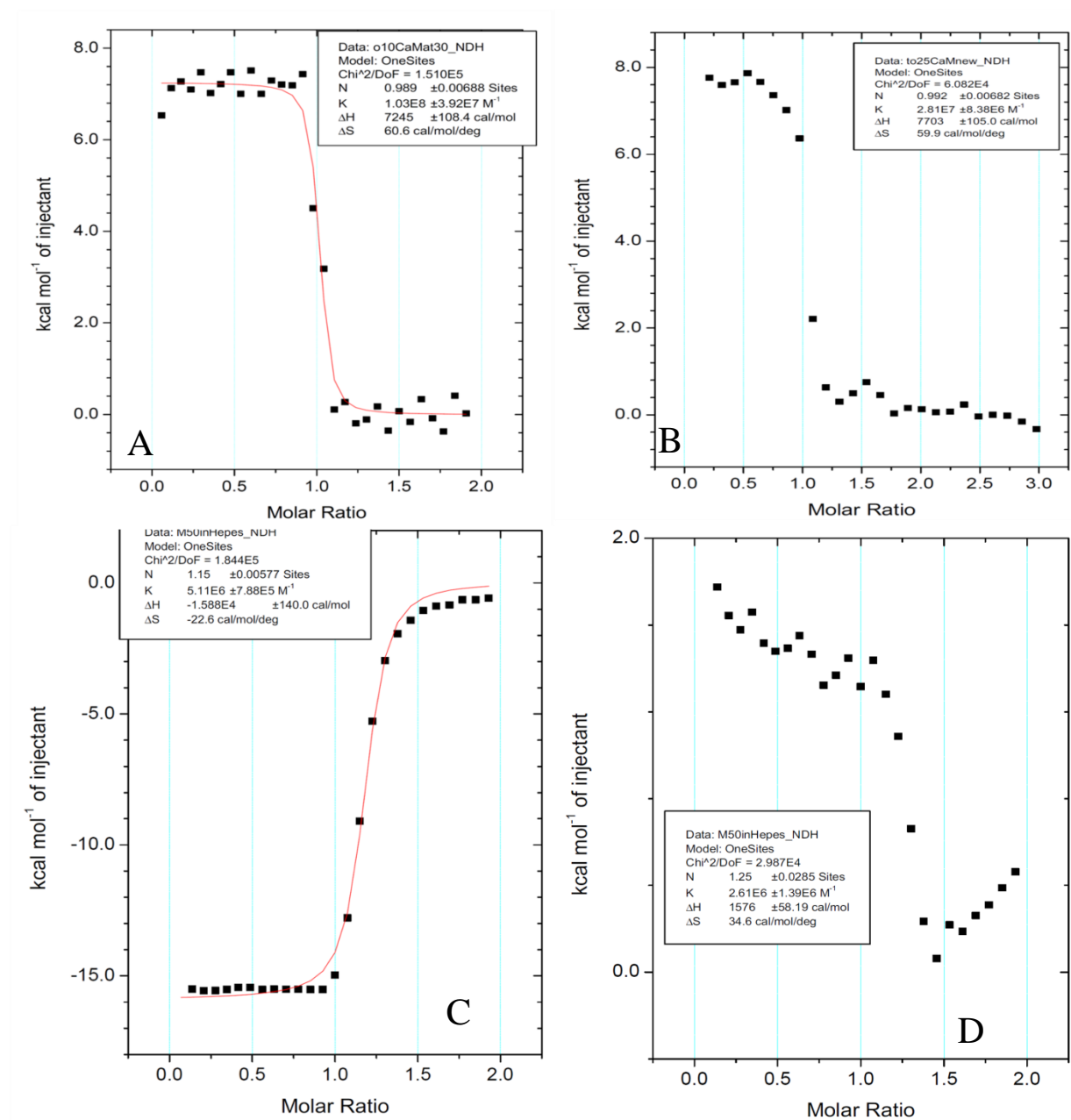
Figure 4.9: Representative isotherms for the wild type CaM and gating brake peptide titrations.
A: LCa$_V$3. B: α1G (Ca$_V$3.1). C: α1H (Ca$_V$3.2). D: α1I (Ca$_V$3.3). All titrations were done in HEPES 10mM (pH 7) with 0.5mM CaCl$_2$, with 200μM peptide (syringe) and 20μM CaM (cell). Ca$_V$3.3 had to be baseline corrected against the heat of dilution (to make all Y-values negative) in order to be fitted.

Wild type CaM was found to bind to the gating brake of LCa$_V$3 with ~nanomolar affinity, the highest of any peptide characterized so far in this dissertation (Table 4.2 and Figure 4.9). The human isoforms had somewhat lower affinities; as well, the Ca$_V$3.2 isoform had an exothermic profile in contrast to Ca$_V$3.1 and LCa$_V$3. Ca$_V$3.3 was found to aggregate at high concentrations (>200µM). At lower concentrations, a negative isotherm (endothermic) was observed but the heats of dilution have a high negative enthalpy (exothermic), which masks the interaction upon first inspection. Integration and baseline adjustment resulted in a more reproducible endothermic curve; however it was not easily fitted to a one-sites model and the SEM values are quite high.

Table 4.2: Summary of ITC results with gating brake peptides.
Each experiment was performed in at least triplicate.

Experiment	N	±	Kd (µM)	±	ΔH (cal/mol)	±	ΔS (cal/mol/deg)
Wild type CaM with gating brake peptides							
LCa$_V$3	0.989	0.00688	0.010	0.004	7245	108	60.6
Ca$_V$3.1	0.992	0.00682	0.036	0.011	7703	105	59.9
Ca$_V$3.2	1.15	0.00577	0.196	0.030	-15880	140	-22.6
Ca$_V$3.3	1.25	0.0285	0.383	0.204	1576	58	34.6
LCa$_V$3 gating brake with EF hand CaMs							
CaM$_{12}$	1.08	0.0121	0.102	0.031	-7217	145	7.8
CaM$_{34}$		N/A					
CaM$_{1234}$	0.949	0.109	4.329	3.561	-6084	964	4.2

CaM$_{34}$ does not appear to bind the LCa$_V$3 gating brake, whereas CaM$_{1234}$ clearly shows an interaction; these experiments were repeated several times to confirm this. The CaM$_{1234}$ isotherm was strong but not typical for a one-set-of-sites interaction; in this case the heat of dilution is endothermic while the interaction appears exothermic, obscuring the analysis greatly. The data had to be baseline-corrected to negative values in order to be fitted.

Both CaM_{1234} and CaM_{12} were exothermic and had a weaker interaction with LCa_V3 gating brake than wild type CaM (Figure 4.10), with the overall order: wtCaM $>CaM_{12}>>CaM_{1234}$. Due to limits on time and equipment, only the *Lymnaea* gating brake peptide was analyzed with the EF hand CaM mutants; additional work is ongoing.
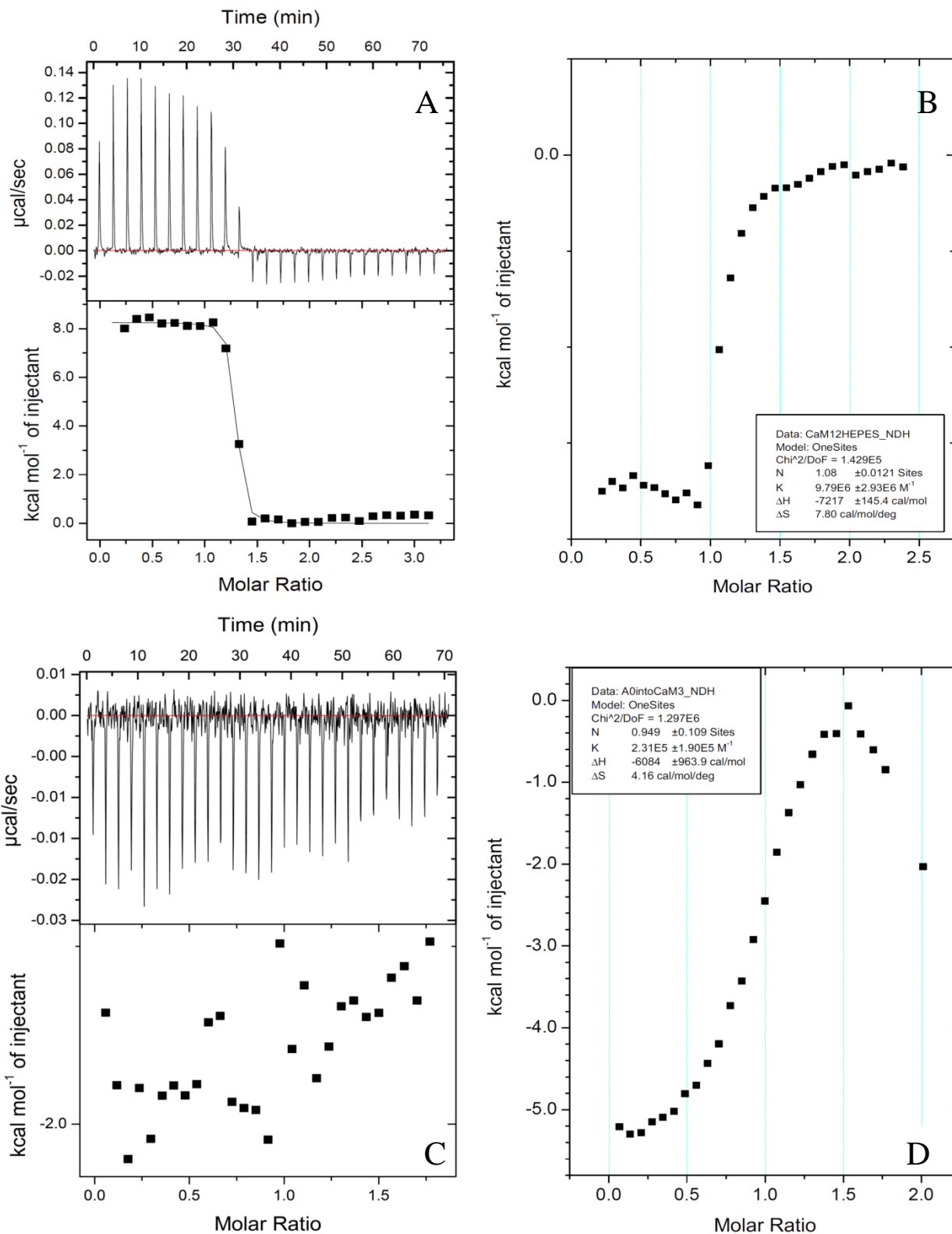
Figure 4.10: EF hand CaM mutants with LCa$_V$3 gating brake peptide.
A) Wild type CaM with LCa$_V$3 (for comparison), including raw data (top panel). B) CaM$_{12}$. C) LCa$_V$3 titrated into CaM$_{34.}$ Raw data in the top panel (for a sense of scale) and integrated data in the bottom panel D) CaM$_{1234}$. Same methodology as Figure 4.9

4.4 Discussion:

In this chapter, we sought to characterize the gating brake of LVA channels (*Lymnaea* Ca$_V$3, human Ca$_V$3.1, 3.2 and 3.3, as well as a mutant of Ca$_V$3.2). Much to our surprise, LCa$_V$3 gating brake peptide has the highest affinity for Ca^{2+}-CaM, followed by α1G (Ca$_V$3.1), α1H (Ca$_V$3.2) and finally α1I (Ca$_V$3.3). The latter has serious aggregation issues due to its hydrophobicity and did not produce a reliable isotherm with ITC, although it does have a weak but detectable gel shift effect on CaM in native PAGE. Urea attenuates the gel shift effects of the mammalian peptides, but does not appear to affect the interaction of LCa$_V$3 gating brake and CaM. As a chaotropic agent, urea likely disrupts both the helical conformational transition of the peptides and destabilizes the hydrophobic interactions between CaM and peptide.

An extremely puzzling observation in our ITC results was that, while having similar affinity, the two mammalian isoform peptides (α1G and α1H) have opposite signs for their enthalpy; i.e. the former is endothermic, like LCa$_V$3, and the latter is exothermic, like all the previously described L-type channel peptides. Enthalpy changes usually accompany electrostatic and hydrogen bond formation, while entropy changes account for solvation and van der Waals effects (Muralidhara et al., 2007; Freyer and Lewis, 2008). Considering that only α1G gating brake peptide is significantly structured when free in solution, we can rule out helix formation as a factor contributing to this difference. Thus, while being fairly similar in sequence and physiochemical properties (i.e. size, isoelectric point, hydrophobicity), the different isoforms have rather distinct biophysical interaction parameters with CaM. It is clear that α1G has a high number of Ala residues, which are known for their alpha-helical propensity, while the other peptides are unstructured when free in solution, but easily converted to an alpha-helix by addition of TFE or somewhat less by CaM. Interestingly, the mutation of α1H with a 6-residue

replacement to the helix-disrupting Pro-Gly(x3) motif completely abolishes any α-helical propensity this motif has, and renders it insensitive to the addition of CaM. We were also unable to detect any binding of the $Ca_V3.2$ mutant peptide to CaM by ITC, and it failed to display a gel shift in either urea+ or urea-free PAGE. While secondary structure most definitely has a role in CaM binding, it is not strictly indicative of strong CaM binding, since LCa_V3 has a much higher CaM affinity and does not form an α-helix on its own. Admittedly, the large PGPGPG substitution in α1H mutant peptide has other effects besides helical disruption. It would be interesting to see if milder helix-disrupting mutations, such as single Pro substitutions in key residues, or A→G mutations in α1G or LCa_V3 gating brake peptides would affect their affinity for CaM. Unfortunately, there was a large standard error in the association constant for $Ca_V3.3$ (α1I) due to aggregation issues at high peptide concentrations (300-500μM). Lower concentrations of peptide (up to 300μM) did produce an isotherm, but it was not easily fitted, and the noise level is high due to the opposite signs for the binding and dilution enthalpies. Of course, it is also possible that the CaM binding site for this isoform is slightly different than the sequence contained within our synthetic peptide, which could be subject of a future study.

Another highly interesting observation is that the gating brake peptide, at least the one from *Lymnaea*, appears to bind CaM_{1234}, as well as CaM_{12}, but not CaM_{34}. The apparent interaction of LCa_V3 gating brake with apo-CaM is completely unexpected.

All of the EF hand CaM mutants produce exothermic peaks, in contrast to wild type CaM. CaM_{1234} transitions to endothermic peaks post-equivalence, likely a contribution of the heats of dilution of peptide, but the overall shape of the curve is exothermic. Whether this is indicative of multiple binding conformations (e.g. apo *versus* holo CaM) with different affinities or some kind of Ca^{2+} specific effect is unclear. This could potentially be due to the mutant CaM

not being representative of 'real' apo-CaM (much like the individual lobe mutants), since the gel-shift results fail to show altered CaM mobility with any of the gating brake peptides in the presence of EDTA. Unfortunately, the gating brake peptides are also subject to aggregation with EDTA, much like the IQ peptides, and thus we were unable to verify this with ITC (the concentrations used in gel shift studies are substantially lower). There is also a possibility that CaM_{34} is ultimately an 'impossible' CaM conformation for peptides to effectively interact with, as there are few cases of native N(2)-C(0) Ca^{2+} CaM conformations (Schumacher et al., 2001). This might mean that the cooperativity for a conformational change leading to holo-CaM's open conformation is reliant on Ca^{2+} binding to the C-lobe (Linse et al., 1991; Ikura, 1996; Vetter and Leclerc, 2003; Yamniuk and Vogel, 2004; Wu et al., 2012). Thus, the gating brake might be pre-associating to apo-CaM, and subsequently 'locking' it on when Ca^{2+} binds. A series of pull-down studies with CaM and mutants may be needed to verify this theory (e.g. using immobilized CaM or apoCaM as 'bait' for isolating whole T-type channels from whole or partially purified cell lysates).

Regrettably, we lack an experimental electro-physiological confirmation of our biochemistry results; T-type channels are notoriously hard to clone (Senatore and Spafford, 2010). There are some interesting I-II linker studies with mammalian T-type channels, which we may attempt to replicate with LCa_V3 in the future, as well as additional CaM-mutant experiments are outlined in the following chapter. There has only been one study suggesting a direct modulation of T-type channels by CaM through the use of CaM synthetic antagonists, namely W7 and trifluoroperazine, which irreversibly altered the biophysical parameters of these channels and reduced the whole cell macroscopic currents in mouse spermatogenic cells (López-González et al., 2001). However, the exact molecular details for this effect have not been described.

Proximal (near IIS6) linker deletion strongly affects channel gating parameters (hyperpolarization of the I-V curve), but these residues precede the second helix of the cognate gating brake where CaM is predicted to bind, so it is unclear what exact role CaM may have on the mechanics of this channel. These effects are reminiscent of the effects of the IIS6-AID rigid helix in β-subunit regulation of HVAs, but there is no such effect known in LVAs. It is possible that the gating brake may have distinct roles for the two helices in its 'helix-loop-helix' motif, suggested by previous (unpublished, Dr. Adriano Senatore) work involving the deletion of distal YYKT residues, i.e. the last 4 residues in the *Lymnaea* gating brake peptide. There is very little biophysical data to describe the molecular effects of the gating brake or how it could produce the varying results in the three different isoforms, and only one relatively modern 'gating brake model' exists (Perez-Reyes, 2010), which places this motif in close contact to the voltage sensor paddle region (S4 helix and the S4-S5 linker coupling it to the activation machinery). As we are the first group to report the binding of CaM to this motif, there is little evidence to base our physiological model on. Tentatively, we predict that the CaM interaction is involved in Ca^{2+}-dependent effects on gating in these channels; this can be tested by various CaM mutant experiments which we will outline in the next Chapter.

4.5 Conclusions:

The main objective of this chapter was to characterize a novel CaM-binding site in the I-II linker of both mammalian and snail T-type channels. This motif is actually part of a previously described 'gating brake' regulatory region in these channels. There is considerable difference in the binding parameters for the three mammalian and the one snail isoform peptides, both in their affinity and thermodynamics. The degree of amino acid conservation is lower for the CaM-

160

binding sequence than the helix preceding it (Perez-Reyes, 2010). More importantly, the snail isoform, at least, is capable of binding apo-CaM, and may serve as a CaM tethering site *in vivo*. A solution structure of both Ca^{2+} replete and deficient CaMs bound to this peptide would be a promising future project.

We propose that this motif is a novel, CaM-centric regulatory mechanism that may affect gating properties of these channels in response to Ca^{2+} entry.

Chapter 5: Conclusions, contributions, and future directions.

5.1 Overview and Summary

The general goals of this dissertation have evolved as a result of new knowledge and concurrent studies that have been published in the course of its completion. At the outset, the main goal was the development of a generalized, universal model of voltage-gated calcium channel (VGCC) regulation by calmodulin (CaM), in both molecular and physiological terms. Over the course of several years and hundreds of experiments, PubMed queries and literature searches, it has become clear that such a generalized model is extremely unlikely. The level of conservation of the putative regulatory sites among the different groups of VGCCs (Ca_V1, 2 and 3) is meager at best, and their biophysical parameters may vary widely, in many cases even within a group (Catterall et al., 1988; Catterall, 2000; Hille, 2001; Liang et al., 2003; Perez-Reyes, 2003; Van Petegem et al., 2005; Zamponi, 2005; Talavera and Nilius, 2006; Dunlap, 2007; Ohrtman et al., 2008; Tuckwell, 2012; Christel and Lee, 2012; Senatore et al., 2012). Thus, a detailed molecular mechanism will have to be constructed independently for each distinct group or even isoform – an undoubtedly gargantuan scientific effort. Thankfully, certain regulatory motifs *within* groups, and the regulation that goes with them, appear to have been evolutionarily conserved from even before the isoform diversification seen in vertebrate channels. Isolating these elements in simple organisms (like *Lymnaea*) will lend important clues to these elements' roles and modes of action.

The IQ and NSCaTE motifs are prime examples of such elements, albeit the ubiquity and importance of the latter is still far from clear. The IQ motif is mostly synonymous with L-type channels; every metazoan genome containing an L-type channel sequence contains at least one exon with this motif (Taiakina et al., 2013). Its structure when bound to holo-CaM and many of the biophysical parameters are known. NSCaTE, in contrast, is more elusive and far less

conserved; possibly having arisen more than once through convergent evolution, although it is conspicuously absent in some invertebrates (see section 2.3.1). Other than basic biophysical properties of its interaction with CaM and some electrophysiology studies with missense and deletion mutants, not much is known about it, despite having been described over a decade ago (Ivanina et al., 2000). More recent research, including our own, points to a possible co-interaction between NSCaTE, IQ and CaM (Johny et al., 2013), although any direct biophysical proof, such as a pull-down or two-hybrid screen, is yet to be reported. More importantly, any concept of how CaM binding to one or both of these motifs actually proceeds to channel inactivation is entirely unknown. There have been numerous attempts to answer this question, through mutagenesis, labeling studies, chimeric constructs, homology modeling with molecular dynamics simulations and so on, but we are still no closer to a three-dimensional picture of how these channels inactivate in response to Ca^{2+} than when the phenomenon was first described (Brehm and Eckert, 1978). The major roadblock has been the inability to obtain a high resolution structure of an entire channel, due to the size limitations of NMR and solubility issues with crystallography. The model we *can* propose involves the construction of a very modest hierarchy of 'if-then' propositions based on all the different pieces of experimental evidence from numerous studies over the years. Below is an attempt at such a construct, where I also point out anywhere we have made contributions throughout this thesis, as well as how additional insights can be gained.
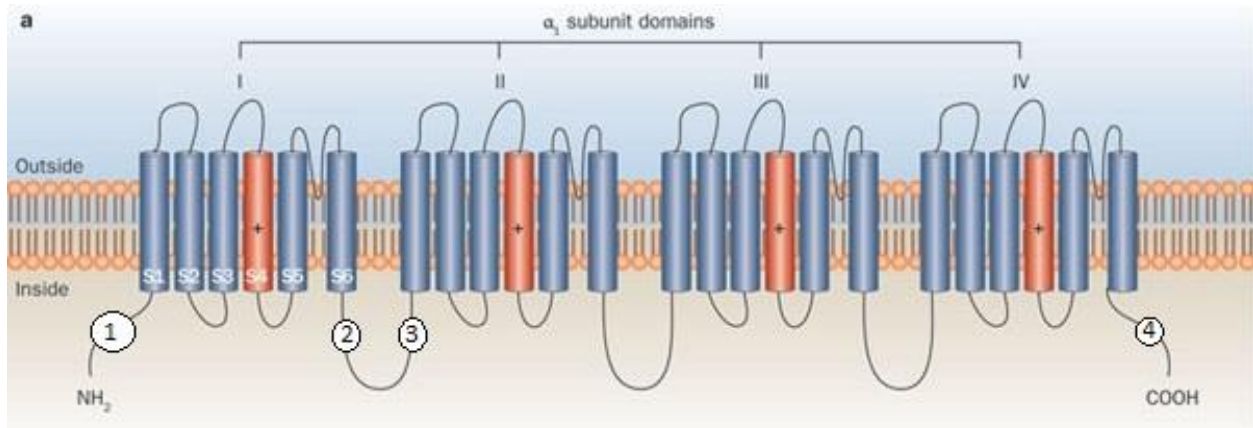
Figure 5.1: Summary of key channel motifs described/studied in this dissertation.
Not to scale**.** 1) NSCaTE (L-type channels only, Chapter 2-3). 2) α-interaction domain (AID) in HVA channels OR the gating brake in T-type channels (Chapter 4). 3) Previously identified CaM-binding site in L-type channels (possible docking site for an IQ-CaM-NSCaTE complex, see sections 5.6.3 and 5.6.4, and also 3.4 and Figure 3.9). 4) IQ motif (HVA channels, Chapter 2-3 and relevant references). Adapted from (Rajakulendran et al., 2012)

5.2 CaM regulation of L-type channels:

5.2.1 Inactivation as a concept

Insofar as CaM-dependent, and therefore, Ca^{2+}-dependent, regulation is observed, HVA channels are the best studied. They have been shown to have robust CDI and VDI, with the latter being strongly modulated by various exogenous factors involving phosphorylation and subunit composition, e.g. the β isoform, and the former being solely orchestrated by CaM^{24} and Ca^{2+} (Pitt et al., 2001; Dafi et al., 2004; Findlay, 2004; Cens et al., 2006; Barrett and Tsien, 2008; Minor and Findeisen, 2010; Tadross et al., 2010; Tekmen and Gleason, 2010; Poomvanicha et al., 2011; Tuckwell, 2012). Nonetheless, actual molecular details of these regulatory effects are less than clear. First and foremost, there is a major question of whether VDI and CDI share a common molecular endpoint – either via pore occlusion by a cytoplasmic channel motif akin to the 'hinged lid' mechanism of Na_Vs, or pore collapse such as that seen in KcsA (Yellen, 1998). So far, most of the experimental evidence points to an allosteric (hinged lid) mechanism, although a combination of different pathways is possible (see Section 2.4). It is also likely that some of these mechanisms share certain molecular features, as well as have their own distinct ones (Findlay, 2004; Cens et al., 2006; Barrett and Tsien, 2008; Findeisen and Minor, 2009; Minor and Findeisen, 2010; Tadross et al., 2010). The majority of evidence supporting the hinged-lid model comes from mutagenesis and chimeric studies involving the I-II linker of L-type channels and its interaction elements with the β-subunits. There is also evidence for a CaM interaction in a distal region of the I-II linker (Findeisen and Minor, 2009; Oz et al., 2011; Christel and Lee, 2012) as well as mutagenesis effects of some of these regions on CDI, a strong indication that

---

[24] While Ca^{2+}-CaM (and the integrity of its binding sites, e.g. the IQ motif and neighboring sequences) is essential for CDI, several other motifs were shown to be essential for CDI, such as the EF hand. Other regions have more modest effects, e.g. the I-II linker (possibly through a common mechanism with VDI) and more recently, NSCaTE.

there is yet a third channel motif in the Ca_V-CaM interactome. One of the key goals of future studies in this field should be to isolate and characterize this interaction and its interplay with the other regulatory elements of these channels.

5.2.2 Identification of apoCaM pre-association site(s):

Shortly after CaM was identified as the principal factor in CDI (Peterson et al., 1999) and the isolation of the IQ motif as the cognate effector sequence (Peterson et al., 2000; Zühlke et al., 2000; Pitt et al., 2001), it was also noted that apo-CaM is able to bind and pre-associate with several regions in the C-terminus of L-type channels (Erickson et al., 2001, 2003; Tang et al., 2003; Kim et al., 2004a). It was noted that while the IQ motif was essential to CDI, it did not bind apo-CaM with strong affinity; however, it did appear to increase the Ca^{2+} affinity of CaM's C-lobe (Tang et al., 2003; Halling et al., 2009). Despite extensive research efforts, so far there is still no clear picture of what constitutes an apo-CaM tethering site in $Ca_V 1$ channels, although it has been narrowed down to a few discontiguous sites in the proximal C-terminus surrounding the IQ motif. These may form a complex tertiary structure that houses apo-CaM in the resting state of the channel, and rearranges significantly upon channel opening and Ca^{2+} entry and binding to CaM, at which point Ca^{2+}(full or partial)-CaM also relocates to a higher affinity site on the channel and initiates an effector cascade. A logical experiment would be to substitute the native IQ motif of an L-type channel with one that binds apo-CaM (e.g. one from a sodium channel, or myosin) and note the effects on CDI.

5.2.3 CaM regulatory elements and their dynamic interplay

5.2.3.1 NSCaTE, CaM and the 'local/global' model.

The canonical ($Ca_V1.2$ and $Ca_V1.3$) L-type channels[25] show robust CDI even in high internal

buffering (10 mM BAPTA) (Budde et al., 2002), which is believed to proceed as a result of Ca^{2+}

binding to the C-lobe of CaM due to the transient elevation in 'local' Ca^{2+} immediately

surrounding the pore vicinity (Tadross et al., 2008). The C-lobe of CaM has a higher affinity and

a slower off-rate for Ca^{2+} than the N-lobe (Linse et al., 1991; Shepherd and Vogel, 2004; Zhang

et al., 2012), which fits well with the 'local' concept of CDI; the transient Ca^{2+} spikes from

single channel opening allow C-lobe of resident CaM to bind and effect channel closure before

Ca^{2+} is able to unbind and dissipate from CaM. The N-lobe, in contrast, has faster Ca^{2+} kinetics

and lower Ca^{2+} affinity, which presumably relegates it to the 'global' regulatory role whereby it

senses a total accumulation of cellular Ca^{2+} from diffuse sources. This renders the N-lobe

sensitive to high concentrations of chelators, either native or experimentally applied. At least,

that's the theoretical prediction of the 'local/global' model found in literature (Tadross, 2009).

On the one hand, this is consistent with the NSCaTE peptide's ability to bind either lobe of CaM

independently (Liu and Vogel, 2012). However, the buffer-resistance effects are not abolished by

EF hand mutations in CaM's C-lobe (CaM_{34}), especially in $Ca_V1.3$, suggesting that the N-lobe

may also play a *local* role – presumably through its interaction with NSCaTE (Dick et al., 2008),

although how this happens is not clear from their data. In order for such an effect to be possible,

the interaction with NSCaTE would have to reciprocally affect the Ca^{2+} binding of the N-lobe of

CaM, i.e. increase its affinity or reduce the dissociation rate for Ca^{2+}. No such effect has yet been

shown; however it is possible – fluorescence experiments with various Ca^{2+} gradients could test

---

[25] $Ca_V1.1$ (skeletal muscle, α1s) and $Ca_V1.4$ (retinal, α1F) channels have unique regulatory features that render them insensitive or incapable of CDI in their native states.

this hypothesis, for example, monitoring the Trp fluorescence change of NSCaTE at varying Ca^{2+} concentrations. Furthermore, our data actually shows a distinct buffer-sensitive component of CDI imparted to LCa_V1 (the invertebrate L-type homolog) by its own NSCaTE (see section 2.2.9). Additionally, we see a significantly lower affinity of both IQ and NSCaTE peptides for CaM_{34}, over either CaM_{12} or wild type CaM, which contradicts the N-lobe preference of NSCaTE reported by (Liu and Vogel, 2012). Whether this is a fundamental difference between the different lengths of peptides used, or a shortcoming of using EF hand mutants instead of 'true' partial-Ca^{2+} CaM conformations will have to be tested.

5.2.3.2 Suggested future experiments with NSCaTE:

To verify which lobe of CaM is most likely interacting with NSCaTE *in vivo*, additional experiments with LCa_V1 and ΔNT-LCa_V1, as well as EF hand CaM mutants and half CaMs will need to be performed. CaM_{12}, CaM_{34} and CaM_{1234} have already been cloned into the eukaryotic expression/reporter vector pIRES-dsRED[26] in our lab. Electrophysiology recordings on heterologously expressed LCa_V1 and ΔNT-LCa_V1 with over-expressed CaM mutants in various levels of internal buffering will either confirm or refute the findings in (Dick et al., 2008). ITC experiments with half-CaMs instead of EF hand mutants and NSCaTE/IQ peptides may yield additional results and establish the validity of the EF hand mutant approach. Ultimately, an NMR solution structure of an NSCaTE-CaM-IQ complex would confirm or refute the co-interaction hypothesis we proposed in Chapter 3 (Taiakina et al., 2013) and also by (Johny et al., 2013). There is a possibility that binding of NSCaTE to the CaM-IQ complex is fundamentally different, both structurally and functionally, than binding of NSCaTE or IQ to CaM alone. For

---

[26] A bicistronic expression vector with a red GFP variant to monitor expression of the construct.

this question to be answered, an expression system for soluble NSCaTE and IQ motif constructs will have to be designed. Our own early work (section 2.2.2) and previous studies aiming to characterize the apo-CaM preassociation site in the C-terminus (Kim et al., 2004a) have shown this to be a challenging process due to inclusion body formation and expression problems in absence of CaM co-expression. While we were able to circumvent the issue somewhat by the addition of exogenous purified CaM during HIS-NSCaTE protein refolding, co-expression of wild type CaM is a viable alternative. An issue may arise if only one of the two has to be isotope-labeled for NMR; in this case the exogenous CaM method may be more desirable.

Thus far, the majority of NSCaTE studies have sought to look for its function through disruptive mutagenesis and isolated *in vitro* peptide studies, like ours. None have yet looked at the possibility that its modest binding affinity and seemingly transient nature of interaction[27] is actually required for its molecular role, whatever that may be. It would therefore be an interesting experimental approach to test if increasing the interaction strength, via improving the amphipathic nature of the peptide, changing the size of hydrophobic anchors or increasing its alpha-helical content/propensity through site-directed mutagenesis, would alter its physiological effects. Alternatively, the entire motif can be replaced with one that binds CaM strongly – for instance, the gating brake peptide of LCa$_V$3. We cannot conceivably predict what such a mutation would do, but it should have a strong impact on CDI.

5.2.3.3 Finding the 'lid': shotgun approach:

Even after (or if) the structure of CaM/IQ/NSCaTE and some of the physiological parameters of such an interaction are determined, it is still unclear what molecular process

---

[27] We have been unable to 'capture' a stable CaM-NSCaTE complex by formaldehyde cross-linking or even gel filtration chromatography; data can be found in the Appendix.

underlies their contribution to CDI. If indeed a 'hinged lid' mechanism is responsible for channel inactivation, the most likely answer is that this CaM-driven complex is driving the docking of an intracellular motif close to the channel pore or activation machinery, that is, at the S6 bundle crossing, or near the S4/5 sensor/linkers. If this is true, a comprehensive, high-throughput search for an interaction site for NSCaTE, IQ, or CaM bound to one or both of these, can be undertaken using a peptide array. Much like DNA microarrays, they aim to find possible leads for novel interactions through exposure of short peptides to a queried partner; in this case, either NSCaTE, IQ, or CaM bound to one or both peptides (Diehnelt, 2013; Hansen et al., 2013; Price et al., 2013). Positive hits can then be further characterized with full length peptides using standard biophysical methods (Chapter 2-4) and mutagenesis for elucidation of a complete mechanism and mode of action. There is a strong possibility that the distal I-II linker of L-type channels will come up as a lead, which would be a triumph for the convergent CDI/VDI molecular endpoint camp of thought (Cens et al., 2006; Minor and Findeisen, 2010; Tadross et al., 2010).

5.3 CaM regulation of non-L-type channels:

5.3.1 Other HVAs:

Unlike the L-type channels, the HVA neuronal (N, R, P/Q type) channels lack any coherent regulatory analysis models. Their molecular and physiological diversity has been as much a roadblock as the lack of structural data for Ca_Vs in general. Chimeric studies and isolated biophysical experiments on channel motifs from these isoforms have had limited success in describing a universal regulatory model for any of these channels; only isolated details for each isoform have so far been described .

```
CaV1.2    WKRTSMKLLDQVVPPAGDDE---VTVGKFYATFLIQEYFRKFKKRKEQGLVGKPSQRN--
LCaV1     WKRTSPKLLDQVVPPAGRDDD--VTVGKFYATFLIQDYFRRFKKRKEQMVKISKGQEH--
LCaV2     WPVQGKKMMDMLMPPSDELDEGKMSVGKIYAGLLISENWKAYKAS--QNASNNFKMRPSL
Cav2.2    WANLPQKTLDLLVPPHKPDE---MTVGKVYAALMIFDFYKQNKTT-----RDQMQQAPGG
Cav2.3    WPHLSQKMLDLLVPMPKASD---LTVGKIYAAMMIMDYYKQSKVKKQRQQLEEQKNAP-M
Cav2.1    WPNLSQKTLDLLVTPHKSTD---LTVGKIYAAMMIMEYYRQSKAKKLQAMREEQDRTPLM
          *       * :* ::.       :    ::***.** ::* : :.   *          .
```

Figure 5.2: CLUSTALW Alignment of the 'IQ' motifs of various HVA channels.
LCa$_V$1 & 2 are *Lymnaea* homologs of Ca$_V$1.2 and Ca$_V$2.x, respectively. Red box indicates the peptide sequences analyzed in this dissertation.

For Ca$_V$2 channels, there is some evidence for IQ-motif-mediated CDI; however it is not present under high internal buffering and in single channel recordings (Peterson et al., 1999; Lee et al., 2003a; Kim et al., 2008; Christel and Lee, 2012). Additionally, the motif sequence conservation is much lower in non-L-type channels, to the point where calling them "IQ" motifs is not really meaningful; for instance, the Gln residue is typically a Phe or Met in these channels (see Figure 5.2). Therefore, basing regulatory models on similarity to L-type channels is likely erroneous. Nonetheless, CaM is most definitely required for CDI in these channels, even if their CDI is limited to the 'global' mode and the CaM-IQ interaction is dissimilar to the more 'canonical' IQ motifs of L-type channels.

We have observed binding of CaM to the IQ motif of α1$_A$ (Ca$_V$2.1, or P/Q-type) that has a 2 : 1 stoichiometry and relatively weak affinity (~1uM) (Chapter 3). Combined with the fact that there were structures published of both parallel and anti-parallel orientations of CaM-IQa, this may be an interesting clue as to how CaM is able to elicit both CDI and CDF within this channel: that is, through a structural rearrangement of the IQa-CaM complex in response to differing Ca^{2+} concentrations (Kim et al., 2008; Mori et al., 2008; Kovalevskaya et al., 2013).

We also tested CaM for interaction with an IQ peptide of LCa$_V$2 (Appendix, Figure A.9), and noted a 2 : 1 stoichiometry, but no CaM gel shift (data not shown). In the future, a comprehensive analysis of Ca$_V$2.x IQ peptides for interaction with CaM may be needed to

explain isoform-specific differences in Ca^{2+}-CaM regulation. Alternatively, a bioinformatics scan of other possible CaM binding sites could reveal novel interactions, which will need to be verified with peptide experiments. Any confirmed interaction will then need to be characterized for its physiological relevance by electrophysiology experiments.

5.3.2 T-type channels:

Although they have been observed in recordings over three decades ago (Llinás and Yarom, 1981), T-type channels are still fairly 'new' in the sense of what is known regarding their molecular mechanisms. Due to the lack of structural information common in this field, very little is known about the exact molecular details of their behavior. Several important features have been described, largely attributed to chimeric and mutagenesis studies involving various cytoplasmic regions of the channels.

A high affinity divalent metal binding site in $Ca_V3.2$ (His191 in DIS3-4 linker), but not other T-type channels, has been used to identify this isoform using Ni^{2+} as a specific blocker (Talavera and Nilius, 2006).

T-type channels are also subject to regulation by phospholipids, G-protein modulation, proton block, phosphorylation (notably, CaMKII) and alternative splicing – for a comprehensive review, see (Senatore et al., 2012). In turn, T-type channels are direct effectors for a number of different pathways involving Ca^{2+}-signaling, such as low-threshold exocytosis, extracellular regulated kinase (ERK) pathways, nitric oxide synthase (NOS) and calcineurin/NFAT[28] activation (Choi et al., 2005; Clapham, 2012; Oliveria et al., 2012; Weiss et al., 2012; Huang et

---

[28] Nuclear factor of activated T-cells, a family of transcription factors; calcium binding to calcineurin results in the translocation of both calcineurin and the associated NFAT to the nucleus. Several oncogenic pathways appear to be triggered by a derailment of NFAT regulation (Rusnak and Mertz, 2000)

al., 2013). There also appears to be a functional and possibly structural link between certain T-type and calcium-gated small conductance (SK) potassium channels and even voltage gated potassium channels (K_V4), although the implications for the latter are somewhat unclear (Wolfart and Roeper, 2002; Anderson et al., 2013)

Unfortunately we still do not fully understand how these channels perform their roles and what molecular features are responsible for their distinctly hyperpolarized (in)activation profiles. One of the more conserved features that has been identified, a gating brake in the I-II linker, appears to have varying effects depending on which region is deleted (or mutated) (Arias et al., 2005; Talavera and Nilius, 2006; Baumgart et al., 2008). The gating brake is a helix-loop-helix motif in the proximal region of the I-II linker and is responsible for gating and activation kinetics of mammalian Ca_V3 channels. Several regions downstream of this motif affect surface trafficking of the channel in both human and *Lymnaea* models. We have described a completely novel interaction between CaM and this second helix in *all* Ca_V3 isoforms (human and snail), although we have not yet been able to characterize the physiological effects of this interaction. Previous studies have suggested a potential role for CaM via the phosphorylation of the II-III linker by CaMKII, as well as the calcineurin/NFAT pathway, but there has been no evidence to date to suggest a direct physical interaction of this channel family with CaM. What is more, this interaction appears to be variable among the three isoforms, at least in biophysical terms, which may explain some of the isoform-specific effects of linker truncations (Baumgart et al., 2008). It also appears that apo-CaM may be able to interact with the gating brake – in a different mode than with holo-CaM. Thus, there may actually be a calcium/CaM-dependent form of regulation for these channels that is universally conserved and has yet to be fully elaborated.

In the future, detailed EF-CaM and half CaM titrations with all of the gating brake peptides (Ca$_V$3.1-3.3), as well as electrophysiology recordings with gating brake/CaM mutant combinations (for human and snail isoforms) will confirm or refute this theory. Additionally, a solution structure of the gating brake-CaM complex can be solved and provide more detailed structural insights into how this interaction occurs, as well as reveal key interacting residues which will be strong candidate for mutagenesis studies. The structure will require a labeled gating brake peptide or a recombinant protein construct, and several different NMR experiments (HSQC/COSY and NOESY) and full residue assignments, all of which will require a considerable time investment. At the present, with such a limited pool of evidence, we cannot conceivably say what role CaM has on the biophysical properties of these channels.

5.4 Other Ca^{2+}-binding proteins:

While CaM is undoubtedly important in the regulation of seemingly every calcium channel, it may not be the only protein capable of such regulation. There are dozens of EF hand proteins with varying degree of similarity to CaM (Ikura, 1996; Gifford et al., 2007). There are also three conservative amino acid changes (Y99F, Q143T and A147S) in *Lymnaea* CaM that are also shared with *Drosophila* and *C.elegans* CaM, which may have small but significant differences in the corresponding CaM-channel interactions in those species – a question perhaps for a future study.

Indeed, CaBP1(calcium binding protein 1, a CaM homolog) has been shown to attenuate CDI in a Ca^{2+}-independent manner and instead causes CDF of Ca$_V$1.2 and enhances its VDI (Findeisen and Minor, 2010; Oz et al., 2011). Interestingly, CaBP1 also binds the C-terminal IQ motif that overlaps the CaM binding site, and *also* the N-terminus of Ca$_V$1.2, however at a site

distal to NSCaTE. CaBP1 and CaM appear to compete for the C-terminal site in their apo-state, although Ca^{2+}-CaM easily outcompetes CaBP1 regardless of the latter's Ca^{2+} state (Findeisen et al., 2013).

Much additional characterization of the interplay between CaM and CaBP1 will be necessary to determine the molecular mechanism by which they elicit their effects and their physiological importance. However, as CaBP1 is primarily a neuronal protein unique to vertebrates (Haeseleer et al., 2000), its relevance to the conserved mechanisms of L-type CDI across other phyla or non-neural tissues is questionable. We have not looked at CaBP1 as a candidate for regulation of heterologously expressed channels, although it may be interesting to see if there is any effect with its co-expression with various Ca_Vs.

5.5 Summary of Original Contributions:

5.5.1 *Lymnaea* NSCaTE is a global regulator of CDI

We have characterized the NSCaTE motif of an invertebrate L-type homolog (LCa_V1) and its binding to CaM under various conditions. Prior to this study, there has been no indication that NSCaTE may be present in non-vertebrate phyla, or that its role may differ based on isoform. Mammalian NSCaTE appears to have a 'local' regulatory effect as evidenced by the seminal work with CaM EF hand and NSCaTE deletion mutants (Dick et al., 2008), in contrast to our results with the invertebrate NSCaTE, which we find to have an increased 'global' effect on CDI. Further studies with *Lymnaea* NSCaTE paralleling these experiments may be necessary to confirm its distinct role as a global regulator of CDI.

5.5.2 NSCaTE as an optional motif:

Through qRT-PCR, we show no difference in NSCaTE-containing transcripts (e.g.

approximately every channel transcript contains an NSCaTE sequence), suggesting that the

downstream Met, if used, is solely a translational regulatory mechanism. To confirm this fully,

detailed histo-immunochemical studies with NSCaTE-specific antibodies will be necessary.

5.5.3 NSCaTE may form a tertiary complex with IQ-CaM:

While we lack direct biophysical evidence for such a complex (e.g. a structure), we have

convincing thermodynamic data to support that a co-interaction between all three partners (CaM,

NSCaTE, IQ) is occurring (see section 3.4 and Figure 3.9). A previous study refuted such a

complex because they were unable to facilitate a pull-down with such a complex by native

PAGE (Benmocha et al., 2009), although neither were we (see Appendix Figure A.4-7). The

complex is likely affected by other parameters *in vivo*, and may be of a weak/transient nature,

which makes it very difficult to capture using standard biophysical methods, consistent with

rapid channel inactivation and recovery. A solution structure or a pull-down study of such a

complex would likely settle the debate.

5.5.4 CaM is capable of interaction with T-type channels directly via the gating brake:

The helix-loop-helix motif in the proximal I-II linker of LVA channels that has been

previously described as important for their inactivation and gating properties was also found to

bind CaM *in vitro*. The peptide corresponding to the second helix from each of the three

mammalian isoforms as well as LCa$_V$3 was subjected to a detailed biophysical analysis using

spectropolarimetry, native PAGE and ITC; all evidence supports a strong interaction with CaM. This novel interaction appears to be variable by isoform, which may hold clues as to its mechanism and role *in vivo*.

EF hand mutant CaM experiments suggest that at least the *Lymnaea* isoform gating brake is capable of binding apo-CaM. Much additional work to determine the physiological impact of these interactions is still needed (see next section).

5.6 Recommendations for future studies:

5.6.1 NSCaTE mutagenesis:

Although the NSCaTE motif has been convincingly established as a regulatory element in L-type channel CDI, the exact molecular mechanism of how it exerts its effects is still unclear. One possible avenue of investigation is chimeric studies with NSCaTEs from different isoforms (or species). If mammalian NSCaTE is a 'local' regulator and the *Lymnaea* NSCaTE is 'global', then a chimeric snail channel with a mammalian NSCaTE should exhibit increased buffer-resistant CDI compared to wild type.

There have been several attempts in our lab to create mammalian-snail NSCaTE/channel hybrids (data not shown); however, none of the partial constructs were able to be cloned into a full-length channel.

Furthermore, instead of deletion and loss-of-function mutants to analyze NSCaTE effects, it would be interesting to see if an increased NSCaTE-CaM affinity would affect CDI. Altering the sequence to create a stronger α-helical propensity, or simply replacing it with a higher-affinity CaM binding sequence altogether may be a viable study.

5.6.2 NSCaTE and CaM binding to Ca^{2+}

It is entirely possible that the 'local' effects of mammalian NSCaTE are actually a result of CaM's altered affinity for Ca^{2+} upon binding NSCaTE. Previous studies, including the IQ motif of other channels, have shown similar properties for other CaM-binding peptides. Biophysical experiments (e.g. ITC or fluorescence) using the NSCaTE peptides and CaM under varying Ca^{2+} concentrations should answer this question.

5.6.3 NSCaTE and co-interaction with IQ-CaM:

To confirm that such a complex exists, either a pull-down of the complex or a solution structure of the peptides in complex with CaM is required. For the former, one can use standard biophysical methods to isolate a complex via CaM, by using an immobilized C- or N-terminal protein construct (e.g. IQ, or NSCaTE, respectively) as 'bait' to isolate the opposing construct in the presence vs. absence of CaM (and Ca^{2+} vs. EDTA). For the latter, isotope-labeled peptides in various combinations (e.g. $^{15}N/^{13}C$ labeled IQ and NSCaTE) will be required, which may also require expression optimization if they are to be produced in-house. Currently we do not have optimized expression constructs for either of these regions. In either scenario (e.g. NMR or protein 'fishing'), an extensive time course for the project is recommended.

5.6.4 Peptide 'fishing study' for the possible docking site of IQ/RN-CaM complex:

To test whether CaM bound to one or more of the CDI effectors (IQ or NSCaTE) is actually a physical component of the 'hinged lid' inactivation particle, a high throughput screen for its binding target in L-type channels can be undertaken. A peptide array consisting of a large number of 10-20 contiguous residues corresponding to a stretch of a cytoplasm-exposed region

of the channel can be generated; these would then be 'probed' for interaction by a fluorescently labeled CaM/IQ/NSCaTE 'bait'. Positive hits can be identified on a standard fluorescence imager and further characterized as potential interactions using larger length peptides. Considering the time and cost involved in such a project, this is a rather risky endeavor but will be most exceptionally fulfilling if the docking hypothesis is indeed correct.

5.6.5 T-type channel recording with CaM mutants:

To verify the role of the gating brake and CaM interaction and its physiological relevance, a combination of gating brake mutants and EF hand CaM mutants, and/or varying the internal buffering conditions will be needed. We have already cloned the necessary CaM mutants ($CaM_{12, 34}$ and $_{1234}$) into a mammalian expression vector, but the gating brake mutations in either mammalian or snail isoforms will have to be made. These mutants can then be recorded in standard whole-cell voltage clamp or patch-clamp mode in various combinations of CaM and channel mutants. Theoretically, altering the CaM-gating brake interaction should affect channel gating.

In addition to electrophysiological data, a solution structure of CaM in complex with the gating brake peptide could be solved; an HSQC spectrum of such a complex (holoCaM and LCa_V3 gating brake) is already available (see Figure 4.3).

Bibliography:

Al-Sayed MD, Al-Zaidan H, Albakheet A, Hakami H, Kenana R, Al-Yafee Y, Al-Dosary M, Qari A, Al-Sheddi T, Al-Muheiza M, Al-Qubbaj W, Lakmache Y, Al-Hindi H, Ghaziuddin M, Colak D, Kaya N (2013) Mutations in NALCN Cause an Autosomal-Recessive Syndrome with Severe Hypotonia, Speech Impairment, and Cognitive Delay. Am J Hum Genet 93:721–726.

Anderson D, Engbers JDT, Heath NC, Bartoletti TM, Mehaffey WH, Zamponi GW, Turner RW (2013) The Cav3-Kv4 complex acts as a calcium sensor to maintain inhibitory charge transfer during extracellular calcium fluctuations. J Neurosci 33:7811–7824.

Anderson P a, Greenberg RM (2001) Phylogeny of ion channels: clues to structure and function. Comp Biochem Physiol B Biochem Mol Biol 129:17–28.

Andrade A, Sandoval A, Oviedo N, De Waard M, Elias D, Felix R (2007) Proteolytic cleavage of the voltage-gated Ca2+ channel alpha2delta subunit: structural and functional features. Eur J Neurosci 25:1705–1710.

Arias JM, Murbartián J, Vitko I, Lee J-H, Perez-Reyes E (2005) Transfer of beta subunit regulation from high to low voltage-gated Ca2+ channels. FEBS Lett 579:3907–3912.

Ashcroft FM (2000) Ion channels and disease: channelopathies, 1st ed. San Diego, CA: Toronto: Academic Press.

Asmara H, Minobe E, Saud Z a., Kameyama M (2010) Interactions of Calmodulin With the Multiple Binding Sites of Cav1.2 Ca2+ Channels. J Pharmacol Sci 112:397–404.

Barel O, Shalev SA, Ofir R, Cohen A, Zlotogora J, Shorer Z, Mazor G, Finer G, Khateeb S, Zilberberg N, Birk OS (2008) Maternally inherited Birk Barel mental retardation dysmorphism syndrome caused by a mutation in the genomically imprinted potassium channel KCNK9. Am J Hum Genet 83:193–199.

Barrett CF, Tsien RW (2008) The Timothy syndrome mutation differentially affects voltage- and calcium-dependent inactivation of CaV1.2 L-type calcium channels. Proc Natl Acad Sci U S A 105:2157–2162.

Baumgart JP, Vitko I, Bidaud I, Kondratskyi A, Lory P, Perez-Reyes E (2008) I-II loop structural determinants in the gating and surface expression of low voltage-activated calcium channels. PLoS One 3:e2976.

Bazykin G a, Kochetov A V (2011) Alternative translation start sites are conserved in eukaryotic genomes. Nucleic Acids Res 39:567–577.

Beeton C et al. (2006) Kv1.3 channels are a therapeutic target for T cell-mediated autoimmune diseases. Proc Natl Acad Sci U S A 103:17414–17419.

Benmocha A, Almagor L, Oz S, Hirsch J a, Dascal N (2009) Characterization of the calmodulin-binding site in the N terminus of CaV1.2. Channels (Austin) 3:337–342.

Bernatchez G, Talwar D, Parent L (1998) Mutations in the EF-hand motif impair the inactivation of barium currents of the cardiac alpha1C channel. Biophys J 75:1727–1739.

Berridge MJ, Lipp P, Bootman MD (2000) The versatility and universality of calcium signalling. Nat Rev Mol Cell Biol 1:11–21.

Bezanilla F (2005) The voltage-sensor structure in a voltage-gated channel. Trends Biochem Sci 30:166–168.

Bezanilla F (2006) The action potential: from voltage-gated conductances to molecular structures. Biol Res:425–435.

Bhat MB, Zhao J, Takeshima H, Ma J (1997) Functional calcium release channel formed by the carboxyl-terminal portion of ryanodine receptor. Biophys J 73:1329–1336.

Bhate MP, McDermott AE (2012) Protonation state of E71 in KcsA and its role for channel collapse and inactivation. Proc Natl Acad Sci U S A 109:15265–15270.

Bichet D, Cornet V, Geib S, Carlier E, Volsen S, Hoshi T, Mori Y, De Waard M (2000) The I-II loop of the Ca2+ channel alpha1 subunit contains an endoplasmic reticulum retention signal antagonized by the beta subunit. Neuron 25:177–190.

Bidaud I, Lory P (2011) Hallmarks of the channelopathies associated with L-type calcium channels: a focus on the Timothy mutations in Ca(v)1.2 channels. Biochimie 93:2080–2086.

Black DJ, Tran Q-K, Persechini A (2004) Monitoring the total available calmodulin concentration in intact cells over the physiological range in free Ca2+. Cell Calcium 35:415–425.

Boschek CB, Sun H, Bigelow DJ, Squier TC (2008) Different conformational switches underlie the calmodulin-dependent modulation of calcium pumps and channels. Biochemistry 47:1640–1651.

Brehm P, Eckert R (1978) Calcium entry leads to inactivation of calcium channel in Paramecium. Cold Spring Harb Symp Quant Biol.

Broecker J, Vargas C, Keller S (2011) Revisiting the optimal c value for isothermal titration calorimetry. Anal Biochem 418:307–309.

Brokx RD, Lopez MM, Vogel HJ, Makhatadze GI (2001) Energetics of target peptide binding by calmodulin reveals different modes of binding. J Biol Chem 276:14083–14091.

Broomand A, Elinder F (2008) Large-scale movement within the voltage-sensor paddle of a potassium channel-support for a helical-screw motion. Neuron 59:770–777.

Brown M, Royer C (1997) Fluorescence spectroscopy as a tool to investigate protein interactions. Curr Opin Biotechnol:45–49.

Budde T, Meuth S, Pape H-C (2002) Calcium-dependent inactivation of neuronal calcium channels. Nat Rev Neurosci 3:873–883.

Burnstock G, Krügel U, Abbracchio MP, Illes P (2011) Purinergic signalling: from normal behaviour to pathological brain function. Prog Neurobiol 95:229–274.

Byerly L, Yazejian B (1986) Intracellular factors for the maintenance of calcium currents in perfused neurones from the snail, Lymnaea stagnalis. J Physiol 370:631–650.

Cain SM, Snutch TP (2010) Contributions of T-type calcium channel isoforms to neuronal firing. Channels (Austin) 4:475–482.

Catterall W a (2000) Structure and regulation of voltage-gated Ca2+ channels. Annu Rev Cell Dev Biol 16:521–555.

Catterall W a (2011) Voltage-gated calcium channels. Cold Spring Harb Perspect Biol 3:a003947.

Catterall W a (2014) Structure and function of voltage-gated sodium channels at atomic resolution. Exp Physiol 99:35–51.

Catterall W a, Yarov-Yarovoy V (2010) Helical motion of an S4 voltage sensor revealed by gating pore currents. Channels (Austin) 4:75–77.

Catterall W, Seagar M, Takahashi M (1988) Molecular properties of dihydropyridine-sensitive calcium channels in skeletal muscle. J Biol Chem 263:3535–3538.

Cens T, Rousset M, Leyris J-P, Fesquet P, Charnet P (2006) Voltage- and calcium-dependent inactivation in high voltage-gated Ca(2+) channels. Prog Biophys Mol Biol 90:104–117.

Censarek P, Beyermann M, Koch K-W (2004) Thermodynamics of apocalmodulin and nitric oxide synthase II peptide interaction. FEBS Lett 577:465–468.

Chanda B, Asamoah OK, Blunck R, Roux B, Bezanilla F (2005) Gating charge displacement in voltage-gated ion channels involves limited transmembrane movement. Nature 436:852–856.

Chen D, Lear J, Eisenberg B (1997) Permeation through an open channel: Poisson-Nernst-Planck theory of a synthetic ionic channel. Biophys J 72:97–116.

Chen L, Chetkovich DM, Petralia RS, Sweeney NT, Kawasaki Y, Wenthold RJ, Bredt DS, Nicoll R a (2000) Stargazin regulates synaptic targeting of AMPA receptors by two distinct mechanisms. Nature 408:936–943.

Chen RF (1968) Dansyl labeled proteins: determination of extinction coefficienc and number of bound residues with radioactive dansyl chloride. Anal Biochem 25:412–416.

Chen X, Wang Q, Ni F, Ma J (2010) Structure of the full-length Shaker potassium channel Kv1.2 by normal-mode-based X-ray crystallographic refinement. Proc Natl Acad Sci U S A 107:11352–11357.

Chen Y-H, Li M-H, Zhang Y, He L-L, Yamada Y, Fitzmaurice A, Shen Y, Zhang H, Tong L, Yang J (2004) Structural basis of the alpha1-beta subunit interaction of voltage-gated Ca2+ channels. Nature 429:675–680.

Cho HJ, Xie QW, Calaycay J, Mumford R a, Swiderek KM, Lee TD, Nathan C (1992) Calmodulin is a subunit of nitric oxide synthase from macrophages. J Exp Med 176:599–604.

Choi J, Park J-H, Kwon OY, Kim S, Chung JH, Lim DS, Kim KS, Rhim H, Han YS (2005) T-type calcium channel trigger p21ras signaling pathway to ERK in Cav3.1-expressed HEK293 cells. Brain Res 1054:22–29.

Chou JJ, Li S, Klee CB, Bax a (2001) Solution structure of Ca(2+)-calmodulin reveals flexible hand-like properties of its domains. Nat Struct Biol 8:990–997.

Christel C, Lee A (2012) Ca2+-dependent modulation of voltage-gated Ca2+ channels. Biochim Biophys Acta 1820:1243–1252.

Ciruela F (2008) Fluorescence-based methods in the study of protein-protein interactions in living cells. Curr Opin Biotechnol 19:338–343.

Clapham D (2012) Calcium Signaling (Islam MS, ed). Dordrecht: Springer Netherlands.

Conti F, Stühmer W (1989) Quantal charge redistributions accompanying the structural transitions of sodium channels. Eur Biophys J 17:53–59.

Cooper EC, Jan LY (1999) Review Ion channel genes and human neurological disease : Recent progress , prospects , and challenges. 96:4759–4766.

Corona JC, Tovar-y-Romo LB, Tapia R (2007) Glutamate excitotoxicity and therapeutic targets for amyotrophic lateral sclerosis. Expert Opin Ther Targets 11:1415–1428.

Corry B, Allen TW, Kuyucak S, Chung SH (2001) Mechanisms of permeation and selectivity in calcium channels. Biophys J 80:195–214.

Crotti L et al. (2013) Calmodulin mutations associated with recurrent cardiac arrest in infants. Circulation 127:1009–1017.

Cui J (2010) Reduction of CaV channel activities by Ca2+-CaM: inactivation or deactivation? J Gen Physiol 135:297–301.

Dafi O, Berrou L, Dodier Y, Raybaud A, Sauvé R, Parent L (2004) Negatively charged residues in the N-terminal of the AID helix confer slow voltage dependent inactivation gating to CaV1.2. Biophys J 87:3181–3192.

Dalsgaard T, Kroigaard C, Simonsen U (2010) Calcium-activated potassium channels - a therapeutic target for modulating nitric oxide in cardiovascular disease? Expert Opin Ther Targets 14:825–837.

Davies A, Douglas L, Hendrich J, Wratten J, Tran Van Minh A, Foucault I, Koch D, Pratt WS, Saibil HR, Dolphin AC (2006) The calcium channel alpha2delta-2 subunit partitions with CaV2.1 into lipid rafts in cerebellum: implications for localization and function. J Neurosci 26:8748–8757.

Davies A, Hendrich J, Van Minh AT, Wratten J, Douglas L, Dolphin AC (2007) Functional biology of the alpha(2)delta subunits of voltage-gated calcium channels. Trends Pharmacol Sci 28:220–228.

Davies AG, Pierce-Shimomura JT, Kim H, VanHoven MK, Thiele TR, Bonci A, Bargmann CI, McIntire SL (2003) A central role of the BK potassium channel in behavioral responses to ethanol in C. elegans. Cell 115:655–666.

Davis TN, Urdea MS, Masiarz FFLR, Thorner J (1986) Isolation of the yeast calmodulin gene: Calmodulin is an essential protein. Cell 47:423–431.

DeMaria CD, Soong TW, Alseikhan B a, Alvania RS, Yue DT (2001) Calmodulin bifurcates the local Ca2+ signal that modulates P/Q-type Ca2+ channels. Nature 411:484–489.

DePristo M a, Zilversmit MM, Hartl DL (2006) On the abundance, amino acid composition, and evolutionary dynamics of low-complexity regions in proteins. Gene 378:19–30.

Dereeper a, Guignon V, Blanc G, Audic S, Buffet S, Chevenet F, Dufayard J-F, Guindon S, Lefort V, Lescot M, Claverie J-M, Gascuel O (2008) Phylogeny.fr: robust phylogenetic analysis for the non-specialist. Nucleic Acids Res 36:W465–9.

Dick IE, Tadross MR, Liang H, Tay LH, Yang W, Yue DT (2008) A modular switch for spatial Ca2+ selectivity in the calmodulin regulation of CaV channels. Nature 451:830–834.

Dickman DK, Kurshan PT, Schwarz TL (2008) Mutations in a Drosophila alpha2delta voltage-gated calcium channel subunit reveal a crucial synaptic function. J Neurosci 28:31–38.

Diehnelt CW (2013) Peptide array based discovery of synthetic antimicrobial peptides. Front Microbiol 4:402.

DiGregorio DA, Nusser Z, Silver RA (2002) Spillover of glutamate onto synaptic AMPA receptors enhances fast transmission at a cerebellar synapse. Neuron 35:521–533.

Dixon HBF (1984) Nomenclature and Symbolism for Amino Acids and Peptides. Recommendations 1983. Eur J Biochem 138:9–37.

Dolphin A (2003a) G protein modulation of voltage-gated calcium channels. Pharmacol Rev 55:607–627.

Dolphin AC (2003b) B subunits of Voltage-Gated Calcium Channels. J Bioenerg Biomembr 35:599–620.

Dolphin AC (2009) Calcium channel diversity: multiple roles of calcium channel subunits. Curr Opin Neurobiol 19:237–244.

Dolphin AC (2013) The α2δ subunits of voltage-gated calcium channels. Biochim Biophys Acta 1828:1541–1549.

Doyle D a (2004) Structural changes during ion channel gating. Trends Neurosci 27:298–302.

Doyle DA (1998) The Structure of the Potassium Channel: Molecular Basis of K+ Conduction and Selectivity. Science (80-) 280:69–77.

Drum CL, Yan SZ, Sarac R, Mabuchi Y, Beckingham K, Bohm a, Grabarek Z, Tang WJ (2000) An extended conformation of calmodulin induces interactions between the structural domains of adenylyl cyclase from Bacillus anthracis to promote catalysis. J Biol Chem 275:36334–36340.

Dudev T, Lim C (2012) Why voltage-gated Ca2+ and bacterial Na+ channels with the same EEEE motif in their selectivity filters confer opposite metal selectivity. Phys Chem Chem Phys 14:12451–12456.

Dunlap K (2007) Calcium channels are models of self-control. J Gen Physiol 129:379–383.

Eckert R, Tillotson D (1981) Calcium-mediated inactivation of the calcium conductance in caesium-loaded giant neurones of Aplysia californica. J Physiol 50:265–280.

Elinder F, Nilsson J, Arhem P (2007) On the opening of voltage-gated ion channels. Physiol Behav 92:1–7.

Erickson MG, Alseikhan B a, Peterson BZ, Yue DT (2001) Preassociation of calmodulin with voltage-gated Ca(2+) channels revealed by FRET in single living cells. Neuron 31:973–985.

Erickson MG, Liang H, Mori MX, Yue DT (2003) FRET two-hybrid mapping reveals function and location of L-type Ca2+ channel CaM preassociation. Neuron 39:97–107.

Ernst O, Zor T (2010) Linearization of the bradford protein assay. J Vis Exp:1–6.

Evans TIA, Hell JW, Shea M a (2011) Thermodynamic linkage between calmodulin domains binding calcium and contiguous sites in the C-terminal tail of Ca(V)1.2. Biophys Chem 159:172–187.

Fallon JL, Baker MR, Xiong L, Loy RE, Yang G, Dirksen RT, Hamilton SL, Quiocho F a (2009) Crystal structure of dimeric cardiac L-type calcium channel regulatory domains bridged by Ca2+* calmodulins. Proc Natl Acad Sci U S A 106:5135–5140.

Feldkamp MD, Yu L, Shea M a (2011) Structural and energetic determinants of apo calmodulin binding to the IQ motif of the Na(V)1.2 voltage-dependent sodium channel. Structure 19:733–747.

Feng Z-P, Zhang Z, van Kesteren RE, Straub V a, van Nierop P, Jin K, Nejatbakhsh N, Goldberg JI, Spencer GE, Yeoman MS, Wildering W, Coorssen JR, Croll RP, Buck LT, Syed NI, Smit a B (2009) Transcriptome analysis of the central nervous system of the mollusc Lymnaea stagnalis. BMC Genomics 10:451.

Findeisen F, Minor D (2010) Structural Basis for the Differential Effects of CaBP1 and Calmodulin on Ca V 1.2 Calcium-Dependent Inactivation. Structure 18:1617–1631.

Findeisen F, Minor DL (2009) Disruption of the IS6-AID linker affects voltage-gated calcium channel inactivation and facilitation. J Gen Physiol 133:327–343.

Findeisen F, Rumpf CH, Minor DL (2013) Apo States of Calmodulin and CaBP1 Control CaV1 Voltage-Gated Calcium Channel Function through Direct Competition for the IQ Domain. J Mol Biol.

Findlay I (2004) Physiological modulation of inactivation in L-type Ca2+ channels: one switch. J Physiol 554:275–283.

Freiburger L, Auclair K, Mittermaier A (2009) Elucidating Protein Binding Mechanisms by Variableâ€•c ITC. ChemBioChem 10:2871–2873.

Freyer MW, Lewis E a (2008) Isothermal titration calorimetry: experimental design, data analysis, and probing macromolecule/ligand binding and kinetic interactions. Methods Cell Biol 84:79–113.

Friel DD, Tsien RW (1989) Voltage-gated calcium channels: direct observation of the anomalous mole fraction effect at the single-channel level. Proc Natl Acad Sci U S A 86:5207–5211.

Gao J, Yin DH, Yao Y, Sun H, Qin Z, Schöneich C, Williams TD, Squier TC (1998) Loss of conformational stability in calmodulin upon methionine oxidation. Biophys J 74:1115–1134.

Gellman SH (1991) On the role of methionine residues in the sequence-independent recognition of nonpolar protein surfaces. Biochemistry 30:6633–6636.

Gifford JL, Walsh MP, Vogel HJ (2007) Structures and metal-ion-binding properties of the Ca2+-binding helix-loop-helix EF-hand motifs. Biochem J 405:199–221.

Gillespie D, Boda D (2008) The Anomalous Mole Fraction Effect in Calcium Channels: A Measure of Preferential Selectivity. Biophys J 95:2658–2672.

Gillespie D, Boda D, He Y, Apel P, Siwy ZS (2008) Synthetic nanopores as a test case for ion channel theories: the anomalous mole fraction effect without single filing. Biophys J 95:609–619.

Gillespie D, Nonner W, Henderson D, Eisenberg RS (2002) A physical mechanism for large-ion selectivity of ion channels. Phys Chem Chem Phys 4:4763–4769.

Gillespie D, Xu L, Wang Y, Meissner G (2005) (De)constructing the ryanodine receptor: modeling ion permeation and selectivity of the calcium release channel. J Phys Chem B 109:15598–15610.

Goldin A (2002) Evolution of voltage-gated Na+ channels. J Exp Biol 584:575–584.

Grabarek Z (2005) Structure of a trapped intermediate of calmodulin: calcium regulation of EF-hand proteins from a new perspective. J Mol Biol 346:1351–1366.

Griessmeier K, Cuny H, Rötzer K, Griesbeck O, Harz H, Biel M, Wahl-Schott C (2009) Calmodulin is a functional regulator of Cav1.4 L-type Ca2+ channels. J Biol Chem 284:29809–29816.

Grueter CE, Abiria S a, Dzhura I, Wu Y, Ham A-JL, Mohler PJ, Anderson ME, Colbran RJ (2006) L-type Ca2+ channel facilitation mediated by phosphorylation of the beta subunit by CaMKII. Mol Cell 23:641–650.

Guo F, Minobe E, Yazawa K, Asmara H, Bai X, Han D, Hao L, Kameyama M (2010) Both N- and C-lobes of calmodulin are required for Ca2+-dependent regulations of CaV1.2 Ca2+ channels. Biochem Biophys Res Commun 391:1170–1176.

Haeseleer F, Sokal I, Verlinde CL, Erdjument-Bromage H, Tempst P, Pronin a N, Benovic JL, Fariss RN, Palczewski K (2000) Five members of a novel Ca(2+)-binding protein (CABP) subfamily with similarity to calmodulin. J Biol Chem 275:1247–1260.

Hagiwara S, Ozawa S, Sand O (1975) Voltage clamp analysis of two inward current mechanisms in the egg cell membrane of a starfish. J Gen Physiol 65:617–644.

Haitin Y, Carlson AE, Zagotta WN (2013) The structural mechanism of KCNH-channel regulation by the eag domain. Nature 501:444–448.

Halling DB, Georgiou DK, Black DJ, Yang G, Fallon JL, Quiocho FA, Pedersen SE, Hamilton SL (2009) Determinants in CaV1 channels that regulate the Ca2+ sensitivity of bound calmodulin. J Biol Chem 284:20041–20051.

Hansen LB, Buus S, Schafer-Nielsen C (2013) Identification and mapping of linear antibody epitopes in human serum albumin using high-density Peptide arrays. Nielsen M, ed. PLoS One 8:e68902.

Harry JB, Kobrinsky E, Abernethy DR, Soldatov NM (2004) New short splice variants of the human cardiac Cavbeta2 subunit: redefining the major functional motifs implemented in modulation of the Cav1.2 channel. J Biol Chem 279:46367–46372.

Hashimoto K, Fukaya M, Qiao X, Sakimura K, Watanabe M, Kano M (1999) Impairment of AMPA receptor function in cerebellar granule cells of ataxic mutant mouse stargazer. J Neurosci 19:6027–6036.

He L-L, Zhang Y, Chen Y-H, Yamada Y, Yang J (2007) Functional modularity of the beta-subunit of voltage-gated Ca2+ channels. Biophys J 93:834–845.

Heiman RG, Atkinson RC, Andruss BF, Bolduc C, Gae E, Beckingham K (2010) Spontaneous avoidance calmodulin expression behavior in Drosophila null for calmodulin expression. 93:2420–2425.

Heine S, Michalakis S, Kallenborn-Gerhardt W, Lu R, Lim H-Y, Weiland J, Del Turco D, Deller T, Tegeder I, Biel M, Geisslinger G, Schmidtko A (2011) CNGA3: a target of spinal nitric oxide/cGMP signaling and modulator of inflammatory pain hypersensitivity. J Neurosci 31:11184–11192.

Henley JM, Wilkinson KA (2013) AMPA receptor trafficking and the mechanisms underlying synaptic plasticity and cognitive aging. Dialogues Clin Neurosci 15:11–27.

Hidalgo P, Neely A (2007) Multiplicity of protein interactions and functions of the voltage-gated calcium channel beta-subunit. Cell Calcium 42:389–396.

Hille B (2001) Ion Channels of Excitable Membranes, 3rd ed. MA: Sinauer Associates, Inc.

Hinrichsen R (1992) 3'-modified antisense oligodeoxyribonucleotides complementary to calmodulin mRNA alter behavioral responses in Paramecium. Proc … 89:8601–8605.

Hoeflich KP, Ikura M (2002) Calmodulin in Action. Cell 108:739–742.

Honoré E (2008) Alternative translation initiation further increases the molecular and functional diversity of ion channels. J Physiol 586:5605–5606.

Houdusse A, Gaucher J-F, Krementsova E, Mui S, Trybus KM, Cohen C (2006) Crystal structure of apo-calmodulin bound to the first two IQ motifs of myosin V reveals essential recognition features. Proc Natl Acad Sci U S A 103:19326–19331.

Hu X, Laragione T, Sun L, Koshy S, Jones KR, Ismailov II, Yotnda P, Horrigan FT, Gulko PS, Beeton C (2012) KCa1.1 potassium channels regulate key proinflammatory and invasive properties of fibroblast-like synoviocytes in rheumatoid arthritis. J Biol Chem 287:4014–4022.

Huang C-H, Chen Y-C, Chen C-C (2013) Physical interaction between calcineurin and Cav3.2 T-type Ca2+ channel modulates their functions. FEBS Lett 587:1723–1730.

Huang LY, Catterall W a, Ehrenstein G (1978) Selectivity of cations and nonelectrolytes for acetylcholine-activated channels in cultured muscle cells. J Gen Physiol 71:397–410.

Ikura M (1996) Calcium binding and conformational response in EF-hand proteins. Trends Biochem Sci 21:14–17.

Ito E, Kobayashi S, Kojima S (1999) Associative learning in the pond snail, Lymnaea stagnalis. Zoolog Sci 16:711–723.

Ivanina T, Blumenstein Y, Shistik E, Barzilai R, Dascal N (2000) Modulation of L-type Ca2+ channels by gbeta gamma and calmodulin via interactions with N and C termini of alpha 1C. J Biol Chem 275:39846–39854.

Jegla TJ, Zmasek CM, Batalov S, Nayak SK (2009) Evolution of the human ion channel set. Comb Chem High Throughput Screen 12:2–23.

Jentsch TJ (2000) Neuronal KCNQ potassium channels: physiology and role in disease. Nat Rev Neurosci 1:21–30.

Jentsch TJ, Poët M, Fuhrmann JC, Zdebik A a (2005) Physiological functions of CLC Cl- channels gleaned from human genetic disease and mouse models. Annu Rev Physiol 67:779–807.

Jiang X, Lautermilch NJ, Watari H, Westenbroek RE, Scheuer T, Catterall W a (2008) Modulation of CaV2.1 channels by Ca2+/calmodulin-dependent protein kinase II bound to the C-terminal domain. Proc Natl Acad Sci U S A 105:341–346.

Jiang Y, Lee A, Chen J, Cadene M, Chait BT, MacKinnon R (2002) Crystal structure and mechanism of a calcium-gated potassium channel. Nature 417:515–522.

Jiang Y, Lee A, Chen J, Ruta V, Cadene M, Chait BT, MacKinnon R (2003a) X-ray structure of a voltage-dependent K+ channel. Nature 423:33–41.

Jiang Y, Ruta V, Chen J, Lee A, MacKinnon R (2003b) The principle of gating charge movement in a voltage-dependent K+ channel. Nature 423:42–48.

Johny M Ben, Yang PS, Bazzazi H, Yue DT (2013) Dynamic switching of calmodulin interactions underlies Ca2+ regulation of CaV1.3 channels. Nat Commun 4:1717.

Jurado L (1999) Apocalmodulin. Physiol … 79:661–682.

Juranic N, Atanasova E, Filoteo AG, Macura S, Prendergast FG, Penniston JT, Strehler EE (2010) Calmodulin wraps around its binding domain in the plasma membrane Ca2+ pump anchored by a novel 18-1 motif. J Biol Chem 285:4015–4024.

Kakiuchi S, Yasuda S, Yamazaki R, Teshima Y, Kanda K, Kakiuchi R, Sobue K (1982) Quantitative determinations of calmodulin in the supernatant and particulate fractions of mammalian tissues. J Biochem 92:1041–1048.

Kang M-G, Campbell KP (2003) Gamma subunit of voltage-activated calcium channels. J Biol Chem 278:21315–21318.

Keller R (2004) Optimizing the process of nuclear magnetic resonance spectrum analysis and computer aided resonance assignment. ETH, Zurich.

Kelly SM, Jess TJ, Price NC (2005) How to study proteins by circular dichroism. Biochim Biophys Acta 1751:119–139.

Keynes R, Elinder F (1999) The screw–helical voltage gating of ion channels. … R Soc … 266:843–852.

Khosravani H, Altier C, Simms B, Hamming KS, Snutch TP, Mezeyova J, McRory JE, Zamponi GW (2004) Gating effects of mutations in the Cav3.2 T-type calcium channel associated with childhood absence epilepsy. J Biol Chem 279:9681–9684.

Kilhoffer MC, Kubina M, Travers F, Haiech J (1992) Use of engineered proteins with internal tryptophan reporter groups and pertubation techniques to probe the mechanism of ligand-protein interactions: investigation of the mechanism of calcium binding to calmodulin. Biochemistry 31:8098–8106.

Kim EY, Rumpf CH, Fujiwara Y, Cooley ES, Van Petegem F, Minor DL (2008) Structures of CaV2 Ca2+/CaM-IQ domain complexes reveal binding modes that underlie calcium-dependent inactivation and facilitation. Structure 16:1455–1467.

Kim J, Ghosh S, Nunziato D a, Pitt GS (2004a) Identification of the components controlling inactivation of voltage-gated Ca2+ channels. Neuron 41:745–754.

Kim S a, Heinze KG, Waxham MN, Schwille P (2004b) Intracellular calmodulin availability accessed with two-photon cross-correlation. Proc Natl Acad Sci U S A 101:105–110.

Kincaid RL, Vaughan M, Osborne JC, Tkachuk VA (1982) Ca2+-dependent interaction of 5-dimethylaminonaphthalene-1-sulfonyl-calmodulin with cyclic nucleotide phosphodiesterase, calcineurin, and troponin I. J Biol Chem 257:10638–10643.

Kochegarov A a. (2003) Pharmacological modulators of voltage-gated calcium channels and their therapeutical application. Cell Calcium 33:145–162.

Kovalevskaya N V, Bokhovchuk FM, Vuister GW (2012) The TRPV5/6 calcium channels contain multiple calmodulin binding sites with differential binding properties. J Struct Funct Genomics 13:91–100.

Kovalevskaya N V, van de Waterbeemd M, Bokhovchuk FM, Bate N, Bindels RJM, Hoenderop JGJ, Vuister GW (2013) Structural analysis of calmodulin binding to ion channels demonstrates the role of its plasticity in regulation. Pflugers Arch 465:1507–1519.

Krauss D, Eisenberg B, Gillespie D (2011) Selectivity sequences in a model calcium channel: role of electrostatic field strength. Eur Biophys J 40:775–782.

Kubota Y, Putkey J a, Waxham MN (2007) Neurogranin controls the spatiotemporal pattern of postsynaptic Ca2+/CaM signaling. Biophys J 93:3848–3859.

Kullmann D, Hanna M (2002) Neurological disorders caused by inherited ion-channel mutations. Lancet Neurol 1:157–166.

Kunzelmann K, Gerlach L, Fröbe U, Greger R (1991) Bicarbonate permeability of epithelial chloride channels. Pflugers Arch 417:616–621.

Lang S, Spratt DE, Guillemette JG, Palmer M (2005) Dual-targeted labeling of proteins using cysteine and selenomethionine residues. Anal Biochem 342:271–279.

Lao QZ, Kobrinsky E, Harry JB, Ravindran A, Soldatov NM (2008) New Determinant for the CaVbeta2 subunit modulation of the CaV1.2 calcium channel. J Biol Chem 283:15577–15588.

Lau K, Chan MMY, Van Petegem F (2014) Lobe-Specific Calmodulin Binding to Different Ryanodine Receptor Isoforms. Biochemistry.

Ledwell JL, Aldrich RW (1999) Mutations in the S4 region isolate the final voltage-dependent cooperative step in potassium channel activation. J Gen Physiol 113:389–414.

Lee A, Zhou H, Scheuer T, Catterall W a (2003a) Molecular determinants of Ca(2+)/calmodulin-dependent regulation of Ca(v)2.1 channels. Proc Natl Acad Sci U S A 100:16059–16064.

Lee W-S, Ngo-Anh TJ, Bruening-Wright A, Maylie J, Adelman JP (2003b) Small conductance Ca2+-activated K+ channels and calmodulin: cell surface expression and gating. J Biol Chem 278:25940–25946.

Lerma J, Marques JM (2013) Kainate receptors in health and disease. Neuron 80:292–311.

Letts V a, Felix R, Biddlecome GH, Arikkath J, Mahaffey CL, Valenzuela a, Bartlett FS, Mori Y, Campbell KP, Frankel WN (1998) The mouse stargazer gene encodes a neuronal Ca2+-channel gamma subunit. Nat Genet 19:340–347.

Letts VA (2005) Stargazer--a mouse to seize! Epilepsy Curr 5:161–165.

Li H. L, Sui H. X, Ghanshani S, Lee S, Walian P. J, Wu C. L, Chandy K. G, Jap B. K (1998) Two-dimensional crystallization and projection structure of KcsA potassium channel. J Mol Biol 282:211–216.

Li Q, Du H-N, Hu H-Y (2003) Study of protein-protein interactions by fluorescence of tryptophan analogs: application to immunoglobulin G binding domain of streptococcal protein G. Biopolymers 72:116–122.

Liang H, DeMaria CD, Erickson MG, Mori MX, Alseikhan B a, Yue DT (2003) Unified mechanisms of Ca2+ regulation across the Ca2+ channel family. Neuron 39:951–960.

Linse S, Helmersson A, Forsén S (1991) Calcium binding to calmodulin and its globular domains. J Biol Chem 266:8050–8054.

Lipkind GM, Fozzard H a (2008) Voltage-gated Na channel selectivity: the role of the conserved domain III lysine residue. J Gen Physiol 131:523–529.

Lipkind GM, Fozzard H a. (2001) Modeling of the Outer Vestibule and Selectivity Filter of the L-Type Ca 2+ Channel †. Biochemistry 40:6786–6794.

Liu Z, Vogel HJ (2012) Structural basis for the regulation of L-type voltage-gated calcium channels: interactions between the N-terminal cytoplasmic domain and Ca(2+)-calmodulin. Front Mol Neurosci 5:38.

Llinás R, Yarom Y (1981) Electrophysiology of mammalian inferior olivary neurones in vitro. Different types of voltage-dependent ionic conductances. J Physiol 315:549–567.

Long SB, Campbell EB, Mackinnon R (2005) Crystal structure of a mammalian voltage-dependent Shaker family K+ channel. Science 309:897–903.

López-González I, De La Vega-Beltrán JL, Santi CM, Florman HM, Felix R, Darszon A (2001) Calmodulin Antagonists Inhibit T-Type Ca2+ Currents in Mouse Spermatogenic Cells and the Zona Pellucida-Induced Sperm Acrosome Reaction. Dev Biol 236:210–219.

Lu Z (2002) Coupling between Voltage Sensors and Activation Gate in Voltage-gated K+ Channels. J Gen Physiol 120:663–676.

Lu Z, Klem a M, Ramu Y (2001) Ion conduction pore is conserved among potassium channels. Nature 413:809–813.

Malasics A, Gillespie D, Nonner W, Henderson D, Eisenberg B, Boda D (2009) Protein structure and ionic selectivity in calcium channels: selectivity filter size, not shape, matters. Biochim Biophys Acta 1788:2471–2480.

Marois R, Croll RP (1992) Development of serotoninlike immunoreactivity in the embryonic nervous system of the snail Lymnaea stagnalis. J Comp Neurol 322:255–265.

Maximciuc A a, Putkey J a, Shamoo Y, Mackenzie KR (2006) Complex of calmodulin with a ryanodine receptor target reveals a novel, flexible binding mode. Structure 14:1547–1556.

McComb C, Varshney N, Lukowiak K (2005) Juvenile Lymnaea ventilate, learn and remember differently than do adult Lymnaea. J Exp Biol 208:1459–1467.

Merrill MA, Malik Z, Akyol Z, Bartos JA, Leonard AS, Hudmon A, Shea MA, Hell JW (2007) Displacement of alpha-actinin from the NMDA receptor NR1 C0 domain By Ca2+/calmodulin promotes CaMKII binding. Biochemistry 46:8485–8497.

Mika YH, Palti Y (1994) Charge displacements in a single potassium ion channel macromolecule during gating. Biophys J 67:1455–1463.

Minor DL, Findeisen F (2010) Progress in the structural understanding of voltage-gated calcium channel (CaV) function and modulation. Channels (Austin) 4:459–474.

Montgomery HJ, Bartlett R, Perdicakis B, Jervis E, Squier TC, Guillemette JG (2003) Activation of constitutive nitric oxide synthases by oxidized calmodulin mutants. Biochemistry 42:7759–7768.

Moorthy a K, Gopal B, Satish PR, Bhattacharya S, Bhattacharya a, Murthy MR, Surolia a (1999) Thermodynamics of target peptide recognition by calmodulin and a calmodulin analogue: implications for the role of the central linker. FEBS Lett 461:19–24.

Mori MX, Vander Kooi CW, Leahy DJ, Yue DT (2008) Crystal structure of the CaV2 IQ domain in complex with Ca2+/calmodulin: high-resolution mechanistic implications for channel regulation by Ca2+. Structure 16:607–620.

Muralidhara BK, Negi SS, Halpert JR (2007) Dissecting the thermodynamics and cooperativity of ligand binding in cytochrome P450eryF. J Am Chem Soc 129:2015–2024.

Napolitano C, Antzelevitch C (2011) Phenotypical manifestations of mutations in the genes encoding subunits of the cardiac voltage-dependent L-type calcium channel. Circ Res 108:607–618.

Nelson MR, Thulin E, Fagan PA, Forsén S, Chazin WJ (2002) The EF-hand domain: a globally cooperative structural unit. Protein Sci 11:198–205.

Nilius B (2007) TRP channels in disease. Biochim Biophys Acta 1772:805–812.

Nishizawa M, Nishizawa K (2008) Molecular dynamics simulation of Kv channel voltage sensor helix in a lipid membrane with applied electric field. Biophys J 95:1729–1744.

Nonner W, Chen DP, Eisenberg B (1998) Anomalous Mole Fraction Effect, Electrostatics, and Binding in Ionic Channels. Biophys J 74:2327–2334.

Numazaki M, Tominaga T, Takeuchi K, Murayama N, Toyooka H, Tominaga M (2003) Structural determinant of TRPV1 desensitization interacts with calmodulin. Proc Natl Acad Sci U S A 100:8002–8006.

O'Donnell SE, Newman R a, Witt TJ, Hultman R, Froehlig JR, Christensen AP, Shea M a (2009) Thermodynamics and conformational change governing domain-domain interactions of calmodulin., 1st ed. Elsevier Inc.

O'Neil KT, DeGrado WF (1990) How calmodulin binds its targets: sequence independent recognition of amphiphilic alpha-helices. Trends Biochem Sci 15:59–64.

Obata K, Nagata K, Iwase M, Odashima M, Nagasaka T, Izawa H, Murohara T, Yamada Y, Yokota M (2005) Overexpression of calmodulin induces cardiac hypertrophy by a calcineurin-dependent pathway. Biochem Biophys Res Commun 338:1299–1305.

Obermair GJ, Tuluc P, Flucher BE (2008) Auxiliary Ca(2+) channel subunits: lessons learned from muscle. Curr Opin Pharmacol 8:311–318.

Ohrtman J, Ritter B, Polster A, Beam KG, Papadopoulos S (2008) Sequence differences in the IQ motifs of CaV1.1 and CaV1.2 strongly impact calmodulin binding and calcium-dependent inactivation. J Biol Chem 283:29301–29311.

Oliveria SF, Dittmer PJ, Youn D, Dell'Acqua ML, Sather W a (2012) Localized calcineurin confers Ca2+-dependent inactivation on neuronal L-type Ca2+ channels. J Neurosci 32:15328–15337.

Opatowsky Y, Chen C-C, Campbell KP, Hirsch J a (2004) Structural analysis of the voltage-dependent calcium channel beta subunit functional core and its complex with the alpha 1 interaction domain. Neuron 42:387–399.

Oz S, Tsemakhovich V, Christel CJ, Lee A, Dascal N (2011) CaBP1 regulates voltage-dependent inactivation and activation of Ca(V)1.2 (L-type) calcium channels. J Biol Chem 286:13945–13953.

Park H-J, Park S-J, Ahn E-J, Lee S-Y, Seo H, Lee J-H (2013) Asp residues of the Glu-Glu-Asp-Asp pore filter contribute to ion permeation and selectivity of the Cav3.2 T-type channel. Cell Calcium 54:226–235.

Park S-H, Raines RT (2004) Fluorescence polarization assay to quantify protein-protein interactions. Methods Mol Biol 261:161–166.

Pathak M, Kurtz L, Tombola F, Isacoff E (2005) The cooperative voltage sensor motion that gates a potassium channel. J Gen Physiol 125:57–69.

Pattnaik BR, Asuma MP, Spott R, Pillers D-AM (2012) Genetic defects in the hotspot of inwardly rectifying K(+) (Kir) channels and their metabolic consequences: a review. Mol Genet Metab 105:64–72.

Payandeh J, Scheuer T, Zheng N, Catterall WA (2011) The crystal structure of a voltage-gated sodium channel. Nature 475:353–358.

Perez-Reyes E (1999) Three for T : molecular analysis of the low voltage-activated. 56:660–669.

Perez-Reyes E (2003) Molecular physiology of low-voltage-activated t-type calcium channels. Physiol Rev 83:117–161.

Perez-Reyes E (2010) Characterization of the gating brake in the I-II loop of CaV3 T-type calcium channels. Channels (Austin) 4:453–458.

Perez-Reyes E, Kim HS, Lacerda a E, Horne W, Wei XY, Rampe D, Campbell KP, Brown a M, Birnbaumer L (1989) Induction of calcium currents by the expression of the alpha 1-subunit of the dihydropyridine receptor from skeletal muscle. Nature 340:233–236.

Persechini A, Stemmer PM (2002) Calmodulin is a limiting factor in the cell. Trends Cardiovasc Med 12:32–37.

Peterson BZ, DeMaria CD, Adelman JP, Yue DT (1999) Calmodulin is the Ca2+ sensor for Ca2+ - dependent inactivation of L-type calcium channels. Neuron 22:549–558.

Peterson BZ, Lee JS, Mulle JG, Wang Y, de Leon M, Yue DT (2000) Critical determinants of Ca(2+)-dependent inactivation within an EF-hand motif of L-type Ca(2+) channels. Biophys J 78:1906–1920.

Pfaffl MW (2001) A new mathematical model for relative quantification in real-time RT-PCR. Nucleic Acids Res 29:e45.

Piontkivska H, Hughes AL (2003) Evolution of vertebrate voltage-gated ion channel alpha chains by sequential gene duplication. J Mol Evol 56:277–285.

Pitt GS, Zühlke RD, Hudmon a, Schulman H, Reuter H, Tsien RW (2001) Molecular basis of calmodulin tethering and Ca2+-dependent inactivation of L-type Ca2+ channels. J Biol Chem 276:30794–30802.

Planells-Cases R, Jentsch TJ (2009) Chloride channelopathies. Biochim Biophys Acta 1792:173–189.

Pless S a, Lynch JW (2008) Illuminating the structure and function of Cys-loop receptors. Clin Exp Pharmacol Physiol 35:1137–1142.

Poomvanicha M, Wegener JW, Blaich A, Fischer S, Domes K, Moosmang S, Hofmann F (2011) Facilitation and Ca2+-dependent inactivation are modified by mutation of the Ca(v)1.2 channel IQ motif. J Biol Chem 286:26702–26707.

Posson DJ, Ge P, Miller C, Bezanilla F, Selvin PR (2005) Small vertical movement of a K+ channel voltage sensor measured with luminescence energy transfer. Nature 436:848–851.

Postea O, Biel M (2011) Exploring HCN channels as novel drug targets. Nat Rev Drug Discov 10:903–914.

Potet F, Chagot B, Anghelescu M, Viswanathan PC, Stepanovic SZ, Kupershmidt S, Chazin WJ, Balser JR (2009) Functional Interactions between Distinct Sodium Channel Cytoplasmic Domains through the Action of Calmodulin. J Biol Chem 284:8846–8854.

Price J V, Jarrell JA, Furman D, Kattah NH, Newell E, Dekker CL, Davis MM, Utz PJ (2013) Characterization of influenza vaccine immunogenicity using influenza antigen microarrays. Turner SJ, ed. PLoS One 8:e64555.

Puljak L, Kilic G (2006) Emerging roles of chloride channels in human diseases. Biochim Biophys Acta 1762:404–413.

Putkey J a, Waxham MN, Gaertner TR, Brewer KJ, Goldsmith M, Kubota Y, Kleerekoper QK (2008) Acidic/IQ motif regulator of calmodulin. J Biol Chem 283:1401–1410.

Radivojac P, Vucetic S, O'Connor TR, Uversky VN, Obradovic Z, Dunker a K (2006) Calmodulin signaling: analysis and prediction of a disorder-dependent molecular recognition. Proteins 63:398–410.

Rajakulendran S, Kaski D, Hanna MG (2012) Neuronal P/Q-type calcium channel dysfunction in inherited disorders of the CNS. Nat Rev Neurol 8:86–96.

Reddy Chichili VP, Xiao Y, Seetharaman J, Cummins TR, Sivaraman J (2013) Structural basis for the modulation of the neuronal voltage-gated sodium channel NaV1.6 by calmodulin. Sci Rep 3:2435.

Rhoads A, Friedberg F (1997) Sequence motifs for calmodulin recognition. FASEB J:331–340.

Rice P, Longden I, Bleasby A (2000) EMBOSS: The European Molecular Biology Open Software Suite. Trends Genet 16:276–277.

Richards MW, Butcher AJ, Dolphin AC (2004) Ca2+ channel beta-subunits: structural insights AID our understanding. Trends Pharmacol Sci 25:626–632.

Robinson P, Etheridge S, Song L, Shah R, Fitzgerald EM, Jones OT (2011) Targeting of voltage-gated calcium channel α2δ-1 subunit to lipid rafts is independent from a GPI-anchoring motif. PLoS One 6:e19802.

Roder H, Maki K, Cheng H, Shastry MCR (2004) Rapid mixing methods for exploring the kinetics of protein folding. Methods 34:15–27.

Rosenmund C, Feltz A, Westbrook GL (1995) Synaptic NMDA receptor channels have a low open probability. J Neurosci 15:2788–2795.

Rothman SM, Olney JW (1995) Excitotoxicity and the NMDA receptor--still lethal after eight years. Trends Neurosci 18:57–58.

Rusnak F, Mertz P (2000) Calcineurin: form and function. Physiol Rev 80:1483–1521.

Sadamoto H, Takahashi H, Okada T, Kenmoku H, Toyota M, Asakawa Y (2012) De novo sequencing and transcriptome analysis of the central nervous system of mollusc Lymnaea stagnalis by deep RNA sequencing. PLoS One 7:e42546.

Saimi Y, Kung C (2002) Calmodulin as an ion channel subunit. Annu Rev Physiol 64:289–311.

Sanabria H, Digman M a, Gratton E, Waxham MN (2008) Spatial diffusivity and availability of intracellular calmodulin. Biophys J 95:6002–6015.

Sandoval A, Oviedo N, Andrade A, Felix R (2004) Glycosylation of asparagines 136 and 184 is necessary for the alpha2delta subunit-mediated regulation of voltage-gated Ca2+ channels. FEBS Lett 576:21–26.

Sanguinetti MC, Krafte DS, Kass RS (1986) Voltage-dependent modulation of Ca channel current in heart cells by Bay K8644. J Gen Physiol 88:369–392.

Sansom MSP, Shrivastava IH, Bright JN, Tate J, Capener CE, Biggin PC (2002) Potassium channels: structures, models, simulations. Biochim Biophys Acta 1565:294–307.

Sarhan MF, Tung C, Van Petegem F, Ahern CA (2012) Crystallographic basis for calcium regulation of sodium channels. Proc Natl Acad Sci U S A 109:3558–3563.

Schumacher M a, Crum M, Miller MC (2004) Crystal structures of apocalmodulin and an apocalmodulin/SK potassium channel gating domain complex. Structure 12:849–860.

Schumacher M a, Rivard a F, Bächinger HP, Adelman JP (2001) Structure of the gating domain of a Ca2+-activated K+ channel complexed with Ca2+/calmodulin. Nature 410:1120–1124.

Senatore A, Boone A, Lam S, Dawson TF, Zhorov B, Spafford JD (2011a) Mapping of dihydropyridine binding residues in a less sensitive invertebrate L-type calcium channel (LCa v 1). Channels (Austin) 5:173–187.

Senatore A, Boone AN, Spafford JD (2011b) Optimized transfection strategy for expression and electrophysiological recording of recombinant voltage-gated ion channels in HEK-293T cells. J Vis Exp.

Senatore A, Monteil A, van Minnen J, Smit AB, Spafford JD (2013) NALCN ion channels have alternative selectivity filters resembling calcium channels or sodium channels. PLoS One 8:e55088.

Senatore A, Spafford JD (2010) Transient and big are key features of an invertebrate T-type channel (LCav3) from the central nervous system of Lymnaea stagnalis. J Biol Chem 285:7447–7458.

Senatore A, Spafford JD (2012) Gene transcription and splicing of T-type channels are evolutionarily-conserved strategies for regulating channel expression and gating. PLoS One 7:e37409.

Senatore A, Zhorov BS, Spafford JD (2012) Cav3 T-type calcium channels. Wiley Interdiscip Rev Membr Transp Signal 1:467–491.

Sencer S, Papineni R V, Halling DB, Pate P, Krol J, Zhang JZ, Hamilton SL (2001) Coupling of RYR1 and L-type calcium channels via calmodulin binding domains. J Biol Chem 276:38237–38241.

Seyferth S, Lee G (2003) Structural studies of EDTA-induced fibrillation of salmon calcitonin. Pharm Res 20:73–80.

Sharma B, Deo S (2005) Competitive binding assay using fluorescence resonance energy transfer for the identification of calmodulin antagonists. Bioconjugate ….

Shcheglovitov a. K, Shuba YM (2006) Sodium/calcium selectivity of cloned calcium T-type channels. Neurophysiology 38:149–157.

Shepherd CM, Vogel HJ (2004) A molecular dynamics study of Ca(2+)-calmodulin: evidence of interdomain coupling and structural collapse on the nanosecond timescale. Biophys J 87:780–791.

Shi C, Soldatov NM (2002) Molecular determinants of voltage-dependent slow inactivation of the Ca2+ channel. J Biol Chem 277:6813–6821.

Shi N, Ye S, Alam A, Chen L, Jiang Y (2006) Atomic structure of a Na+- and K+-conducting channel. Nature 440:570–574.

Shieh CC, Coghlan M, Sullivan JP, Gopalakrishnan M (2000) Potassium channels: molecular defects, diseases, and therapeutic opportunities. Pharmacol Rev 52:557–594.

Simons TJ (1988) Calcium and neuronal function. Neurosurg Rev 11:119–129.

Sine SM, Engel AG (2006) Recent advances in Cys-loop receptor structure and function. Nature 440:448–455.

Singh B, Monteil A, Bidaud I, Sugimoto Y, Suzuki T, Hamano S, Oguni H, Osawa M, Alonso ME, Delgado-Escueta A V, Inoue Y, Yasui-Furukori N, Kaneko S, Lory P, Yamakawa K (2007) Mutational analysis of CACNA1G in idiopathic generalized epilepsy. Mutation in brief #962. Online. Hum Mutat 28:524–525.

Slavov N, Carey J, Linse S (2013) Calmodulin transduces Ca(2+) oscillations into differential regulation of its target proteins. ACS Chem Neurosci 4:601–612.

Snijder J, Rose RJ, Raijmakers R, Heck AJR (2011) Site-specific methionine oxidation in calmodulin affects structural integrity and interaction with Ca2+/calmodulin-dependent protein kinase II. J Struct Biol 174:187–195.

Sobey CG (2001) Potassium Channel Function in Vascular Disease. Arterioscler Thromb Vasc Biol 21:28–38.

Spafford JD, Dunn T, Smit AB, Syed NI, Zamponi GW (2006) In vitro characterization of L-type calcium channels and their contribution to firing behavior in invertebrate respiratory neurons. J Neurophysiol 95:42–52.

Splawski I, Yoo DS, Stotz SC, Cherry A, Clapham DE, Keating MT (2006) CACNA1H mutations in autism spectrum disorders. J Biol Chem 281:22085–22091.

Spratt DE, Newman E, Mosher J, Ghosh DK, Salerno JC, Guillemette JG (2006) Binding and activation of nitric oxide synthase isozymes by calmodulin EF hand pairs. FEBS J 273:1759–1771.

Spratt DE, Taiakina V, Guillemette JG (2007) Calcium-deficient calmodulin binding and activation of neuronal and inducible nitric oxide synthases. Biochim Biophys Acta - Proteins Proteomics 1774:1351–1358.

Stotz SC, Jarvis SE, Zamponi GW (2004) Functional roles of cytoplasmic loops and pore lining transmembrane helices in the voltage-dependent inactivation of HVA calcium channels. J Physiol 554:263–273.

Striessnig J (2007) C-terminal tailoring of L-type calcium channel function. J Physiol 585:643–644.

Striessnig J, Bolz HJ, Koschak A (2010) Channelopathies in Cav1.1, Cav1.3, and Cav1.4 voltage-gated L-type Ca2+ channels. Pflugers Arch 460:361–374.

Stroffekova K (2011) The IQ motif is crucial for Cav1.1 function. J Biomed Biotechnol 2011:504649.

Sukhareva M, Hackos DH, Swartz KJ (2003) Constitutive activation of the Shaker Kv channel. J Gen Physiol 122:541–556.

Swartz KJ (2004a) Opening the gate in potassium channels. Nat Struct Mol Biol 11:499–501.

Swartz KJ (2004b) Towards a structural view of gating in potassium channels. Nat Rev Neurosci 5:905–916.

Tadross MR (2009) MECHANISM OF SENSING CALCIUM FROM NEAR OR AFAR.

Tadross MR, Ben Johny M, Yue DT (2010) Molecular endpoints of Ca2+/calmodulin- and voltage-dependent inactivation of Ca(v)1.3 channels. J Gen Physiol 135:197–215.

Tadross MR, Dick IE, Yue DT (2008) Mechanism of local and global Ca2+ sensing by calmodulin in complex with a Ca2+ channel. Cell 133:1228–1240.

Taiakina V, Boone AN, Fux J, Senatore A, Weber-Adrian D, Guillemette JG, Spafford JD (2013) The calmodulin-binding, short linear motif, NSCaTE is conserved in L-type channel ancestors of vertebrate Cav1.2 and Cav1.3 channels. PLoS One 8:e61765.

Talavera K, Janssens A, Klugbauer N, Droogmans G, Nilius B (2003) Pore structure influences gating properties of the T-type Ca2+ channel alpha1G. J Gen Physiol 121:529–540.

Talavera K, Nilius B (2006) Biophysics and structure-function relationship of T-type Ca2+ channels. Cell Calcium 40:97–114.

Tang W, Halling DB, Black DJ, Pate P, Zhang J-Z, Pedersen S, Altschuld R a, Hamilton SL (2003) Apocalmodulin and Ca2+ calmodulin-binding sites on the CaV1.2 channel. Biophys J 85:1538–1547.

Tekmen M, Gleason E (2010) Multiple Ca2+-dependent mechanisms regulate L-type Ca2+ current in retinal amacrine cells. J Neurophysiol 104:1849–1866.

Tombola F, Pathak MM, Isacoff EY (2006) How does voltage open an ion channel? Annu Rev Cell Dev Biol 22:23–52.

Toutenhoofd SL, Strehler EE (2000) The calmodulin multigene family as a unique case of genetic redundancy: multiple levels of regulation to provide spatial and temporal control of calmodulin pools? Cell Calcium 28:83–96.

Tuckwell HC (2012) Quantitative aspects of L-type Ca2+ currents. Prog Neurobiol 96:1–31.

Turnbull WB, Daranas AH (2003) On the value of c: can low affinity systems be studied by isothermal titration calorimetry? J Am Chem Soc 125:14859–14866.

Unneberg P, Merelo JJ, Chacón P, Morán F (2001) SOMCD: method for evaluating protein secondary structure from UV circular dichroism spectra. Proteins 42:460–470.

Van den Ent F, Löwe J (2006) RF cloning: a restriction-free method for inserting target genes into plasmids. J Biochem Biophys Methods 67:67–74.

Van Petegem F, Chatelain FC, Minor DL (2005) Insights into voltage-gated calcium channel regulation from the structure of the CaV1.2 IQ domain-Ca2+/calmodulin complex. Nat Struct Mol Biol 12:1108–1115.

Van Petegem F, Lobo P a, Ahern C a (2012) Seeing the forest through the trees: towards a unified view on physiological calcium regulation of voltage-gated sodium channels. Biophys J 103:2243–2251.

Venkatachalam K, Montell C (2007) TRP channels. Annu Rev Biochem 76:387–417.

Vetter SW, Leclerc E (2003) Novel aspects of calmodulin target recognition and activation. Eur J Biochem 270:404–414.

Vivian JT, Callis PR (2001) Mechanisms of tryptophan fluorescence shifts in proteins. Biophys J 80:2093–2109.

Walker D, Waard M De, De Waard M (1998) Subunit interaction sites in voltage-dependent Ca 2+ channels: role in channel function. Trends Neurosci 21:148–154.

Walsh CPC, Davies A, Butcher AAJ, Dolphin AC, Kitmitto A (2009) Three-dimensional Structure of CaV3. 1 COMPARISON WITH THE CARDIAC L-TYPE VOLTAGE-GATED CALCIUM CHANNEL MONOMER ARCHITECTURE. J Biol … 284:22310–22321.

Wang C, Wang H-G, Xie H, Pitt GS (2008) Ca2+/CaM controls Ca2+-dependent inactivation of NMDA receptors by dimerizing the NR1 C termini. J Neurosci 28:1865–1870.

Weiss N, Zamponi GW, De Waard M (2012) How do T-type calcium channels control low-threshold exocytosis? Commun Integr Biol 5:377–380.

Welsby PJ, Wang H, Wolfe JT, Colbran RJ, Johnson ML, Barrett PQ (2003) A mechanism for the direct regulation of T-type calcium channels by Ca2+/calmodulin-dependent kinase II. J Neurosci 23:10116–10121.

Whitmore L, Wallace B a (2004) DICHROWEB, an online server for protein secondary structure analyses from circular dichroism spectroscopic data. Nucleic Acids Res 32:W668–73.

Whitmore L, Wallace B a (2008) Protein secondary structure analyses from circular dichroism spectroscopy: methods and reference databases. Biopolymers 89:392–400.

Wilson SM, Brittain JM, Piekarz AD, Ballard CJ, Ripsch MS, Cummins TR, Hurley JH, Khanna M, Hammes NM, Samuels BC, White F a, Khanna R (2011) Further insights into the antinociceptive potential of a peptide disrupting the N-type calcium channel-CRMP-2 signaling complex. Channels (Austin) 5:449–456.

Wolfart J, Roeper J (2002) Selective coupling of T-type calcium channels to SK potassium channels prevents intrinsic bursting in dopaminergic midbrain neurons. J Neurosci 22:3404–3413.

Wu C, Zhang J, Abu-Soud H, Ghosh DK, Stuehr DJ (1996) High-level expression of mouse inducible nitric oxide synthase in Escherichia coli requires coexpression with calmodulin. Biochem Biophys Res Commun 222:439–444.

Wu G, Gao Z, Dong A, Yu S (2012) Calcium-induced changes in calmodulin structural dynamics and thermodynamics. Int J Biol Macromol 50:1011–1017.

Wu X, Bers DM (2007) Free and bound intracellular calmodulin measurements in cardiac myocytes. Cell Calcium 41:353–364.

Xiong L, Zhang J-Z, He R, Hamilton SL (2006) A Ca2+-binding domain in RyR1 that interacts with the calmodulin binding site and modulates channel activity. Biophys J 90:173–182.

Xiong L-W, Kleerekoper QK, Wang X, Putkey J a (2010) Intra- and interdomain effects due to mutation of calcium-binding sites in calmodulin. J Biol Chem 285:8094–8103.

Yamniuk AP, Vogel HJ (2004) Calmodulin's flexibility allows for promiscuity in its interactions with target proteins and peptides. Mol Biotechnol 27:33–57.

Yap KL, Kim J, Truong K, Sherman M, Yuan T, Ikura M (2000) Calmodulin target database. J Struct Funct Genomics 1:8–14.

Yellen G (1998) The moving parts of voltage-gated ion channels. Q Rev Biophys 31:239–295.

Yu F, Catterall W (2003) Overview of the voltage-gated sodium channel family. Genome Biol 4:207.

Yuan T, Vogel HJ (1999) Substitution of the methionine residues of calmodulin with the unnatural amino acid analogs ethionine and norleucine: biochemical and spectroscopic studies. Protein Sci 8:113–121.

Yuzawa Y, Niki I, Kosugi T, Maruyama S, Yoshida F, Takeda M, Tagawa Y, Kaneko Y, Kimura T, Kato N, Yamamoto J, Sato W, Nakagawa T, Matsuo S (2008) Overexpression of calmodulin in pancreatic beta cells induces diabetic nephropathy. J Am Soc Nephrol 19:1701–1711.

Zalk R, Lehnart SE, Marks AR (2007) Modulation of the ryanodine receptor and intracellular calcium. Annu Rev Biochem 76:367–385.

Zamponi GW (2005) Voltage Gated Calcium Channels. New York, NY: Kluwer Academic/Plenum Publishers.

Zhang M, Abrams C, Wang L, Gizzi A, He L, Lin R, Chen Y, Loll PJ, Pascal JM, Zhang J (2012) Structural basis for calmodulin as a dynamic calcium sensor. Structure 20:911–923.

Zhang M, Li M, Wang JH, Vogel HJ (1994) The effect of Met-->Leu mutations on calmodulin's ability to activate cyclic nucleotide phosphodiesterase. J Biol Chem 269:15546–15552.

Zhang M, Tanaka T, Ikura M (1995) Calcium-induced conformational transition revealed by the solution structure of apo calmodulin. Nat Struct Mol Biol 2:758–767.

Zhang R, Dzhura I, Grueter C, Thiel W (2005) A dynamic α-β inter-subunit agonist signaling complex is a novel feedback mechanism for regulating L-type Ca2+ channel opening. FASEB J 16:1–16.

Zhang S, Ehlers MD, Bernhardt JP, Su CT, Huganir RL (1998) Calmodulin mediates calcium-dependent inactivation of N-methyl-D-aspartate receptors. Neuron 21:443–453.

Zhou H, Yu K, McCoy KL, Lee A (2005) Molecular mechanism for divergent regulation of Cav1.2 Ca2+ channels by calmodulin and Ca2+-binding protein-1. J Biol Chem 280:29612–29619.

Zhou Y, Xue S, Yang JJ (2013) Calciomics: integrative studies of Ca2+-binding proteins and their interactomes in biological systems. Metallomics 5:29–42.

Zühlke RD, Pitt GS, Tsien RW, Reuter H (2000) Ca2+-sensitive inactivation and facilitation of L-type Ca2+ channels both depend on specific amino acid residues in a consensus calmodulin-binding motif in the(alpha)1C subunit. J Biol Chem 275:21121–21129.

Appendix

Sequence of the HIS-RN construct (in pET22b) used in Chapter 2:

```
tttaagaaggagatataccatgggcagcagccatcatcatcatcatcacagcagcggcctg
                  M  G  S  S  H  H  H  H  H  H  S  S  G  L
gtgccgcgcggcagccatatggtgaacgaaaacacccgcatgtatgtgccggaagaaaac
 V  P  R  G  S  H  M  V  N  E  N  T  R  M  Y  V  P  E  E  N
catcagggcagcaactatggcagcccgcgcccggcgcatgcgaacatgaacgcgaacgcg
 H  Q  G  S  N  Y  G  S  P  R  P  A  H  A  N  M  N  A  N  A
gcggccggcctggcgccggaacatattccgaccccgggcgcggccctgagctggcaggcg
 A  A  G  L  A  P  E  H  I  P  T  P  G  A  A  L  S  W  Q  A
gcgattgatgcggcgcgccaggcgaaactgatgggcagcgcgggcaacgcgaccattagc
 A  I  D  A  A  R  Q  A  K  L  M  G  S  A  G  N  A  T  I  S
accgtgagcagcacccagcgcaaacgccagcagtatggcaaaccgaaaaaacagggcggc
 T  V  S  S  T  Q  R  K  R  Q  Q  Y  G  K  P  K  K  Q  G  G
accaccgcgacccgcccgccgcgcgcgctgctgtgcctgaccctgaaaaacccgattcgc
 T  T  A  T  R  P  P  R  A  L  L  C  L  T  L  K  N  P  I  R
cgcgcgtgcattagcattgtggaatgggtcgacaagcttgcggccgcactcgagcaccac
 R  A  C  I  S  I  V  E  W  V  D  K  L  A  A  A  L  E  H  H
caccaccaccactgagatccggctgctaacaaagcccgaaaggaagctgagttggctgct
 H  H  H  H
gccaccgctgagcaataactagcataacccccttggggcctctaaacgggtcttgagggt

tttttgctgaaaggaggaactatatccggattggcgaatgggacgcgccctgtagcggcg

cattaagcgcggcgggtgtggtggttacgcgcagcgtgaccgctacacttgccagcgccc

tagcgcccgctcctttcgctttcttcccttcctttctcgccacgttcgccggctttcccc

gtcaagctctaaatcggggggctccctttagggttccgatttagtgctttacggcacc
```

NSCaTE is highlighted in red. Expressed construct start site Met is in bold black (extra residues left over from cloning). Start site found in native $Ca_V1.2$ sequences (Met1) is blue and the 'alternative' start site omitting NSCaTE (Met2) is in red.

ATGGCCAGCCCACTGGTCAACATCGTGAGACTGGAGGAGGAGGGGGGACATAATCCAGGTGGCGCTGTCAACTCGCCTTCTGGAGCAGGAGGTGG
M A S P L V N I V R L E E E G D I I Q V A L S T R L L E Q E V

TGGAGGTAGAGGAGGAGGAGGAGGAGGGGGAGGACCCTGGTGGTACGGGCGGAGGTAGTGGATACAAACCCCTCGTCCCGCAGAACACTACAAGC
V E V E E E E E G R T L V V R A E V V D T N P S S R R T L Q A

SacI
GCTTGCCACTGTCGTCAGGTGGCTTGTCTCTGAATACAACAGACTCTGGCAGAGCTCTAAGTACAGGTTGGAGCACCGCCTTAGCAGCTGCGCA
L A T V V R W L V S E Y N R L W Q S S K Y R L E H R L S S C A

                                                                                    FseI
AGGTGCTGCTACTGTACGAAAACGAGCCAACATGAGGAAGCAACAAAACCAAAATGTGCGGCCGGCCAGGGCACTTCTTTGCTTGACTCTGAAA
R C C Y C T K T S Q H E E A T K P K C A A G Q G T S L L D S E

         AccI   EcoRI   5LREcoRIb
AATCCCATACGCAAATTTGTATACAGGTTGCAGAATACAAAGCATTTGAATTCTTGGTATTAATCACCATTTTTGCCAATTGTGTTGCTCTTGC
K S H T Q I C I Q V A E Y K A F E F L V L I T I F A N C V A L A

TATTTATACACCGTATCCAATGTCTGACTCCAATGAAGTTAACTCTGCACTGGATCGGATTGAATATGTCTTCTTAGTGATATTCTTATTGGAG
I Y T P Y P M S D S N E V N S A L D R I E Y V F L V I F L L E

                                                                              NsiI
GGAATACTCAAGATCATAGCTTACGGCTTCGTCATGCACCAAGGAGCTTATTTACGAAATGGATGGAATGCATTAGATTTTACCATTGTTGTCA
G I L K I I A Y G F V M H Q G A Y L R N G W N A L D F T I V V

                                                                              L5R41
                                                             L5R42   StuI
TAGGTATTATTAGTTCGATTTTATCCTTCGTCCAAGAAAAGGGTTTTGACGTGAAAGCCCTGAGAGCATTCAGAGTATTGAGGCCTTTAAGACT
I G I I S S I L S F V Q E K G F D V K A L R A F R V L R P L R L

GGTGTCAGGGCAACCAAGTCTCCAAGTGGTGTTAAATTCTATTGTACGTGCCATGGTCCCTTTGTTGCACATTGCCCTTCTTGTAATATTTGTC
V S G Q P S L Q V V L N S I V R A M V P L L H I A L L V I F V

                                                        L5R5   BstEII
ATCATCATCTATGCTATCATCGGATTGGAGCTGTTTTATGGAAAACTTCACAACGCTTGCTACAAGATAAattcaactgaattttcAGGTGACC
I I I Y A I I G L E L F Y G K L H N A C Y K I N S T E F S G D

CAAGAATATGTGGGCAAGGCTACACTTGTGACGACATAGCATCTGGAGGTGAAAAGGGGGAGTGCAGAGAGGGGTGGGAAGGACCCAAACTATGG
P R I C G Q G Y T C D D I A S G G E K G E C R E G W E G P N Y G

AATAACAAATTTTGATAATTTTGGTCTGGCCATGTTGACTGTCTTCCAGTGTATCACCATGGAGGGGTGGACCACAGTGCTCTATGATGTAAAT
I T N F D N F G L A M L T V F Q C I T M E G W T T V L Y D V N

        L5R3 SalI
        LD1S5B   L5R2
AATGCGTTGGGCAATGAGTGGCCGTGGATTTACTTTATTAGCCTCATCATCATTGGCTCATTTTTTGTCCTTAACCTTGTTCTTGGTGTCCTAA
N A L G N E W P W I Y F I S L I I I G S F F V L N L V L G V L

L5R1
GTGGAGAGTTTTCCAAAGAAAGAGAGAAAGCAAAAGCCAGAGGTGACTTCCAGAAACTGAGAGAGAAACAGCAGCTTGAAGAAGATCTTAGAGG
S G E F S K E R E K A K A R G D F Q K L R E K Q Q L E E D L R G

                                                                              1401
TTATTTGGACTGGATTACACAAGCTGAGGACATAGATCCAGAGGTTGAGGATGAAAATGAGGAAGGAGCAACACCACGTCACTCCAAAATTACG
Y L D W I T Q A E D I D P E V E D E N E E G A T P R H S K I T

AGTGATATAGATTCAGGGGACAAGGTGGAGGAAGGAGAGAATGTAGAGATCCAACAGTCTTGGCTCCAGCAGAAAAGACTGCACTTACAGAAAC
S D I D S G D K V E E G E N V E I Q Q S W L Q Q K R L H L Q K

**Figure A.3: Sequence of LCa$_V$1 with primers.**
The two possible start Met are boxed.

Figure A.4: Gel filtration chromatogram of wild type Ca^{2+}-CaM with IQ and NSCaTE peptides (at stoichiometric ratios).
Hi-Load Superdex 75 (10/60) from GE Healthcare was used; holoCaM alone reliably elutes at ~67mL on this column. Due to their small size (both <3kDa), both IQ and NSCaTE, when unbound to CaM, elute at well past the resolution limit (peak near 110mL), thus the only other resolvable peaks should contain various CaM-bound peptides. Only one such peak was noted (~77mL), and collected for analysis by ESI MS. Due to the salt used in gel filtration protocols (which interferes with ESI MS), this sample had to be extracted with Zip Tip (C18 reverse-phase media-containing pipette tip used for 2D gel spot extraction, Millipore) before submitting the sample for MS analysis. Subsequently, only CaM and the IQ peptide (but not NSCaTE) mass peaks were found in the ESI MS spectrum (see Figure A.5 and Figure A.6).
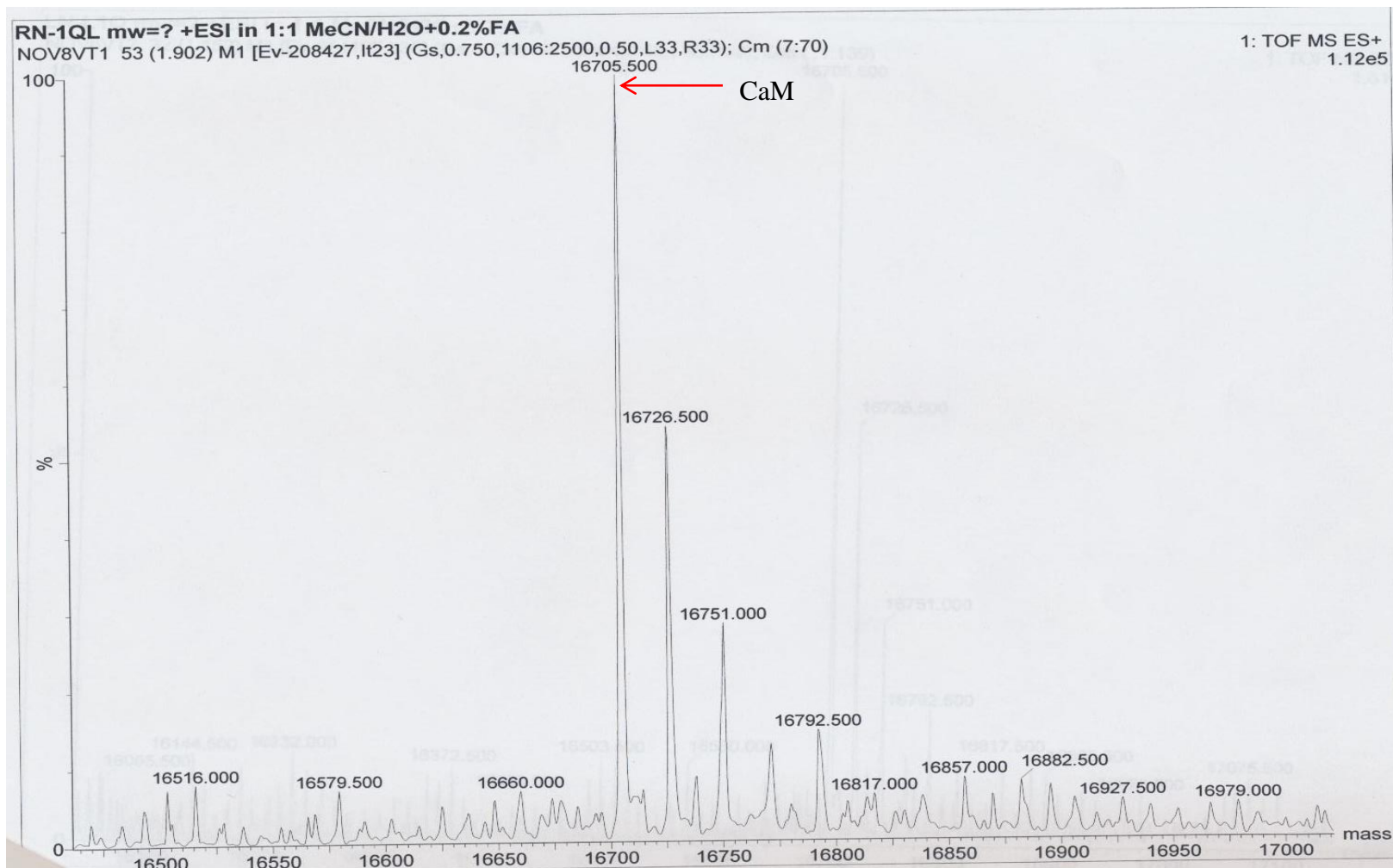
Figure A.5: Deconvoluted MS spectrum of CaM.
Desalted (using the Zip Tip protocol) samples from the gel filtration treatment of CaM-RN-IQc mixture (Figure A.4) were analyzed by ESI MS (Waters Q-TOF Ultima Global at University of Waterloo, under the supervision of Dr. Richard Smith) .
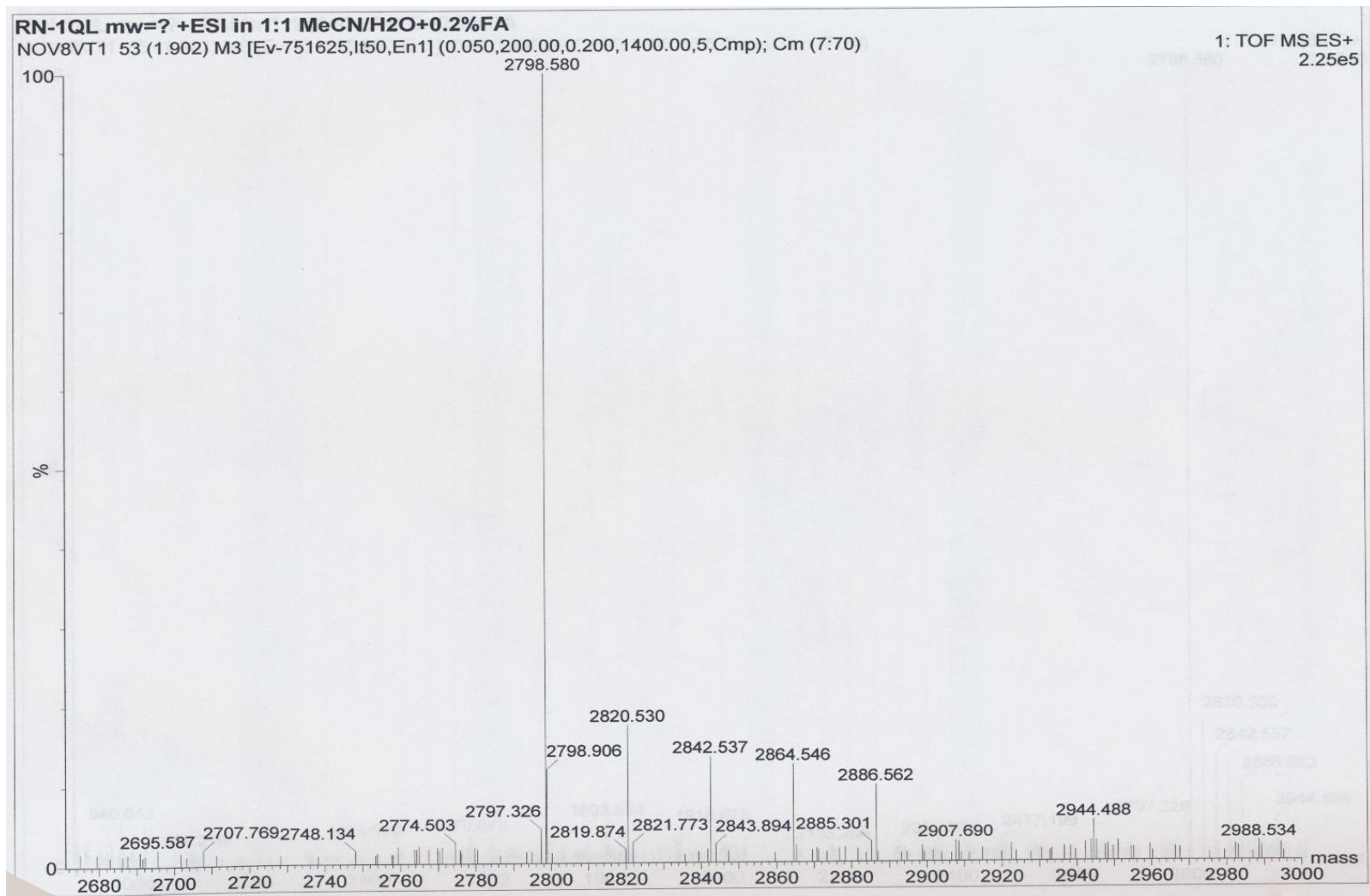
Figure A.6: Deconvoluted spectrum (peptide range) of CaM/IQc/RN (same raw data as Figure A.5).
The same sample as in Figure A.5 but using the peptide algorithm for peak integration /deconvolution. The ~2.8 kDa peak corresponds to the IQc peptide; no peaks were obtained for the RN peptide (MW ~1.8 kDa). Judging by the presence of IQc and a rather low absorbance of this fraction at 280nm, corresponding to Trp fluorescence, which should be high for NSCaTE (Figure A.4), we judged that RN was not co-eluting with CaM under the gel filtration conditions used.
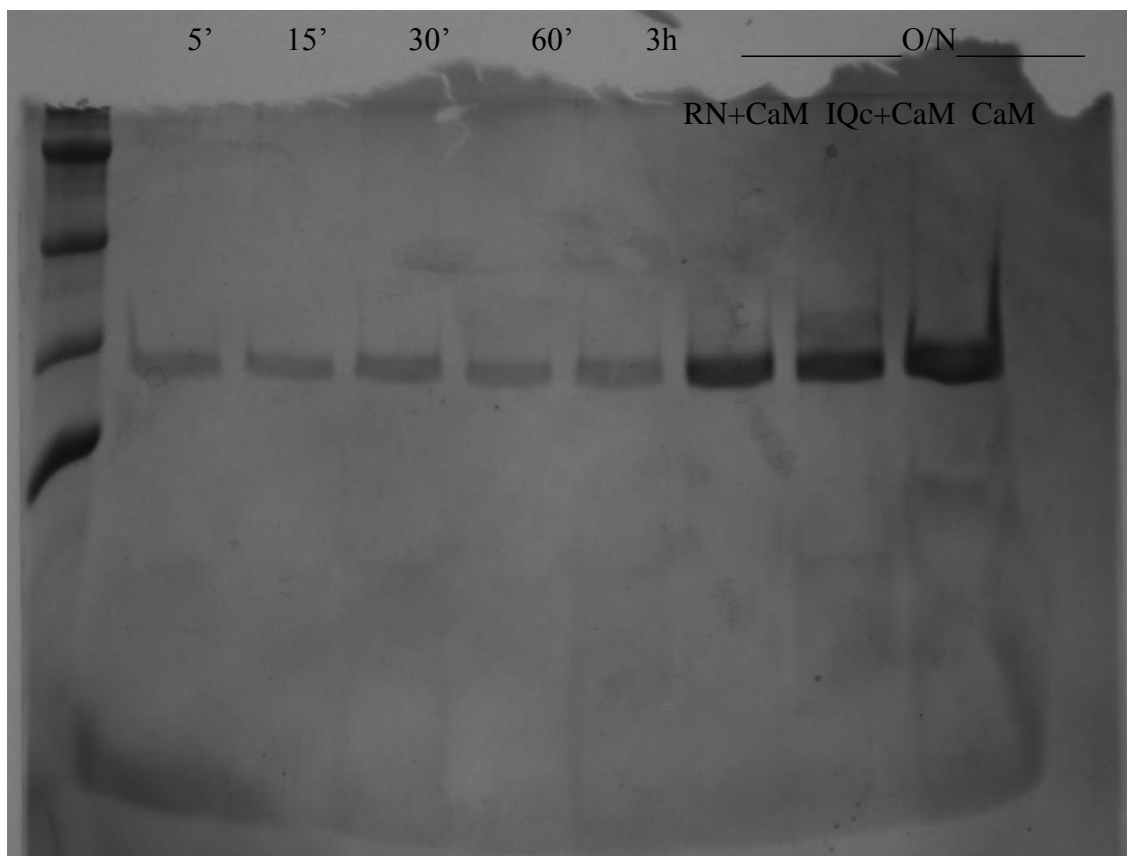
Figure A.7: Formaldehyde cross linking time trial.
Equal molar amounts of peptide and Ca^{2+}-CaM (300pmol each, in gel filtration buffer with 1mM $CaCl_2$) were pre-incubated for 20-30 minutes on ice. Incubation times (indicated at the top) were started upon adding up to 0.5% w/v paraformaldehyde (from dissolved 10% stock made fresh) to the CaM-peptide complex, and terminated by quenching with excess Tris-Cl. To the quenched samples (kept on ice), 1 : 1 loading dye was added and they were then run on a native PAGE (same protocol as for gel-shift mobility assays, see section 2.2.4). Initially, the goal was to identify a tripartite complex by chromatography and then ESI-MS, but the PAGE was performed as a preliminary screen for successful cross-linking. Unfortunately no higher-MW bands can be seen except for the IQc-CaM control (which is expected based on the results covered in Chapter 2). The last three lanes are overnight incubations in 1% formaldehyde of CaM and a single peptide each lane (CaM + RN, CaM + IQc, CaM alone), ran as controls.
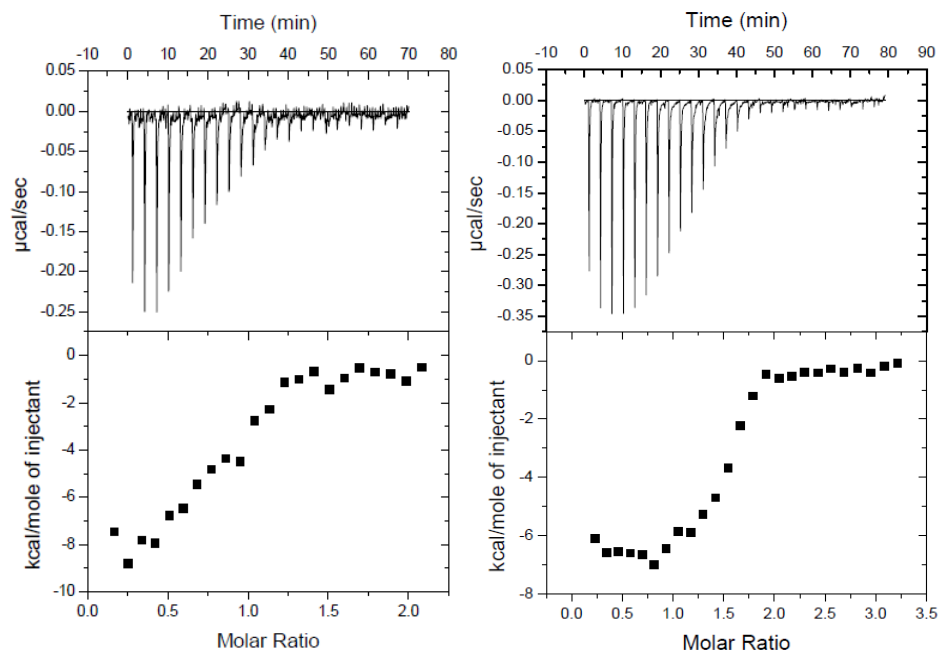
Figure A.8: Preliminary binding of the L-type channel I-II linker peptides to Ca^{2+}-CaM.
Ca$_V$1.2 (LHLQKLNRRYRRFCRRIVKS, left) and LCa$_V$1 (GENCRARLAHRISKSKFSRY, right) peptides (Genscript, >98% purity) were titrated into CaM (500µM peptide in the syringe, 50µM CaM in the cell). Clear exothermic interaction was observed for both, but the stoichiometry for LCa$_V$1 appears to be non 1 : 1 (although this could be due to insufficient peptide resuspension; the experiment has not since been repeated). LCa$_V$1 I-II linker peptide also appears to have a higher affinity for CaM (~0.4µM) than Ca$_V$1.2 (1.8µM). Further characterization of these fragments is recommended.
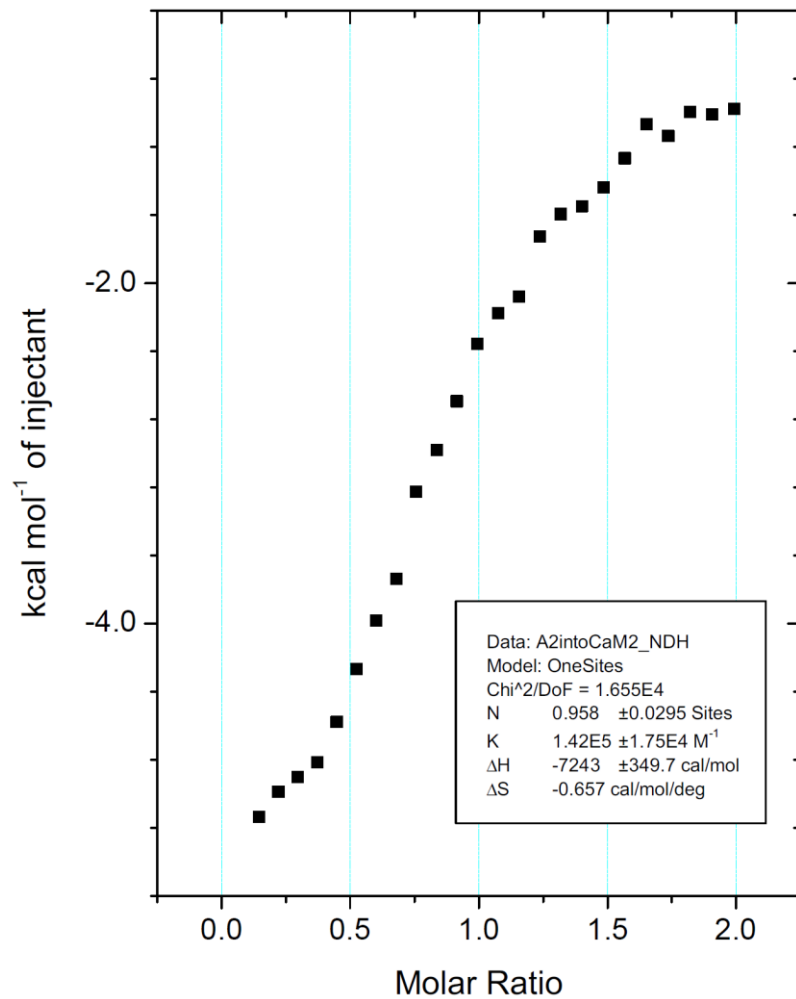
Figure A.9: ITC results (fitted) of LCa$_V$2 IQ peptide (KIYAGLLISENWKAYKASQNA) with holoCaM.

Same methods as L-type peptides; see section 3.1.1.